1-1-1998

Rheology of molten polystyrene with dissolved gases

Choongyong Kwag

RHEOLOGY OF MOLTEN POLYSTYRENE WITH DISSOLVED GASES

by

CHOONGYONG KWAG

DISSERTATION

Submitted to the Graduate School

of Wayne State University,

Detroit, Michigan

in partial fulfillment of the requirements

for the degree of

DOCTOR OF PHILOSOPHY

1998

MAJOR: CHEMICAL ENGINEERING

Approved by:

Co-advisor Date 3/5/98

Co-advisor Date 3/5/98

Kyung W. Suh 2/19/98

Ronald F. Gibson 2/19/98

Chau Mao 2/24/98

Because the foolishness of God is wiser than men; and the weakness of God is stronger than men.

1 Corinthians 1:25

ACKNOWLEDGEMENTS

I would like to express my sincere gratitude to my supervisors Dr. Esin Gulari and Dr. Charles W. Manke Jr. They provided this opportunity and have guided me to achieve the goal with thankful encouragement and invaluable advice.

Also I acknowledge Dr. Kyung W. Suh and Dr. Lawrence Hood in Dow Chemical Company for their technical advice and support.

My thanks are to Dr. Linda Gerhardt who originally designed the experimental equipment and gave helpful suggestions, to Khan Vickar for his excellent theoretical modeling, to Dr. Ashok Garg for providing experimental data, to Dr. Joseph Smolinski for numerous technical supports, and to other members of our research group. Eugene Snowden and the members of Engineering Machine Shop are also gratefully appreciated for their reliable service at anytime.

I wish to thank my parents in Korea for their persistent love and care and Pastor John H. Lee and friends in KFCUMC for their prayers and spiritual provisions.

The endurance and support of my wife, Ji-Young and my son, Han-Wook was the most important help to complete this work.

TABLE OF CONTENTS

LIST OF TABLES

LIST OF FIGURES

CHAPTER 1

INTRODUCTION

Multitudes of thermoplastics having diverse ranges of chemical and physical properties are manufactured in the modern polymer industry. The process of converting raw polymers to finished commercially useful articles involves polymer processing. Polymer processing includes a variety of mainly physical processes for the conversion of raw polymers to final products. The transport phenomena associated with the processing are quite complex and attract interests of chemical engineers who are pursuing the process development and optimization of an individual and/or integrated manufacturing processes. Most of individual operations and shaping steps of polymer processing involve the flow of molten or softened polymeric materials through geometrically complex conduits at elevated temperatures and pressures and under either isothermal or non-isothermal conditions.

Rheology is the science engaged in the relationships between the deformation or deformation rate and the applied stress. The polymer rheology becomes a major scope of rheology due to the abundance and versatility of polymers and their distinctive rheological properties. Frequently special rheological properties of polymer systems are artificially tailor-made for research or engineering. The rheological characteristics are essential for the study of the flow behavior of polymer that provides an important information to the process analysis and equipment design. In addition, it is invaluable to investigate rheological properties for a comparative study of polymers, evaluation of novel polymers, and demonstration of special processing characteristics of polymers.

It is common that diverse types of additives are incorporated with the base

thermoplastic polymer as a processing aid in order to facilitate processing and/or to provide a specific performance of final product. The modified rheological and thermodynamic properties of polymer system should be characterized thoroughly to attain the optimum processing condition and design. When the viscosity of a polymer needs to be reduced for more effective processing, usually a plasticizer is incorporated as a processing aid for the reduction of the glass transition temperature (T_g), which causes the viscosity reduction. As the glass transition temperature is lowered, the process can be carried out at a lower temperature that leads to the reduction of energy consumption and thermal or mechanical degradation during processing. The plasticizer added for the reduction of viscosity may be removed after processing to prevent the undesired loss of product performance due to the residual additives.

Frequently, however, the plasticizer is mixed with the base polymer for the accomplishment of a special function of product. For instance, electric cables are coated with flexible polymer which is a blend of poly(vinylchloride) and appropriate organic plasticizers for the improvement of flexibility. Gaseous plasticizers are primarily used as physical or chemical blowing agents in the plastic foam production. In both cases, the plasticizer acts as a processing aid and a special functional additive for the final product.

Conventional plasticizers are mostly low molecular weight organic compounds that are mostly liquids. Among gaseous plasticizers chlorofluorocarbons (CFC's) and hydrochlorofluorocarbons (HCFC's) have been widely used as blowing agents for manufacturing foam products. The discharge of such plasticizers into air provokes an environmental problem during processing and diffusion through the product surface. Therefore, in addition to the functional consideration, the environmental aspect must be also examined in the selection of plasticizers.

1.1 Application of Supercritical Gases in Polymer Processing

When a gas is heated above its critical temperature, T_c, and pressurized beyond its critical pressure, P_c, the gas behaves as a single dense fluid phase. This is called a supercritical gas (SCG) having a liquid-like density and intermediate diffusivity and viscosity between the values of gas and liquid. Due to their great solvating power and controllability, SCG's have been used in diversified chemical, pharmaceutical and food industries for various separation processes [McHugh and Krukonis, 1986]. Supercritical solutions are applied for the development of new micro-coating material in the drug delivery systems due to the rapid volume expansion of supercritical solution and enhanced extraction power [Jaarmo et al, 1997; Mishima et al., 1997]. Supercritical carbon dioxide is used as a reaction medium for both homogeneous and heterogeneous polymerization of polymers which are insoluble in most common organic solvents, such as fluorinated polymers [DeSimone et al., 1992; Guan et al., 1993; Clark and DeSimone, 1994; Kendall and DeSimone, 1997]. For the polymer processing applications, SCG's received substantial attention recently as a processing aid or plasticizer [Wang et al., 1982; Chiou et al., 1985; Sefcik, 1986]. Numerous application of SCG's in polymer processing is reviewed by Garg [1993] for instance, extraction, fractionation, fiber deposition, devolatilization, foam production, microcellular plastics, gas separation membranes, etc. Most of thermoplastics are processed at elevated temperatures and pressures providing the conditions of supercritical behavior of SCG's.

The plasticization of polymer melts with dissolved gases leading to reduction of viscosity is possible through two mechanisms, the dilution effect of chain entanglement and the addition of free volume by the diluent or plasticizer. The dilution of chain entanglement is the main effect of the organic solvent plasticizers because organic

solvents and the molten polymers have similar densities, and therefore the additive free volume effect is relatively low. However, both mechanisms contribute to the viscosity reduction for polymer–SCG systems. Since SCG's have much more free volume than organic solvents, the significantly increased free volume enhances the viscosity reduction. Wang et al. [1982] reported 50 °C or more reduction of T_g of polystyrene plasticized with supercritical carbon dioxide. Although the thermodynamic and rheological data for polymer-SCG systems are required for the processing applications, only few limited data are available. The thermodynamic and rheological investigations of polymer-SCG systems are essential to provide the fundamental information for the processing of polymer-SCG mixtures.

CFC's and HCFC's, generally known as Freon gases, have been used as a physical-blowing agent in plastic foam industries and as a refrigerant, a propellant, and a solvent in many other applications. Because the CFC's cause the destruction of the ozone layer, according to the Montreal protocol voted in 1990, their production will be phased-out by the year 2000 in developed countries. Therefore, environmentally benign SCG's, particularly carbon dioxide, are candidate materials to replace the CFC's and HCFC's. The hydrofluoroalkanes (HFA's), such as 1,1-difluoroethane (R152a), 1,1,1,2-tetrafluoroethane (R134a), etc. have been developed for the replacement of the CFC's and HCFC's. Also carbon dioxide, a non-toxic and economic gas is a good alternative. The environmental consideration is expected to be important in the selection of SCG's for polymer processing.

1.2 Research Objectives

The primary objective of this dissertation is the experimental measurements of the

rheological properties of polymer-SCG solutions over a wide range of shear rates. There was no systematic study on the rheological characterization of molten polymers with dissolved gases, such as PS-CO_2, PS-R152a, and PS-R134a mixtures in open literature. This study builds on the previous work for mixture of liquid poly(dimethylsiloxane) (PDMS) and CO_2 performed by Dr. Linda J. Gerhardt [1994].

The thermoplastic polymer used for this study is polystyrene (PS), a widely used common thermoplastic which is employed for plastic foam production. Blowing agents for the foam production are now changing from ozone-depleting CFC's to non-hazardous SCG's. Carbon dioxide (CO_2), 1,1-difluoroethane (refrigerant R152a), and 1,1,1,2-tetrafluoroethane (refrigerant R134a) are environmentally acceptable gases used in this study. Carbon dioxide is a very common and non-ozone depleting gas having the near ambient T_c, 31.05 °C. Both of R152a and R134a are typical substitutive refrigerants replacing ozone-depleting CFC's and HCFC's.

The solubility of a gas into polystyrene is necessary to determine the adequate composition range of a PS-gas mixture to be characterized. The primary property determining the rheological behavior of molten polymers or concentrated polymer solutions is the shear viscosity, which is the main rheological property experimentally measured in this study. A pressurized capillary rheometer is used to measure the viscosities of PS-CO_2, PS-R152a, and PS-R134a solutions. Gerhardt [1994] originally designed the rheometer for measuring the viscosity of PDMS-CO_2 solutions. The modified rheometer is capable of measuring PS-SCG solution viscosities with further modifications for sample loading. The experimental apparatus and technique will be mentioned in detail in Chapter 5.

The viscosity reduction due to dissolved gas is assessed by the concentration shift

factor, the ratio of zero-shear viscosity of diluted polymer melt to that of pure molten polymer. The concentration shift factor is evaluated by the shift of viscosity curves of diluted polymer making a concentration-invariant master curve. Gerhardt [1994] successfully applied this procedure to PDMS-CO_2 mixture. In the current study, the shift factors representing the viscosity reduction due to changes in temperature, pressure, and concentration are evaluated for molten PS-SCG mixtures.

The contribution of diluent to the chain entanglement dilution can be evaluated through a series of experiments using additives having the identical free volume fraction as the polymer where the fractional free volume is unchanged by dissolving diluents. Low molecular weight PS is chosen as the diluent for this purpose providing iso-free volume experiments.

The viscosity reduction of polymer-diluent mixture can be estimated theoretically by the free volume model which employs the concept of free volume to explain the properties of liquids and polymeric fluids. The viscosity decreases with the increase of fractional free volume which is dependent of temperature, concentration of diluent, and pressure. The viscosity reduction due to dissolved diluent is correlated with the relative increment of fractional free volume contributed by the diluent. The Kelly-Bueche equation [1961] is one of earlier theories based on the assumption of simple additivity between free volumes of polymer and diluent. Gerhardt et al. [1997] employed an extended free volume rheological model which is modified from the Kelly-Bueche equation and adopted lattice based-equation of state models in order to compute specific volumes of PDMS-CO_2 mixtures instead of using a mixing rule for polymer and diluents. The extended free volume model with the Sanchez-Lacombe equation of state [1976, 1978] is applied in the current study for the prediction of viscosity of PS-SCG mixtures.

1.3 Significance of Research

The flow behavior of polymers is strongly dependent on how the temperature of interest departs from the T_g of polymer. The fractional free volume increases linearly with the temperature departure from T_g. The dissolved diluent contributes to the increase of fractional free volume of mixture and the solubility is dependent on the departure of temperature from the T_c of diluent. Therefore, for polymer-SCG mixtures, the inter-relationship of the operating temperature of interest (T), the T_c of SCG, and the T_g of polymer, determines the principal trend of solubility and viscosity reduction.

Garg, et al. [1994] confirmed that the highest solubility is obtained when the critical temperature and pressure of the SCG are closely matched to the processing conditions of the polymer. The critical properties of selected supercritical gases are shown in Table 1.1.

Table 1.1
Critical Constants of selected Supercritical Gases

	Carbon Dioxide	1,1-Difluoroethane (R152a)	1,1,1,2-Tetrafluoroethane (R134a)
Molecular Weight M_w	44.01	66.05	102.03
Critical Temperature T_c (°C)	31.04	113.5	101.1
Critical Pressure P_c (MPa)	7.38	4.49	4.06
Critical Density ρ_c (g/cm^3)	0.468	0.365	0.515

Garg et al. [1994] investigated that the solubility of carbon dioxide to PDMS reaches up to 21 weight percent at 50 ^{0}C which is above and closed to the T_c of CO_2.

Practical processing conditions of PS (e.g., $T > 150\ ^0C$ and $P > 100$ atm) are within the supercritical regime of above SCG's. In the current study, a back-pressure greater than the equilibrium pressure of each PS-SCG solution is exerted on the measurement system allowing the single phase of PS-SCG solutions at supercritical states during measurement. Since carbon dioxide has much lower T_c than R152a or R134a, its solubility to PS is expected relatively lower at processing conditions and it is well known that PS is CO_2-phobic. The PS-CO_2 system is invaluable for the investigation of the effect of dissolved SCG in less favorable combinations of polymer and SCG. The PS-R152a and PS-R134a systems provide practical interests because they are used in plastic foam production in place of CFC's and the processing temperatures are relatively closer to their T_c's enabling higher solubilities. The influence of T_c upon the viscosity reduction of PS will be elucidated in the current study.

The viscosity reduction, the ratio of reduced viscosity to the reference viscosity of pure polymer, is influenced by the relative change of fractional free volume caused by the diluent rather than the absolute value of fractional free volume of mixture. In the previous research performed by Gerhardt [1994], for PDMS-CO_2 solutions, viscosity measurements were made at 50 and 80 $^{\circ}$C, 173 and 203 degrees above the T_g of PDMS (-123.0 $^{\circ}$C) respectively whereas, in the current study the viscosity of PS-SCG solution is measured at 150 and 175 $^{\circ}$C, about 50 to 75 $^{\circ}$C above the T_g of PS. The PDMS at the measurement conditions exists as a viscous liquid at an expanded state, having a substantial fractional free volume and little chain entanglement while the PS at given conditions has very high viscosity with considerable chain entanglement and little fractional free volume. In contrast to the PDMS-CO_2 case, the dissolved SCG into PS is

expected to exhibit the effect of added free volume more significantly.

In this study, based on the solubility data for a given polymer-SCG system, the viscosity reductions are measured experimentally and predicted theoretically by the free-volume rheological model. The influences of pressure, temperature, and composition are thoroughly investigated and correlated. Finally, a database providing possible viscosity reductions is constructed for each PS-SCG system. In addition, the optimum operating conditions for the viscosity reduction are explored.

CHAPTER 2

RHEOLOGICAL PROPERTIES OF MOLTEN POLYMERS AND CONCENTRATED POLYMER SOLUTIONS: AN OVERVIEW

In general, the rheological behaviors of concentrated polymer solutions resemble that of molten polymers. One of principal properties representing the rheological behavior of molten polymers or concentrated polymer solutions is the shear viscosity. For low molecular weight liquids the viscosity is only a function of temperature and pressure and not dependent on the deformation rate and time. In addition, the two normal stress differences are zero and the uni-axial extensional viscosity becomes three times the shear viscosity. Such liquids are entitled "Newtonian" fluids. Fluids showing deviations from any Newtonian behavior are termed as non-Newtonian fluids.

Among non-Newtonian features, the non-zero normal stress differences and time-dependent and high extensional viscosity are attributed to the elasticity of materials. When such an elastic property is observed during flow, the fluid is classified as a "viscoelastic" fluid which specifies that both of viscous and elastic characteristics coexist. Although such a classification needs to be accounted with the time scale of experiment with respect to the characteristic time of material that extremely influences the response of material, the categorizing will be retained in this chapter. Molten polymers and polymer solutions are grouped as typical viscoelastic fluids. One of observable viscoelastic behavior of them is the Weissenberg effect (rod-climbing phenomena) and the die swelling which are ascribed to the non-zero normal stress difference. The open-siphon effect demonstrates the substantial extensional viscosity exposed by certain polymer solutions.

Molten polymers and concentrated polymer solutions have shear rate dependent viscosities, especially shear-thinning viscosities. In the current study, the shear viscosity of molten polymer is emphasized as a main controlling rheological property. Viscoelastic properties influencing the capillary rheometry will be discussed in Chapter 6.

2.1 Shear-thinning non-Newtonian Viscosity

The shear viscosity η is defined as the ratio of stress component in the direction of shear deformation to the velocity gradient perpendicular to the direction of shear deformation, or the shear rate:

$$\eta = \frac{\tau}{dv/dx} = \frac{\tau}{\dot{\gamma}} \tag{2.1}$$

where τ is the shear stress and $\dot{\gamma}$ is the shear rate.

Molten polymers and concentrated polymer solutions are categorized as shear-thinning fluids: the viscosity is Newtonian at very low and high rates of shear but strongly dependent upon the shear rate at the intermediate range of shear rates. The transition from the Newtonian viscosity at low shear rate region to the shear rate dependent viscosity, non-Newtonian viscosity, is sharp for mono-dispersed molten polymers and broad for poly-dispersed molten polymers. The Newtonian viscosity at very low rates of shear is called zero shear viscosity, η_0. Generally the zero shear viscosity is not directly measured, but determined by extrapolation of viscosity data as a function of shear rate:

$$\eta_0 = \lim_{\dot{\gamma}\to 0} \eta(\dot{\gamma}) \tag{2.2}$$

The zero shear viscosity simply represents the molecular characteristics and is widely

used for the comparative rheological study of materials.

The rheological properties are determined experimentally by using a rheometer for specified range of deformation rates and stresses. The experimental results are analyzed by means of the constitutive equation that governs the relationship between the applied stress and the deformation or rate of deformation with essential parameters including rheological properties. The parameters are computed through fluid dynamic calculations.

Various constitutive equations have been developed for the prediction of the shear-thinning viscosity behavior [Darby, 1976; Barnes et al., 1989; Whorlow, 1992]. A general equation with four parameters was given by Cross [1965]:

$$\frac{\eta-\eta_\infty}{\eta_0-\eta_\infty}=\frac{1}{\left(1+(K\dot{\gamma})^m\right)} \tag{2.3}$$

where η_0 and η_∞ are the asymptotic values of Newtonian viscosity at very low and very high shear rates respectively, K is a time constant and m is a dimensionless constant. The simplified Cross model is obtained when the upper asymptotic Newtonian viscosity is excluded:

$$\frac{\eta}{\eta_0}=\frac{1}{\left(1+(K\dot{\gamma})^m\right)} \tag{2.4}$$

The Carreau [1972] model is an alternative to the Cross model:

$$\frac{\eta-\eta_\infty}{\eta_0-\eta_\infty}=\left[1+(\lambda\dot{\gamma})^2\right]^{(n-1)/2} \tag{2.5}$$

where λ is a time constant having the same meaning as K in the Cross model and n is a dimensionless constant.

For $\eta >> \eta_\infty$, the Cross model reduces to the well known power-law model.

$$\eta = K'(\dot{\gamma})^{n-1} \tag{2.6}$$

where n is the power-law index ranging from 0.2 to 0.8 for most molten polymers and K' is the consistency index, which is directly proportional to the zero shear rate viscosity. The slope of viscosity curve as a function of shear rate in a log-log scale is *(n-1)*. Although the lower and upper asymptotic Newtonian viscosities can not be described, the power-law model is one of the most widely used empirical models in molten polymers and concentrated polymer solutions.

When the Newtonian viscosity at very high shear rates is concerned, the Sisko (1958) model is an appropriate selection. For $\eta << \eta_0$, the Cross model is modified to

$$\eta = \eta_\infty + K''\dot{\gamma}^{n-1} \tag{2.7}$$

where K'' is similar to the consistency in the power-law model. The Sisko model retains the Newtonian viscosity at very high shear rates.

2.2 Effect of Molecular Weight and Concentration

The viscosity of a molten polymer or a concentrated polymer solution increases with increasing molecular weight. For molecular weights higher than a critical value, M_c, the zero shear viscosity of molten polymer is represented as: [Fox and Flory, 1948]

$$\log \eta_0 = a\,(\log M_w) + A, \qquad M_w > M_c \tag{2.8}$$

where a is a system dependent parameter and A is an empirical constant dependent on the nature of polymer and system temperature. The value of a is often accepted as 3.4 for linear polymer melts [Ferry, 1980; Bird et al., 1987]. For molecular weights lower than

M_c, the parameter a varies from 0.5 to 1.0. It is thought that the formation of chain entanglements results in the transition of the molecular weight dependence of zero shear viscosity. Bueche [1952, 1956] also derived Equation (2.8) with a large number of assumptions and proposed that the existence of M_c is associated with the beginning of the formation of an entanglement node in the polymer. Consequently the chain entanglements does not influence the flow behavior of polymers if M_w is less than M_c. The values of M_c may vary from 2,000 to 60,000, depending on the structure of polymer. For polystyrene, the critical molecular weight was reported as 31,200 [Graessley, 1974] and 33,000 [Stratton, 1966].

Concentrated polymer solutions show the same phenomena of the M_c as in the case of polymer melts, but M_c increases with decreasing polymer composition and vice versa. A critical concentration, c_c can be computed when *log n* is plotted with *log c* for a constant M_w. Onogi et al. [1966] reported that for a variety of polymer solutions the critical concentration follows

$$c_c^{\,p} \cdot M_c = constant \tag{2.9}$$

where $p \approx 1.5$.

The viscosity of a concentrated polymer solution is given by a power-law expression [Johnson et al., 1952; Onogi et al., 1966]

$$\eta = K\ c^{\alpha} M_w^{\beta} \tag{2.10}$$

It is adopted approximately that $\alpha = 5.4$ and $\beta = 3.4$.

2.3 Effect of Temperature

The effect of temperature on the viscosity of polymer melt and polymer solution

is quite complex and no relationship has been found to be valid for the entire range of temperatures for a given polymer [Rodriguez, 1982].

Andrade [1930] formulated a simple relationship based on Arrhenius type equation for temperatures far enough above the melting point of the polymer (T_m)

$$\eta_0 = B \exp\left(\frac{E_\eta}{RT}\right) \tag{2.11}$$

where B is a constant and E_η is the activation energy.

According to Eyring theory [Glasstone et al., 1941], a liquid contains unoccupied sites or holes, which move at random throughout the liquid as they are filled and created by molecules jumping from one site to another. Each jump needs to overcome an energy barrier of magnitude E_η. The activation energy is related to the heat of vaporization for low molecular weight liquids, but, in polymers, E_η levels off at a value independent of molecular weight. The viscous flow of polymers happens by successive jumps of segments until the whole chain has shifted because the unit of flow or jumping segment is much smaller than the complete molecule.

Magill and Greet [1969] asserted that the Arrhenius type relationship, Equation (2.11) does not hold in the vicinity of the melting point, even for low molecular weight polymers. For temperature ranges between T_g and slightly above T_m, Equation (2.11) cannot be applied.

As the temperature increases, E_η is found to decrease due to the created extra fractional free volume by thermal expansion. For polymer solutions, E_η depends upon the concentration too. Among several attempts to formulate this temperature dependence of activation energy, Doolittle [1951] suggested the equation

$$\eta = A \exp(B/f) \tag{2.12}$$

where A and B are constants and f is the fractional free volume.

Equation (2.12) is the first formulation of free volume theory and becomes the basis of future modified free volume theories which will be stated in Section 4.4.

A linear dependence of fractional free volume on temperature may be assumed:

$$f = f_g + \alpha_f (T - T_g) \tag{2.13}$$

The parameter f represents the fractional free volume and f_g is the fractional free volume at T_g of polymer. The α_f is the thermal expansion coefficients of free volume. The substitution of Equation (2.13) into Equation (2.12) yields the WLF equation which was proposed by Williams, Landel and Ferry [1955].

$$\ln \frac{\eta(T)}{\eta(T_g)} = -\frac{B}{f_g}\left(\frac{T - T_g}{f_g/\alpha_f + T - T_g}\right) \tag{2.14}$$

The WLF equation shows a fair degree of accuracy for numerous polymers in the temperature range $T_g < T < (T_g + 100\,^{o}C)$ and can be generalized as

$$\ln \frac{\eta(T)}{\eta(T_s)} = -\frac{C_1(T - T_s)}{C_2 + (T - T_s)} \tag{2.15}$$

where T_s is a standard temperature.

When the standard temperature is chosen as T_g, the values of C_1 and C_2 are 17.44 and 51.6 respectively. If the standard temperatures are arbitrarily chosen in order to obtain the best universal function, the values of C_1 and C_2 are 8.86 and 101.6, respectively. For most of polymers, the T_s is about 43 °C higher than T_g. [van Krevelen, 1990].

More recently Lomellini [1992] measured the dynamic melt viscosity of PS up to 290 °C (about T_g + 185 °C) and the viscosity data according to the WLF equation and

Arrhenius type relationship. The WLF equation was found to fit the experimental data accurately, but there was no evidence of Arrhenius-like behavior at those high temperature ranges.

2.4 Effect of Diluent

Kelly and Bueche [1961] suggested a method, which can be applied for the prediction of polymer solution viscosity under the assumption of a linear mixing rule of free volumes of solvent and polymer, where the molecular weight of polymer is greater than the critical molecular weight, M_c:

$$\eta = Bc_p^4 \exp\left(\frac{1}{f}\right), \qquad M_w > M_c \tag{2.16}$$

$$f = \phi_p f_p + \phi_s f_s \tag{2.17}$$

$$f_p = f_g + \alpha_f (T - T_g) \tag{2.18}$$

$$f_s = f_g + \alpha_s (T - T'_g) \tag{2.19}$$

In Equation (2.16), B is an empirical constant which incorporates the effect of molecular weight of polymer, c_p is the concentration of polymer, and f represents the fractional free volume of polymer solution, which is expressed as the linear mixing rule in Equation (2.17). The parameters f_p and ϕ_p are the fractional free volume and the volume fraction of the pure polymer and f_S and ϕ_S are those of the solvent, respectively. In Equations (2.18) and (2.19), f_g represents the fractional free volume of the system at T_g and α_S and T'_g are the thermal expansion coefficient and the T_g of the solvent. Although the concentration dependence of viscosity is governed by fourth power in Kelly-Bueche theory, a range of the power values can be found in literature and summarized by Gerhardt [1994]. Modified versions of Kelly-Bueche theory will be introduced in Section

4.4.

The viscosity reduction of polymer is caused by the depression of glass transition temperature of polymer when a low molecular weight solvent is dissolved into the polymer. The viscosity reduction depends upon the concentration of the solvent. Only a few theoretical predictions are available for the glass transition temperature depression of polymer brought by the addition of diluent The theoretical approach developed by Bueche [1962] gives and equation for the glass transition temperature of plasticized polymer:

$$T_g = \frac{T_g^P + (K_\alpha T_g^S - T_g^P)\phi_S}{1 + (K_\alpha - 1)\phi_S} \tag{2.20}$$

where K_α is a constant and $\approx (\alpha^S - \alpha_g^S) / (\alpha^P - \alpha_g^P)$, ϕ_S is the volume fraction of solvent, α and α_g are the volume expansion coefficients at temperatures above and below T_g respectively, and the superscripts S and P represent the solvent (plasticizer) and polymer respectively. The constant K_α normally has values between 1 and 3.

Chow [1980] developed an explicit equation giving the depression of T_g of polymer-diluent systems based on the Gibbs-Dimarzio theory [1958] and the classical lattice model. The equation has been proven experimentally various polymer-diluent mixture systems [Chiou et al., 1985; Wissinger and Paulaitis, 1987]:

$$\ln\left(\frac{T_g}{T_{g0}}\right) = \beta\{(1-\theta)\ln(1-\theta) + \theta(1-\theta)\} \tag{2.21}$$

$$\beta = zR / M_p \Delta C_{pp} \tag{2.22}$$

$$\theta = (M_p / zM_d)(w/(1-w) \tag{2.23}$$

where T_g and T_{g0} are the glass transition temperature of mixture and pure polymer, R is the gas constant, ΔC_{pp} is the excess transition isobaric specific heat of the polymer defined as $\Delta C_p = m_p \Delta C_{pp}$, where m_p is the mass of polymer and ΔC_p is the isobaric specific heat of polymer, z is the lattice coordination number, M_p and M_d are the molecular weights of polymer and diluent respectively, and w is the weight fraction of diluent.

2.5 Effect of Pressure

The effect of pressure on the viscosity of a polymer melt or a polymer solution should not be overlooked in polymer processing. Usually the processing is executed under very high pressures compared with the conditions of the usual viscosity measurements. The viscosity data obtained at relatively low pressures might be erroneous when applied to the analysis of actual processing data.

For the polymer solutions, especially polymer-SCG mixtures, an equilibrium pressure should be kept to conserve the mixed phase at a certain composition and temperature. Higher SCG compositions and higher processing temperatures need increased pressurization.

From the definition of free volume, the pressure increase is expected to decrease the free volume. This effect leads to the depression of T_g and consequently the increase of viscosity. Cogswell [1981] represented a practical procedure to evaluate the effect pressure. From the published experimental data on the pressure dependent viscosity, the influence of pressure on viscosity is qualitatively similar bur opposite in sign to that of temperature. Thus for an increase in pressure, the equivalent decrease of temperature can be assumed. An isoentropic thermodynamic function has a similar appearance which is

the instantaneous temperature rise resulting from the application of pressure. The advantage of this approach is that the thermodynamic function may be utilized as a guide if no pressure dependent viscosity data is available. The values of this function for a group of polymers are available [Cogswell, 1981].

Similar approach is described by van Krevelen [1990]. The pressure coefficient of viscosity, χ is defined as:

$$\chi = \frac{1}{\eta}\left(\frac{\partial \eta}{\partial P}\right)_T \tag{2.24}$$

Since experimental data of χ are quite limited, the theoretical prediction is possible using the following thermodynamic derivation.

$$\lambda = \frac{1}{\eta}\left(\frac{\partial \eta}{\partial T}\right)_P \tag{2.25}$$

The pressure coefficient of viscosity can be approximately estimated from the compressibility and thermal expansion coefficient data using the relationship, $\chi/\lambda \approx -\kappa/\alpha$, where κ is the compressibility and α is the thermal expansion coefficient.

Miller [1971] and Penwell et al. [1971] used the identical definition of pressure coefficient as:

$$b = \left(\frac{\partial \ln \eta}{\partial P}\right)_T \tag{2.26}$$

A practical equation was developed by both authors from this definition for the evaluation of pressure coefficient:

$$b = \left(\frac{\partial \ln \eta}{\partial P}\right)_T \cong \frac{2.303 B \ dT_g}{(T - T_0)^2 \ dP} \tag{2.27}$$

where B is a constant and T_0 is a reference temperature.

The derivations of pressure coefficient by Miller [1971] and Penwell et al. [1971]

are given and discussed in Section 4.1.2. Penwell et al. [1971] and Yamada and Porter [1974] considered the influence of pressure in the measurement of viscosity using capillary rheometers which will be discussed in Chapter 6.

2.6 Correlation of Rheological Data

Over a wide range of temperatures, the viscosity versus shear rate curves of polymer systems have similar shapes. Also the zero shear viscosity varies with temperature and shows a similarity. The departure of zero shear viscosity from the value at a reference temperature T_0 is termed the shift factor, a_T. For concentrated polymer solutions and polymer melts, a_T is given by Vinogradov and Malkin [1980]:

$$a_T = \frac{\eta_0(T)\rho_0 T_0}{\eta_0(T_0)\rho_0 T_0} \tag{2.28}$$

where ρ is the density at temperature T, and ρ_0, the density at T_0.

If the term $\rho_0 T_0/\rho T$ is neglected as compared with the variation of viscosity, then

$$a_T = \frac{\eta_0(T)}{\eta_0(T_0)} \tag{2.29}$$

Introducing Equation (2.29) to the WLF equation, Equation (2.15) and taking T_g as a reference temperature provides

$$\ln a_T = \ln \frac{\eta_0(T)}{\eta_0(T_g)} = -\frac{C_1(T - T_g)}{C_2 + (T - T_g)} \tag{2.30}$$

The viscosity data are generalized by means of constructing master curves. From the plot of viscosity versus shear rate in log-log scale, the curve at T is shifted vertically by the amount of $log\ [\eta_0(T_0)/\eta_0(T)]$ to make two curves overlap. For the complete superposition of two curves, the vertically shifted curve is translated horizontally by a certain amount,

which is defined by log a_T. Consequently the viscosity versus shear rate curves in log scale can be shifted to make a single master curve.

The WLF equation, Equation (2.15) or (2.30) has been found to hold for a variety of polymers [Williams et al., 1955] The pure molten polystyrene is a typical polymer system that is precisely described by the WLF equation.

In Chapter 4, the concept of shift factor is generalized to any viscosity behavior of polymers or polymer solutions that depends upon a certain parameter, such as the pressure or concentration.

CHAPTER 3

LITERATURE REVIEW

For systematic investigation of polymer-SCG solutions, thermodynamic and rheological characterizations are essential. Most data for polymer solutions are obtained near ambient conditions of temperature and pressure [Bonner, 1975, 1977]. Only a few data [Garg, 1993] are available for the solutions of polymer melts and SCG's at the supercritical conditions.

3.1 Solubility of Supercritical Fluids in Polymers

The solubility of SCG's in polymers approaches a maximum near the critical condition of SCG, when the dissolved SCG exist at the most dense state [Daneshvar, 1989; Daneshvar et al., 1990]. The investigations of polymer-SCG systems at extremely high pressures are available in literature [Hunter and Richards, 1945; Kumar et al., 1987; Saraf and Kiran, 1988]. Measurements of solubilities of SCG's to polymers are summarized below.

Shah et al., [1986, 1993] investigated the solubility of carbon dioxide, methane, and propane in a variety of silicone polymers, which have different side chains and backbone structures, at temperatures of 10 to 55 ^{0}C and pressures up to 26 atm.

The interaction of polymers with near critical carbon dioxide was considered by Berens and Huvard [1989]. Gravimetric measurements were carried out at 25 ^{0}C using thin film polymer samples. The transport kinetics were found to be Fickian and the diffusivity increased with CO_2 concentration. For several glassy polymers, the sorption

isotherms were sigmoid in shape, combining dual -mode type at low activity and Flory-Huggins form at high activity.

An optical high-pressure cell, including sapphire windows, was employed for the examination of microscopic and macroscopic interactions between supercritical carbon dioxide and a polyurethane elastomer by Briscoe and Kelly [1993]. Fourier transform IR spectroscopy was used to investigate the effect of increasing ambient gas pressure on the molecular conformation of the polymer, and the corresponding gas-induced volume changes were quantified by a simple visual observations at CO_2 pressures up to 16 MPa. Zinc selenide windows were utilized for the spectroscopic study. A correlation was observed between the extent of swelling and spectroscopic shift data. The potential for high-pressure spectroscopy and visualization for the study of gas-polymer interactions were postulated.

Recently Shieh et al. [1996A, 1996B] presented the solubilities of carbon dioxide in a variety of crystalline and amorphous polymers at the temperature from 25 to 70 ^{0}C and for the pressure range of 1000 to 3000 psi. A visual cell unit and a high-pressure windowless reactor were used for the monitoring and treatment of polymer samples. The CO_2 solubility was evaluated by gravimetry. The interaction of carbon dioxide and a series of polymers were investigated and the effect of treatment was examined by thermal and mechanical characterizations. The amorphous polymer was found to absorb the CO_2 at a great extent compared with crystalline polymers. The polarity of the polymer was crucial in determining the solubility of polymer in CO_2.

Daneshvar [1989] developed a unique high-pressure apparatus based on the circulation of polymer-rich lower phase and the SCG phase from one section of the

equilibration cell to another. A lattice fluid model was used to describe the PVT behavior of the liquid polymer-SCG system [Daneshvar et al, 1990]. The model contains only one adjustable binary interaction parameter. The polyethylene glycol and CO_2 system was examined experimentally at temperatures up to 100 ^{0}C and pressures to 35 MPa and theoretically.

Kim [1992] measured the solubility of supercritical CO_2 in two coexisting phases in a series of different molecular weights PDMS (M_w=4,000 to 13,000) using the method developed by Daneshvar [1989]. The temperatures ranged from 40 to 50 ^{0}C and the pressures varied from 0 to 25 MPa. Theoretical modeling was performed using Sanchez and Lacomb [1976, 1977] and Panayiotou and Vera [1982] equations of state, in which both models incorporate a single adjustable binary interaction parameter. The modeling was successfully accomplished with detailed information regarding the extent of polymer fractionation into supercritical phase.

Garg [1993] measured the solubility of supercritical gas in the lower phase of polymer-SCG solutions. The solubility of 1,1-difluoroethane (R152a) in PS was measured at 135 and 165 ^{0}C and at pressures ranging from 1 to 17 MPa. These data are used in the current study. Also the solubility of CO_2 in PDMS (M_w =308,000) was obtained at temperatures of 50, 80 and 100 ^{0}C and pressures from 0.5 MPa to 26 MPa. When the system temperature is close to the T_c of CO_2, the solubility is more than 40 weight percent. As the temperature increases, the solubility decreases slightly. Those data were compared with the theoretical modeling results. Two lattice-based equations of state were used for the modeling with a single binary interaction parameter. The solubility data were employed for the determination of the binary interaction parameter for each model.

The Sanchez-Lacomb equation of state is applied later in this work for the theoretical prediction of viscosity reduction along with a free volume rheological model [Gerhardt et al., 1997].

Selected works on the measurement of the solubility in polymers are reviewed by Garg [1993]. Wissinger and Paulaitis [1987] presented experimental data on gas sorption and polymer swelling in poly(methyl methacrylate) (PMMA) and PS at temperatures from 33 to 65 ^{0}C and pressures up to 100 atm. The glass transition pressures were estimated from the swelling data of PS- CO_2 mixture and used to obtain the relationship between the T_g of PS and the CO_2 solubility. A monotonic decrease in T_g of PS was observed as CO_2 pressure increased from 1 to 60 atm. The relationship was in good agreement with a theoretical correlation for T_g of PS-liquid diluent mixtures.

Sato et al. [1996] measured the solubility of carbon dioxide and nitrogen into PS at elevated temperatures. They determined the amount of a gas dissolved in a polymer sample from the difference between the amount of gas initially contacted with the polymer and that remaining in the gas phase after equilibration using three sorption cells. Solubilities of carbon dioxide and nitrogen at 100, 140, and 180 ^{0}C and pressures up to 20 MPa were presented with the theoretical modeling based on the Sanchez-Lacomb equation of state. Binary interaction parameters were calculated for each solubility isotherm. In addition, Henry's constants were evaluated using the Sanchez-Lacomb equation of state and correlated with temperature showing relatively good agreement with those of Durill and Griskey [1966].

The summary of solubility data of carbon dioxide and common gases into polystyrene are shown in Table 3.1.

Table 3.1
Solubility Measurements of Supercritical Gases in Polystyrene

System	Temperature (^{0}C)	Pressure (MPa)	Reference
PS-CO_2	35	1 – 7	Wissinger and Paulaitis [1987]
	50	1 – 7	
	100	1 – 20	Sato et al. [1996]
	140	1 – 20	
	180	1 – 20	
PS-R152a	135	1 – 16	Garg et al. [1994]
	160	1 - 16	

3.2 Plasticization effect of SCG

Typical observations of previous studies on the effect of SCG's include the swelling [Fleming Koros, 1986; Sefcik, 1986; Hirose et al, 1986; Wissinger and Paulaitis, 1987] and the depression of T_g. Important contributions to the subject are summarized below.

Wang et al. [1982] evaluated the plasticization of PS by CO_2 through measuring the Young's modulus and creep compliance. Higher solubility of CO_2 is correlated with greater depressions of T_g. They reported that depression of T_g by as much as 65 ^{0}C could be caused by sorption of CO_2 at a pressure of 200 atm. In the plot of T_g of sorbed PS versus the CO_2 pressure, the T_g passes a minimum value and increases gradually as the pressure increases. The counteracting effect of pressure on free volume and on CO_2 sorption prevails after the minimum T_g pressure. The hydrostatic pressure effect was represented by the increase of T_g using the WLF equation and the pressure dependence of

T_g [Gee, 1966]. By separating the effect of hydrostatic pressure, the net effect of plasticization by CO_2 is elucidated showing rapid decrease of T_g followed by a gradual decline as the CO_2 pressure increases.

Differential scanning calorimetry was utilized to obtain the T_g of polymers containing dissolved gas by Chiou et al. [1985]. The effect of CO_2 at pressures up to 25 atm was investigated for PMMA and its blend with poly(vinylidene fluoride). Also, less extensive results were obtained for PS, polycarbonate (PC), PVC and poly(ethylene terephthalate) (PET). The depression of T_g up to 50 ^{0}C was observed. The theoretical equation of Chow [1980] for estimating the T_g depression was found to be reasonable agreement with the experimental results.

Smith and Moll [1990] employed the ^{2}H NMR spectroscopy with the quadruple echo pulse technique to probe the effect of CO_2 pressure on the molecular dynamics of polymers. The result showed that the mobility of the polymer is enhanced by dissolved CO_2 at relatively low pressures for PC, PS and polyester carbonate. Diffusion was found to be aided by the microscopic molecular dynamics. The presence of dissolved gas caused plasticization of polymer, giving rise to increased molecular mobility and enhanced gas diffusivity. Thus, the molecular mobility and the diffusivity are both a function of the plasticization of the polymer by the dissolved gas but are mutually independent.

Condo et al. [1992] presented a theoretical model to predict the T_g reduction of polymer in the presence of a diluent as a function of pressure. A lattice fluid theory was applied with the Gibbs-Di Marzio criterion, which is based on the hypothesis that an ideal glass transition temperature, T_2 exists at infinitely slow cooling and at T_2 the polymer essentially becomes frozen and has zero entropy [Gibbs and Di Marzio, 1958]. For the

limited data for the PS- CO_2 and PMMA- CO_2 systems, the predictions were in good agreement with experiment. A new phenomenon, which they called retrograde vitrification, was predicted where a liquid to glass transition occurs with increasing temperature. This was a consequence of the complex effects of temperature and pressure on sorption. In this vitrification region at a constant pressure, theoretically, the sorption increases markedly with a reduction in temperature, thus causing a glass to liquid transition. Therefore, if this phenomenon is confirmed experimentally, then polymers may be plasticized with compressed fluids under much milder conditions than expected presently.

Handa et al. [1993, 1994] employed a calorimetric method to obtain the T_g of polymers swollen with CO_2 and ethylene. For PS and ethylene system, the largest depression of T_g was 67 ^{0}C at 78 atm. The ethylene was found to have almost the same plasticization effect as CO_2. The change of T_g of poly(2,6-dimethyl phenylene oxide), (PPO), due to the pressurized CO_2 was measured and the highest depression was 31.6 ^{0}C. In addition, a quasi-lattice solid-solution model for polymer-diluent systems was in fair agreement with the experimental results. There was a considerable discrepancy of the value of T_g at 60 atm with the work of Hachisuka, et al. [1990] who also used the calorimetric method.

Goel and Beckman [1993] used a dielectric measurement for the investigation of the PMMA and CO_2 system. A mean-field lattice gas model was applied to describe the free energy of mixing with an additional term to account for the elastic free energy. The model equation predicted the swelling of mixtures by dissolved gases as a function of pressure and temperature. The degree of plasticization increased at pressures up to 1200

psi and leveled off at higher pressures. They stated that the counteracting effects of pressure on free volume and gas sorption were the possible reason.

3.3 Experimental Measurements of Pressure dependent Viscosity of Polymers

Since the viscosity measurement of polymer-SCG solution needs to be conducted above the vapor pressure of diluent, it is worthwhile to review the measurement of pressure dependent viscosity of polymers. The experimental investigations on the influence of pressure upon viscosity were done mostly in the sixties and seventies. A group of important works were performed using the equipment designed by Semjonow [1962], consisting of a pressurized concentric cylinder geometry where a Coutte type of flow is generated by rotation of the outer cylinder and the torque exerted on the inner cylinder is measured. Hellwege et al. [1967] and Herrmann and Knappe [1969] measured the viscosity of PS and PMMA under pressure and showed that a temperature and pressure invariant master curve can obtained from both polymers. Christmann and Knappe [1974] surveyed the viscosities of low-density polyethylene (LDPE) and PMMA using the same equipment. The zero shear viscosity of both polymers was correlated by an exponential relationship for the pressure effect and an Arrhenius type expression for temperature dependency. Later Christmann and Weber [1978] worked on high-density polyethylene (HDPE) using the same technique. The measurements of Cogswell and McGowan [1972] employed a similar apparatus allowing a limited shear rate range of 0.1 to 25 s-1. The above measurements were confined to the low shear rate range and relatively low pressure due to the restrictions of equipment capability.

Westover [1961] developed a double piston rheometer for the measurement of

viscosity under elevated pressure. A capillary die is pressurized from both sides by two pistons acting in two cylinders on each side. The pressure on each side is derived by the force applied on each piston and can reach up to 25,000 psi. The pressure difference between ends of the die and the average hydrostatic pressure in the die can be varied. The viscosity of PS is increased by a factor of 100 when the hydrostatic pressure is increased from 2,000 to 25,000 psi. The obtained pressure difference, however, may be subject to errors due to friction of the pistons.

Karl [1979] also used the same rheometer and reported a substantial decrease of the pressure coefficient with increasing pressure for LDPE. Lord [1979] used a similar system to measure the viscosity of PC.

More than a decade later, Kadijk et al. [1994] developed a slit viscometer consisting of a slit die which is pressurized from both sides by two servo-hydraulic pistons capable of generating pressures up to 1,800 bar. Several polymers were investigated for the shear rate range of 0.01 to 3,000 s-1 at pressures 200, 500, and 1,000 bar. Shear thinning viscosity data were fitted using the Cross-Carreau model and the zero shear viscosity was evaluated by a modified Arrhenius-WLF equation. When the pressure increases from 200 bar to 500 and 1,000 bar, the zero shear viscosity increases by a factor of 3.2 and 18.6 at 202 ^{0}C for PS. If the pressure is raised from 200 to 500 bar at 162 ^{0}C for PS, the viscosity increased by a factor of 5.8.

3.4 Rheological Characterization of Polymer-SCG Solutions

Majority of earlier investigations dealt with the solution viscosities of polymers and organic solvents at concentrations less that fifty percent of solvent [Spencer and

Williams, 1947; Bueche, 1953, 1955; Nishimura, 1965; Fujita and Maekawa, 1962; Grasessley, 1965, 1967, 1974; Graessley and Segal, 1970; Ide and White, 1974; Blockmeir and Westphal, 1974; Riande et al., 1975]. These solvents are much less volatile than the supercritical gases of interest here. The shear rate ranges were limited to the Newtonian regime, thereby excluding the shear dependent region which is important in actual processing.

Few rheological data of thermoplastic polymers swollen with solvents, however, are available at the condition of supercritical state of the solvent. The high volatility of SCG at elevated temperature makes such measurements difficult. Bae [1996] measured the viscosity of poly(ethylene) glycol - CO_2 solutions indirectly from diffusivity data measured by photon correlation spectroscopy at the pressures up to 8 MPa and temperatures ranging 30 to 60 ^{0}C. Later Bae and Gulari [1997] worked on the viscosity measurement of PDMS- CO_2 solutions at ambient temperature and relatively low pressure condition (1 - 3 MPa) using a falling ball viscometer. The modified Kelly-Bueche free volume theory was useful to interpret the viscosity change due to the dissolved CO_2.

The plastic foam processing is a typical application of polymer-SCG mixtures using appropriate blowing agents. The blowing agent used in the foam processing have two types, i.e., the chemical blowing agent and the physical blowing agent. Both methods include the direct contact between the rubbery or liquid phase of polymer and gaseous components.

The chemical blowing agent decomposes at a certain elevated temperature producing a mixture of gases. The chemical blowing agent is dispersed in the polymer

pellets or powder and supplied through the feeding funnel. The gases produced by the decomposition of blowing agent are blended with fused polymer, making a polymer-gas solution at elevated temperature and pressure. The physical blowing agent is usually supplied between the end of extruder or injection molding machine, where a vigorous blending with molten polymer occurs through a supplementary mixing equipment preceding the shaping unit. Frequently the mixture is bypassed to an in-line rheometer for rheological characterization.

Blyer and Kwei [1979] measured the viscosity of the LDPE foam and HDPE foam using a capillary extrusion rheometer. A chemical blowing agent, azodicarbonamide was blended with the polymer and the mixture was premolded at the temperature less than the decomposition temperature of blowing agent, making disks fitted into the rheometer barrel. The added blowing agent of 5 percent by weight to both LDPE and HDPE gave the viscosity reduction of approximately 20 percent at constant shear rate. The Doolittle free volume equation was used to account for the viscosity reduction.

PS foam and LDPE foam were investigated by Oyanagi and White [1979], extruding the polymer blended with the azodicarbonamide through a capillary rheometer. Also the flow visualization of injection molding was performed using a mold with glass windows attached to the rheometer. The viscosity was evaluated for each plastic foam at three different blowing agent compositions, i.e., 0.5, 1.0, and 1.5 percent, at temperatures of 170, 190 and 210 ^{0}C. The viscosity of polymer melts with blowing agent was less than that without blowing agent, especially at high temperatures. The bubble size and void fraction increased with temperature, decreasing extrusion rate, and decreasing die aspect ratio.

Fridman et al. [1989] appraised the viscosity of LDPE foam, which was prepared using the azodicarbonamide blowing agent. From the measurement, they found that the critical pressure, beyond which the polymer-gas mixture constitutes one phase, as a function of shear rate. They also explained the flow properties of the mixture in terms of free volume and the distribution of free holes in the melt. One of the conclusions is that the dissolved gas behaves as a free gas in the gas-containing thermoplastic melts according to statistical thermodynamics.

Shuler et al. [1994] evaluated the viscosity of polymer solutions of three phase fiber suspensions, the mixture of polyamide 6.6 filled with long glass fibers foamed with the azodicarbonamide blowing agent. A plunger-type capillary rheometer was used for the study without any modification for high pressure sealing of dissolved gases. The rheometer was equipped with two capillary dies in parallel; one of them is zero-length die with the same diameter with the normal die. The experimental data taken from the zero-length die was used for the Bagley correction and also the computation of extensional viscosity which will be discussed in Chapter 6 in detail. The reduction of both shear and extensional viscosities were observed and found to be independent of deformation rate.

When the azodicarbonamide blowing agent decomposes, a mixture of gases, such as nitrogen, carbon monoxide, small amount of carbon dioxide and ammonia, are produced. Therefore, the mixture needs to be considered as a multi-component system raising complexity of thermodynamic approach.

Han and Ma [1983A, 1983B] measured the wall normal stress along the longitudinal axis of a capillary die using an equipment consisting of a plasticating extruder, a gas supplying unit, static mixers, and a capillary rheometer [Han, 1974]. The blowing agents mixed with different grades of LDPE, HDPE and PS were

dichlorodifluoromethane (Refrigerent FC-12), dichlorotetrafluoroethane (Refrigerent FC-114), a blend of 50 weight percent of FC-12 and FC-114, trichlorofluoromethane (FC-11), a blend of 50 weight percent of FC-11 and FC-12. The viscosity of the mixture of each combination was measured over the overall concentration range from 5 to 20 percent and temperatures ranging from 110 to 170 ^{0}C. They claimed that the defined viscosity reduction factor, which is given as the ratio of the viscosity of mixture to that of pure polymer, depends only on the type of blowing agent, not on the shear rate or temperature for the measurement conditions. The measurement covers the shear thinning range of shear rates. The viscosity reduction factor is obtained from viscosity versus shear rate plots, by a single shift of viscosity curves along viscosity axis.

Although above viscosity measurements of polymer solution with blowing agents were conducted at elevated temperature over practically wide range of shear rates, the extrudates were forced out to atmospheric pressure. As reaching the die exit, the extrudate experiences a foaming or degassing, which greatly deteriorates the stability of pressure or stress measurement. Therefore considering the thermodynamic equilibrium of polymer solution at elevated temperatures, the viscosity measurement should be done under stable back-pressure control to keep the equilibrium and single phase of polymer solution.

Mendelson [1979, 1980] made a modification to a plunger type viscometer for the measurement of the viscosity of concentrated polymer solution at elevated temperatures and pressures. A pressurized reservoir at the exit of a capillary prevented the degassing of dissolved solvent, while a relatively tight-fitting Teflon ball inserted between the sample and the plunger tip was used to block the back flow of the sample and the degassing of solvent in the barrel. The viscosity of solutions PS in ethyl benzene were measured at the

concentration range of 50 to 90 weight percent of polymer and temperatures ranging from 100 to 225 ^{0}C [Mendelson, 1979]. He utilized the modified rheometer later for the same polymer solution [Mendelson, 1980], presenting the temperature dependence of viscosity described by an Arrhenius type relationship over the concentration range from 40 to 100 percent of polymer for temperatures well above T_g. Also the Newtonian limiting viscosity, i.e., zero shear viscosity, was evaluated for the polymer solution at both isothermal and iso-free volume conditions.

A similar modified plunger-type rheometer was employed by Foster and Lindt [1987] for the investigation of PS-ethylbenzene solution viscosity over the concentration range from 60 to 100 percent of PS and temperatures ranging from 132 to 240 ^{0}C. A strain gauge was inserted into the barrel wall before the inlet of capillary assembly to directly measure pressures, which alleviate the need for corrections to the shear stress low levels due to barrel friction. For the prevention of upstream degassing, a fluorocarbon rubber O-ring was employed. The viscosity data were correlated using an empirical viscosity model and the temperature dependence was represented by an Arrhenius type equation. The experimental relaxation times, such as Rouse time and Bueche relaxation time were computed and the Williams theory [1967] for the concentration dependence of the relaxation time was found to be applicable.

Gerhardt [1994] accomplished a pioneering rheological investigation of polymers swollen with supercritical CO_2. The viscosity measurement of PDMS swollen with supercritical CO_2 was conducted over the concentration ranges up to 20 percent of CO_2, wide range of shear rates and at temperatures of 50 and 80 ^{0}C. Since its T_g is around -123 ^{0}C, the behavior of PDMS at 50 and 80 ^{0}C depicts that of typical thermoplastic melts far above T_g. A capillary rheometer was modified for sealed operation under elevated

pressure. A back-pressure assembly equipped with a pressure transducer is attached at the end of capillary die to seal the capillary and prevent the degassing of dissolved gas. A back-pressure regulator assembly, which is linked to an air cylinder, is used to apply the force to create the back-pressure. The load reading at the rheometer plunger and the back-pressure reading from a pressure transducer at the capillary outlet determine the pressure differential exerted on the capillary die, implementing the viscosity evaluation. Gerhardt [1994] observed almost an order of magnitude reduction in viscosity for a 21 weight percent CO_2 system at 50 ^{0}C; a considerably larger reduction compared with that brought by the iso-free volume solvent, low molecular weight PDMS. The concentration-dependent shift factor was evaluated by constructing master curves in the logarithmic plot of viscosity versus shear rate. The free volume rheological model based on two lattice-based equations of state, Sanchez-Lacomb and Panayiotou and Vera, exhibit a close match with the experimental result. The Table 3.2 represents the survey of existing literature on the viscosity measurement of polymer-diluent mixtures at elevated temperatures and pressures over a wide range of shear rates.

Table 3.2
Viscosity Measurements of Polymer-Diluent Mixtures at elevated Pressures and wide Ranges of Shear Rates

Polymer(s)	Diluent	Apparatus	Temp.(^{0}C)	Back-Pressure Control	References
LDPE & HDPE	Azocarbonamide	Constant Pressure Capillary Rheometer	200	Atmospheric	Blyer & Kwei [1979]
LDPE, PS & HDPE	Azocarbonamide	Capillary Rheometer	170, 190 & 210	Atmospheric	Oyanagi & White [1979]
LDPE, HDPE & PS	Refrigerants F-11, FC-12 & FC-114	Screw Extruder & Capillary Rheometer	110 - 170	Atmospheric	Han & Ma [1983A, 1983B]
LDPE	Azocarbonamide	Capillary Rheometer	190	Atmospheric	Fridman et al. [1989]
Mixtures of Polyamide 6,6 with glass fiber	Azocarbonamide	Capillary Rheometer	275	Atmospheric	Shuler et al. [1994]
PS	Ethylbenzene	Pressurized Capillary Rheometer	60 - 225	Constant Gas Pressure higher than Equilibrium Pressure	Mendelson [1979, 1980]
PS	Ethylbenzene	Pressurized Capillary Rheometer	132 - 240	Constant Gas Pressure higher than Equilibrium Pressure	Foster & Lindt [1987]
PDMS	CO_2	Pressurized Capillary Rheometer	50 & 80	Constant Gas Pressure higher than Equilibrium Pressure	Gerhardt [1994]

CHAPTER 4

THEORIES AND APPLICATIONS

4.1 Extensive Application of Shift Factor

The temperature shift factor a_T, which was introduced in Section 2.5, can be extensively utilized for the computation of any viscosity change due to variations of temperature, pressure, and concentration if the viscosity curves have similar shapes at different conditions.

$$a_T = \frac{\eta_0(T)}{\eta_0(T_0)} \tag{2.29}$$

The pressure shift factor, a_P and concentration factor, a_C are defined as

$$a_P = \frac{\eta_0(T,P,c)}{\eta_0(T,P_0,c)} \tag{4.1}$$

$$a_C = \frac{\eta_0(T,P,c)}{\eta_0(T,P,c_0)} \tag{4.2}$$

where P_0 and c_0 represent reference pressure and concentration respectively.

The viscosity change of a polymer system at a given condition can be described as the deviation of viscosity using a single or multiple shift factors from a reference state. In general any changes of viscosity due to variations of temperature, pressure or concentration are calculated using a combined shift factor, $a_{T,\,Overall}$

$$a_{T,Overall} = a_T\, a_P\, a_c \tag{4.3}$$

Such a generalization of shift factors is specifically discussed in Vinogradov and Malkin [1980]. The contributions of individual and combined shift factors are depicted in Figure 4.1.

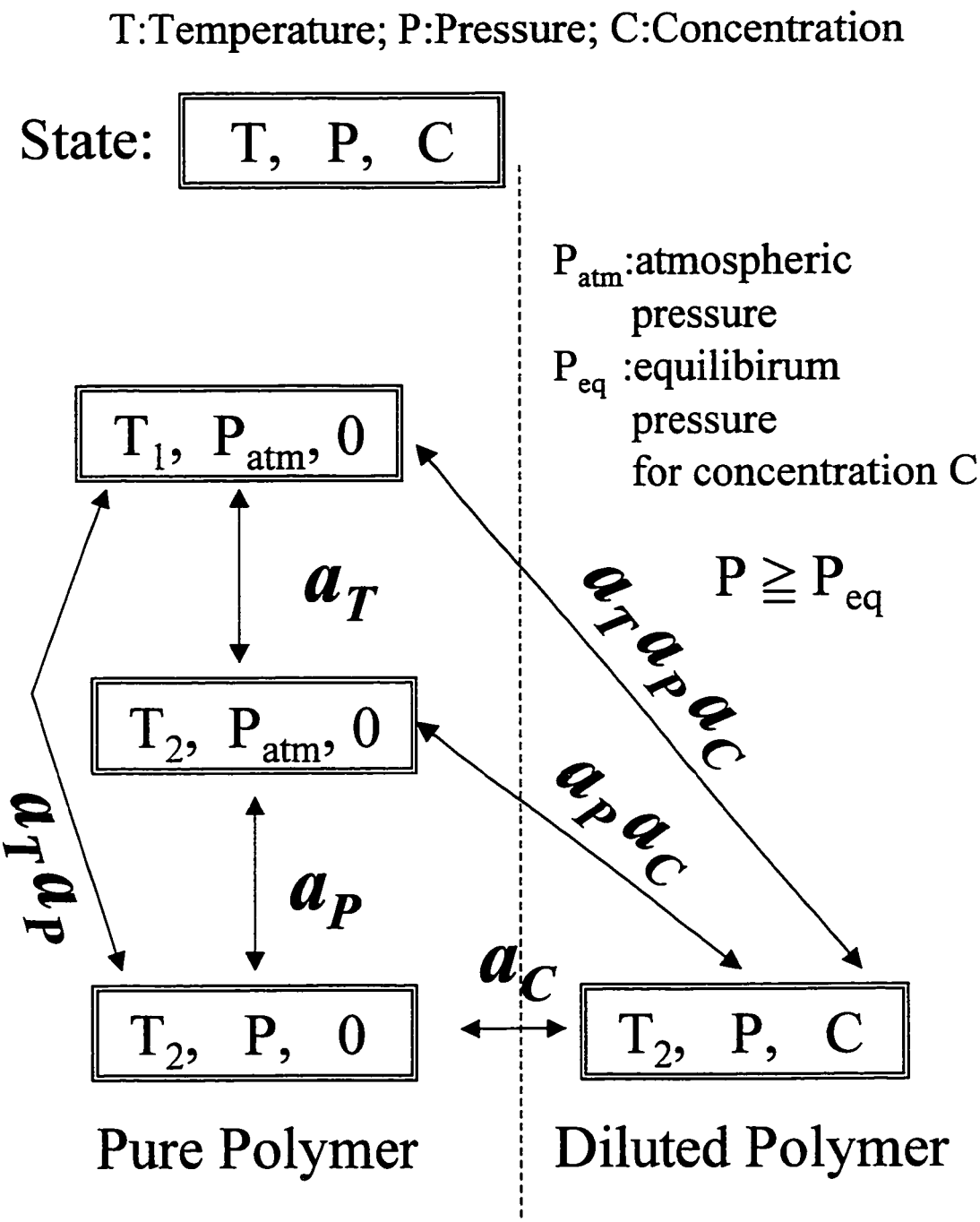

Figure 4.1
Contribution of Individual and Combined Shift Factors.

4.2 Evaluation of Shift Factors from Viscosity Curves

The evaluation of shift factor is practical from the experimental viscosity data of polymer systems. The viscosity reduction by a dissolved gas at an elevated pressure is computed as the product of a_P and a_C at a constant temperature.

$$\frac{\eta_0(T,P_{eq},c)}{\eta_0(T,P_{atm},0)}=\frac{\eta_0(T,P_{eq},0)}{\eta_0(T,P_{atm},0)}\frac{\eta_0(T,P_{eq},c)}{\eta_0(T,P_{eq},0)}=a_P\,a_C \tag{4.4}$$

where P_{eq} is the equilibrium pressure of diluted polymer at the composition c and P_{atm} is the atmospheric pressure. Figure 4.2 shows the shifting of viscosity curves having similar shapes at varying pressures and concentrations.

The concentration shift factor, a_C is evaluated at a constant temperature and at a constant pressure as

$$a_{C_i}=\frac{a_{T_2}}{a_{T_1}}=\frac{\eta_0(T,P_{eq},c_i)/\eta_0(T_g,P_{atm},0)}{\eta_0(T,P_{eq},0)/\eta_0(T_g,P_{atm},0)}=\frac{\eta_0(c_i)}{\eta_0(0)};\quad a_C=\frac{a_{c_2}}{a_{c_1}}=\frac{\eta_0(c_2)}{\eta_0(c_1)} \tag{4.5}$$

where a_{T1} or a_{T2} denotes an arbitrary shift factor during the evaluation procedure and c_i is an arbitrary concentration.

Similarly the pressure shift factor, a_P is given at a constant temperature and at a constant concentration as

$$a_{P_i}=\frac{a_{T_2}}{a_{T_1}}=\frac{\eta_0(T,P_i)/\eta_0(T_g,P_{atm})}{\eta_0(T,P_{atm})/\eta_0(T_g,P_{atm})}=\frac{\eta_0(T,P_i)}{\eta_0(T,P_{atm})};\quad a_P=\frac{a_{P_2}}{a_{P_1}}=\frac{\eta_0(T,P_2)}{\eta_0(T,P_1)} \tag{4.6}$$

where P_i is an arbitrary pressure.

The viscosity curves are shifted horizontally and vertically according to the shift factor. A master curve can be constructed by shifting of viscosity curves for wide ranges of conditions.

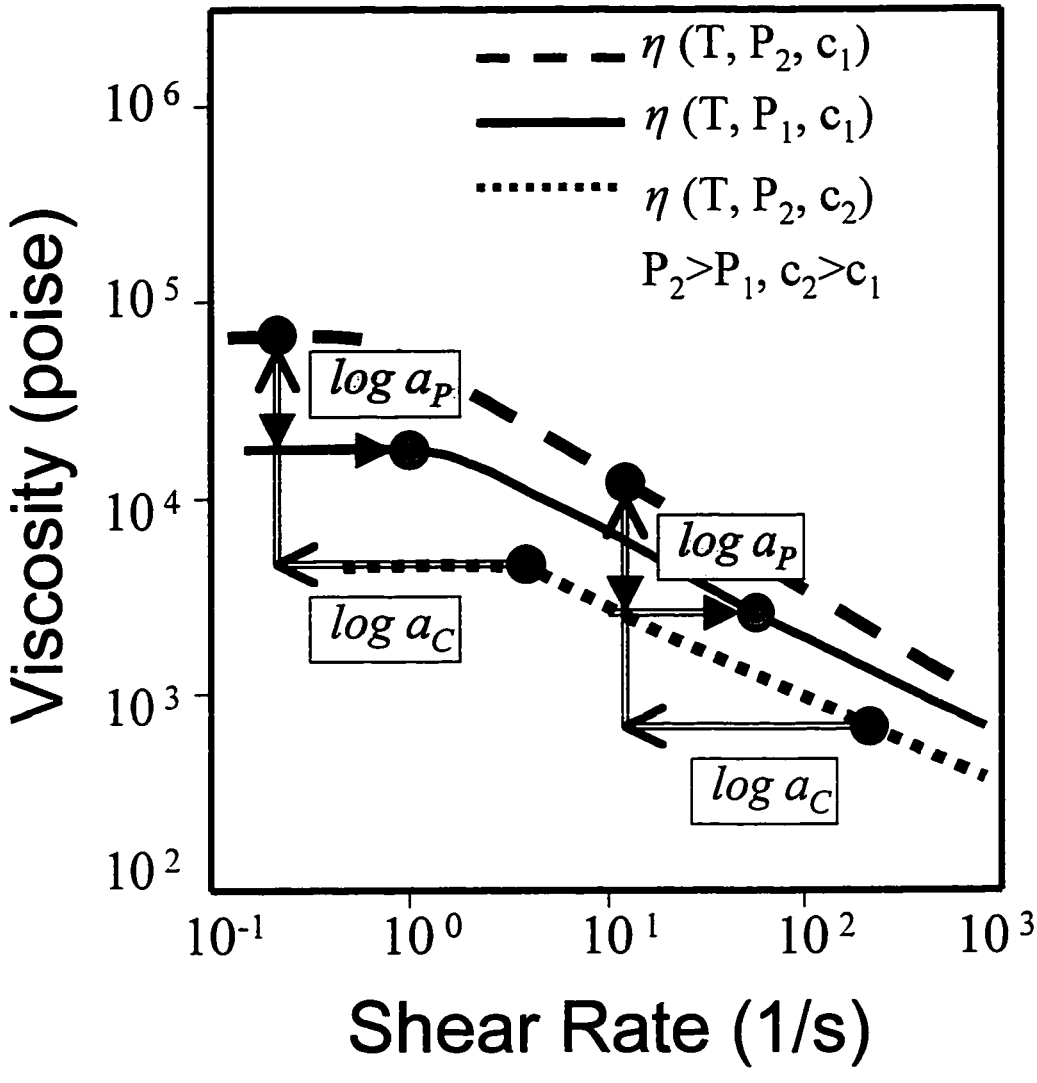

Figure 4.2
Schematic of Pressure and Concentration Shift of Viscosity Curves using a_C and a_P.

4.3 Calculation of Shift Factors using WLF equation

As in the case of temperature shift factor, if the viscosity versus shear rate curves have similar shapes under different pressures and concentrations, the pressure or concentration shift factor might be considered as an equivalent temperature shift factor. The temperature shift factor is readily calculated by introducing a given temperature to Equation (2.30).

$$\ln a_T = \ln \frac{\eta_0(T)}{\eta_0(T_g)} = -\frac{C_1(T - T_g)}{C_2 + (T - T_g)} \tag{2.30}$$

The effect pressure and concentration on viscosity can be estimated theoretically by the WLF equation if the dependence of T_g, C_1 and C_2 upon pressure and concentration is known. The changes of pressure and/or concentration would modify the T_g of polymer system. When the dependencies of T_g upon pressure and concentration is known, the pressure or concentration shift factor is calculated using the modified T_g from Equation (2.30).

The concentration shift factor, a_C can be evaluated using the concentration dependent T_g of diluted polymer system under the assumption that C_1 and C_2 are independent of concentration.

$$\ln a_C = \ln\left[\frac{\eta_0(T, P_{eq}, c)}{\eta_0(T, P_{eq}, c_0)}\right] = -\frac{C_1\{T - T_g(P_{eq}, c)\}}{C_2 + \{T - T_g(P_{eq}, c_0)\}} \tag{4.7}$$

where P_{eq} is the equilibrium pressure of diluted polymer system at a given concentration and the concentration dependent T_g can be estimated by the Chow's formula, Equation (2.21) through (2.23).

A similar equation is used for the evaluation of pressure shift factor under the same assumption that C_1 and C_2 are independent of concentration

$$\ln a_P = \ln\left[\frac{\eta_0(T,P_2)}{\eta_0(T,P_1)}\right] = -\frac{C_1\{T - T_g(P_2)\}}{C_2 + \{T - T_g(P_1)\}} \tag{4.8}$$

Linear dependence on pressure is approximated for T_g

$$T_g = T_{g0} + (dT_g/dP)(P - P_{atm}) \tag{4.9}$$

where T_{g0} is the T_g at atmospheric pressure.

When the pressure dependence of T_g is available, Equation (4.8) and (4.9) give the pressure shift factor.

Alternatively the pressure shift factor is calculated using the pressure coefficient, Equation (2.26).

$$b = \left(\frac{\partial \ln \eta}{\partial P}\right)_T \tag{2.26}$$

The pressure shift factor is obtained using the pressure coefficient

$$a_P = \frac{\eta_0(T,P,c)}{\eta_0(T,P_0,c)} = \exp\{b(P - P_0)\} \tag{4.10}$$

Miller [1971] and Penwell et al. [1971] derived the equation for pressure coefficient from the definition of pressure coefficient.

According to Miller [1971]:

$$b = \left(\frac{\partial \ln \eta}{\partial P}\right)_T \cong -\left(\frac{\partial \ln \eta}{\partial T}\right)_P \left(\frac{\partial T}{\partial P}\right)_\eta \tag{4.11}$$

Assume:

$$H = \left(\frac{\partial V}{\partial T}\right)_\eta - \left(\frac{\partial V}{\partial T}\right)_P = \left(\frac{\partial V}{\partial P}\right)_T \Big/ \left(\frac{\partial T}{\partial P}\right)_\eta \tag{4.12}$$

For any polymer, H is independent of temperature at atmospheric pressure.

At $T = T_g$,

$$\left(\frac{\partial T}{\partial P}\right)_{\eta} \cong \frac{\partial T_g}{\partial P} \tag{4.13}$$

$$H = \left(\frac{\partial V}{\partial P}\right)_T \Big/ \left(\frac{\partial T}{\partial P}\right)_{\eta} = \frac{(\beta V)_{T_g}}{\partial T_g / \partial P} \tag{4.14}$$

where β is the compressibility.

$$\left(\frac{\partial T}{\partial P}\right)_{\eta} = \frac{(\beta V)_{T_g}}{H} \cong \frac{\partial T_g}{\partial P} \tag{4.15}$$

Then

$$\left(\frac{\partial \ln\eta}{\partial P}\right)_T \cong -\left(\frac{\partial \ln\eta}{\partial T}\right)_P \left(\frac{\partial T}{\partial P}\right)_{\eta} \cong \left(\frac{\partial \ln\eta}{\partial T}\right)_P \frac{\beta V}{H} \tag{4.16}$$

From Vogel's equation,

$$\ln\eta = A + \frac{2.303B}{(T - T_0)} \qquad or \qquad \left(\frac{\partial \ln\eta}{\partial T}\right)_P = -\frac{2.303B}{(T - T_0)^2} \tag{4.17}$$

Finally,

$$b = \left(\frac{\partial \ln\eta}{\partial P}\right)_T = -\frac{2.303B}{(T - T_0)^2} \frac{dT_g}{dP} \frac{\beta V}{(\beta V)_{T_g}} \tag{4.18}$$

From the comparison of Vogel's equation with WLF equation, it is shown that $B = C_1 C_2$ and $T_0 = T_g - C_2$.

Penwell et al. [1970] used the WLF equation with the linear pressure dependence of glass transition temperature:

$$\log\frac{\eta}{\eta_g} = \frac{-C_1 (T - T_g(P))}{C_2 + T - T_g(P)} \tag{4.19}$$

$$T_g(P) = T_{g0} + \frac{dT_g}{dP}(P - P_{atm}) \tag{4.20}$$

Assuming that C_1 and C_2 are independent of pressure,

$$\frac{d\log\eta}{dP} = \frac{d\log\eta_g}{dP} + \frac{C_1 C_2}{\left[C_2 + (T - T_g)^2\right]}\left(\frac{\partial T}{\partial P}\right)_\eta$$

$$\cong \frac{d\log\eta_g}{dP} + \frac{C_1 C_2}{\left[C_2 + (T - T_g)^2\right]}\frac{\partial T_g}{\partial P} \tag{4.21}$$

Let $B = C_1 C_2$ and $T_0 = T_g - C_2$, then Equation (2.27) is derived

$$b = \left(\frac{\partial \ln\eta}{\partial P}\right)_T \cong -\frac{2.303B}{(T - T_0)^2}\frac{dT_g}{dP} \tag{2.27}$$

Penwell et al. [1970] reported that Equation (2.27) is good for the temperature ranges $T_g < T < T_g + 100\ ^0C$. The results show that the pressure shift factor can be approximately computed by the temperature shift factor based on the WLF equation with the pressure dependence of T_g.

In Chapter 6, the pressure coefficient will be used for the pressure correction of capillary rheometry data.

4.4 Evaluation Viscosity Reduction by Free Volume Equation

The viscosity reduction of polymer-diluent mixture can be estimated theoretically by free volume theory which employs the concept of free volume to explain the viscosity of liquids and polymeric fluids. Pioneering free volume theories have been developed by Doolittle [1951], Cohen and Turnbull [1959], Williams, Landel, and Ferry [1955], and Kelly and Bueche [1961]. The Kelly-Bueche equation, Equation (2.16) comprises the expression for the segmental friction factor suggested by Cohen and Turnbull [1957] and adopts the WLF equation for the fractional free volume. For the study of viscosity reduction of polymer melt brought by added diluent, the Kelly-Bueche equation provides

a simple foundation based on the assumption of free volume additivity between polymer and diluent, Equation (2.17).

Bae [1989] applied a modified Kelly-Bueche equation to predict the viscosity reduction of poly(ethylene) glycol-CO_2 and PDMS-CO_2 systems. The non-ideal mixing effect is handled through the estimation of the realistic fractional free volume of mixture computed by swollen volume data fitting.

Gerhardt [1994] applied an extended free volume model associated with the lattice based-equation of state models for PDMS-CO_2 system successfully. The Kelly-Bueche Equation, Equation (2.16) is rewritten for the ratio of polymer solution viscosity, η_m to that of pure polymer, η_p as:

$$\frac{\eta_m}{\eta_P} = w_P^n \left(\frac{\rho_m}{\rho_P}\right)^n \exp\left[\frac{1}{f_m} - \frac{1}{f_P}\right] \tag{4.22}$$

$$f_P = \frac{V_P - V_P^0}{V_P} \tag{4.23}$$

$$f_m = \frac{V_m - V_m^0}{V_m} \tag{4.24}$$

$$V_m^0 = w_P V_P^0 + (1 - w_P) V_d^0 \tag{4.25}$$

where w is the weight fraction of diluent, f is the fractional free volume, V is the specific volume, V^0 is the occupied specific volume, ρ is the density , n is an exponent to be determined by experiment, and subscripts p, d, and m represent polymer, diluent, and mixture respectively.

The densities of pure components and PS-SCG mixtures, the occupied volumes of pure components, and the exponent should be determined.

4.4.1 Evaluation of Density

Densities of pure components and mixtures can be evaluated directly by an equation of state model. Khan [1997] applies the Sanchez-Lacombe equation of state [1976,1978], that was successfully employed for PDMS-CO_2 system by Gerhardt et al. [1997], for the current study.

Densities of pure components are obtained directly using the Sanchez-Lacombe equation of state for pure component. The evaluation of mixture density needs the binary interaction parameter, δ_{ij}, that accounts for the non-linear mixing effect and replaces a mixing rule for binary mixtures [Garg, 1993]. The binary interaction parameter can be evaluated from the solubility isotherm data for each binary mixture. Computed binary interaction parameters for current study will be presented in Chapter 7. Detailed description of density computation is referred to Garg [1993].

4.4.2 The Occupied Volume of Supercritical Gases

Goldhamer [1910] suggested the rule for the estimation of density for most liquids:

$$\rho_L - \rho_V = M\rho_C\left(1-\frac{T}{T_C}\right)^{1/3} \tag{4.26}$$

where ρ_L and ρ_V are the liquid and vapor phase densities, respectively, M is a disposable constant generally equal to 3.8, and the subscript c refers to the critical condition.

$$\rho_L - \rho_V = C''(T-T_C)^{1/3} \tag{4.27}$$

Matthews [1916] presented Equation (4.27) which is equivalent to Equation (4.26) and Equation (4.28) for the estimation of occupied volume at 0 ^{0}K.

$$\rho_0 = C'' T_C^{1/3} \tag{4.28}$$

where ρ_0 is the occupied volume and C''is a constant computed by Equation (4.27). Also he applied the assumptions of van der Waals that the density at absolute zero is approximately equal to Sd_C:

$$\rho_0 \cong Sd_C = \frac{RT_C}{P_C V_C} \rho_C \tag{4.29}$$

Bondi [1964A] estimated the occupied volume of 0.589 cm^3/g for carbon dioxide from the reconciliation of x-ray diffraction data with extrapolated crystal density at 0 ^0K. The equation of state model can be used to predict the occupied volume of supercritical gases through the optimization of experimental thermodynamic data given in literature [Wissinger and Paulitis, 1991; Garg, 1993]. Heuse [1930] estimated the density of carbon dioxide to be 1.702 cm3/g at a temperature of -253 ^0C, which gives the occupied volume of 0.5875 cm^3/g or lower. A specific volume of carbon dioxide was measured by Newitt et al. [1948] to be 0.615 cm3/g at -130 ^0C for solid phase saturated with the vapor phase. The existing investigations on the occupied volumes of carbon dioxide are shown in Table 4.1.

Table 4.1
Occupied Volumes of Carbon Dioxide

V_0 (cm^3/g)	Method	Reference
0.5797	Equation (3.2) & (3.3)	Matthews [1916]
0.6031	Equation (3.4)	Matthews [1916]
0.6158	Group Contribution	Sugden [1927]
0.5880	Measurement of Density at –253 ^0C	Heuse [1930]
0.5890	X-ray Diffraction and Extrapolation of Crystal Density	Bondi [1964A]
0.7010	Sanchez-Lacombe Equation of State	Garg [1993]
0.7690	Panayiotou-Vera Equation of State	Garg [1993]
0.8710	Panayiotou-Vera Equation of State	Wissinger & Paulaitis [1991]

The group contribution theory given by Haward [1970] is useful to estimate the occupied and molar volumes of low molecular weight compounds and polymers. The molar occupied volumes of functional groups are available [Haward, 1970; van Krevelen, 1990] and include the atomic constants of molar occupied volumes of Sugden [1927] and Blitz [1934]. While Sugden estimated the occupied volumes by extrapolating liquid densities, Blitz did from the crystalline state. The estimated occupied volumes based on Sugden's data are generally 2 to 3 % above those using Blitz's data for low molecular weight compounds. Bondi [1964B] presented the van der Waals volumes (V_w) of simple compounds and functional groups which can be used in the group contribution method. Later Bondi [1968] suggested that the occupied volume is approximately 1.3 times of van der Waals volume. For the current study, the occupied volume of R152a (1,1-diflluoroethane) and R134a (1,1,1,2-tetrafluoroethane) are necessary. Garg [1993] presented the occupied volume of R152a by the optimization of thermodynamic data in literature. The group contribution method is useful to estimate the occupied volumes of R152a and R134a. The occupied volumes of R152a and R134a are summarized at Table 4.2.

Table 4.2
Occupied Volumes of R152a and R134a

Gas	V_0 (cm^3/g)	Method	Reference
R152a	0.7509	Group Contribution	Sugden [1927]
	0.6277	Group Contribution & $V_0 = 1.3\ V_w$	Bondi [1964B]
	0.8251	Sanchez-Lacomb Eqaution of State	Garg [1993]
	0.8951	Panayiotou-Vera Eqaution of State	Garg [1993]
R134a	0.5552	Group Contribution	Sugden [1927]
	0.4740	Group Contribution & $V_0 = 1.3\ V_w$	Bondi [1964B]

For polymer melts, the extrapolation of the density to absolute zero is difficult because polymers become glasses as the temperature decreases, and the coefficient of expansion in the liquid state cannot be obtained at temperatures well above absolute zero. For the current experimental study, the occupied volume of pure polystyrene is obtained from an optimized fit of Newtonian viscosity data over a wide range of temperatures to an equation of the form given by the Doolittle free volume equation. The procedure will be explained in detail in Section 5.7.

CHAPTER 5

EXPERIMENTAL TECHNIQUES

5.1 Materials for PS-SCG Systems

The materials used in the rheological measurement of PS-SCG system are listed in Table 5.1. Each material was used without further purification.

Table 5.1 Materials used for PS-SCG systems

Material	Molecular Weight (M_w)	Supplier
Polystyrene	132,000 (polydispersed)	Dow Chemical Co.
Carbon Dioxide	44.0 (99 %, bone dry)	Scott Specialty Gases
1,1-difluoroethane (R152a)	66.1 (100%)	Du Pont Chemicals
1,1,1,2-tetrafluoroethane (R134a)	102.0 (100%)	Du Pont Chemicals

5.2 Equipment for Equilibration of PS and SCG

The schematic of equilibration equipment for PS-SCG mixtures is shown in Figure 5.1. The equilibrium chamber is a stainless steel pressure vessel (Parr Instrument Company, Moline, IL) with a nominal capacity of 321 cm^3 and rated for 350 °C and 3000-psig pressure. It is equipped with a safety valve (rated for 1500 psig), a pressure gauge (set for 2000 psig) on the vessel head, a purging port, and a gas inlet valve. The gas inlet tube is connected to the gas cylinder. When the pressurization of gas is necessary, a metering pump Model 396-89 (Milton Roy) was used. The pump is a displacement type and rated for 6000 psig, with a maximum flow rate of 460

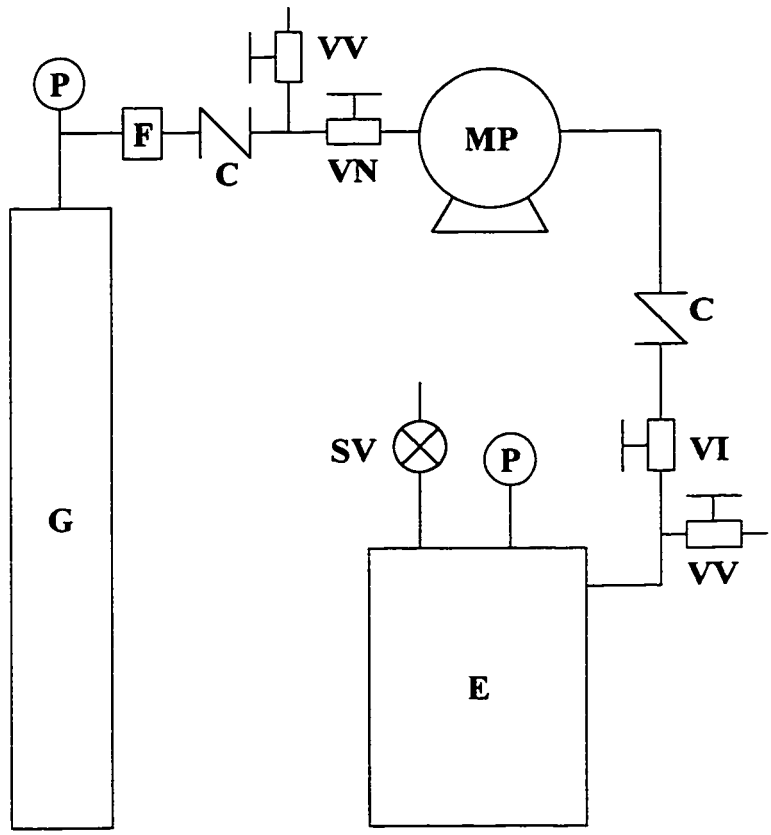

C Check Valve
E Equilibrium Vessel
F Micron Filter
G Gas Cylinder
MP Metering Pump
P Pressure Gauge
SV Safety Valve
VI Gas Inlet Valve
VN Needle Valve
VV Gas Release Valve

Figure 5.1
Schematic of Equilibration Equipment

ml/hour. Because the refrigerants R152a and R134a are supplied under their own vapor pressures (roughly 70 to 80 psig at ambient temperature), pressurization is necessary for the sorption experiment.

5.3 Equilibration of PS and SCG

About 20 g of PS pellets, enclosed in a steel mesh bag is put into the pressure vessel. The steel mesh bag gives enough vacant space for the contact of pellet with gas. The mass of PS and the steel mesh bag are weighed before the charging of gas. Initially the vessel needs to be purged to expel pre-existed air in the vessel. After the purging, the gas is loaded into the vessel until the desired pressure is built. It is easy for CO_2, which is supplied from a full cylinder at 850 psig. The refrigerants R152a and R134a need to be pressurized through the metering pump up to 600 psig. To facilitate the sorption of R134a, which has very low solubility compared to CO_2 and R152a, into PS, the granular PS rather than the conventional pellet was used. The granule PS was milled to pass through the U.S. standard #14 sieve but not a #35 sieve.

As will be mentioned in Section 5.2, since the pellet or granule is ideal for the loading into the rheometer barrel, any fusion of PS pellets is not desirable. The dissolved SCF contributes to the substantial T_g depression of the PS [Chiou et. al., 1985]. When the PS pellets are highly sorbed at room temperature or even slightly sorbed at a warm temperature, the sorbed pellets in the steel mesh bag might fuse together. Thus the resultant T_g of sorbed PS should not be lower than the temperature of equilibration. Holding the equilibration system at room temperature was effective to restrain the fusion of pellets as well as for the safety. The equilibration pressure was kept at 900 psi or higher for carbon dioxide and 600 or higher for R152a and R134a.

After equilibration with gas, the weight gain of the lower polymer-rich phase was measured to assess the amount of gas absorbed preceding the rheological measurement. The upper phase in the equilibrium phase can be assumed a pure gas, since the high molecular weight polystyrene has negligible solubility in a gaseous upper phase at ambient room temperature. The gas pressure was rapidly released and the steel mesh bag was placed on the pan of a fast-response electronic digital balance readable to 0.0001g (Mettler H80). Using a computerized data acquisition system, the sample weight during the desorption period at atmospheric were monitored and recorded at every 30 second. The weight changes due to desorption of gas is shown in Figure 5.2 for each PS-SCG combination. The amount of sorbed gas was controlled by the equilibration pressure. A minimum 5 days of equilibration was found necessary. The maximum weight concentration of carbon dioxide was about 5 percent for the viscosity measurement of PS-CO_2. The gradual slopes of desorption of R152a and R134a enable the viscosity measurement at higher concentrations.

5.4 Pressurized Capillary Rheometer System

The measurement of PS-SCF solution viscosity was conducted on the pressurized capillary rheometer [Gerhardt, 1994], which was modified to enable the pressurization of total system. The conventional capillary rheometer system is the Instron Model 4202 universal testing machine equipped with an Instron Model 3210 capillary rheometer (Instron Corporation, Canton, MA). Capillary dies used in the measurement were two stainless steel dies of L_c/D_c = 40.3 (1.999 in. length and 0.0496 in. diameter with 90 ^{o} entry angle) and an L_c/D_c = 74.67 (3.7482 in. length and 0.0502 in. diameter with 90 ^{o} entry angle), both supplied by the Instron Company. Also a zero-length die with 0.05 in.

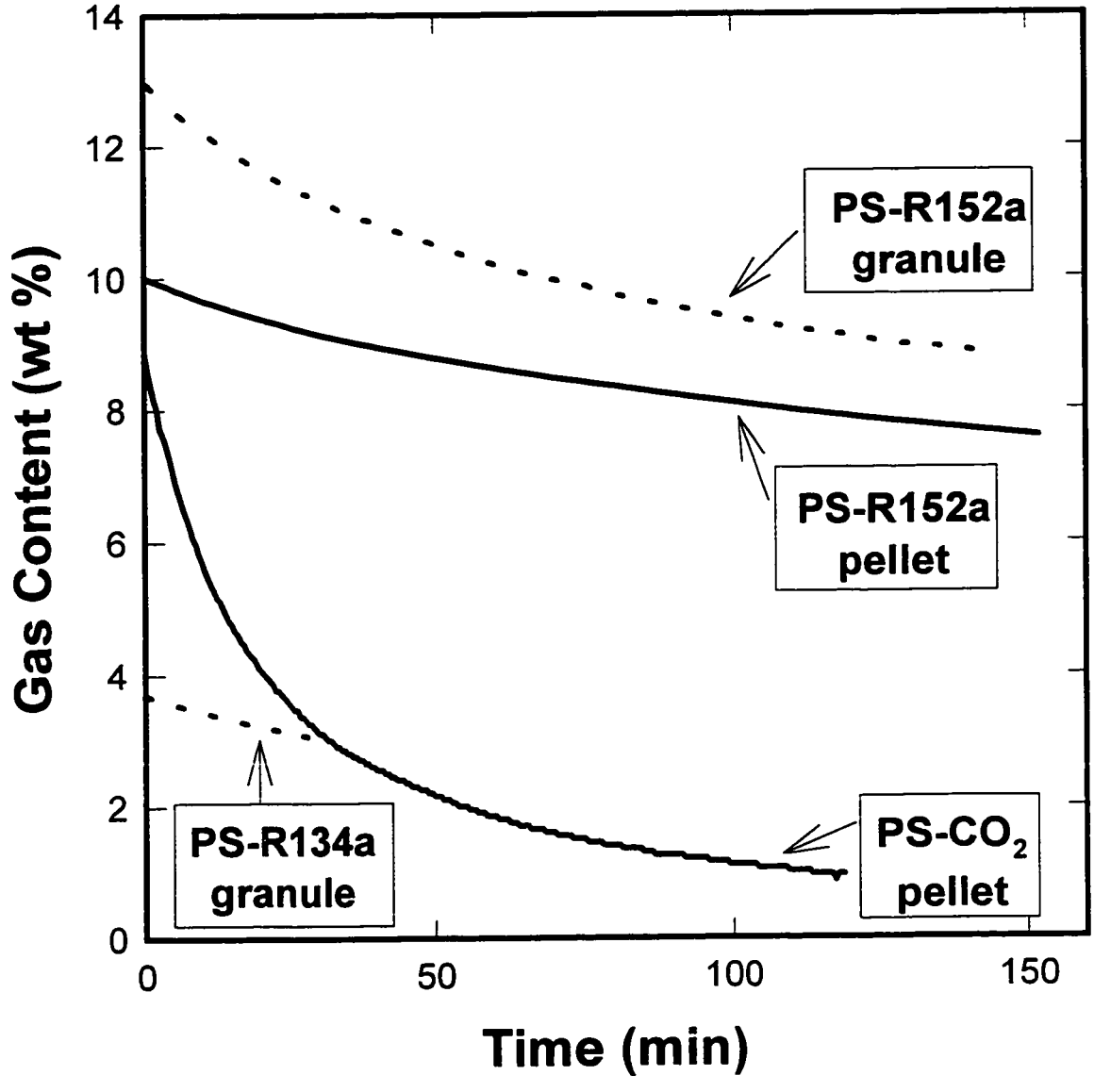

Figure 5.2
Desorption Behavior of absorbed Gases at atmospheric Pressure and ambient Temperature.

diameter and 90 ° entry angle was utilized.

The pressurized capillary rheometer system is shown in Figure 5.3. The main apparatus added unto the conventional capillary rheometer is the back-pressure assembly, which was originally designed and applied for the viscosity measurement of the PDMS-CO_2 system by Gerhardt [1994]. A back-pressure chamber, connected to the outflow end of capillary die, has a piston (1 in. diameter) to provide back-pressure to insure that the PS-SCG solution remains single-phase during the viscosity measurement. The piston, linked to the piston rod (6-in. diameter) of an air cylinder in tandem, is held at constant force exerted by the air cylinder. The air cylinder is supplied a regulated air pressure through a pneumatic pressure regulator (maximum 250 psig) which is connected to a standard blended air (20-21% of Oxygen) cylinder. A piezoresistive quartz pressure sensor (Type 6153C, Kistler Instruments AG of Winterthur, Switzerland) is flush mounted at the bottom the back-pressure chamber, directly below the outlet of the capillary die. The piezoelectric signal is converted to a voltage signal by the charge amplifier (Type 5041B, Kistler Instruments AG of Winterthur, Switzerland). The voltage signal and the load cell reading of the Instron machine are sent to a personal computer for monitoring and recording during the measurement. A ceramic insulated resistance wire is inserted through a series of horizontally drilled holes penetrated through the wall of back-pressure chamber to provide temperature control. The wire and a thermocouple are coupled with a temperature controller for the temperature control of the back-pressure chamber.

5.5 Sealing under High Pressure

Since the PS-SCF solution needs to be pressurized to keep the SCF from flushing,

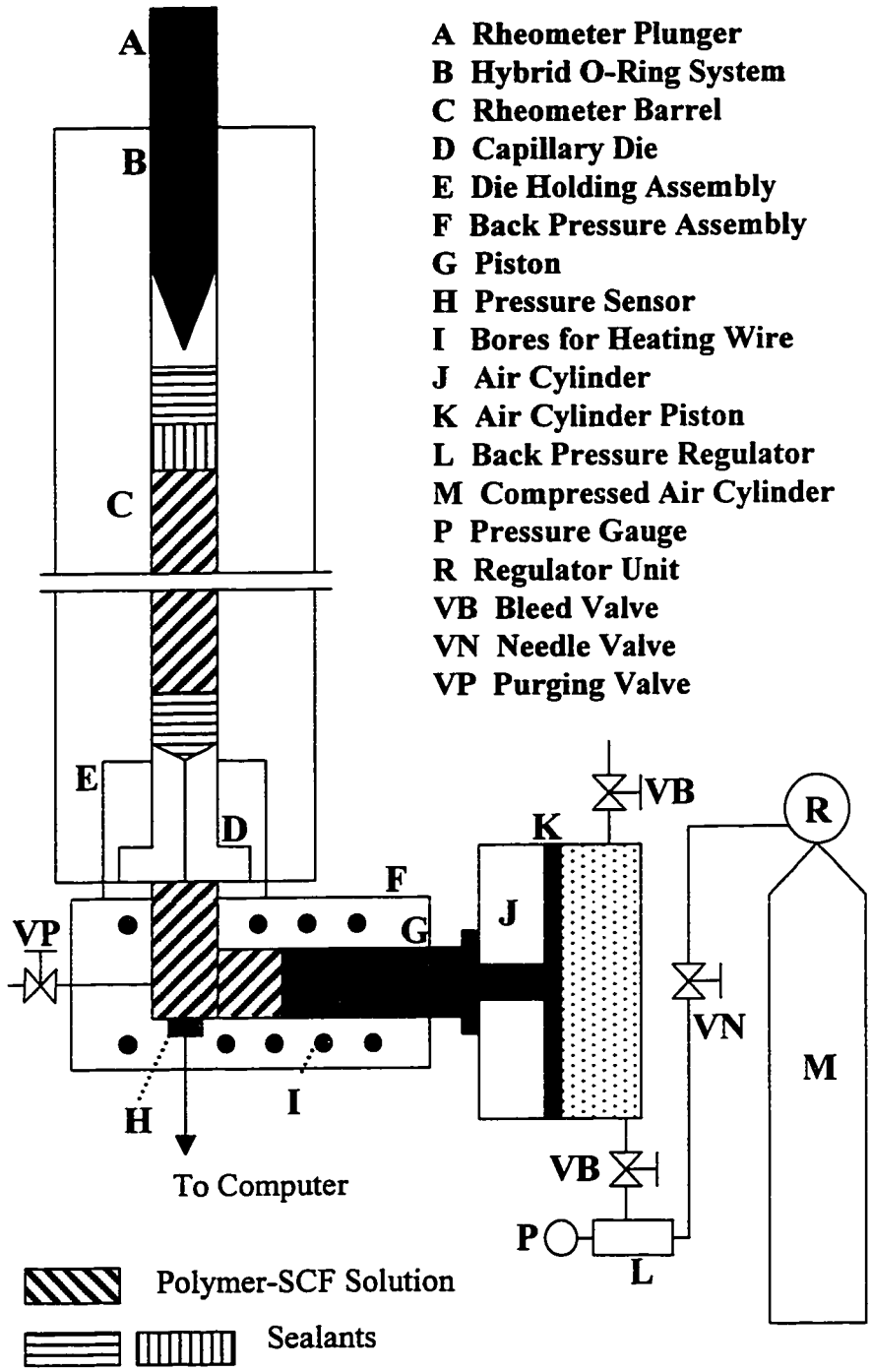

Figure 5.3
Modified Capillary Rheometer System for the Measurement of PS-SCG Solution at Elevated Back-Pressure

the sealing of the total rheometer assembly is very important. The PS-SCF mixture is confined between the plunger tip and the piston of chamber. The piston of back-pressure chamber moves about 7 times slowly compared with one in the rheometer barrel during the extrusion. The space between the piston head in the chamber and the entry region of capillary die is filled with pure PS prior to loading the PS-SCF sample. The plunger tip is equipped with double grooves. Each one is packed with a Viton (hardness 90) O-ring and two Teflon washers. One O-ring and two washer system gives an excellent sealing effect in a dynamic situation. The Viton O-ring has a superior elasticity and long-term durability even at high temperatures in static or weakly dynamic conditions. It may easily be torn, however, at highly pressurized static and moderate dynamic situations. The Teflon washers support and protect the Viton O-ring, so that the inherent characteristics of Viton O-ring work better and longer.

The sealing of that O-ring assembly is one-dimensional, the circumferential direction only. The hybrid block sealing, i.e., cylinder blocks of pure PS and Teflon, both 3/8-in. diameter and 3/8-in. length achieve the additional sealing, which offer a two-dimensional sealing effect. The Teflon block, on the top of PS-SCF sample, works as a separator and a sealant. The pure PS block is seated on the Teflon block. Also a little amount of high molecular weight PDMS is squeezed on the pure PS block. Each material has widely different glass transition temperatures, so that, throughout the temperature ranges from cryogenic to 200 ^{o}C or higher, one or more liquid seal is always functional. The friction effect of cylinder block sealing is evaluated by running the rheometer for pure PS (1) without back-pressure assembly and using the O-ring and washer system and (2) with back-pressure assembly and using the O-ring and washer system and the hybrid block sealing. Both viscosity data were identical.

The additional friction due to this O-ring and washer sealing system needs to be evaluated. The measured wall friction will be discussed in Chapter 6.

5.6 Procedure of Rheological Measurement under High Pressure

The rheometer is chilled to sub-zero temperatures to suppress degassing of the sample during the PS-SCG solution (sorbed PS pellets) loading. The equilibration chamber is disassembled and the meshed sample bag containing PS pellets absorbed with a SCG is placed on a balance. The sample bag is frozen in the liquid nitrogen bath when the gas content reaches the appropriate level. The frozen pellets are loaded unto the pre-cooled barrel of the rheometer in the same manner of normal pellet loading. The sorbed PS pellets are blocked with the hybrid block sealing explained in Section 5.3 and the plunger equipped with O-ring and washers is lowered to pressurize. At the same time, the compressed air regulated at a pre-determined pressure is supplied to the back-pressure assembly. In addition, the heating of overall rheometer system is begun. The piston is lowered manually giving compression and pressurization. The rheometer system reaches a thermal equilibrium after about 30 minutes and a mechanical balance between the load cell reading and back-pressure after another 30 minutes approximately. If an appreciable degassing occurs in this period, it is detected by the continuous increase of load without stabilization.

The pressure sensor is zeroed at the thermal and mechanical equilibrium and the computer is started for data recording. The shear rates are scanned from lowest to highest or highest to lowest value. At the end of measurement, the load cell reading is monitored further after the piston is stopped to evaluate pressure stability. For the reproducibility of experiment, the same experiment is repeated at a reverse scanning of shear rates.

Based on the equilibrium pressure of a certain composition, an extra back-pressure is needed to ensure a single phase solution, in dynamic situations, such as the plunger movement during capillary rheometry. For higher shear rates, more back-pressure is necessary to keep a single phase [Suh, 1997]. The reverse shear rate scanning is invaluable to obtain reproducible data.

The appropriate composition range of PS-SCF solution is determined by the solubility data, the extra back-pressure, and the load limit of the rheometer system. The solubility isotherms for PS-CO2 [Sato et al., 1996] and PS-R152a [Garg et al., 1994] available in literature are shown in Figure 5.4 and 5.5 with the modeling by Vikhar [1997]. The Table 5-2 represents the experimental system of PS-SCF solution for the current study.

Table 5.2
Experimental Systems

Polymer-SCF	Temperature (deg C)	Pressure (MPa)	Composition (weight fraction of SCF)
PS-CO_2	150	1 – 17	0 – 0.051
	175	1 – 17	0 – 0.052
PS-R152a	150	1 – 16	0 - 0.11
	175	1 – 17	0 - 0.10
PS-R134a	150	1 - 12	0 - 0.03
	175	1 - 10	0 - 0.028

5.7 Iso-Free-Volume Polymer Solutions

The only effect of chain dilution can be verified by the measurement of viscosity of the mixture with the materials that have similar chemical nature and identical

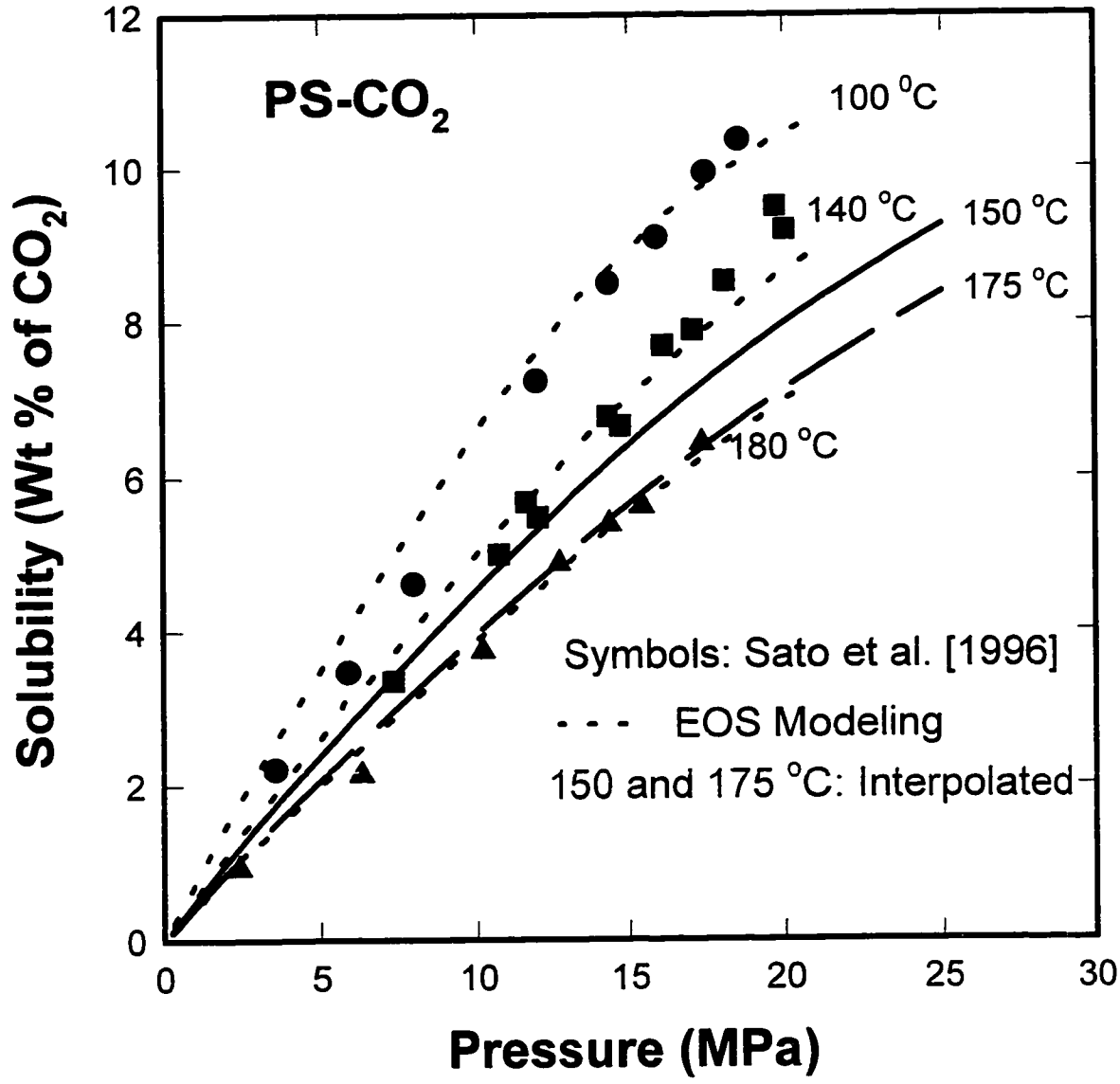

Figure 5.4
Solubility Isotherms of PS-CO_2 by Sato et al. [1996] and Modeling by Equation of State

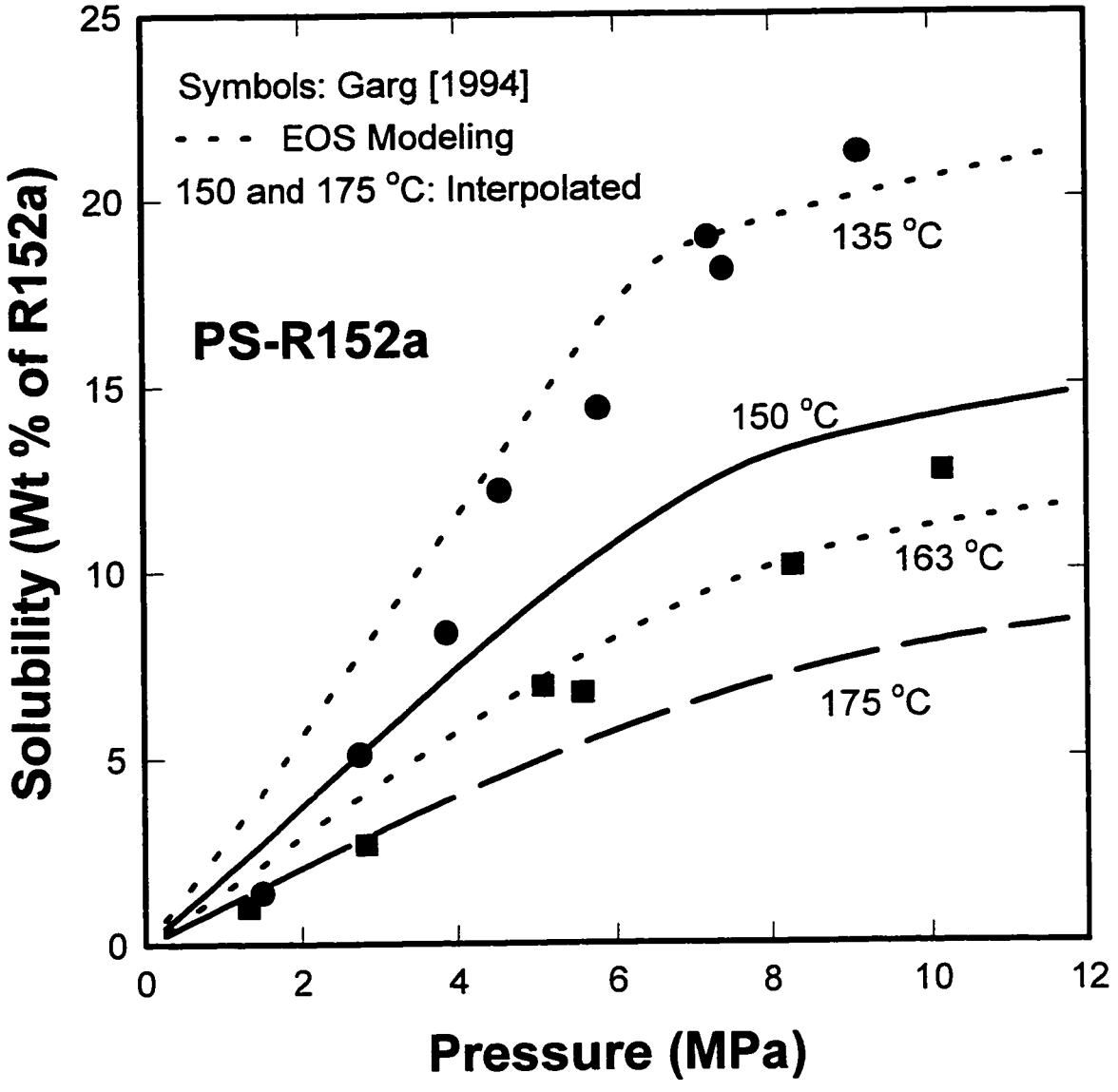

Figure 5.5
Solubility Isotherms of PS-R152a by Garg et al. [1994] and Modeling by Equation of State

fractional free volume. Mono-dispersed low molecular weight polystyrene (M_w=4,000, Pressure Chemical) is mixed with the high molecular weight polystyrene (M_w=160,000, Pressure Chemical) using the common solvent toluene. Total weight of both polystyrenes was 2 grams, more than 3 times the necessary amount to make a 0.5-mm thick and 4cm-diameter disk. The weight fractions of low molecular weight polystyrene were 0, 0.05, 0.1, 0.2, 0.3 and 0.4. The solution was made using a small Aluminum pan which has the volume of 10 cm^3 and advantage of easy releasing of polystyrene disk. A tiny Teflon-coated magnetic stirrer was used for vigorous mixing of solution at ambient temperature. Fresh solvent was added during the mixing period to counter-balance the evaporation of solvent. The completely mixed solution was dried in a fume hood at ambient condition for preliminary drying for 3 days. Later the solution was gradually heated from room temperature up to the boiling point of Toluene at atmospheric pressure for 7 days. A vacuum was applied progressively and the solution was kept at 150 ^0C for 14 days. After this vacuum drying, the weight change of the Aluminum pan with solution was monitored regularly. The vacuum drying was stopped when the weight gain of dried sample is within 1 percent of the original weight of polystyrene. Normally it took 4 weeks to obtain a desired dried sample. The dried sample was easily peeled off out of the pan and machined to make a 0.5 to 1 mm-thick and 4 cm-diameter disk. The center of disk was made thicker than the circumference for better wetting at the measurement using the Weissenberg Rheogoniometer. The cone and plate configuration was used for the viscosity measurement at the range of shear rate from 0.01 rad/s to 0.1 rad/s. The result was used for the computation of concentration dependence factor at the free volume rheological model.

CHAPTER 6

ANALYSIS OF CAPILLARY RHEOMETER DATA

6.1 Introduction

The raw data from capillary rheometry, the plunger speed and the force measured by load-cell are converted to the apparent wall shear stress (τ_{wa}) and shear rate ($\dot{\gamma}_{wa}$) giving the apparent viscosity (η_a) by means of the geometric information of barrel and capillary die.

$$\eta_a = \frac{\tau_{wa}}{\dot{\gamma}_{wa}} \tag{6.1}$$

$$\dot{\gamma}_{wa} = \frac{4Q}{\pi R^3}; \quad \tau_{wa} = \frac{\Delta P}{4(L/D)} \tag{6.2}$$

where Q is the volumetric flow rate, R is the radius of capillary, D is the capillary diameter, L is the length of capillary, and ΔP is the pressure drop across the capillary die.

For a Newtonian fluid, the apparent viscosity represents the true viscosity exactly and the apparent shear stress and apparent shear rate can be given by

$$\dot{\gamma}_{wa} = \frac{8V_x D_p^2}{D^3}; \quad \tau_{wa} = \frac{F}{4A_p \frac{L}{D}} \tag{6.3}$$

where V_x is the cross head speed, D_p is the plunger diameter, F is the force acting on the plunger, and A_p is the cross-sectional area of plunger.

Since the apparent viscosity is valid only for Newtonian fluids, appropriate corrections of shear stress and shear rate are necessary to obtain true rheological data for non-Newtonian fluids. The Bagley-Rabinowitsch correction is a widely accepted and

standardized procedure to correct the apparent wall shear stress and the apparent shear rate for non-Newtonian fluids giving corrected viscosity data [Dealy, 1982; Brydson, 1988; Whorlow, 1990]. Sometimes the effect of wall friction, viscous heating, and the pressure dependence of viscosity may need to evaluated to acquire accurate viscosity data from capillary rheometry.

6.1.1 Wall Friction

The wall friction is the force to push the plunger through an empty barrel at a given shear rate and temperature. Usually the magnitude of wall friction is within the experimental error range. When the plunger is equipped with extra sealing, however, it is necessary to check the magnitude of wall friction which must be subtracted from the total load reading to obtain the net force driving flow.

6.1.2 Correction of Wall Shear Stress

The entry pressure loss, ΔP_e, in the entrance region of capillary die is the major bias giving increased wall shear stress. Entry pressure is caused by the viscoelastic behavior of the test fluid, and it must be subtracted from the apparent pressure drop to calculate an effective pressure drop for the fully developed flow. The Bagley correction [1957, 1961] is the conventional procedure dealing the entry pressure. Methods of correcting entry pressure loss are briefly presented and discussed below.

The Bagley correction can be performed by the elimination of the entry effect by using two dies with same diameter and entry angle but different lengths. Each die should have large (L/D) ratio to provide an enough length of fully developed flow. The difference of two measured pressures represent the pressure drop over the fully developed

region and the true wall shear stress is evaluated.

$$\tau_w = \frac{\Delta F_2 - \Delta F_1}{4\,A_P(L_2 - L_1)/D} = \frac{\Delta P_2 - \Delta P_1}{4(L_2 - L_1)/D} \tag{6.4}$$

Another type of Bagley correction is the evaluation of the Bagley correction factor, e representing the artificial supplementary die length for the extra pressure drop caused by the entry loss, which is applied to calculate the true shear stress as:

$$\tau_w = \frac{F}{4A_p\left(\frac{L}{D}+e\right)} = \frac{\Delta P}{4\left(\frac{L}{D}+e\right)} \tag{6.5}$$

The factor is calculated through a series of experiments using several dies with different length and the same diameter and entry angle. The measured pressure drops are plotted as a function of *(L/D)* ratio for a range of shear rates. From the plot, known as the Bagley plot, the data points showing linear relationships are extrapolated to give intercepts on the abscissa, e and on the vertical axis, ΔP_e. Since slight curvatures of the plot in the vicinity of zero *(L/D)* ratio are observed in many cases [Dealy, 1982], only the linear segment of the plot at higher (L/D) ratios should be used for the extrapolation.

Another approach of is to measure ΔP_e directly with orifice die having zero *(L/D)* ratio. The pressure drop obtained from the measurement with the orifice die, ΔP_O has been used for the estimation elongational viscosity as proposed by Cogswell [1972A, 1972B] and Binding [1990]. The procedure has been examined experimentally [Tremblay, 1989, 1992; Shroff et al., 1977; Laun and Schuch, 1989] and numerically [Kwag, 1992; Davies et al., 1993]. The orifice pressure drop is directly subtracted from the total pressure drop to give the pressure drop for fully developed flow [Shuler et al.,

1994; Kazatchikov et al. 1995].

$$\tau_w = \frac{\Delta P - \Delta P_0}{4(L/D)} \tag{6.6}$$

For polypropylene melt, this method gives identical values of Bagley correction with those evaluated from the Bagley plot using dies with finite lengths [Kazatchikov et al. 1995].

6.1.3 Non-linear Bagley Plots and Pressure Correction

When the Bagley plot shows a significant non-linearity, only the orifice die method can be applied directly. Laun [1983] and Hatzikiriakos and Dealy [1992] adopted quadratic data fittings to evaluate e from non-linear Bagley plots. The source of this non-linearity, especially at higher shear rates, is the viscous heating effect and/or pressure-dependent viscosity as suggested [Dealy, 1982]. The viscous heating effect is due to viscous dissipation within the fluid during flow through the die. The pressure-dependent viscosity of polymers may also cause the total pressure drop measured by the load cell to vary nonlinearly with L, especially at lower temperatures and higher shear rates As the pressure increases at higher shear rates, the viscosity of polymer in the die increases according to the pressure dependence. Both effects contribute to non-linear increase in pressure drop at higher shear rates.

Kamal and Nyun [1983] performed an excellent analysis on the viscous heating and pressure effect on the capillary rheometry for polystyrene. While the result clarifies the effect of end correction, pressure effect, and viscous heating systematically, very extensive experimental data were necessary in their analysis. Other group of investigators applied only the pressure dependence of viscosity successfully [Penwall et al., 1970;

Kazatchkov et al., 1995]. Earlier works of pressure corrections are briefly reviewed below.

6.1.3.1 Approach by Penwell et al.

Penwell et al. [1971] derived the equation for the pressure coefficient, Equation (4.14) which includes terms depending upon temperature, molecular weight, and pressure. They computed pressure coefficients of polystyrene melts through extensive data obtained with a capillary rheometer. The obtained pressure coefficients for polystyrene are 0.0029 *deg C/bar* (M_w = 670,000 at 165 ^{0}C) and 0.0055 *deg C/bar* (M_w = 20,400 at 140 ^{0}C). The pressure distribution across die length was computed from the pressure dependent viscosity equation (Equation 2.26) and the equation of motion for power-law fluid as:

$$\frac{z}{L} = \frac{e^{-bP} - e^{-bP_0}}{e^{-bP_L} - e^{-bP_0}} \tag{6.7}$$

where b is the pressure coefficient defined as Equation (2.26), L is the die length, and P_0 and P_L is the pressure at the inlet and outlet respectively.

The derivation of Equation (6.7) will be done at Section 6.2.4. Penwell et al. calculated the average pressure, P_{avg}, by numerical integration and the viscosity at the average pressure was evaluated as:

$$\eta_{Pavg} / \eta = exp\,(b\,P_{avg}) \tag{6.8}$$

6.1.3.2 Yamada and Porter's approach

The pressure coefficient equation, Equation (4.14) was adopted for the pressure

correction directly. Using Equation (4.14), the Newtonian viscosity can be represented as

$$\eta_0 = \eta_g \exp\left[2.303\frac{A_2 + A_3 P}{A_4 - A_1 P}\right] \tag{6.9}$$

where $A_1=dT_g/dP$, $A_2=-C_1(T-T_{g0})$, $A_3=C_1A_1$, and $A_4=C_2+T-T_{g0}$ and T_{g0} is the glass transition temperature at atmospheric pressure.

They assumed that the change of zero-shear viscosity dominates the overall viscosity change under a pressure effect.

$$\eta\,(P+\Delta P) = \eta_0\,(P+\Delta P)\,f(\dot{\gamma}\lambda) \tag{6.10}$$

The equation of motion for capillary rheometry is

$$\frac{\partial P}{\partial z} - \frac{1}{r}\frac{\partial}{\partial r}(r\tau_{rz}) = 0 \tag{6.11}$$

The generalized Newtonian model is used.

$$\tau_{rz} = \eta\frac{\partial v_z}{\partial r} = \eta_0\ f(\lambda\dot{\gamma})\frac{\partial v_z}{\partial r} = \eta_g \exp(f(P))\ f(\lambda\dot{\gamma})\frac{\partial v_z}{\partial r} \tag{6.12}$$

$$f(P) = 2.303\ (A_2 + A_3P)/(A_4 - A_1P) \tag{6.13}$$

The pressure function $f(P)$ corresponds to the pressure coefficient, b in Equation (6.8).

Introducing the generalized Newtonian model gives

$$\frac{dP/dz}{\eta_g \exp(f(P))} = C = \frac{1}{r}\frac{\partial}{\partial r}\left(r\,f(\lambda\dot{\gamma})\frac{\partial v_z}{\partial r}\right) \tag{6.14}$$

where C is an integration constant.

For pressure dependent terms,

$$\int_{P_0}^{P_L}\frac{dP}{\exp(f(P))} = C\int_0^L \eta_g\,dz = C\eta_g L \tag{6.15}$$

The integration constant can be calculated by a numerical integration over the die length. Using the integration constant, the pressure distribution is computed by solving the ordinary differential equation and the average pressure is obtained concurrently.

$$\frac{dP}{dz} = C\eta_g \exp(f(P)) \quad ; P_{avg} = \int_0^L P\,dz / L \tag{6.16}$$

The resultant viscosity change due to pressure is

$$\frac{\eta_p}{\eta} = \frac{\eta_{0p} f(\lambda\dot{\gamma})}{\eta_0 f(\lambda\dot{\gamma})} = \exp\left[2.303\left(\frac{A_2 + A_3 P_{avg}}{A_4 - A_1 P_{avg}} - \frac{A_2}{A_4}\right)\right] \tag{6.17}$$

where η_{0P} represent the zero-shear viscosity at elevated pressure.

Yamada and Porter applied this method for the evaluation of viscosity data of polycarbonate which varied with different length capillary dies at the same temperature.

Rather than evaluating the pressure coefficient from extensive capillary rheometry, this method provides a convenient procedure using the pressure dependence of glass transition temperature that is available for typical polymers in literature [Schouten et al.,1991; Simha and Simha, 1971; Miller, 1971].

6.1.4 Correction of Shear Rates

The apparent shear rate, which is based on the parabolic velocity profile of Newtonian fluids, is corrected for non-Newtonian fluids having non-parabolic velocity profiles.

The Rabinowitsch correction [Rabinowitsch, 1929] is a useful technique to evaluate true shear rates. The correction is performed using the true wall shear stress and apparent shear rate. The slope of the logarithmic plot of true stress and apparent shear

rate is calculated.

$$h = \frac{d \log \dot{\gamma}_{wa}}{d \log \tau_w} \tag{6.18}$$

For a power-law fluid, the exponent n is equal to $1/h$. The corrected true shear rate is calculated by

$$\dot{\gamma}_w = \frac{(3n+1)}{4n} \dot{\gamma}_{wa} \tag{6.19}$$

The Schuemmer correction [Chmiel and Schuemmer, 1971; Schuemmer and Worthoff, 1978] is a convenient approximate procedure giving true shear rates to within about 3%. The representative shear rate is defined, at which the true viscosity equals the apparent viscosity at the same flow rate.

$$\eta(\dot{\gamma}^*) = \eta_0(\dot{\gamma}_{wa}) \tag{6.20}$$

The representative shear rate is given as some fraction, x*, of the apparent shear rate:

$$\dot{\gamma}^* = x^* \dot{\gamma}_{wa} \tag{6.21}$$

where, for a power-law fluid,

$$x^* = \left(\frac{3n+1}{4n} \right)^{n/(n-1)} \tag{6.22}$$

For the values of n ranging from 0.35 to 1.2, Schuemmer and Worthoff [1978] noted that x* is a weak function of n: $x^* = 0.83 \pm 4\%$.

The Schuemmer correction is usefully applied when the true wall shear stress is not available, since the Rabinowitsch correction can not be performed in such cases. Laun [1983, 1989] reported that this single point correction is as accurate as the Rabinowitsch correction for several polymer melts and solutions.

6.2 Pure Polystyrene

Capillary rheometry was performed for pure polystyrene at 150, 175, 188, and 200 ^{0}C discharging from the capillary at atmospheric pressure, using three capillary dies with different *(L/D)* ratios of 0, 40, and 75 and the same diameter and entry angle. These viscosity data of pure PS are used as the reference in comparison with those of gas-loaded PS.

6.2.1 Wall Friction

The wall friction needs to be considered in the current study because the spcial sealing with a series of grooves filled up by Teflon washers and Viton O-rings was adopted causing additional friction at the barrel wall. Figure 6.1 shows the variation of wall friction force as the plunger passes the empty barrel at 188 ^{0}C. A sudden increase of the wall friction in the beginning of movement followed by a fast decay to a steady value was monitored for all conditions of temperatures ranging 150 to 200 ^{0}C and apparent shear rates from 0.5 to 2000 s^{-1}. The initial high friction is caused by the initial concentric alignment of plunger and barrel, and does not persist after alignment has occurred. Therefore, all the data were chosen after 3-inch movement of plunger from the beginning. The measured wall friction data is fitted to logarithmic equation as a function of shear rate at each temperature as shown in Figure 6.2. The wall friction was subtracted from the raw force reading giving net force for further calculations.

6.2.2 Bagley Correction

The Bagley plots are constructed in Figures 6.3(a) through 6.3(d) for pure polystyrene at 150, 175, 188 and 200 ^{0}C along with three *(L/D)* ratios of 0, 40, and 75.

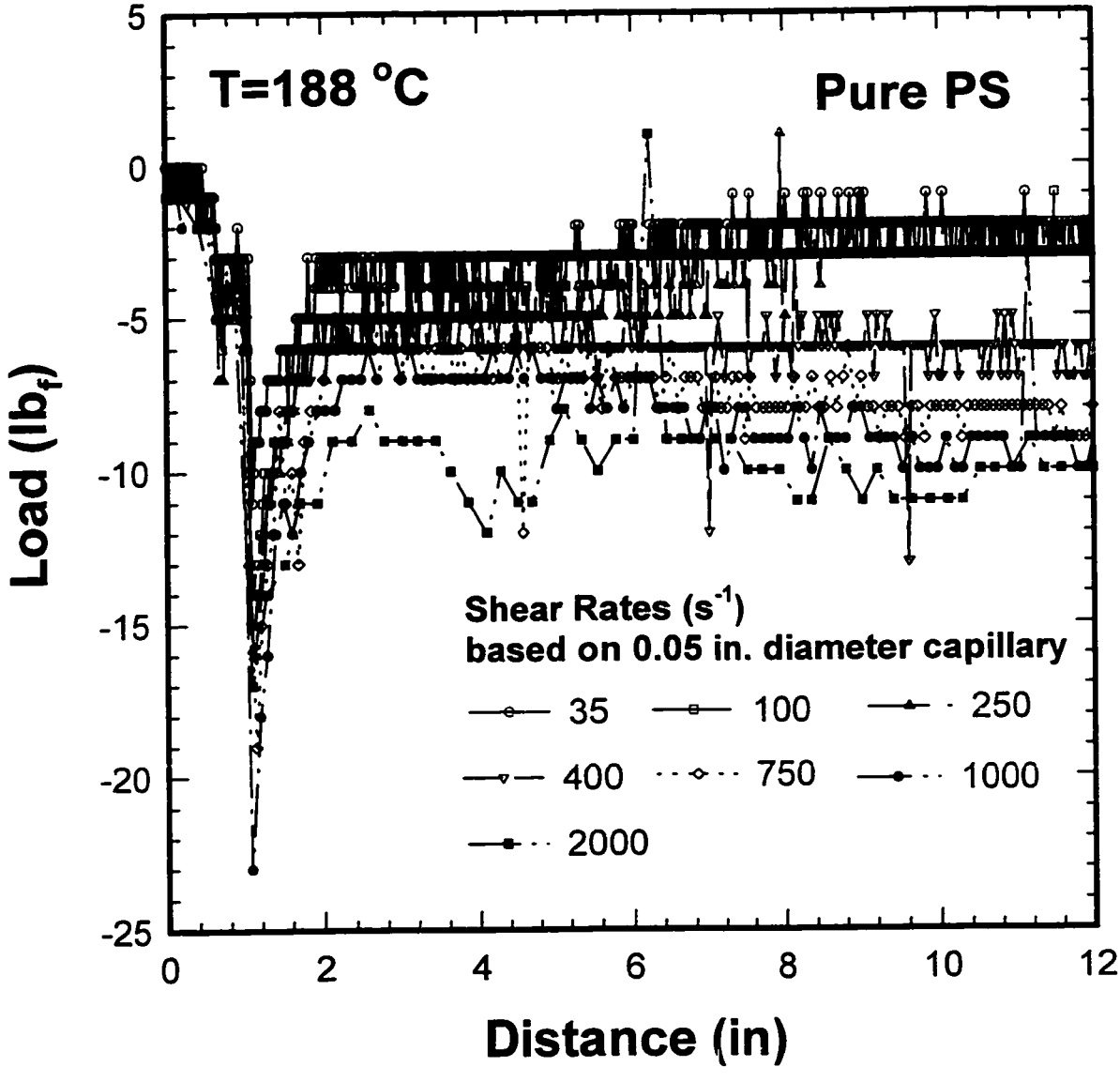

Figure 6.1
Variation of Wall Friction Force measured at empty Barrel at T=188 ^{0}C

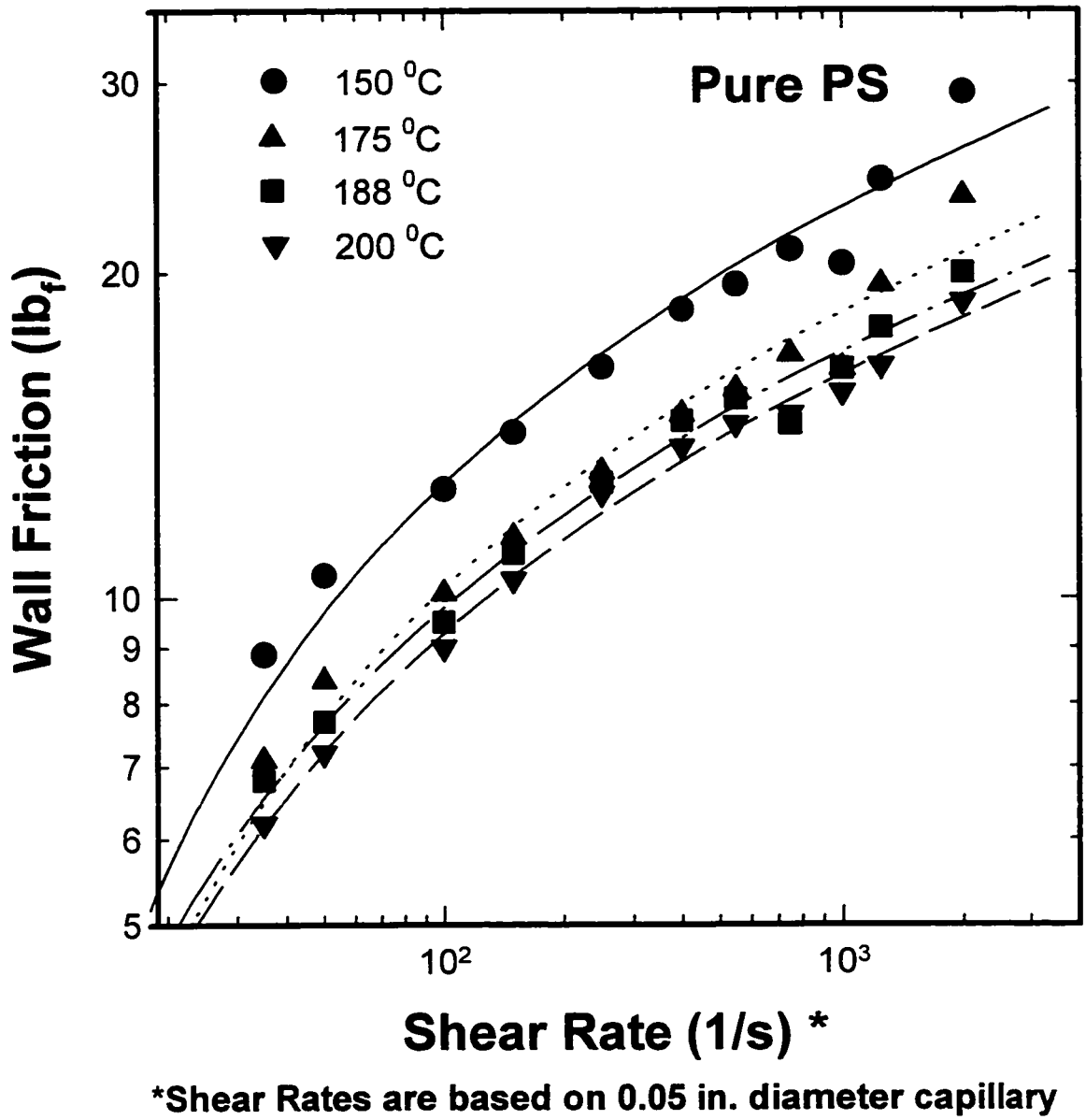

Figure 6.2
Wall Friction Force fitted by Logarithmic Equation at T=150, 175, 188, and 200 °C

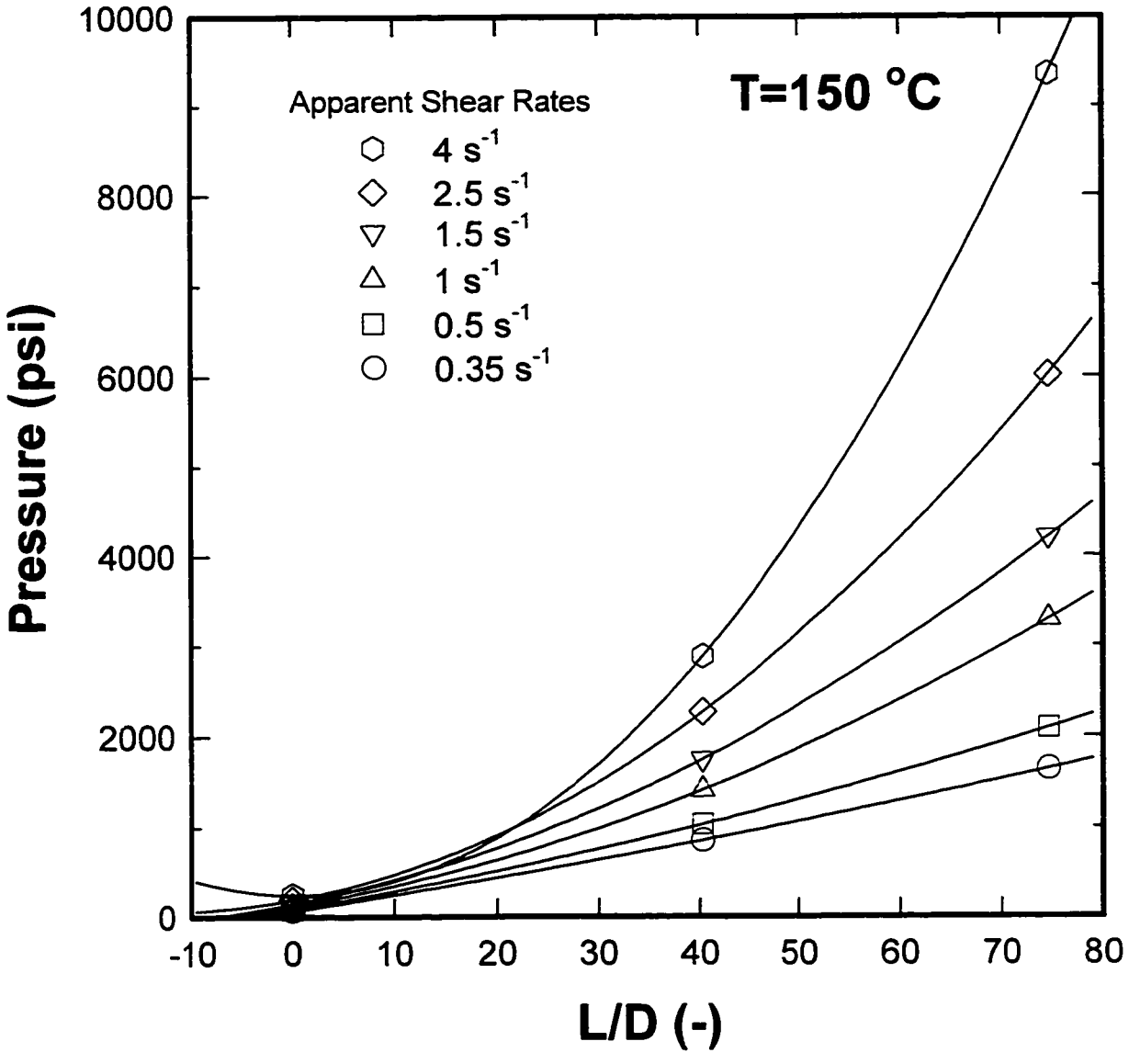

Figure 6.3(a)
Bagley Plots for pure PS at T=150 ^{0}C

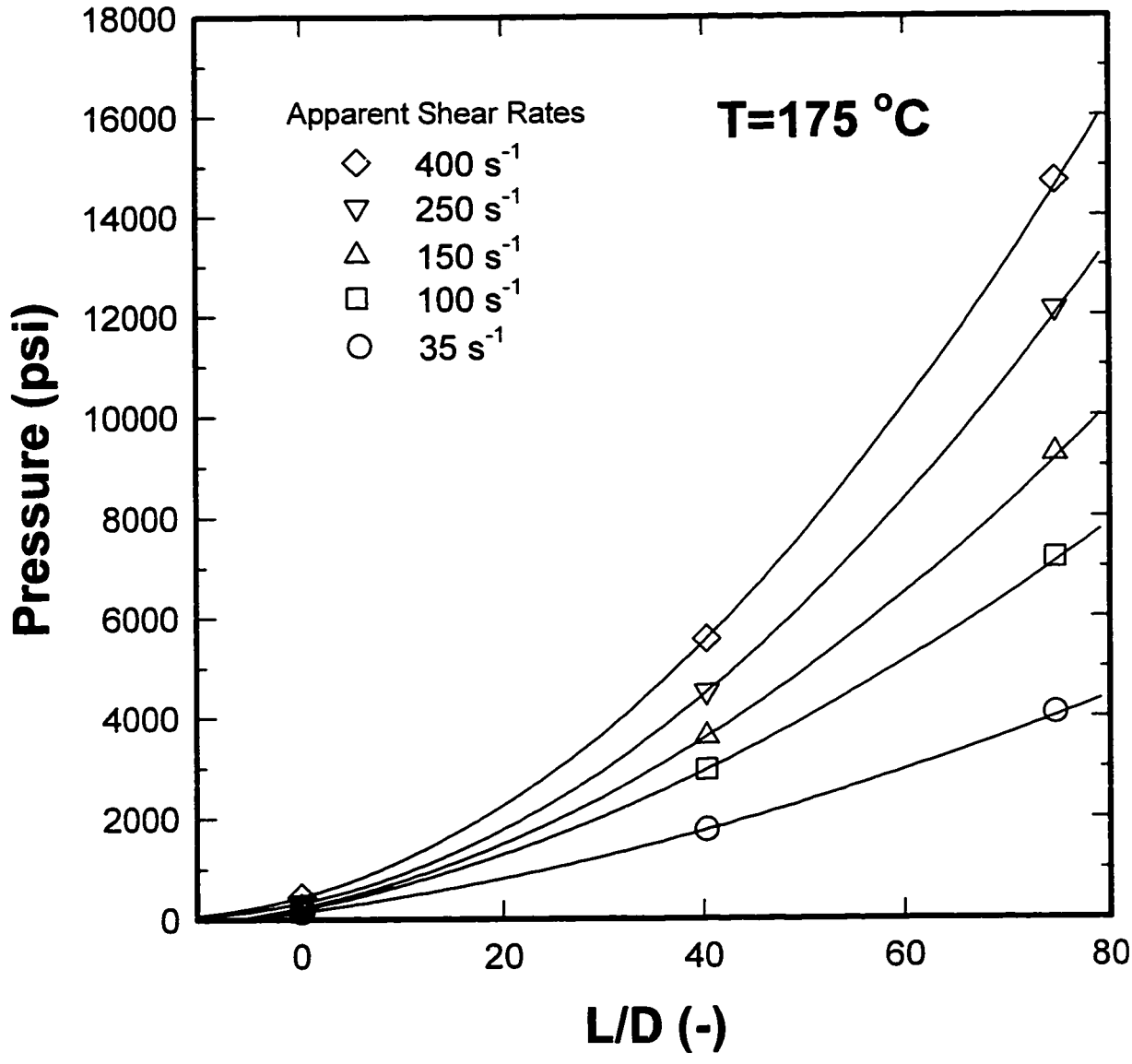

Figure 6.3(b)
Bagley Plots for pure PS at 175 ^{0}C

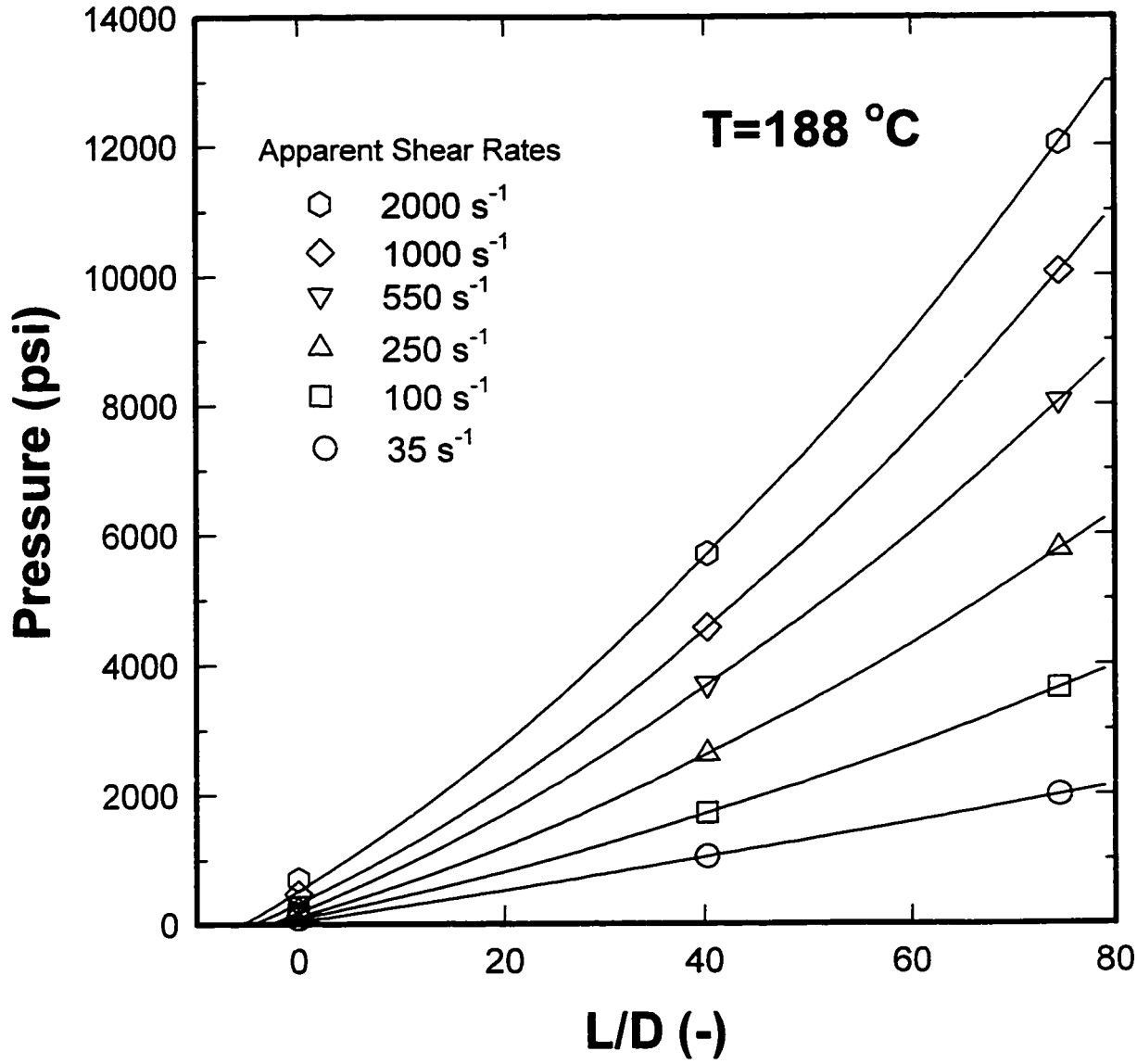

Figure 6.3(c)
Bagley Plots for pure PS at 188 ^{0}C

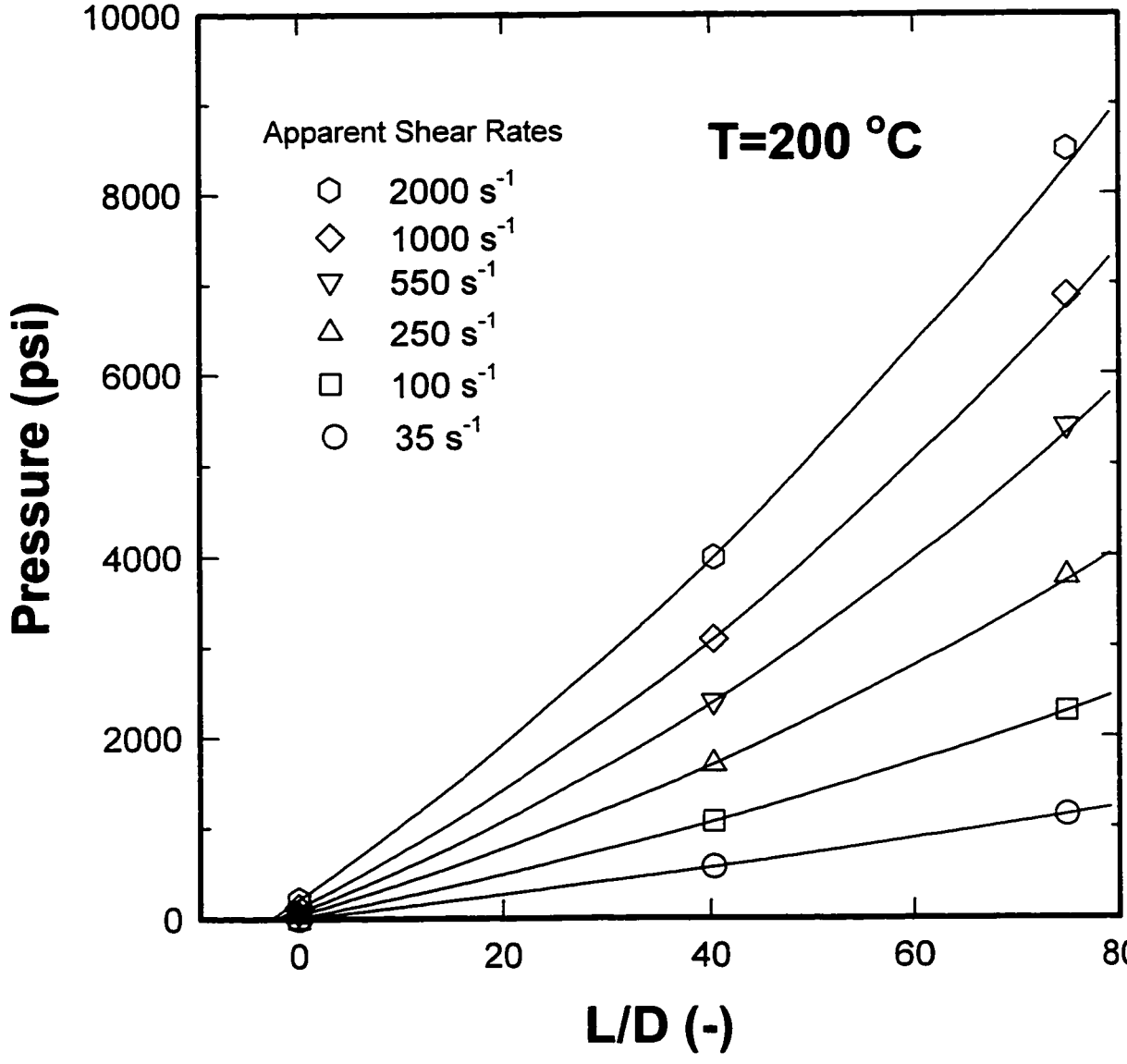

Figure 6.3(d)
Bagley Plots for pure PS at 200 ^{0}C

For lower temperatures and higher shear rates, the pressure drop shows significant increase causing non-linearity. The shear rate at which the non-linearity begins is higher for higher temperature and vice versa.

The orifice pressure drop, ΔP_0, which represents the magnitude of entry pressure loss, is plotted as a function of apparent shear rate in Figure 6.4(a). The orifice pressure drop is highest at 150 ^{0}C and shows sudden decreases at 175 ^{0}C and higher temperatures. In Figure 6.4(b) the ratio of orifice pressure drop to upstream pressure drop also shows decrease as temperature increases. Since the ratio is less than 6 percent for the highest shear rate at 200 ^{0}C, it is a reasonable assumption that the Bagley correction is negligible for temperatures higher than 200 ^{0}C, i.e., $(T - T_g) \geq 100$. Accordingly, for gas loaded systems having same $(T - T_g)$, the Bagley correction can be excluded with less than 6 percent error.

Since Equations (6.4) and (6.5) can not be directly applied due to the non-linearity, the method with orifice pressure drop is adopted here (Equation 6.6). The Bagley corrected pressure drops are plotted as a function of (L/D) ratio in Figure 6.5(a) and 6.5(d). The non-linearity of Bagley corrected plots indicates that further corrections for the effects of pressure-dependent viscosity are necessary, especially at 150 ^{0}C.

6.2.3 Schuemmer Correction

Due to the non-linearity of Bagley plots, the true wall shear stress is not obtained by the Bagley correction. Unfortunately the Rabinowitsch correction requires the true wall shear stress under conditions where the pressure gradient is linear. Therefore the approximate Schuemmer correction rather than the Rabinowitsch method was employed for the correction of apparent shear rates.

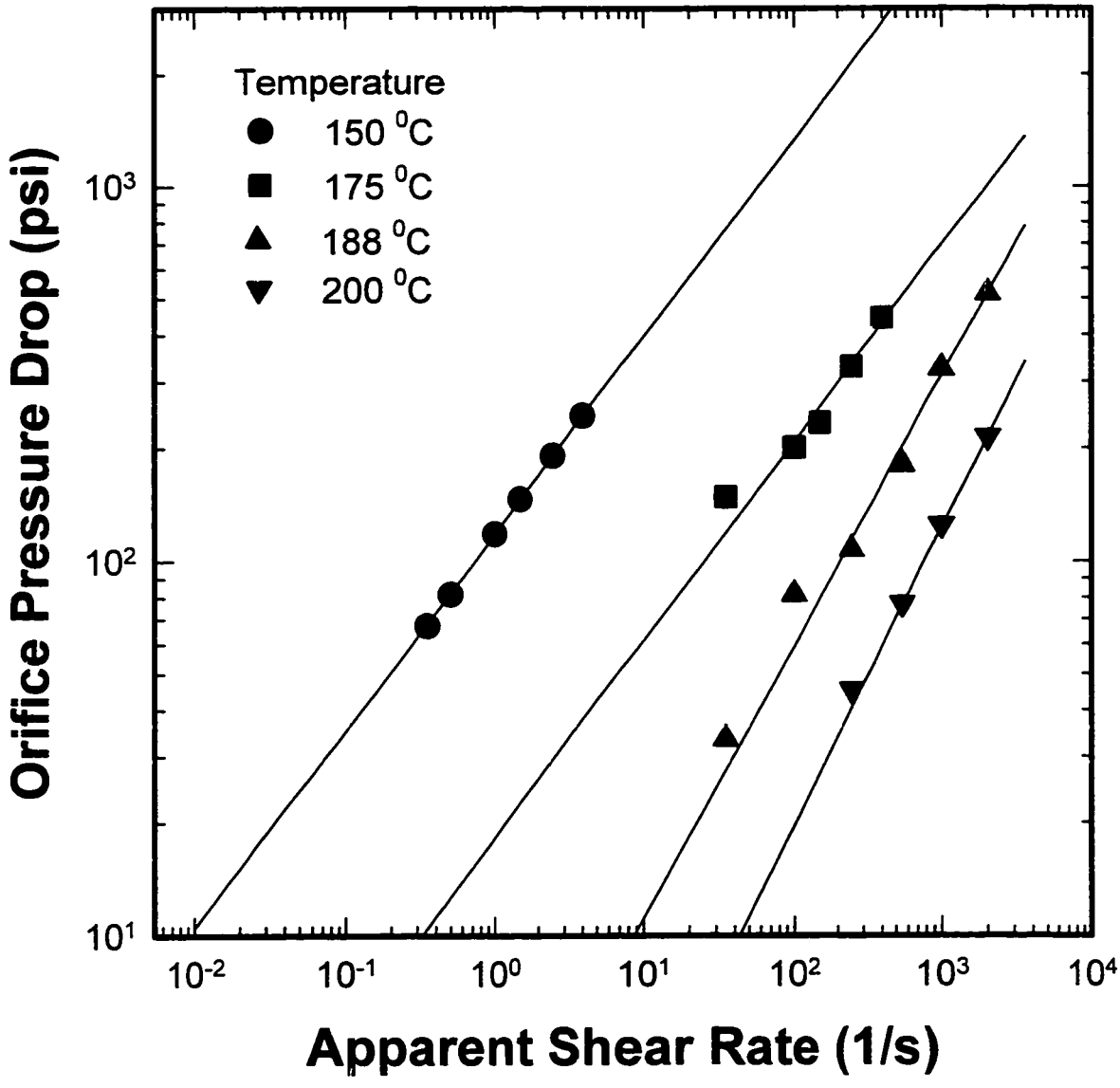

Figure 6.4(a)
Orifice Pressure Drops for pure PS at T=150, 175, 188, and 200 ^{0}C.

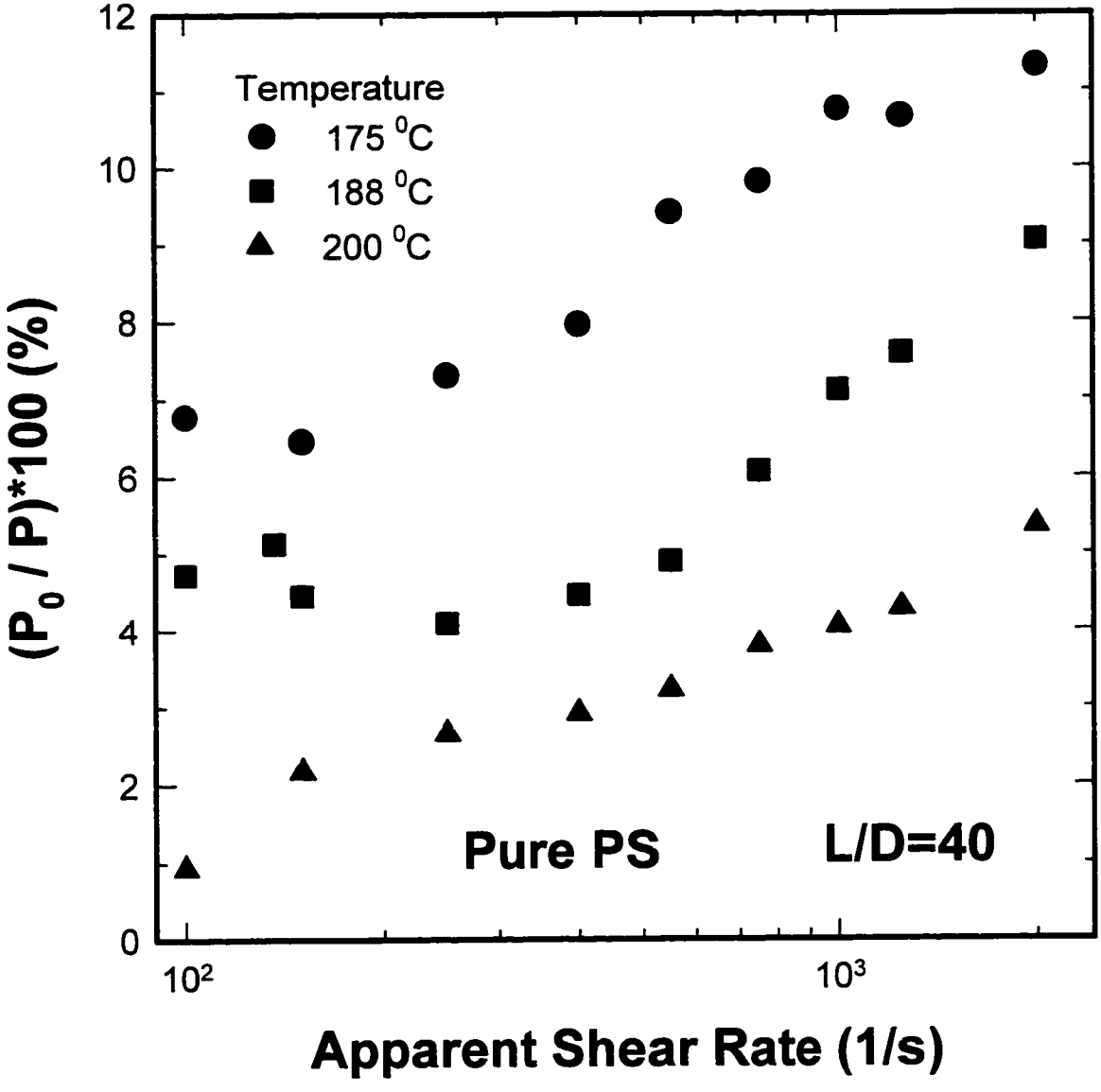

Figure 6.4(b)
Relative Magnitude of Orifice Pressure Drops with respect to Total Pressure Drops measued using Capillary Die with (L/D)=40 for pure PS at *T*=150, 175, 188, and 200 °

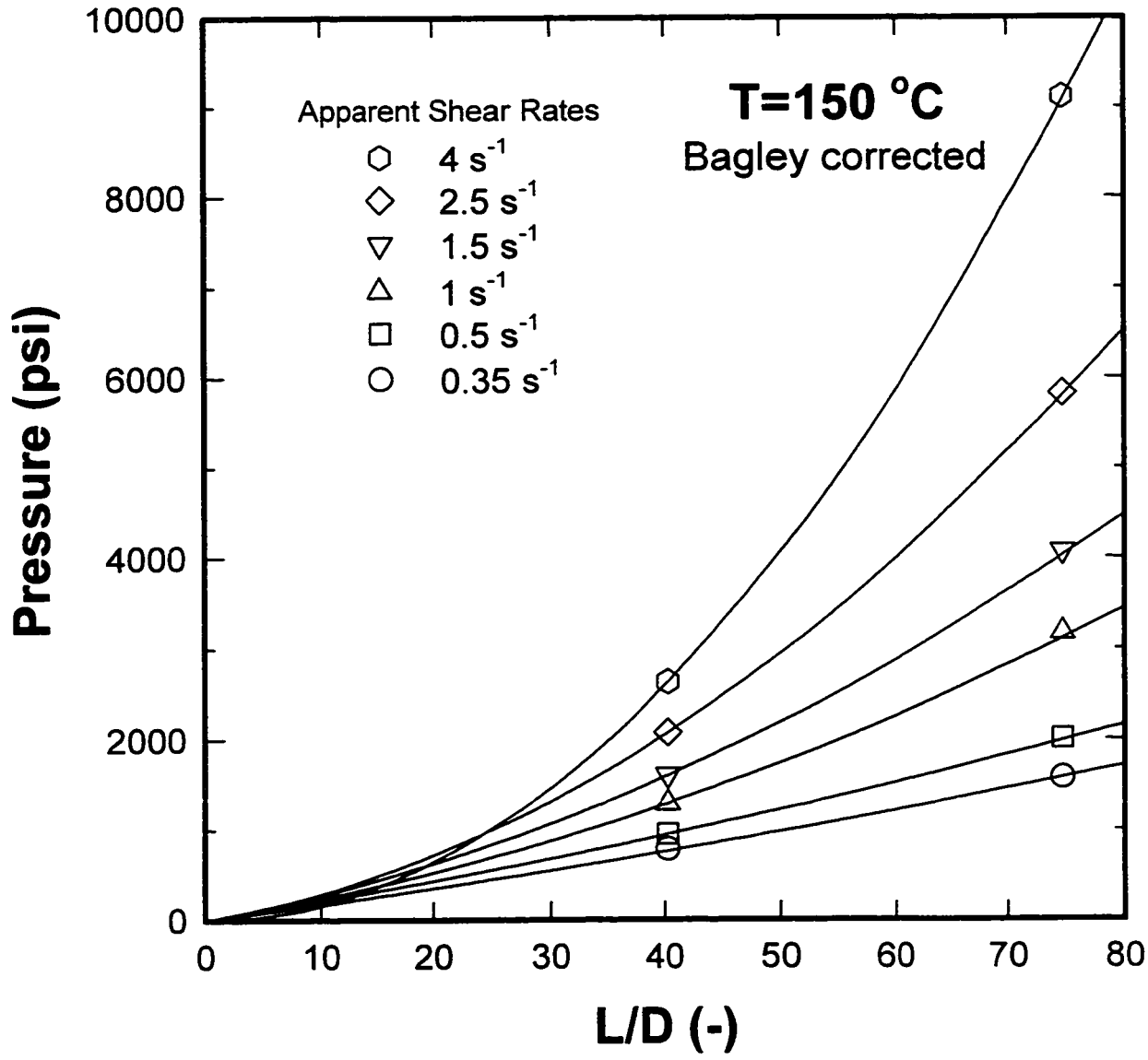

Figure 6.5(a)
Bagley Plots for pure PS at T=150 ^{0}C after Bagley Correction

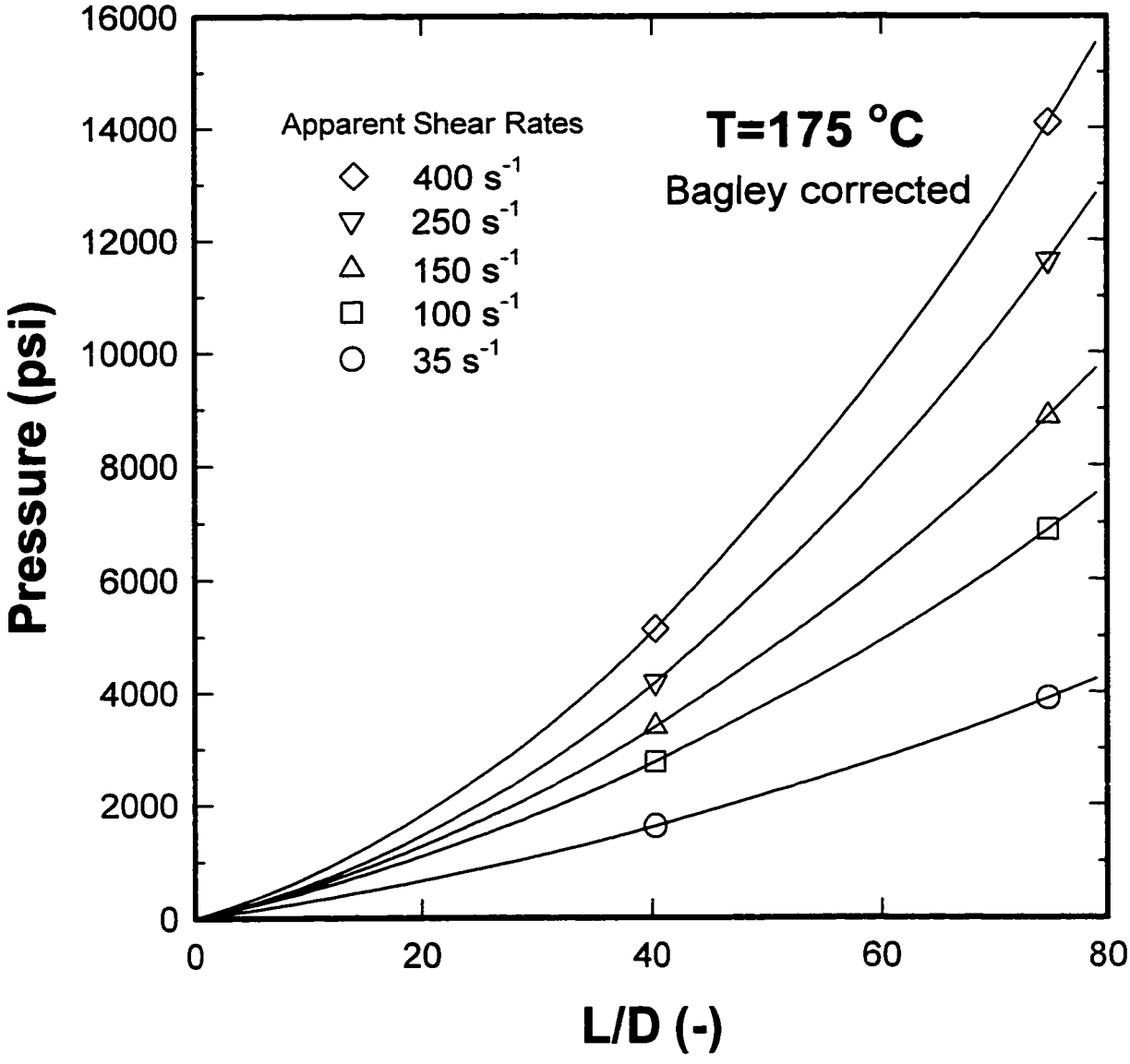

Figure 6.5(b)
Bagley Plots for pure PS at T=175 ^{0}C after Bagley Correction

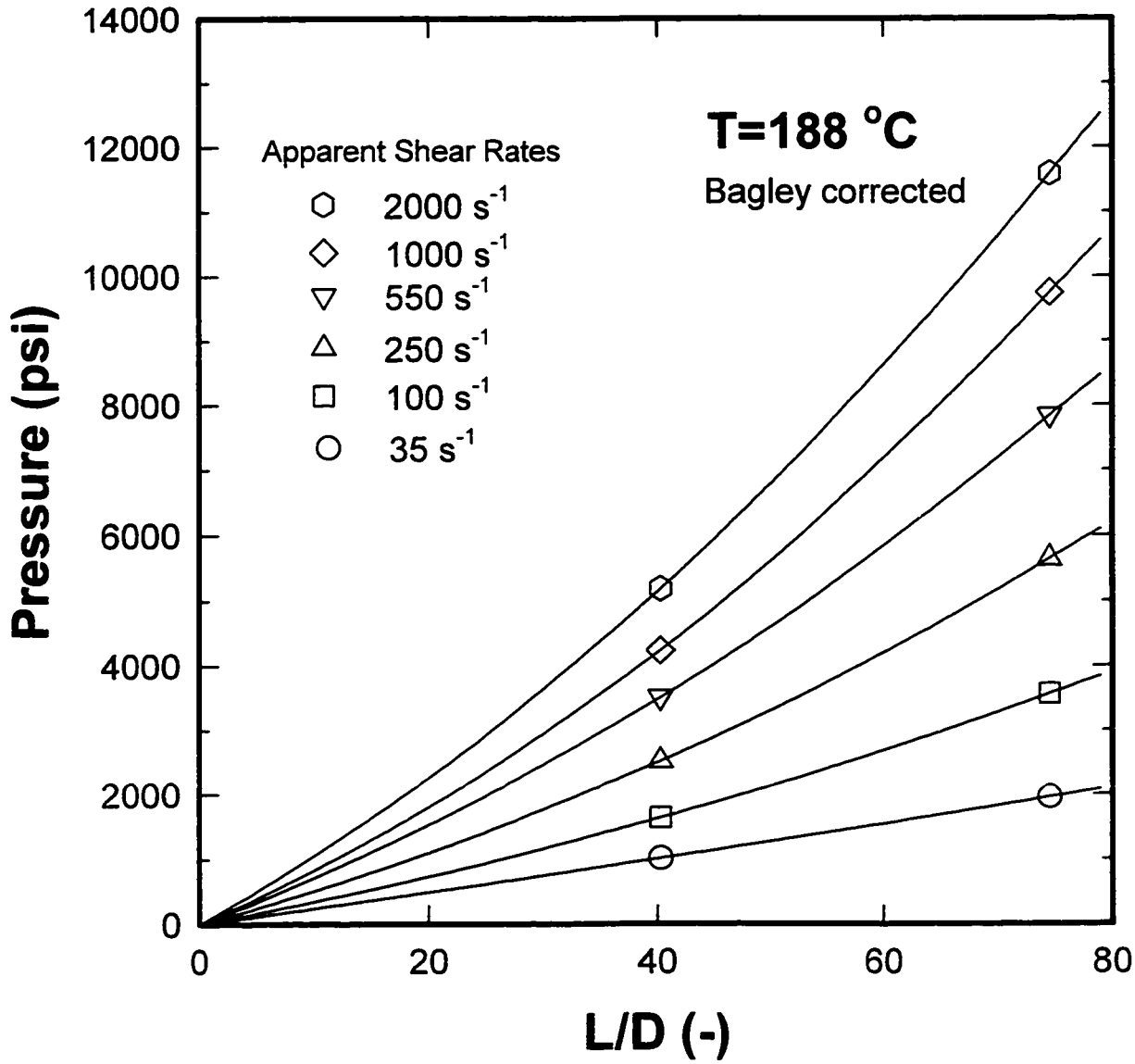

Figure 6.5(c)
Bagley Plots for pure PS at T=188 ^{0}C after Bagley Correction

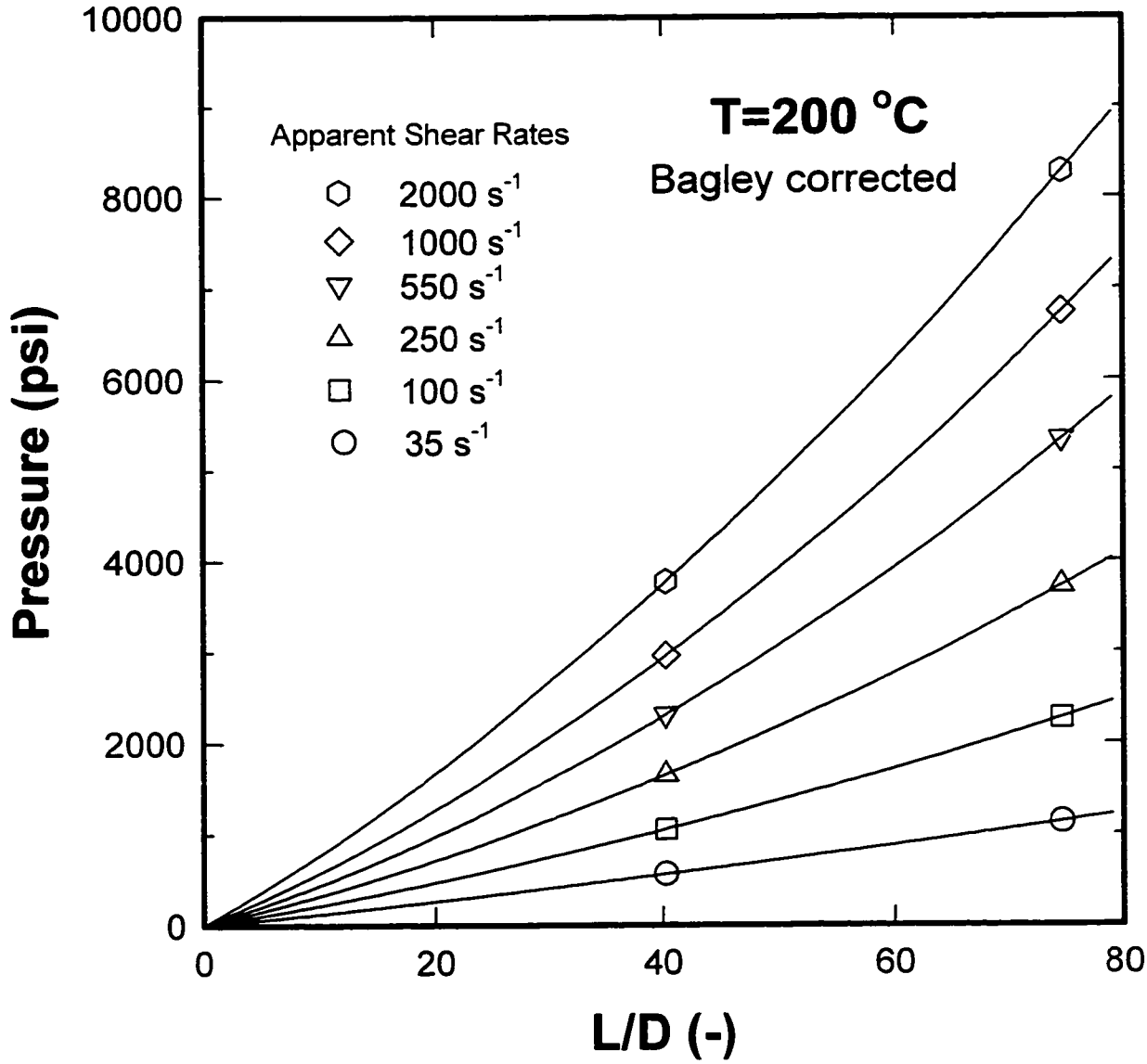

Figure 6.5(d)
Bagley Plots for pure PS at T=200 ^{0}C after Bagley Correction

The Bagley-Schuemmer corrected viscosity is represented for two *(L/D)* ratios and compared with the complex viscosity measured by the Weissenberg Rheogoniometer in Figure 6.6. The discrepancy of Bagley-Rabinowitsch corrected viscosities for two different *(L/D)* ratios is evident and becomes substantial at lower temperatures, indicating the necessity of further corrections for the dependence of viscosity on pressure, as expected from the non-linear Bagley plots.

An apparent shear thickening behavior, which is contrary to the known behavior of polystyrene melts, is observed at 150 ^{0}C for high shear rates. Such a peculiar viscosity increase was observed earlier by Ballman [1964] along with non-linear Bagley plots for polystyrene at 149 ^{0}C.

As the die length increases, the contribution of pressure dependent viscosity becomes more significant, resulting higher load cell readings and accordingly overestimated viscosities. If the Bagley-Schuemmer corrected viscosity is utilized without further correction, the data from shorter dies, where the effect of pressure on viscosity is less pronounced, is preferred (of course, the die length should be sufficiently long enough to neglect the length for entry effect). In the current study the Bagley-Schuemmer corrected viscosity values were obtained using the shorter die having the (L/D) ratio of 40.

The complex viscosity and the Bagley-Schuemmer corrected shear viscosity superimpose successfully at transitional shear rates, supporting the Cox and Merz rule [1958] and enabling the modeling over a wide range of shear rates. The modified Cross model, Equation (2.4) was applied for the Bagley-Schummer corrected viscosity and the complex viscosity as shown in Figure 6.7. The parameters of the modified Cross model are tabulated in Appendix II.

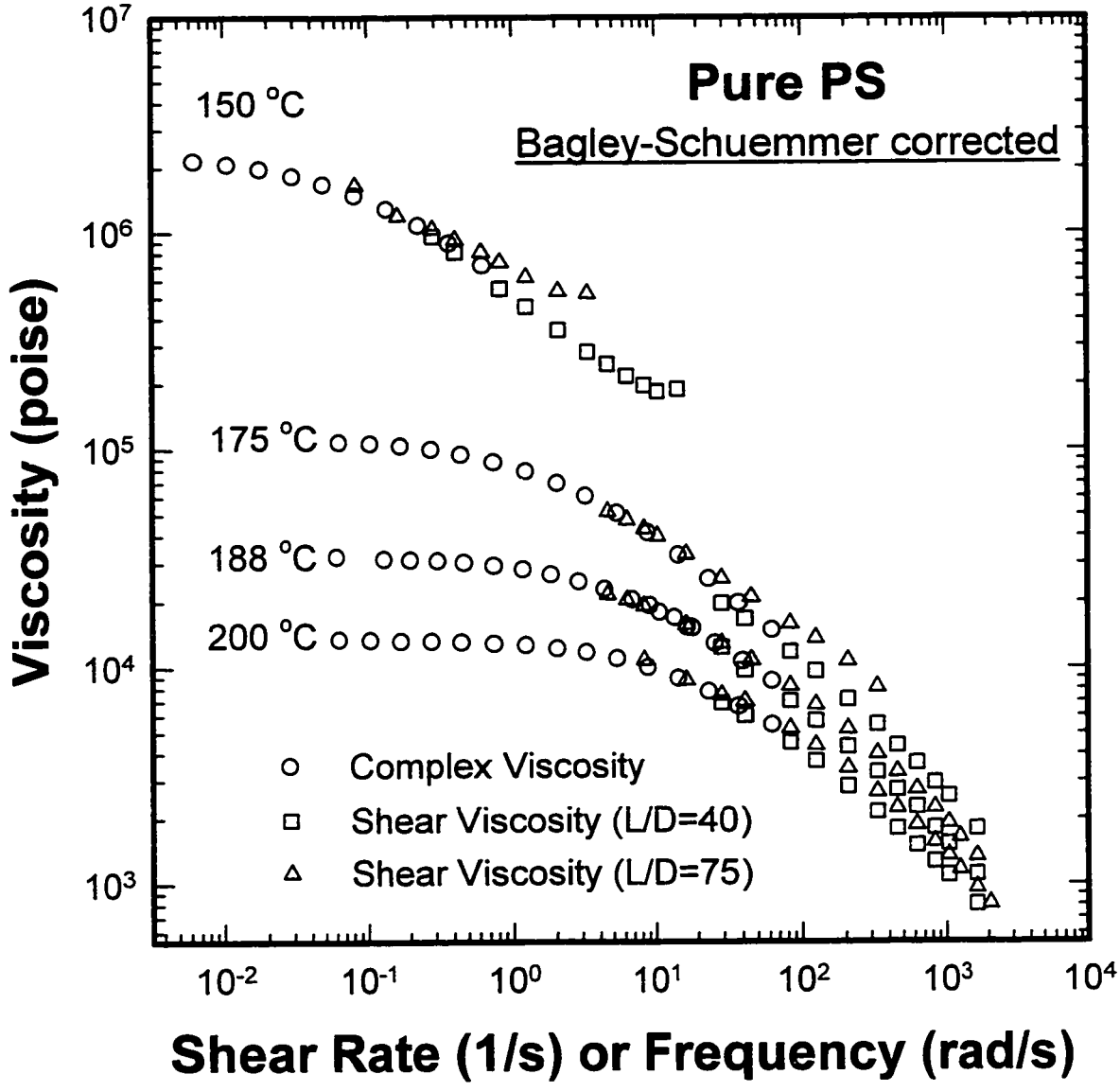

Figure 6.6
Complex Viscosity and Bagley-Schuemmer corrected Viscosity using Dies with (L/D)=40 and 75 for pure PS at T= 150, 175, 188, and 200 ^{0}C.

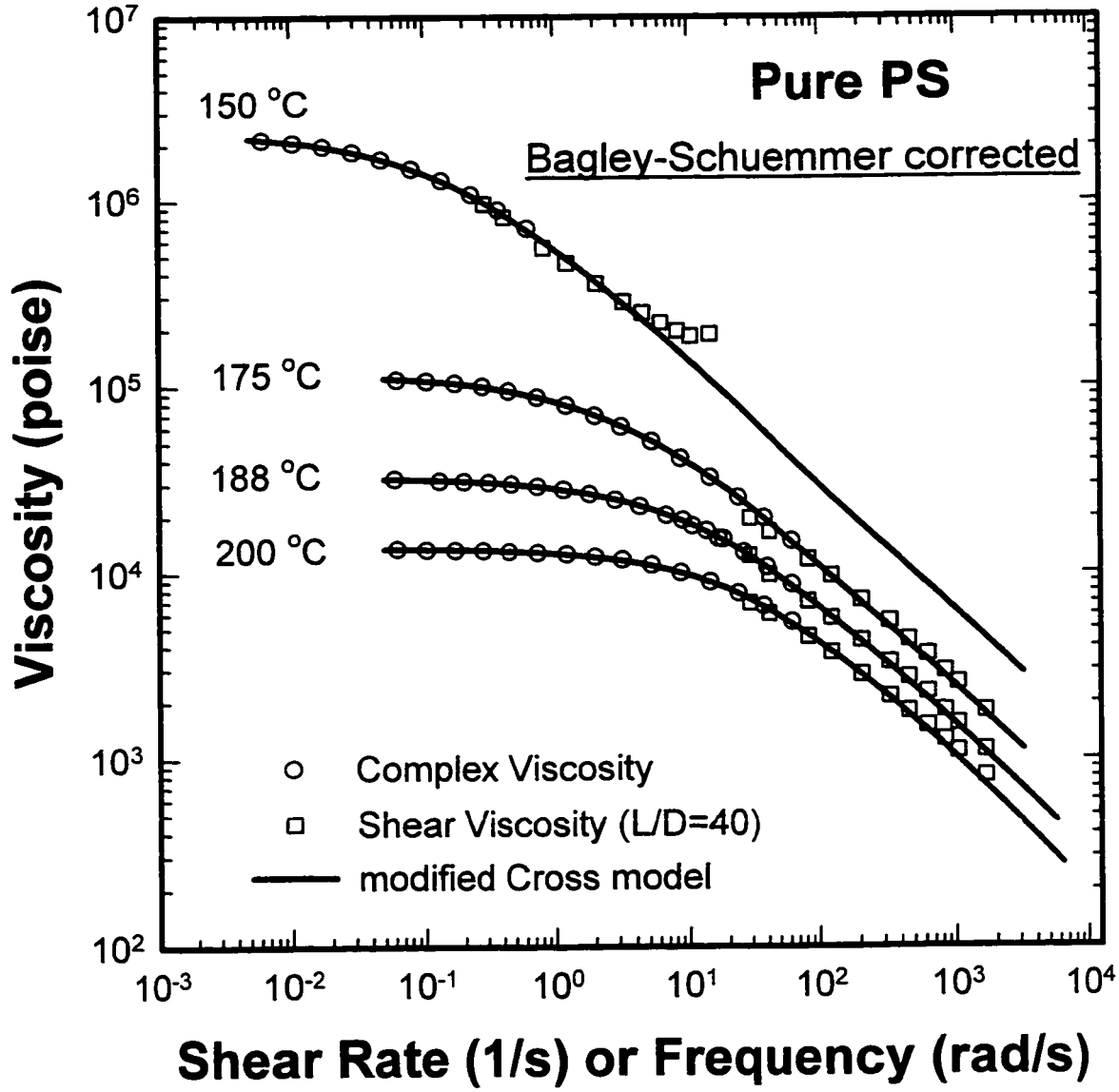

Figure 6.7
Modified Cross Modeling of Complex Viscosity and Bagley-Schuemmer corrected Viscosity using Dies with (L/D)=40 and 75 for pure PS at T=150, 175, 188, and 200 ^{0}C.

6.2.4 Pressure Correction

In order to refine the Bagley-Schuemmer corrected viscosity data, a pressure correction was performed on the Bagley corrected pressure drops. The pressure correction procedure in the current study was based on the method of Penwell [1971] but modified for the determination of pressure coefficient and the computation of the average pressure used in Equation (6.8).

$$\frac{\eta_p}{\eta} = \exp(bP_{avg}) \tag{6.8}$$

6.2.4.1 Determination of Pressure Coefficients

The determination of pressure coefficient in the current study was for power-law fluids. The z-component of equation of motion for steady flow of incompressible fluid is

$$-\frac{\partial P}{\partial z} - \frac{1}{r}\frac{\partial}{\partial r}(r\tau_{rz}) = 0 \tag{6.23}$$

Assuming that the pressure correction factor is independent of shear rate:

$$\tau_{rz} = \tau_{rz}^{\,0}\, e^{bP} = m\dot{\gamma}^{n} = m_0 e^{bP}\dot{\gamma}^{n} \quad ; \quad \dot{\gamma} = -\frac{\partial v_z}{\partial r} \tag{6.24}$$

where m is the consistency, n is the flow index, and the subscript and superscript 0 designate values at a reference state.

Substituting Equation (6.23) into Equation (6.22) and rearranging gives

$$\frac{e^{-bP}}{m_0}\frac{\partial P}{\partial z} = -\frac{1}{r}\frac{\partial}{\partial r}\left\{r\left(-\frac{\partial v_z}{\partial r}\right)^{n}\right\} = C_1 \tag{6.25}$$

where C_1 is an integration constant.

The integration constant C_1 is calculated by solving the z-dependent equation of Equation

(6.24) with the boundary condition.

$$\int \frac{e^{-bP}}{m_0} dP = C_I \int dz \quad or \quad \frac{e^{-bP}}{m_0} = C_I z + C_{II} \tag{6.26}$$

$$At \quad z = 0, \quad P = P_0$$
$$z = L, \quad P = P_L$$

where C_{II} is an integration constant.

Integration constants are computed as:

$$C_I = \frac{e^{-bP_L} - e^{-bP_0}}{-bm_0 L} \qquad and \qquad C_{II} = \frac{e^{-bP_0}}{-bm_0} \tag{6.27}$$

The pressure distribution across die length is obtained as:

$$\frac{z}{L} = \frac{e^{-bP} - e^{-bP_0}}{e^{-bP_L} - e^{-bP_0}} \qquad or \qquad P = \frac{\ln\left\{e^{-bP_0} + \frac{z}{L}\left(e^{-bP_L} - e^{-bP_0}\right)\right\}}{-b} \tag{6.28}$$

Equation (6.27) is the same as Equation (6.7) derived by Penwell et al. [1971]. Once the pressure coefficient is determined, the pressure distribution across the die length is calculated.

Integration of r-dependent terms of Equation (6.24) yields

$$\left(-\frac{\partial v_z}{\partial r}\right)^n = -\frac{C_I}{2} r + \frac{C_{III}}{r} \tag{6.29}$$

At $r = 0$, both side terms should be finite. Then C_{III} needs to be zero giving

$$\frac{dv_z}{dr} = -\left(-\frac{C_I}{2} r\right)^{\frac{1}{n}} \tag{6.30}$$

Integration of Equation (6.30) gives

$$v_z = -\frac{n}{n+1}\left(-\frac{C_I}{2}\right)^{\frac{1}{n}} r^{\frac{n+1}{n}} + C_{IV} \tag{6.31}$$

At $r = R$, $v_z = 0$ (no-slip condition).

The velocity profiles is represented as:

$$v_z = v_{\max}\left(1-\left(\frac{r}{R}\right)^{\frac{n+1}{n}}\right) \quad ; \quad v_{\max} = \frac{n}{n+1}\left(-\frac{C_1}{2}\right)^{\frac{1}{n}} R^{\frac{n+1}{n}} \tag{6.32}$$

The volumetric flow rate, Q is calculated as:

$$\begin{aligned} Q = \pi R^2 v_{avg} &= \pi R^2 \int_0^{2\pi}\int_0^R v_{\max}\left(1-\left(\frac{r}{R}\right)^{\frac{n+1}{n}}\right) r\,dr\,d\theta \\ &= \frac{n\pi R^3}{3n+1}\left(\frac{-C_1 R}{2}\right)^{\frac{1}{n}} \end{aligned} \tag{6.33}$$

where R is the radius of capillary die and v_{avg} is the average velocity.

Rearranging Equation (6.27),

$$C_1 = \frac{e^{-bP_L} - e^{-bP_0}}{-bm_0 L} = \frac{\Delta P}{-m_0 L}\,\frac{e^{-bP_L} - e^{-bP_0}}{b\Delta P} \tag{6.34}$$

where $\Delta P = P_0 - P_L$.

Introducing Equation (6.34) into Equation (6.33) gives

$$Q = \frac{n\pi R^3}{3n+1}\left(\frac{\Delta P R}{2m_0 L}\,\frac{e^{-bP_L} - e^{-bP_0}}{b\Delta P}\right)^{\frac{1}{n}} \quad or \quad Q = \frac{n\pi R^3}{3n+1}\left(\frac{\Delta P R}{2m_0 L}\right)^{\frac{1}{n}} e^{\frac{-bP^*}{n}} \tag{6.35}$$

Since $Q = V_P\,\pi\,R_B^2$, where V_P is the plunger speed and R_B is the radius of barrel, Equation (6.35) can be written as:

$$\frac{V_P}{R^3 / R_B^{\,2}} = \frac{n}{3n+1}\left(\frac{\Delta P R}{2m_0 L}\right)^{\frac{1}{n}}\left(\frac{e^{-bP_L} - e^{-bP_0}}{b\Delta P}\right)^{\frac{1}{n}} \tag{6.36}$$

For pure polystyrene, the exit pressure, P_L becomes 0, since the capillary rheometry is performed against atmospheric pressure.

In Equation (6.36), unknown parameters, b, m_0, and n, were determined by curve fitting analysis. At a given temperature, a series of data set from capillary rheometry of pure polystyrene at different shear rates are used to estimate the three parameters.

Figures 6.8(a) through 6.8(d) exhibit curve fittings of Equation (6.36) for pure polystyrene. Obtained pressure coefficients are shown in Figure 6.9 with calculated values using Equation (6.13) and those by Penwell et al.[1971]. The pressure coefficient decreases as temperature increases.

6.2.4.2 Computation of Effective Pressure

From the pressure distribution, Equation (6.28), Penwell et al. [1971] calculated the average pressure by numerical integration. However in the current study, an effective pressure, P^* is taken for the pressure correction. The effective pressure, P^* is defined as the pressure at which the local pressure gradient equals to the apparent one,

$$At \quad P = P^*, \qquad \frac{\partial P}{\partial z} = \frac{P_L - P_0}{L} = \frac{-\Delta P}{L} \tag{6.37}$$

Then P^* can be calculated as:

$$P^* = \frac{\ln\left\{\dfrac{b\Delta P}{e^{-bP_L} - e^{-bP_0}}\right\}}{b} \tag{6.38}$$

Using the effective pressure, the viscosity at $P = P_L$ can be computed as:

$$\eta(P_L) = \eta(P^*)e^{-bP^*} = \frac{e^{-bP_L} - e^{-bP_0}}{b\Delta P}\eta(P^*) \tag{6.39}$$

In Figure 6.10, as the pressure coefficient increases, the non-linearity of pressure profile increases and the effective pressure becomes smaller. Also the non-linearity of pressure distribution develops as the shear rate increases at the same pressure coefficient due to

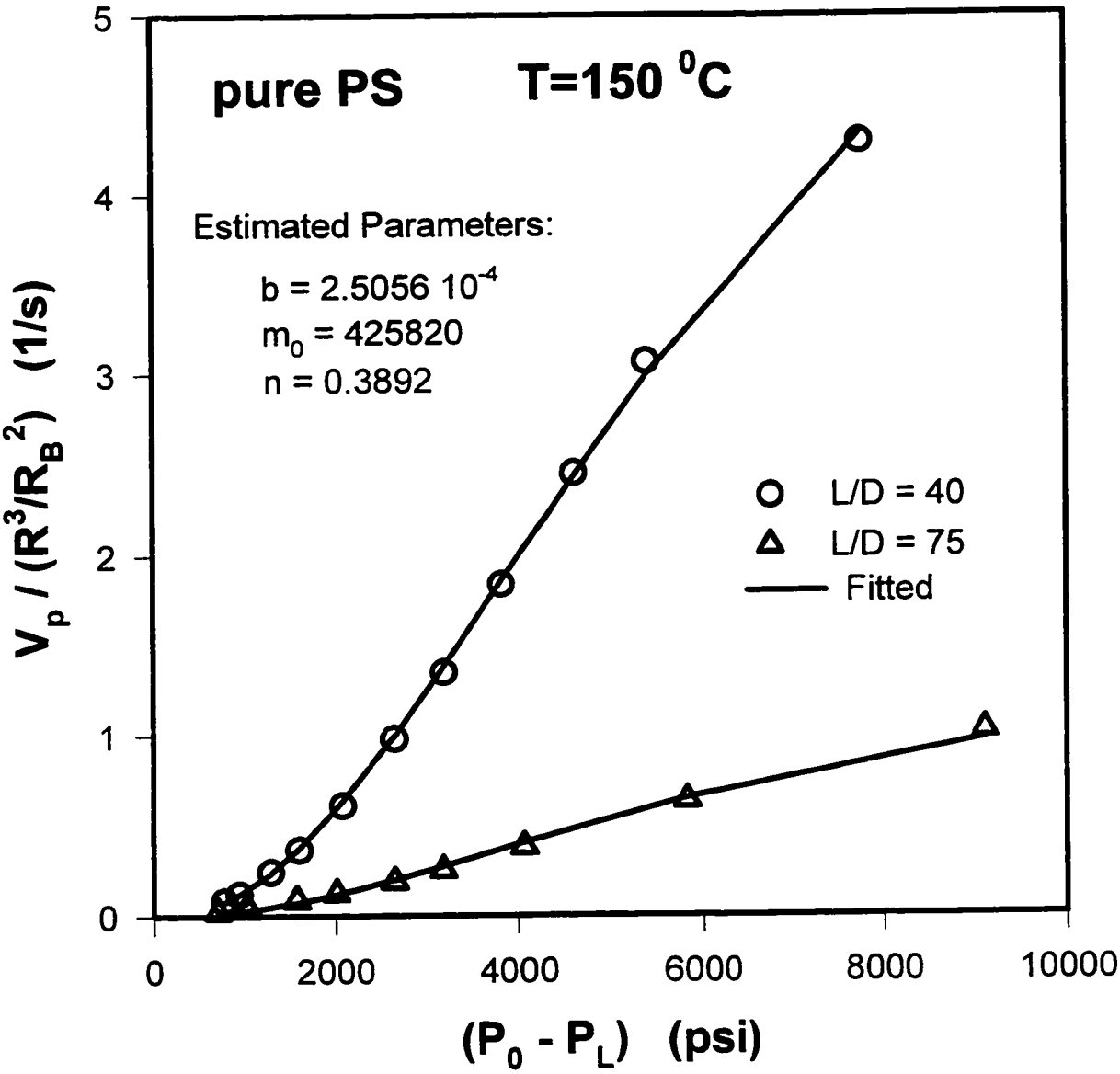

Figure 6.8(a)
Curve Fit of Three Parameter Estimation (Equation 6.35) for pure PS at T=150 ^{0}C.

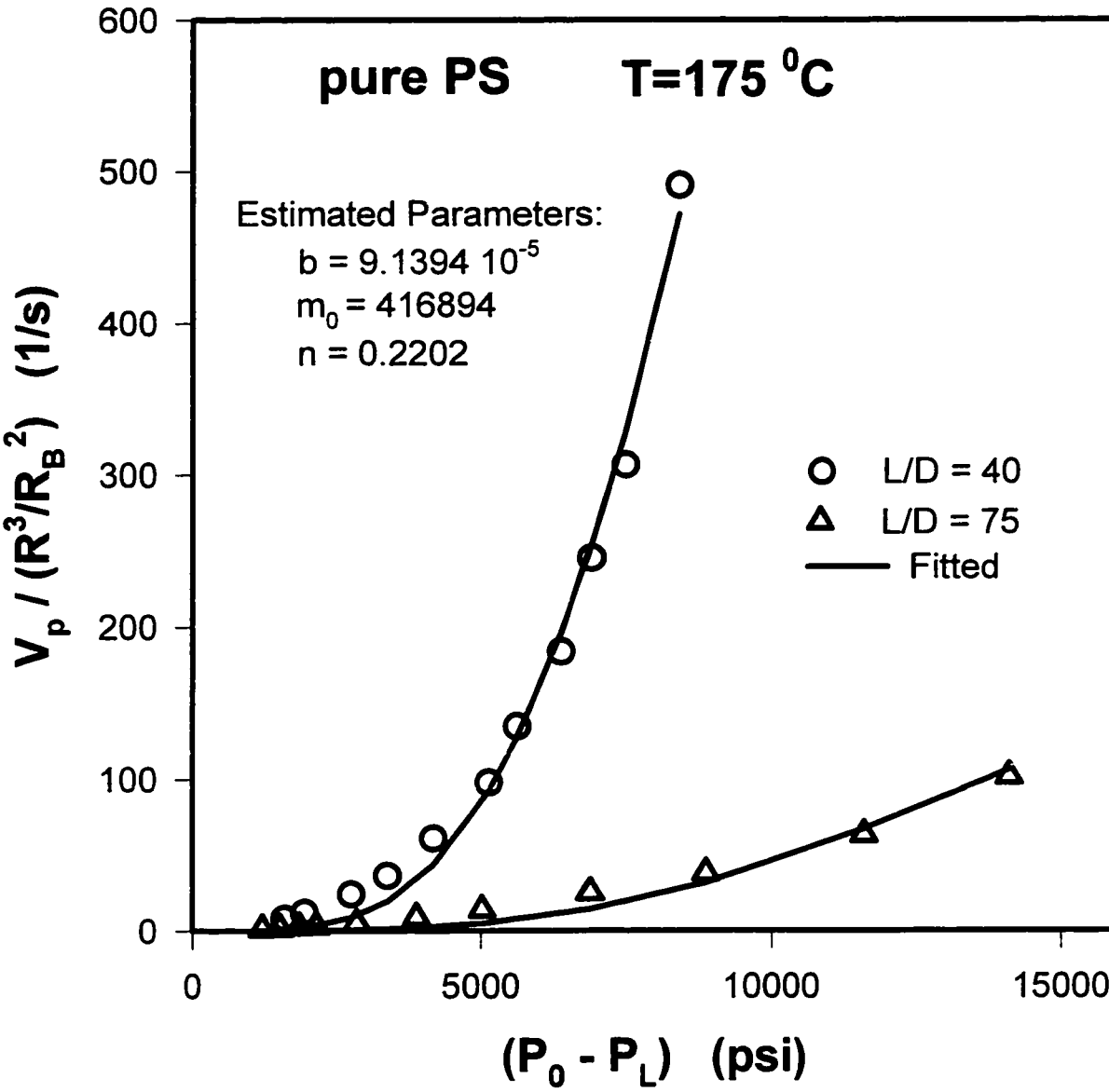

Figure 6.8(b)
Curve Fit of Three Parameter Estimation (Equation 6.35)
for pure PS at *T*=175 ^{0}C.

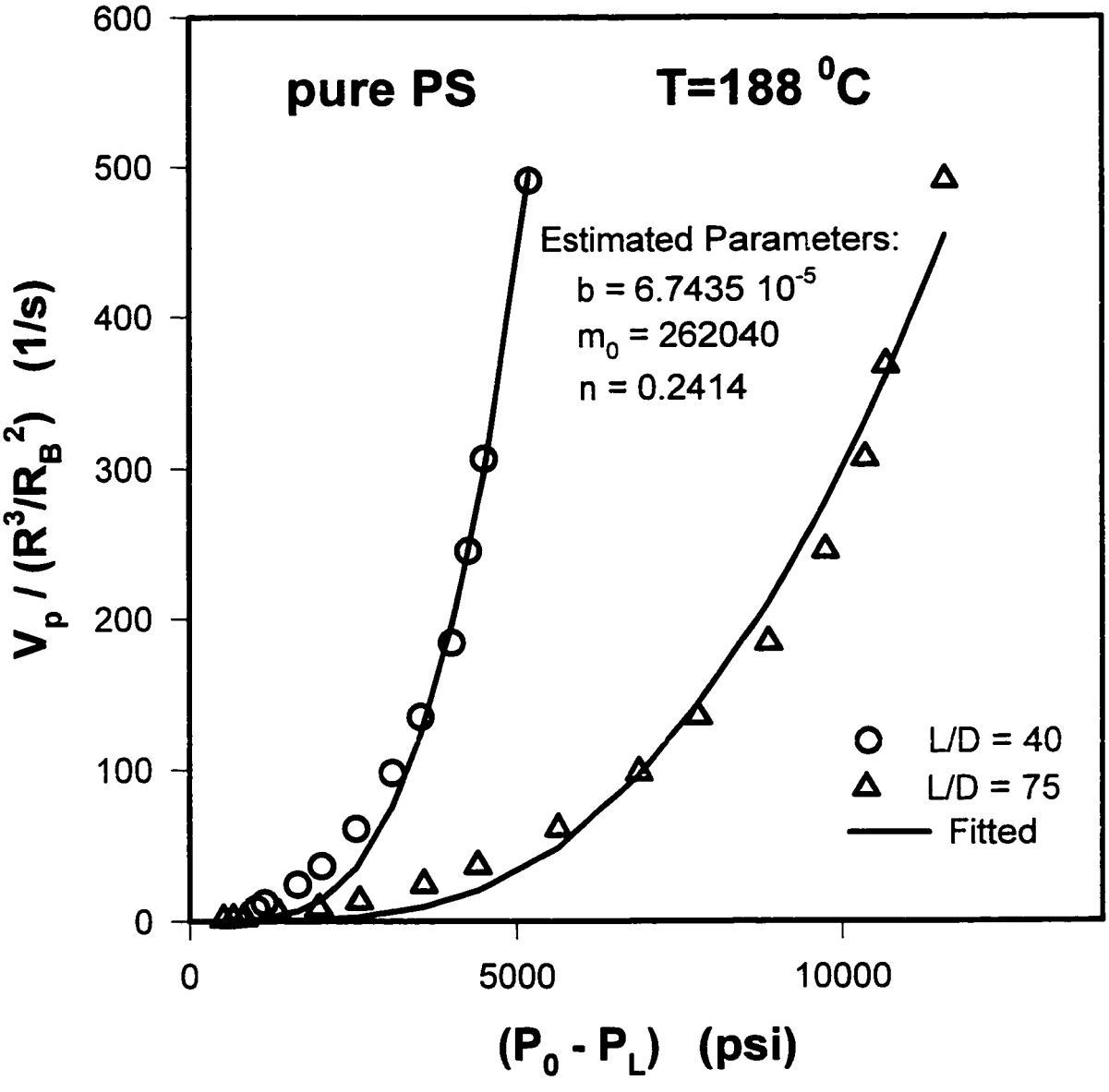

Figure 6.8(c)
Curve Fit of Three Parameter Estimation (Equation 6.35) for pure PS at T=188 ^{0}C.

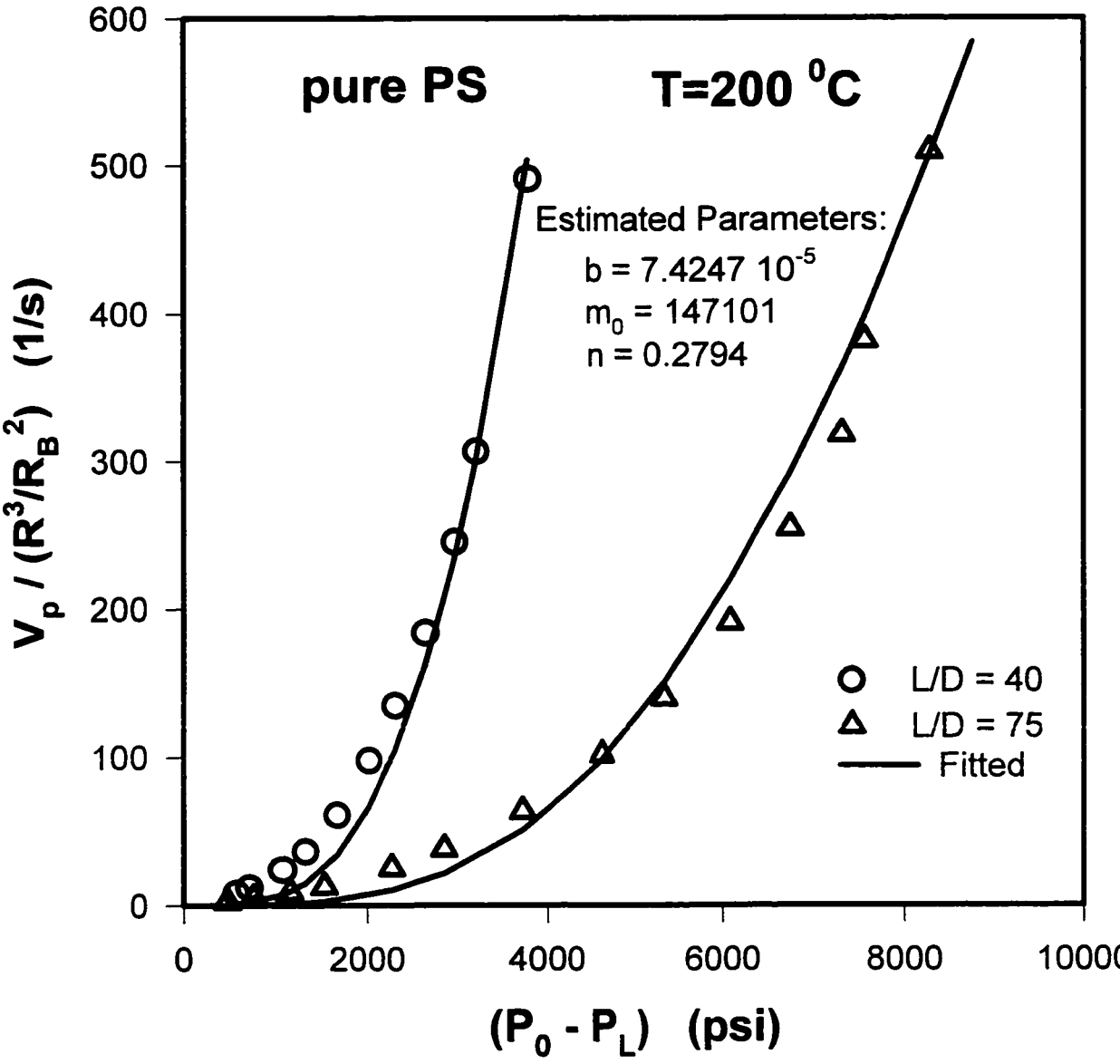

Figure 6.8(d)
Curve Fit of Three Parameter Estimation (Equation 6.35) for pure PS at *T*=200 ^{0}C.

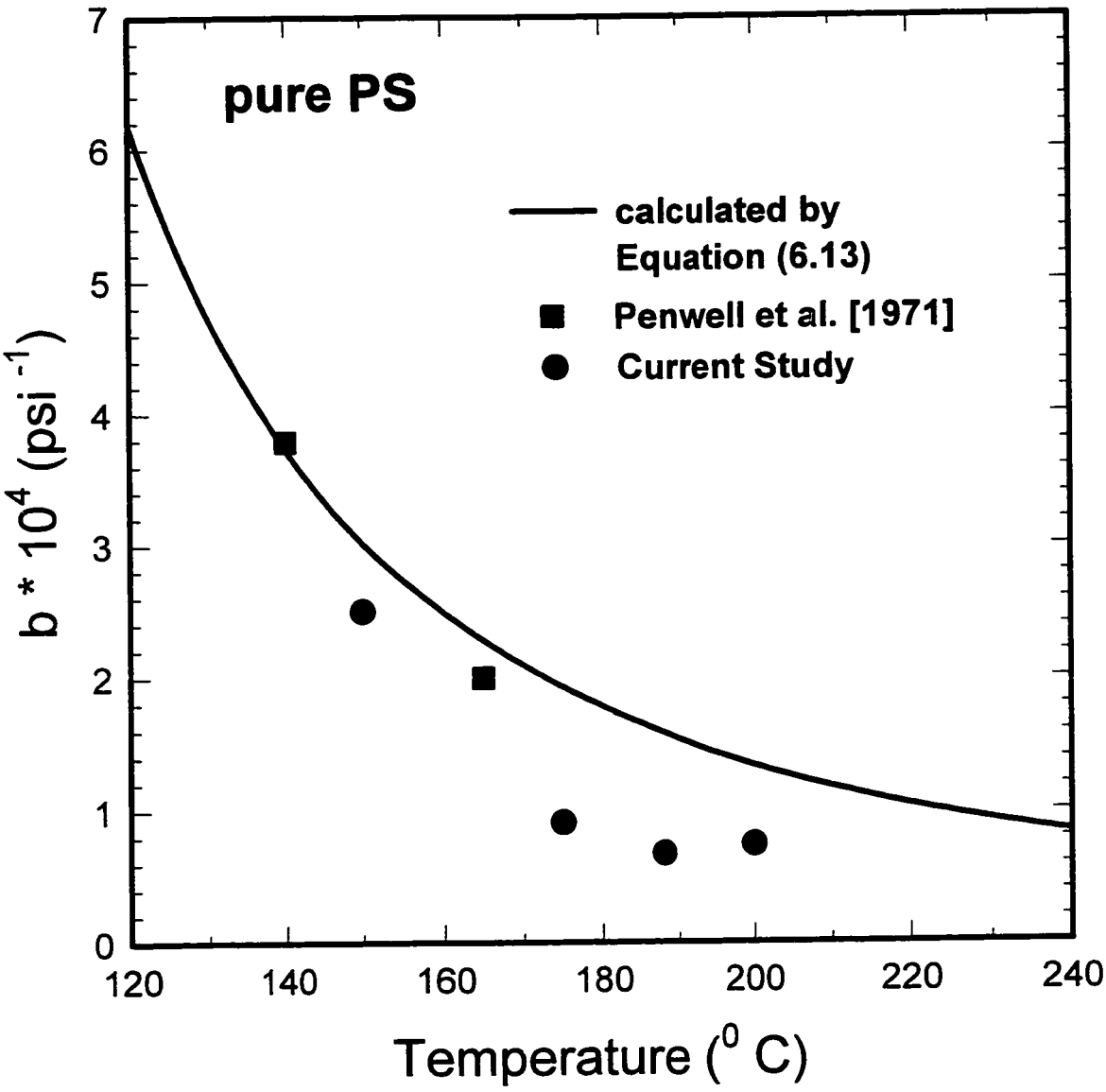

Figure 6.9
Evaluated Pressure Coefficients for pure PS.

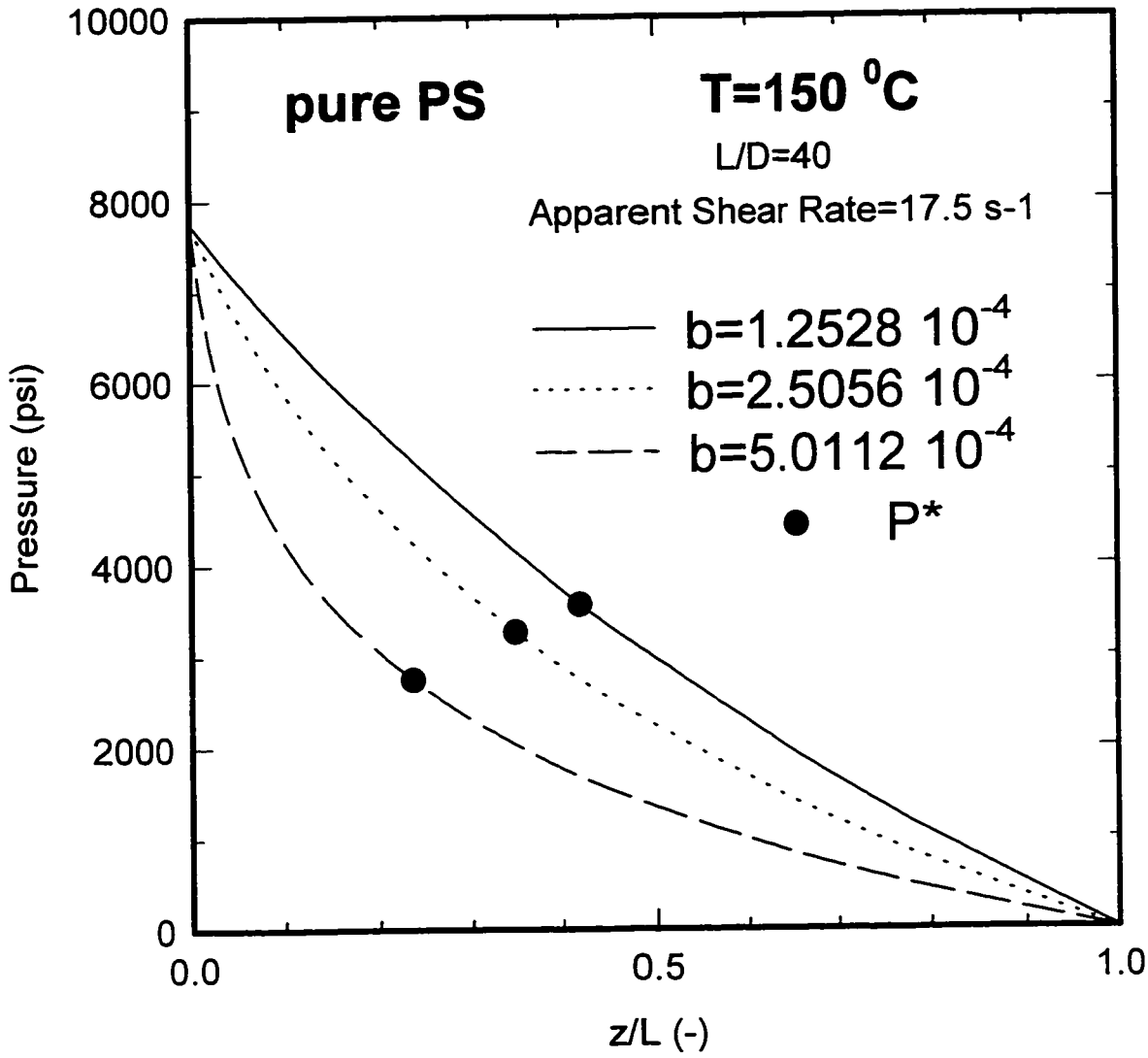

Figure 6.10
Variations of Pressure Distribution and Effective Pressure with Pressure Coefficient for pure PS at T=150 0^0C when (L/D)=40 and apparent Shear Rate is 17.5 s^{-1} .

elevated pressures in Figure 6.11.

The pressure correction was performed on Bagley-Schuemmer corrected viscosity data using Equation (6.39). The procedure to obtain Bagley-Schuemmer-Pressure corrected viscosity is summarized in Figure 6.12.

The Bagley-Schuemmer-Pressure corrected viscosity is depicted with uncorrected ones in Figures 6.13(a) through 6.13(d), where the viscosity data for (L/D) of 40 and 75 match closely indicating the pressure correction is practical. The pressure correction is satisfactory to generate refined viscosity data for the current study and no further correction is necessary. In Figure 6-13(a) the apparent shear-thickening behavior of polystyrene at 150 ^{0}C for Bagley-Schuemmer corrected viscosity is rectified and the expected shear-thinning behavior emerges. The effect of pressure correction is largest at 150 ^{0}C and becomes progressively smaller for higher temperatures.

The Bagley-Schuemmer-Pressure corrected viscosity of pure PS that was fitted to the modified Cross model along with the complex Newtonian viscosity data in Figure 6.14. The fitted model parameters are given in Appendix II.

The Bagley-Schuemmer-Pressure corrected viscosity and complex viscosity in Figure 6.14 indicate the migration of transition shear rate at which the shear-thinning behavior begins to higher shear rates as temperature increases. Graesley [1974] suggested that the decrease in viscosity with increasing shear rate could be understood qualitatively as due to a decrease in the density of entanglement occurred during flow. The reciprocal of the transition shear rate is a characteristic time λ_η that is found similar in magnitude to the longest relaxation time. Consequently, the onset of non-Newtonian behavior is related to the time required for complete rearrangement of an entangled molecule. Any factors influencing the density of entanglement would affect the transition shear rate as well as

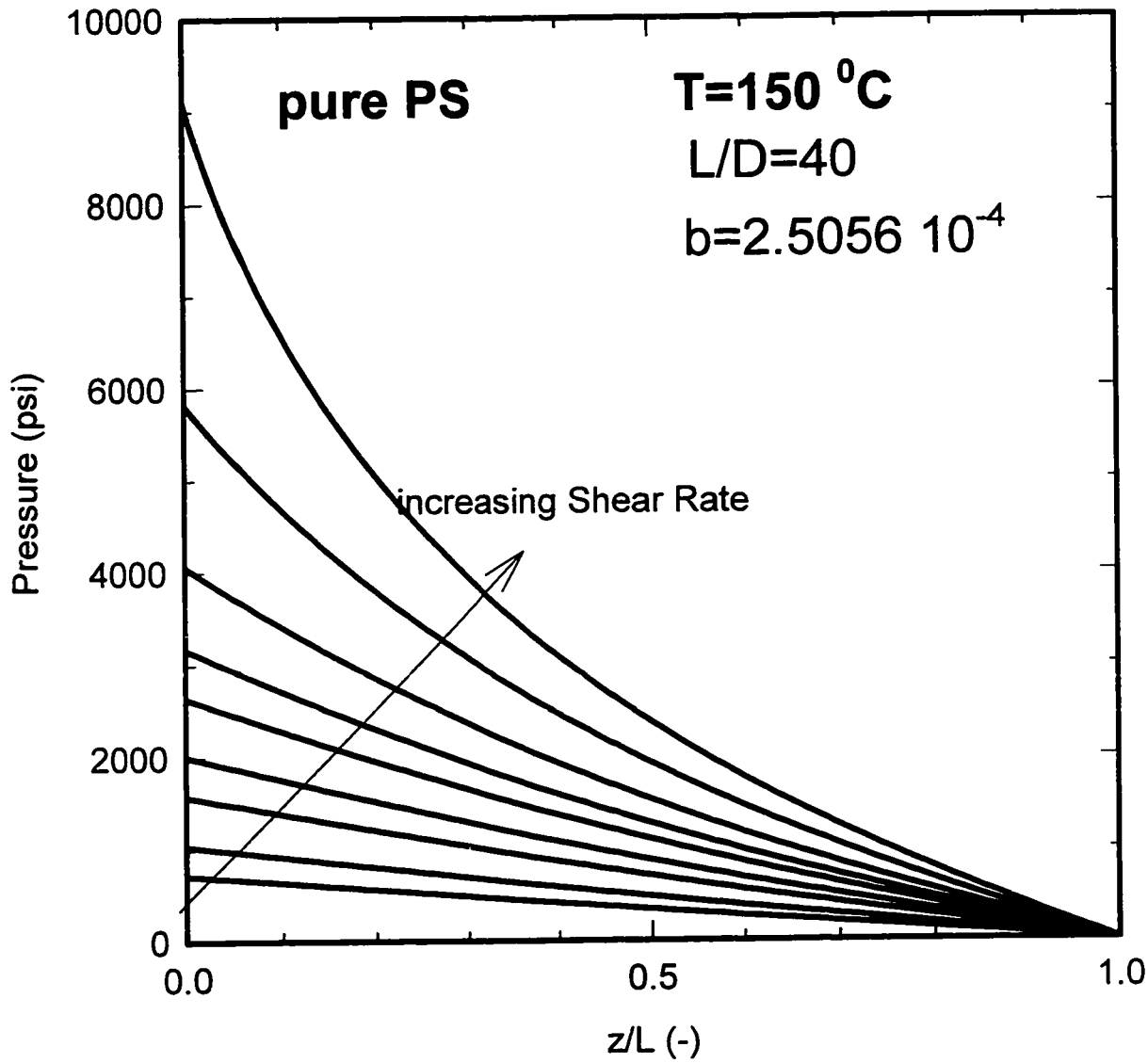

Figure 6.11
Pressure Distributions with varying Shear Rates at a fixed Pressure Coefficient for pure PS at T=150 ^{0}C and (L/D)=40.

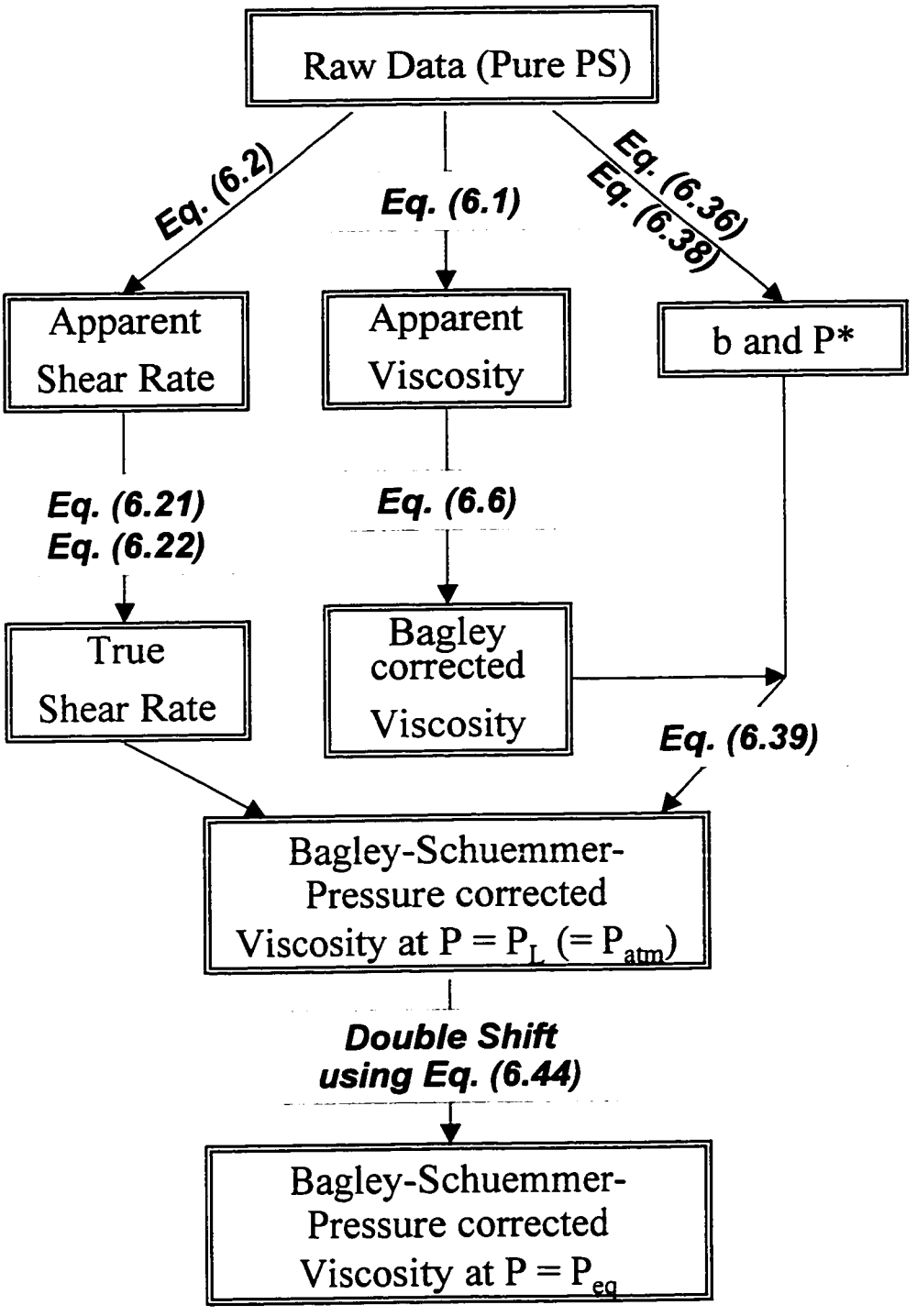

Figure 6.12
Procedure to obtain Bagley-Schuemmer-Pressure corrected Viscosity of pure PS at $P=P_{atm}$ or $P=P_{eq}$.

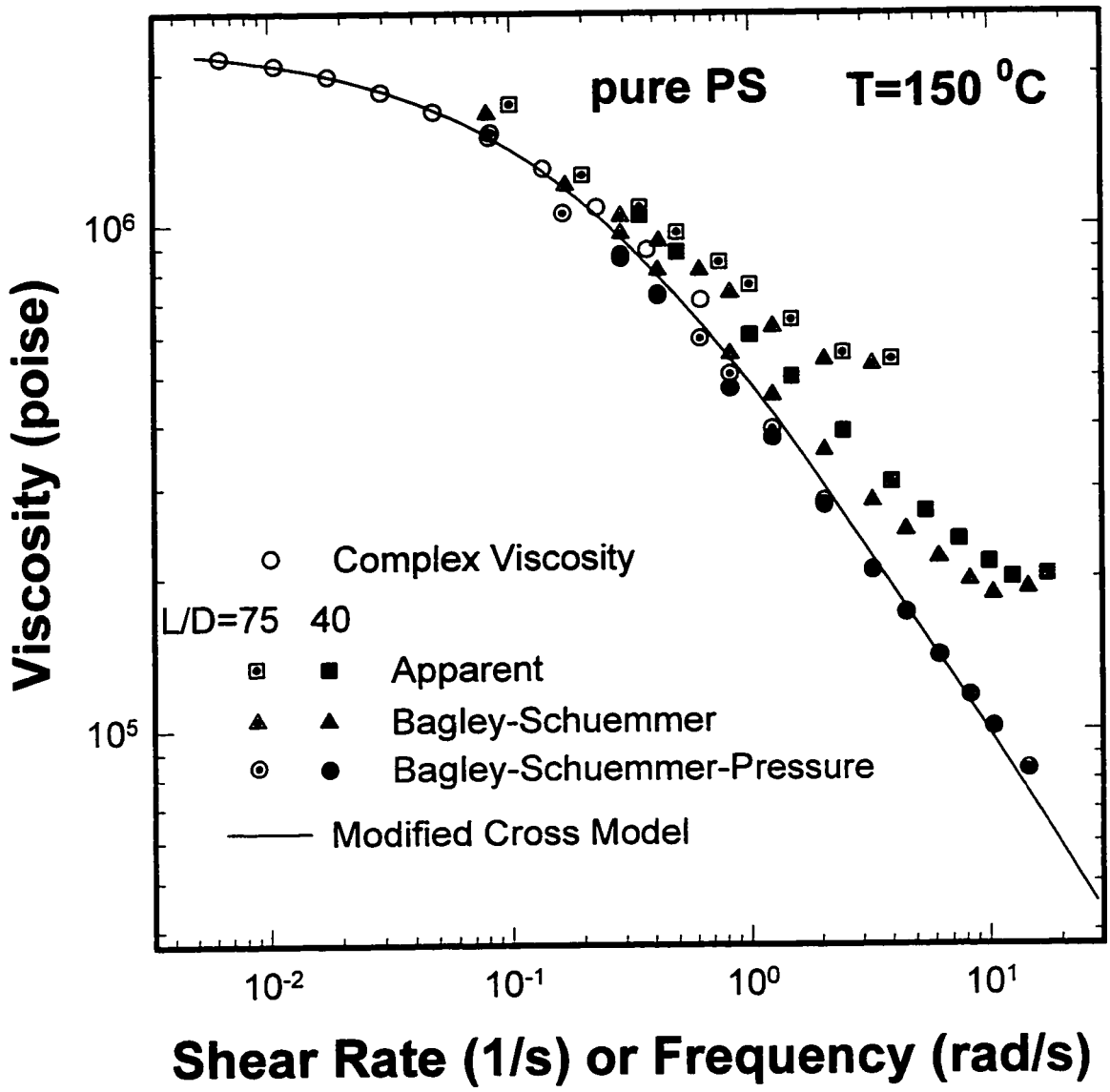

Figure 6.13(a)
Modified Cross Modeling of Bagley-Schuemmer-Pressure corrected Viscosity for (L/D)=40 and 75 and Complex Viscosity compared with apparent Viscosity and Bagley-Schuemmer corrected Viscosity for pure PS at T=150 ^{0}C.

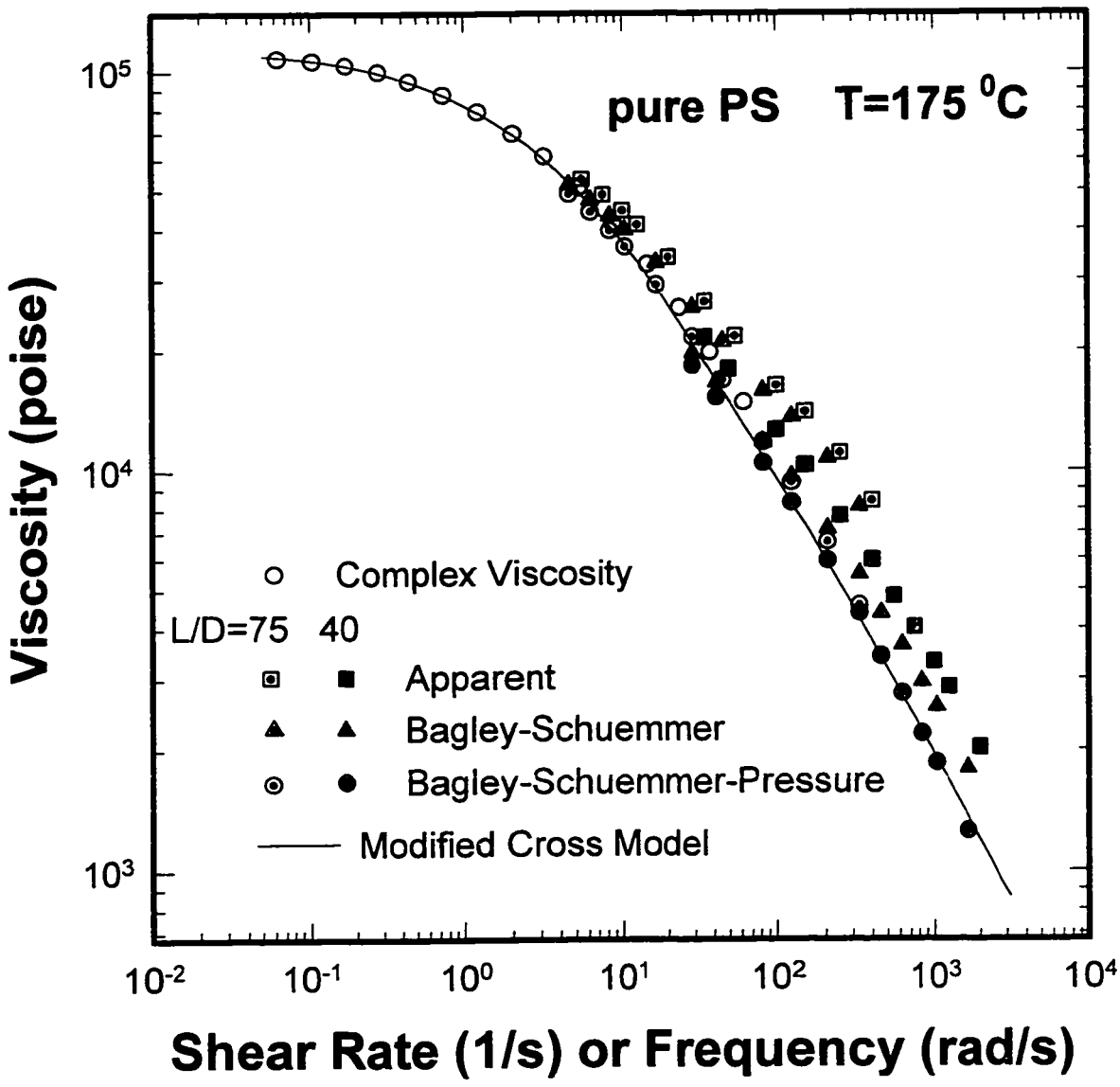

Figure 6.13(b)
Modified Cross Modeling of Bagley-Schuemmer-Pressure corrected Viscosity for (L/D)=40 and 75 and Complex Viscosity compared with apparent Viscosity and Bagley-Schuemmer corrected Viscosity for pure PS at T=175 ^{0}C.

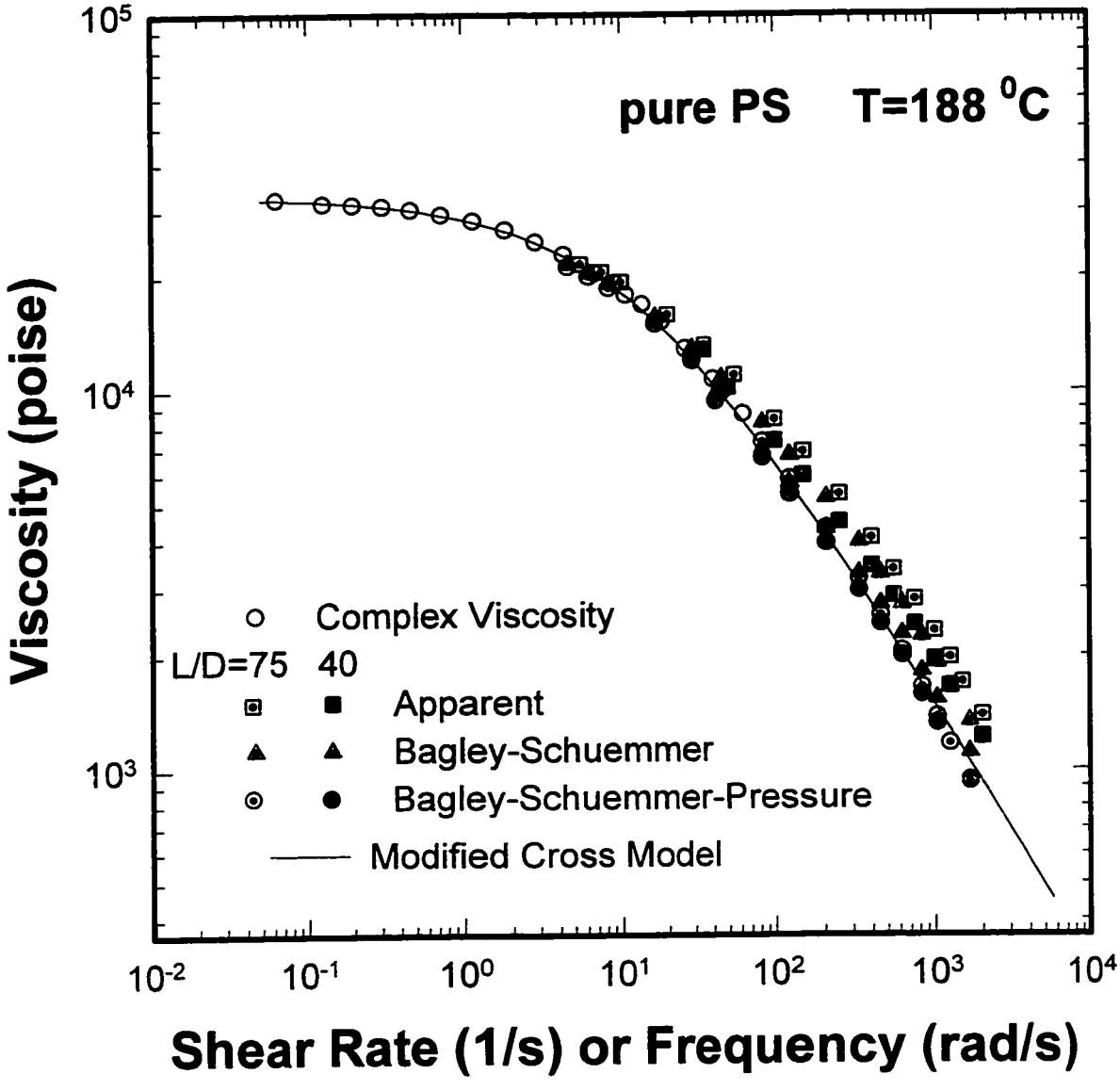

Figure 6.13(c)
Modified Cross Modeling of Bagley-Schuemmer-Pressure corrected Viscosity for (L/D)=40 and 75 and Complex Viscosity compared with apparent Viscosity and Bagley-Schuemmer corrected Viscosity for pure PS at T=188 °C.

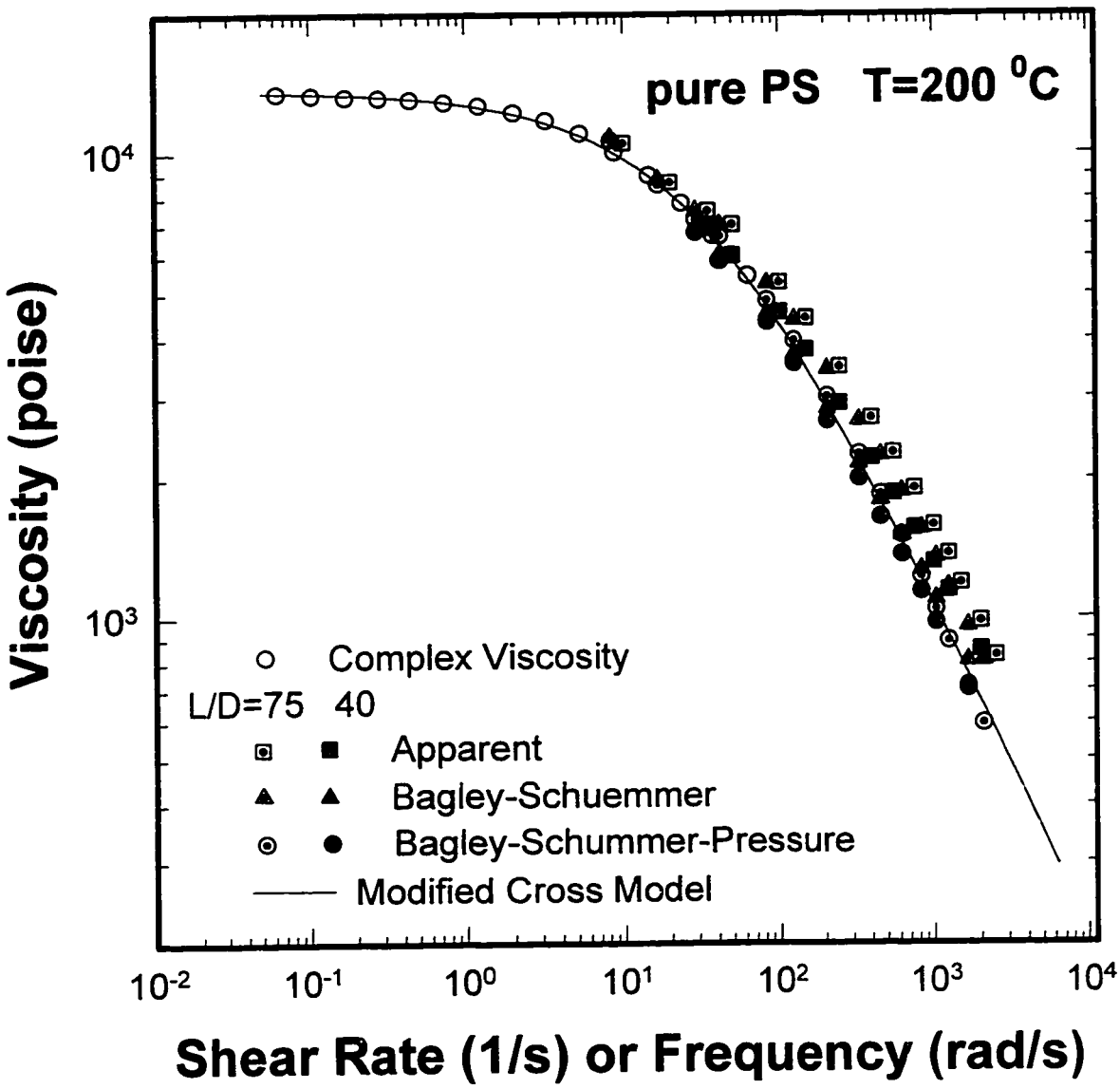

Figure 6.13(d)
Modified Cross Modeling of Bagley-Schuemmer-Pressure corrected Viscosity for (L/D)=40 and 75 and Complex Viscosity compared with apparent Viscosity and Bagley-Schuemmer corrected Viscosity for pure PS at T=200 °C.

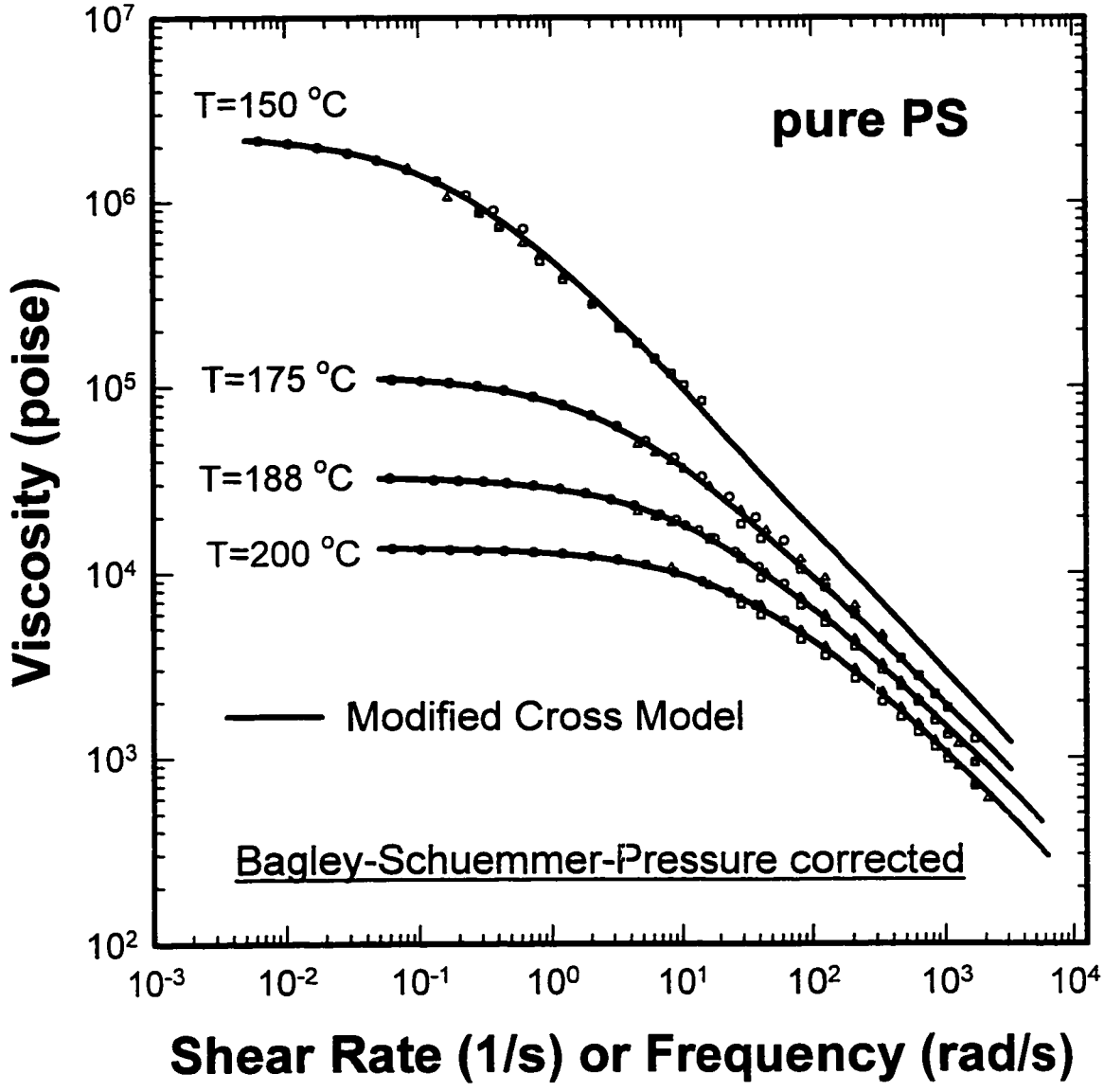

Figure 6.14
Modified Cross Modeling of Complex Viscosity and Bagley-Schuemmer-Pressure corrected Viscosity for (L/D)=40 and 75 for pure PS.

the viscosity. Changes in temperature, pressure, and concentration are expected to bring shifts of viscosity curves in both shear rate and viscosity axes confirming the validity of double shifting of the viscosity curve.

6.2.4.3 Significance of Bagley and Pressure Corrections

The significance of two corrections can be examined by comparing their correction effects. In order to assess the only effect of pressure correction, the Schuemmer-Pressure corrected viscosity was obtained by performing the pressure correction unto the Schuemmer corrected viscosity data without Bagley correction.

The correction effect can be compared from Figure 6.15(a) for 150 ^{0}C and Figure 6.15(b) for 200 ^{0}C representing viscosity data corrected by various procedures. The correction action making two viscosity data from different (L/D) ratios superimposed is attributed to the pressure correction at 150 and 200 ^{0}C. The Schuemmer-pressure corrected viscosity data approach closely to the Bagley-Schuemmer-Pressure corrected ones and the fitted model curves at both temperatures. The viscoelastic effect (Bagley correction) is found to be less significant as the influence of pressure dependent viscosity for the current study at 150 ^{0}C. Also at 200 ^{0}C, although both corrections are less important as at 150 ^{0}C, the pressure correction is the major contribution to obtain matched viscosity data from different (L/D) ratios.

Consequently for pure polystyrene, the analysis of capillary rheometer data should include the pressure correction which is more important than the Bagley correction, especially when the measurement temperature is closer to its T_g. For higher measurement temperatures, the significance of pressure correction becomes less and so does that of Bagley correction.

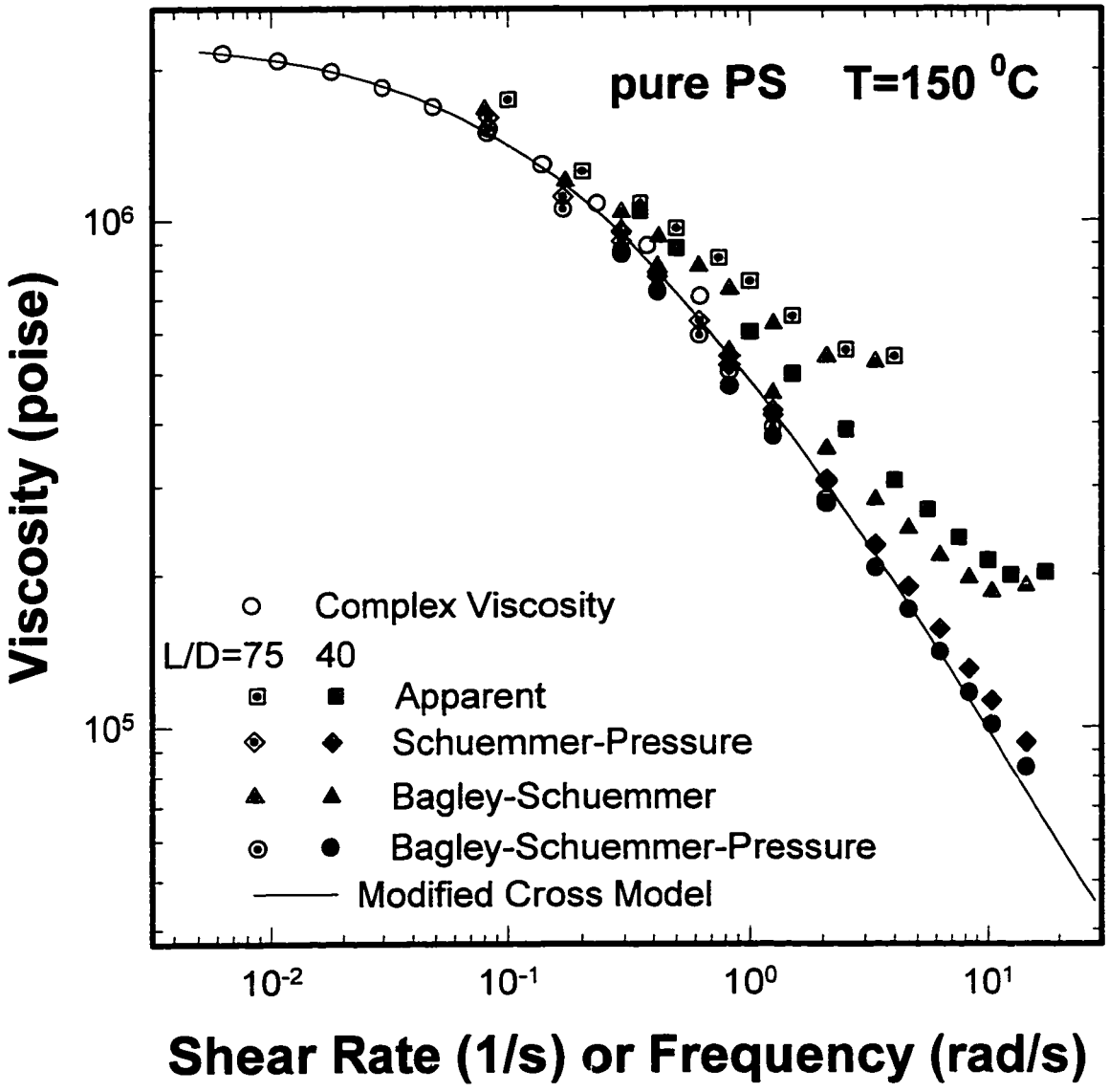

Figure 6.15(a)
Modified Cross Modeling of Bagley-Schuemmer-Pressure corrected Viscosity for (L/D)=40 and 75 and Complex Viscosity compared with apparent, Schuemmer-Pressure corrected, and Bagley-Schuemmer corrected Viscosity for pure PS at T=150 °C.

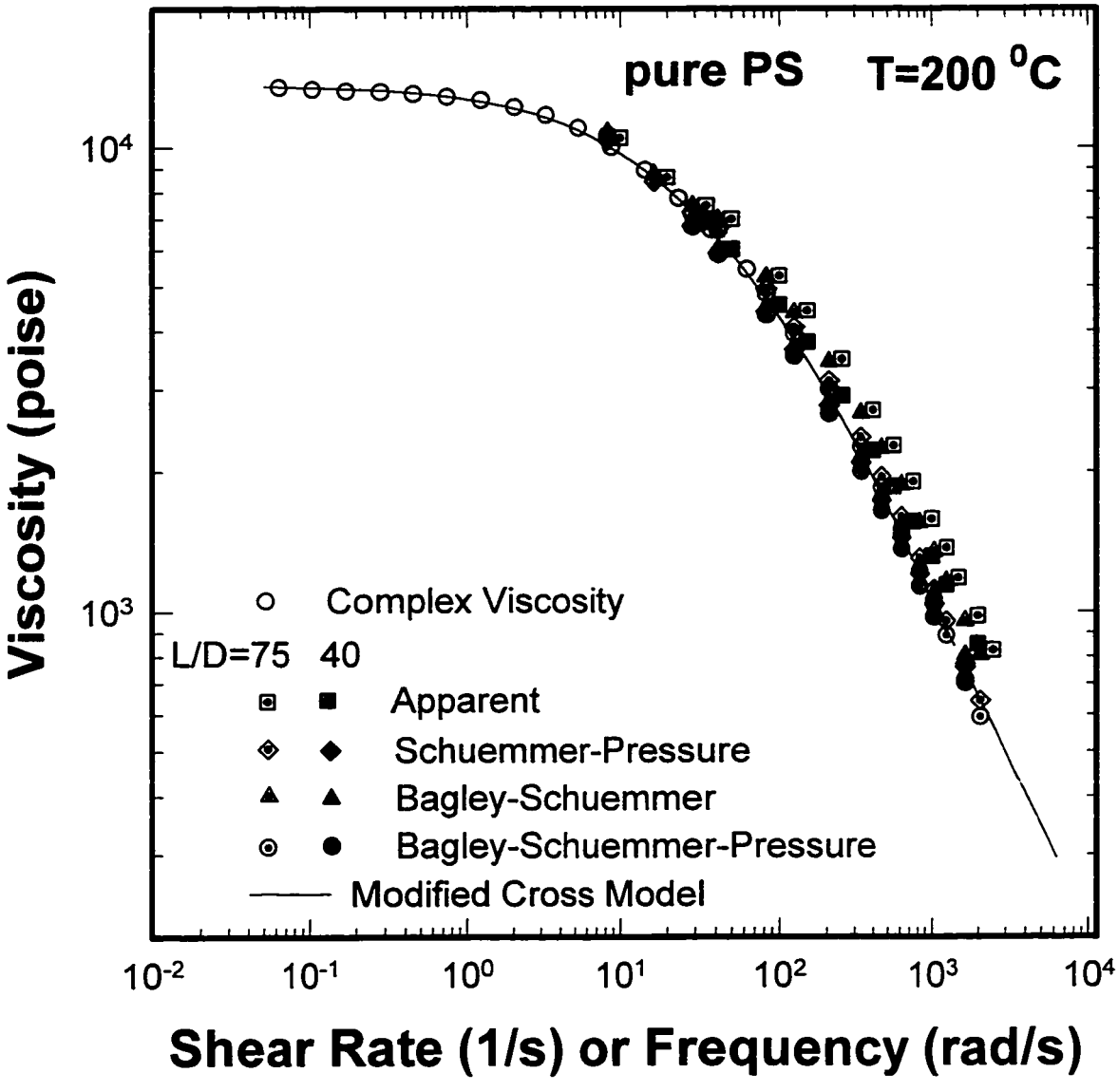

Figure 6.15(b)
Modified Cross Modeling of Bagley-Schuemmer-Pressure corrected Viscosity for (L/D)=40 and 75 and Complex Viscosity compared with apparent, Schuemmer-Pressure corrected, and Bagley-Schuemmer corrected Viscosity for pure PS at T=200 °C.

When the Bagley correction can not be applied due to any reason, the pressure correction alone is expected to provide reliable viscosity data. Especially if the pressure is high due to high shear rate or high viscosity of material or the total measurement system is under elevated pressures, the pressure correction will be very important and essential to obtain dependable viscosity data from capillary rheometry.

6.2.5 Temperature Shift Factors and Master Curves

The WLF equation was used for the temperature shift of viscosity curves constructing the temperature-independent viscosity curve for pure polystyrene. Rather than using empirical values, coefficients of WLF equations, C_1 and C_2 were evaluated using the method by Williams [1953] which is introduced in Appendix III. The evaluated T_g (99.24 ^{0}C) and WLF coefficients (C_1 = 13.81 and C_2 = 48.87) were used to calculate the temperature shift factor, a_T which provides the amount of shift of viscosity curves along both axes.

In Figure 6.16 the widely spread viscosity data for various temperatures are shifted giving a single temperature-independent master curve which shows the relevance of double shifting. The modified Cross model was applied to the master curve also and the evaluated parameters are given in Appendix II. The spread of shifted data points in the intermediate range of shear rate is expected for polymers with wide molecular weight distribution [Malkin and Vinogradov, 1980].

6.3 PS-SCG mixtures

The shear viscosity of PS-SCG mixtures were measured using the pressurized capillary rheometer at 150 and 175 ^{0}C and elevated pressures using a capillary die with

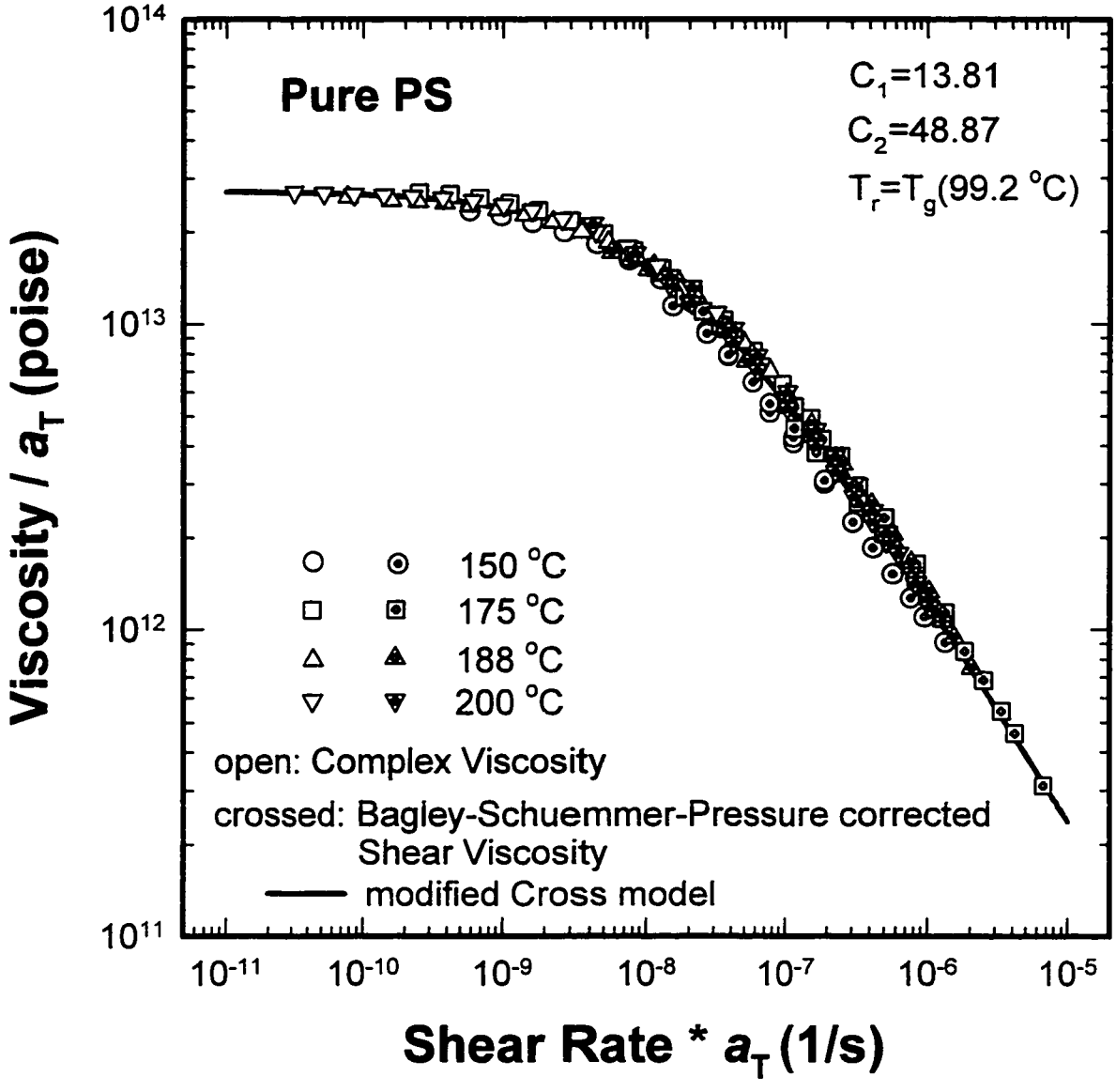

Figure 6.16
Master Curve constructed by Temperature Shift of Bagley-Schuemmer-Pressure corrected Viscosity for (L/D)=40 and 75 and Complex Viscosity for pure PS using the WLF Equation.

(L/D) ratio 40. The data analysis procedure is modified to account the pressure effect.

6.3.1 Wall Friction

The wall friction was examined in order to check any additional wall friction brought by the attachment of back-pressure assembly. When the alignment of back-pressure assembly and rheometer unit is straight, however, the magnitude of wall friction is identical with that obtained without the back-pressure assembly. Consequently, the wall friction data taken without the back-pressure assembly was used the same way.

6.3.2 Schuemmer-Pressure Corrected Viscosity

Since the measured force reading by the load cell comprises the force against the exerted back-pressure from the back-pressure assembly, the actual force applied to the flow of PS-SCG mixture is obtained by subtracting the force by back-pressure from the total force measured by the load cell. The pressure at the exit of capillary die was monitored by the pressure transducer which was set to zero at the initial equilibrium stage prior to the measurement.

As mentioned in Section 6.2.4.3, since the measurement system is under elevated pressures, the pressure correction becomes more crucial and relatively the weight of Bagley correction is decreased. Therefore it will be a reasonable procedure to perform only the pressure correction unto Schuemmer corrected viscosity data for PS-SCG mixtures.

The load cell measures the upstream pressure and the inlet pressure is corrected by the wall friction. The exit pressure is the sum of constant back-pressure regulated by gas cylinder and the pressure fluctuation measured at the die exit. The exit pressure, P_L is

controlled greater than the equilibrium pressure, P_{eq} of the PS-SCG mixture at a given temperature.

$$P_L = (P_{BACK} + P_{tr}) \quad > \quad P_{eq} \tag{6.40}$$

where P_{BACK} is the regulated back-pressure steadily supplied by the gas cylinder and P_{tr} is the reading of pressure transducer located at the die exit monitoring the fluctuation of pressure during measurement. In fact the exit pressure P_L increases during measurement as the back-pressure chamber is filled with fresh extrudates through the capillary die. The shear stress calculated by Equation (6.41) is used for further calculation of viscosity and the determination of pressure coefficient.

$$\tau_w = \frac{(F - F_w)/A_P - P_{BACK} - P_{tr}}{4(L/D)/\pi} \tag{6.41}$$

6.3.2.1 Determination of Pressure Coefficients

The pressure coefficient of PS-SCG mixture is determined by the same procedure as for the pure polystyrene. Equation (6.36) is used for the curve fitting of experimental data. The presence of SCG is expected to reduce the viscosity in the same manner when the temperature is increased or the T_g is lowered. Accordingly we assume that the viscosity curve of PS-SCG mixtures would have the identical power-law index, n with the pure PS in the power-law regime of high shear rates.

Power-law indexes computed from the Bagley-Schuemmer-pressure corrected viscosity data of pure PS were used for the curve fitting of Equation (6.36). Thus two unknowns, m_0 and b were evaluated for each mixture.

The computation of pressure coefficient was very sensitive to a single raw data entry and a wide spread of evaluated pressure coefficients was obtained. A specific

correlation between b and weight fraction was not possible for both temperatures. An alternative procedure is to use the overall average with standard deviation as shown in Figures 6.17(a) for 150 ^{0}C and Figure 6.17(b) for 175 ^{0}C.

It was shown that the pressure coefficient decreases and the decreasing rate of b decays as temperature rises or $(T-T_g)$ increases experimentally and theoretically for pure PS from Figure 6.9. For PS-SCG mixtures the pressure coefficient is expected to be less than that for pure polystyrene due to the depression of T_g. It is shown from Figures 6.16(a) that the pressure coefficients for pure PS locate at the above or upper half of the span of b for PS-SCG at 150 ^{0}C, supporting the decreasing tendency of b. In contrast, the decrease of b for PS-SCG was not evidently proven for 175 ^{0}C as shown in Figure 6.16(b), where b's for pure PS remain within the spread of b for PS-SCG mixture. Such a trend of decreasing b with temperature was found from Figure 6.9.

6.3.2.2 Pressure Correction

Using the average b, the Schuemmer corrected viscosity data were pressure corrected by Equation (6.39) giving the viscosity of PS-SCG at $P=P_L$. The Schuemmer-pressure corrected viscosity of PS-SCG mixtures at $P=P_L$ is shown in Figure 6.18(a) through 6.18(f) for 150 and 175 ^{0}C. Since the exit pressure varies during measurement, a series of data for a given concentration, which include the viscosity measured at each shear rate, are not under same pressure. It is advantageous to represent the viscosity of PS-SCG mixture with a concentration at a fixed reference pressure, such as the equilibrium pressure.

6.3.3 Pressure Shift of Viscosity

From the Schuemmer-pressure corrected viscosity at $P=P_L$, the viscosity data at

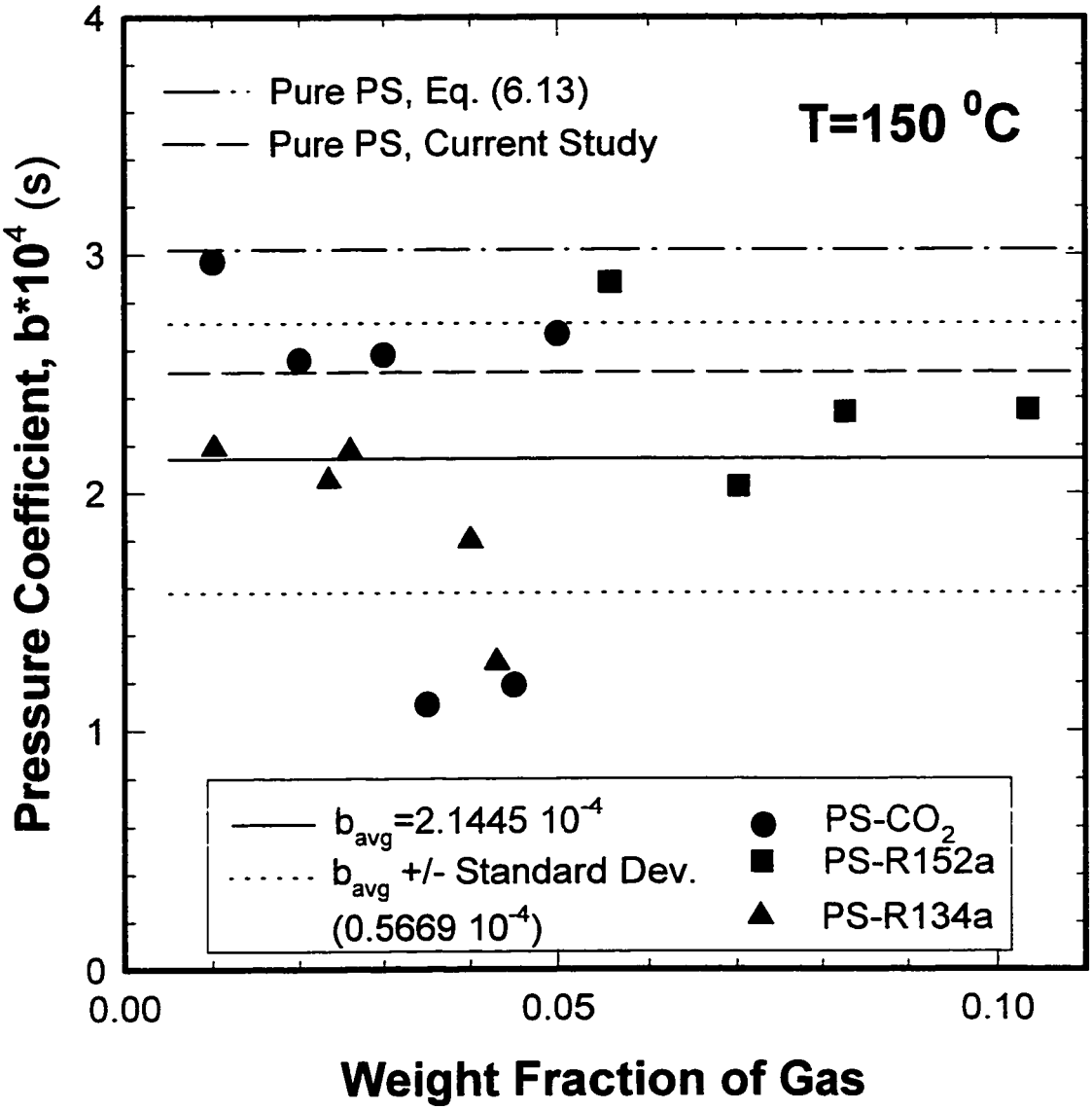

Figure 6.17(a)
Evaluated Pressure Coefficients for PS-SCG mixtures compared with that of pure PS at T=150 ^{0}C.

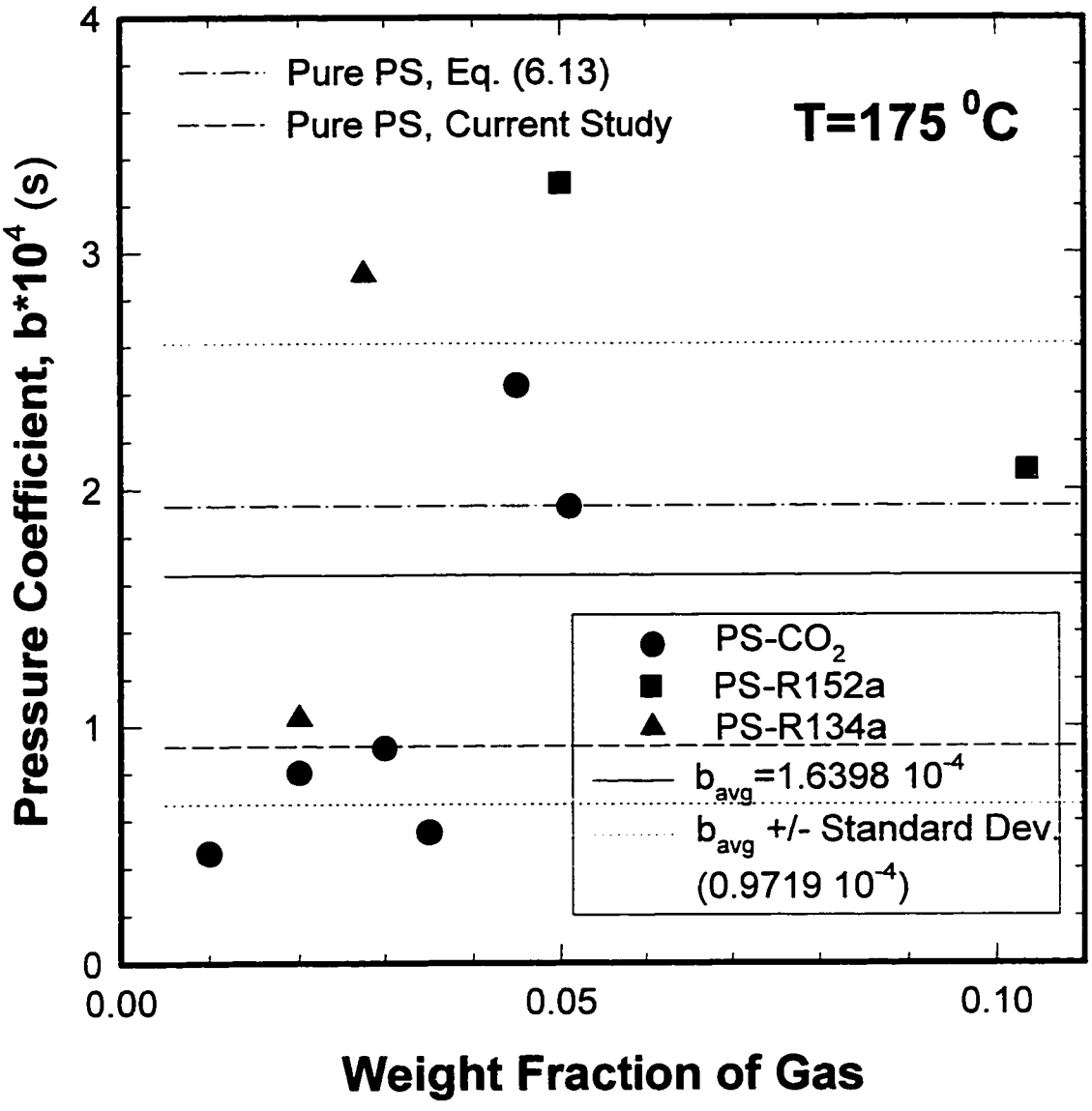

Figure 6.17(b)
Evaluated Pressure Coefficients for PS-SCG mixtures compared with that of pure PS at T=175 ^{0}C.

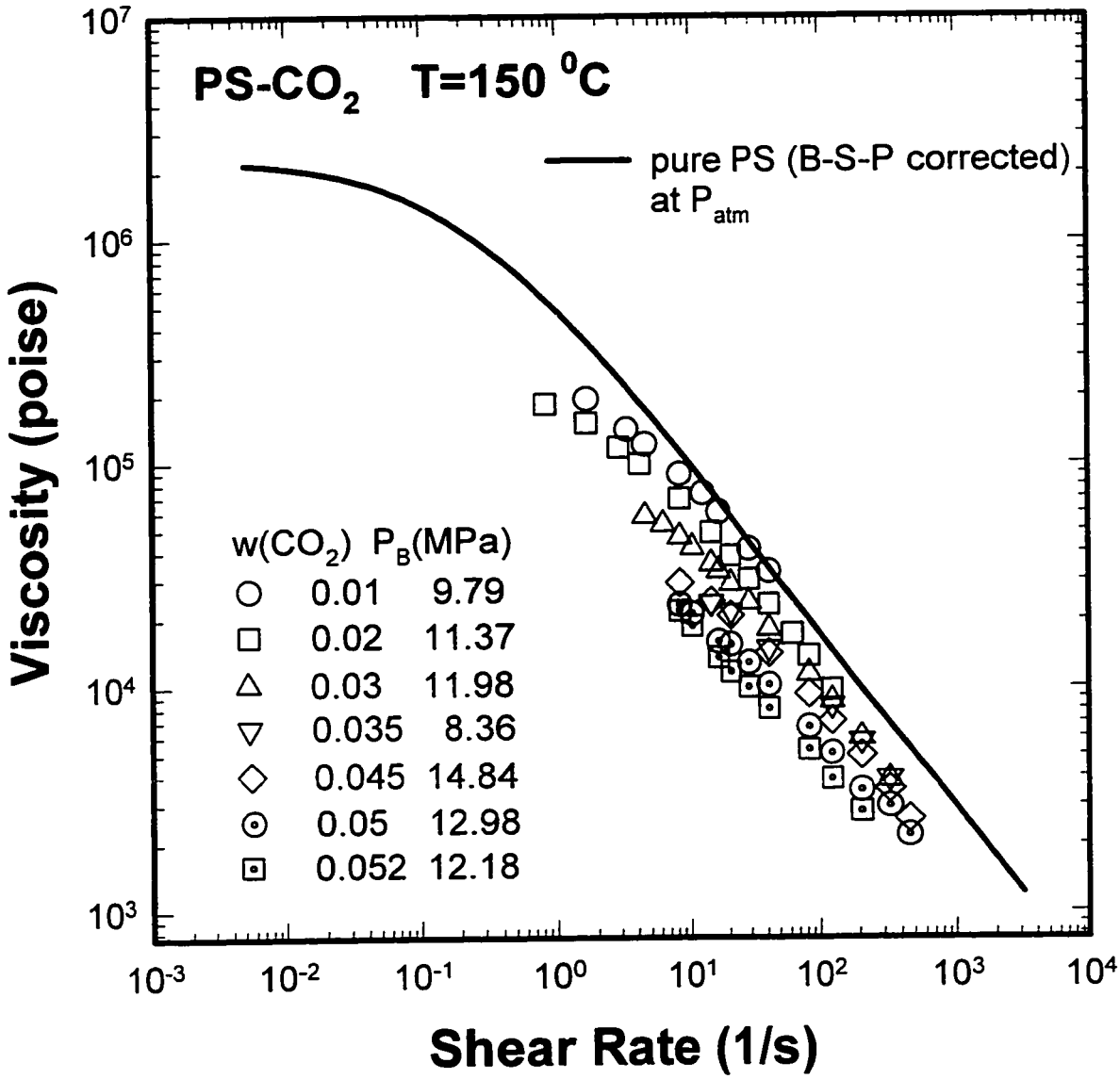

Figure 6.18(a)
Schuemmer-Pressure corrected Viscosities of PS-CO_2 at $P=P_B$ (Back Pressure) and at T=150 ^{0}C compared with Bagley-Schuemmer-Pressure corrected Viscosity of pure PS at $P=P_{atm}$.

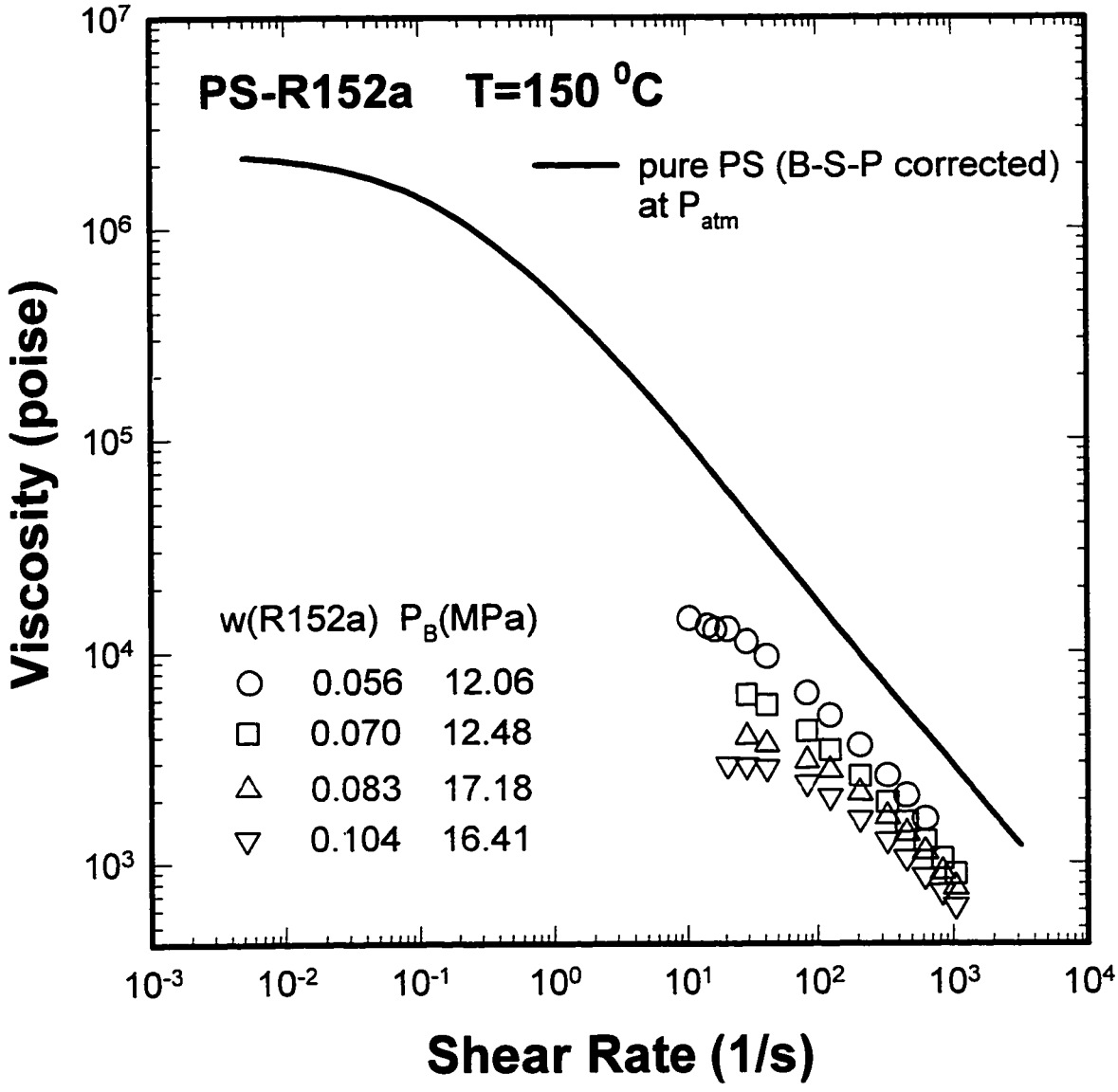

Figure 6.18(b)
Schuemmer-Pressure corrected Viscosities of PS-R152a at $P=P_B$ (Back Pressure) and at T=150 °C compared with Bagley-Schuemmer-Pressure corrected Viscosity of pure PS at $P=P_{atm}$.

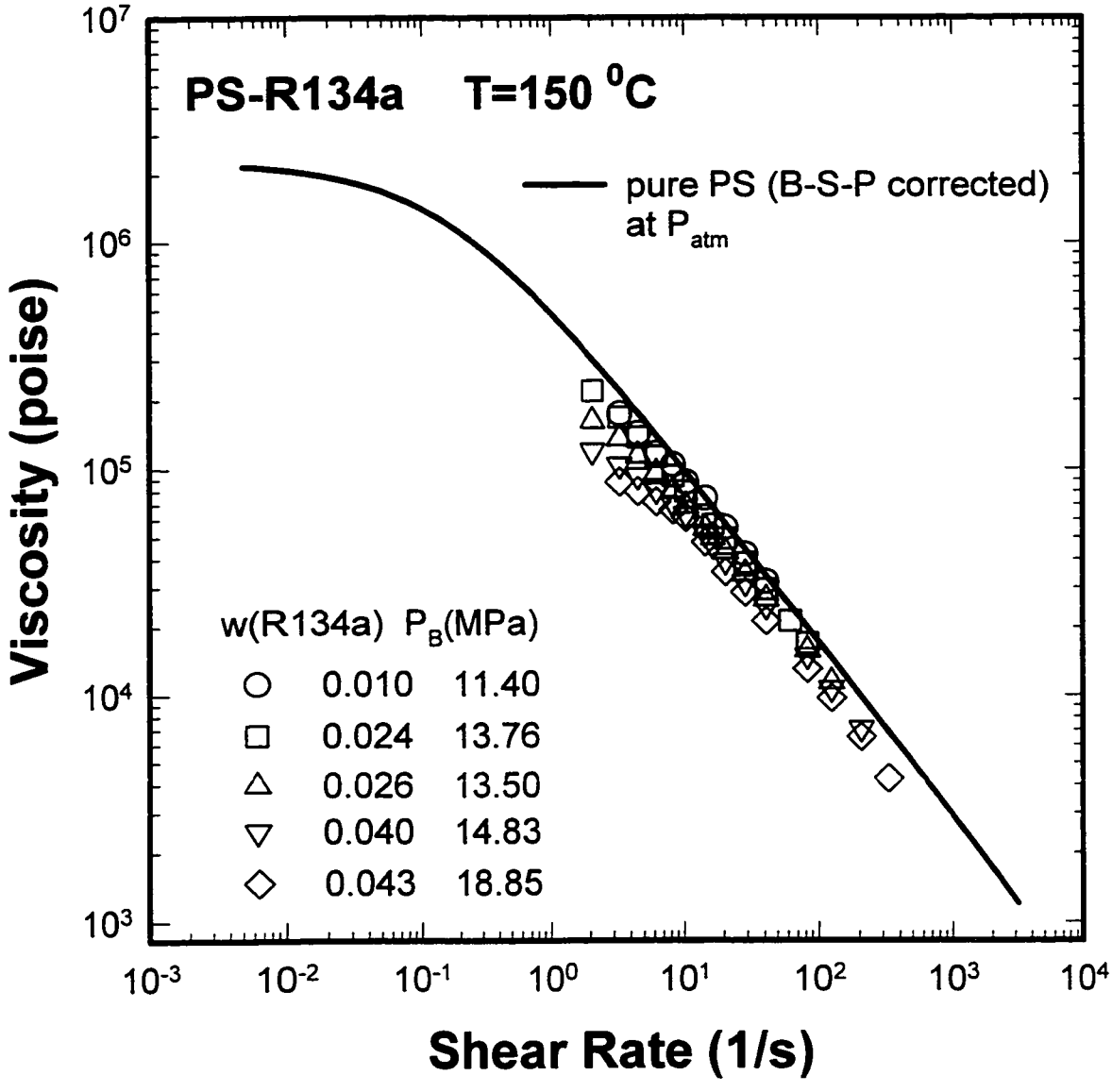

Figure 6.18(c)
Schuemmer-Pressure corrected Viscosities of PS-R134a at $P=P_B$ (Back Pressure) and at T=150 °C compared with Bagley-Schuemmer-Pressure corrected Viscosity of pure PS at $P=P_{atm}$.

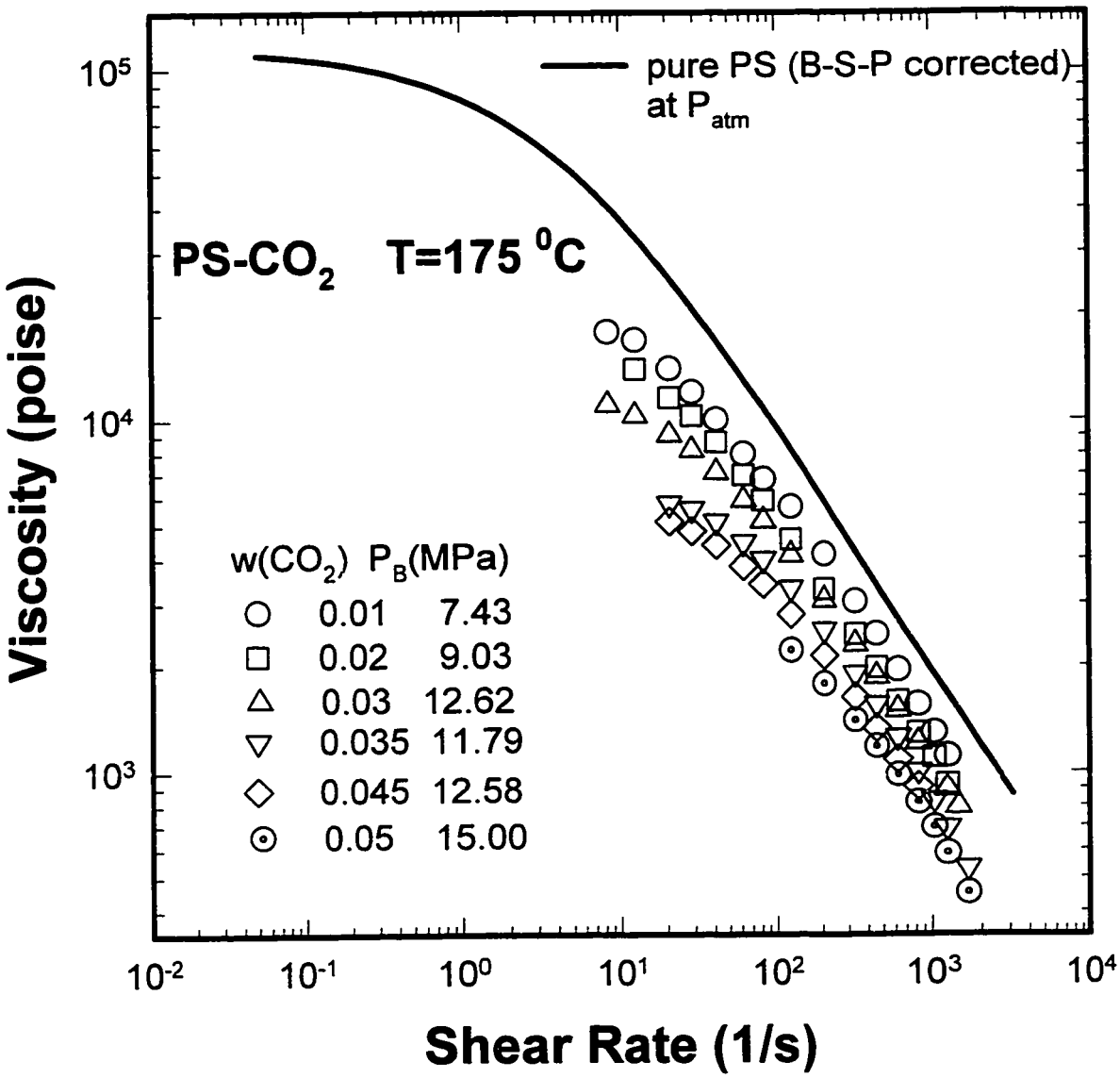

Figure 6.18(d)
Schuemmer-Pressure corrected Viscosities of PS-CO_2 at $P=P_B$ (Back Pressure) and at T=175 ^{0}C compared with Bagley-Schuemmer-Pressure corrected Viscosity of pure PS at $P=P_{atm}$.

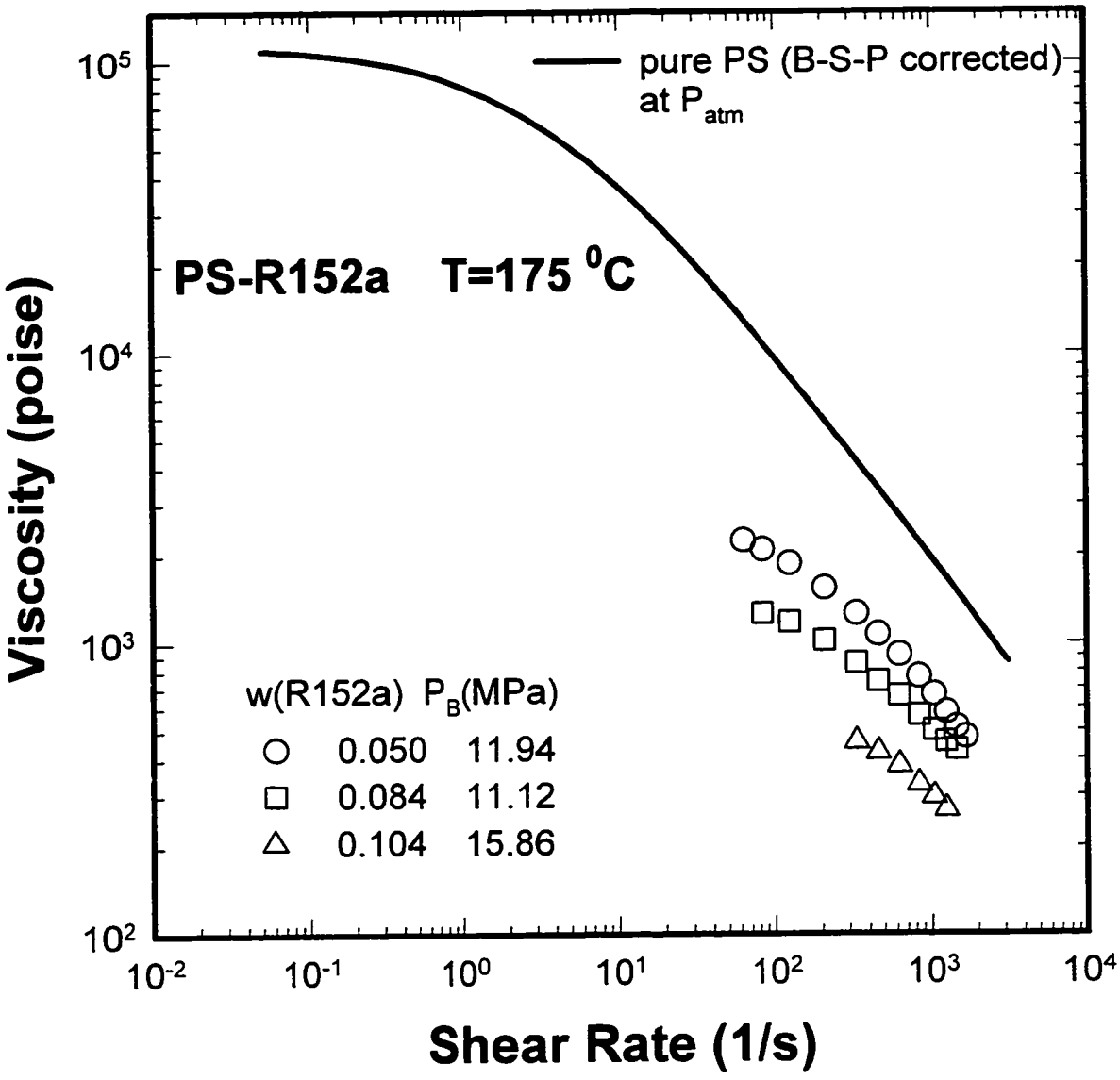

Figure 6.18(e)
Schuemmer-Pressure corrected Viscosities of PS-R152a at $P=P_B$ (Back Pressure) and at T=175 ^{0}C compared with Bagley-Schuemmer-Pressure corrected Viscosity of pure PS at $P=P_{atm}$.

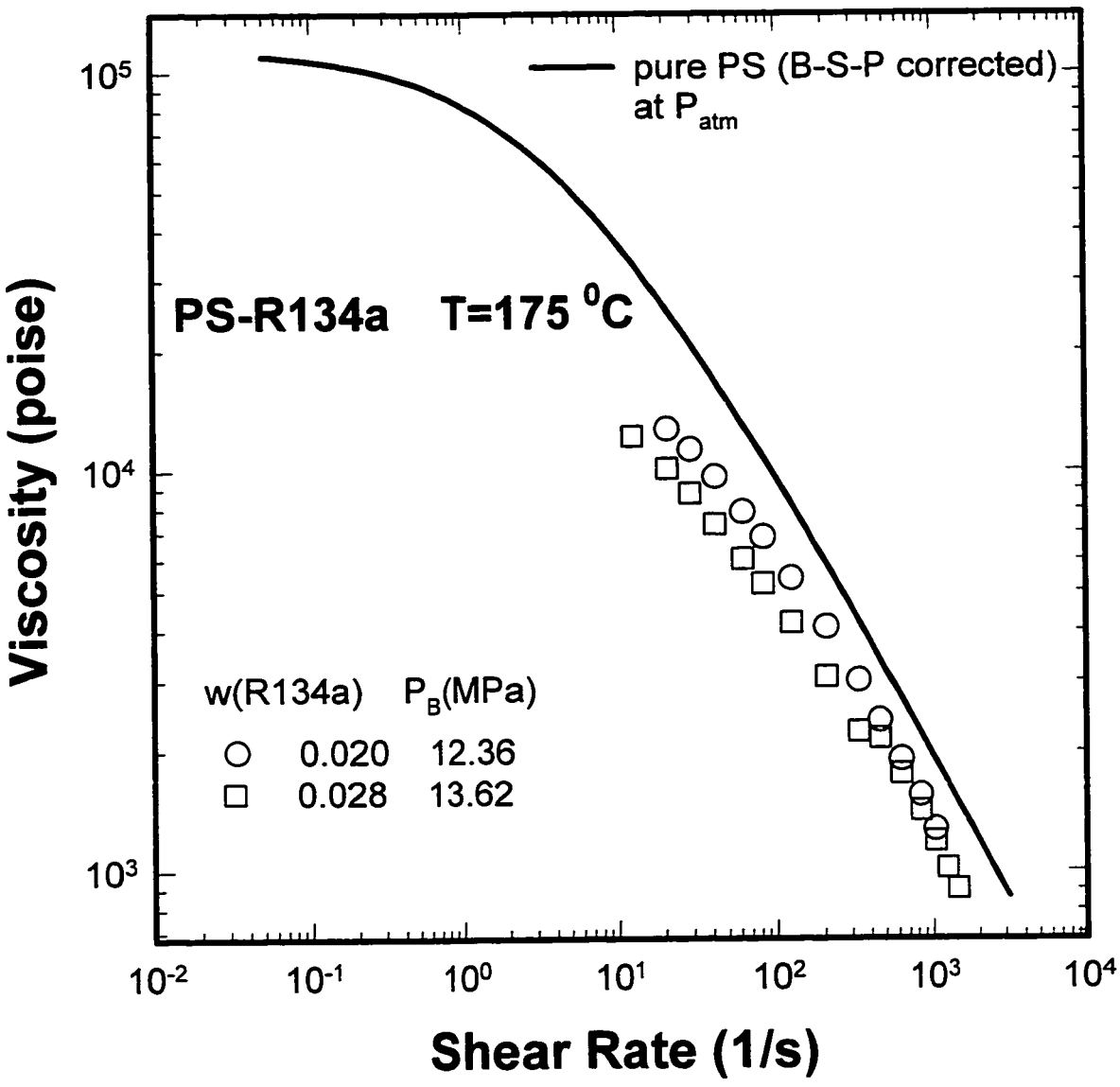

Figure 6.18(f)
Schuemmer-Pressure corrected Viscosities of PS-R134a at $P=P_B$ (Back Pressure) and at T=175 ^{0}C compared with Bagley-Schuemmer-Pressure corrected Viscosity of pure PS at $P=P_{atm}$.

any pressure can be calculated by using the pressure shift factor, a_P. Usually the viscosity of PS-SCG mixture at the corresponding equilibrium pressure is worthwhile to determine in the thermodynamic point of view. The equilibrium pressures are found from the modeling of solubility isotherms shown in Figure 5.4 and 5.5 for PS-CO_2 and PS-R152a. For PS-R134a mixtures, however, the viscosity at atmospheric pressure is evaluated since the solubility isotherms are not available.

The pressure coefficient, b is calculated for a single shift of viscosity data at power-law regime, i.e., the modifying of viscosity at the same shear rate and not for a double shift of overall viscosity curve. Therefore the pressure coefficient for double shift, b_D is necessary for a double shift of viscosity data. Figure 6.19 elucidates the difference between two pressure coefficients. From Figure 6.19 the pressure coefficient is represented as:

$$\log \eta_S = \log \eta^* - bP \tag{6.42}$$

where η_S is the viscosity obtained by single shift.

If the two viscosity curves are parallel in the power-law regime, having the slope *(n-1)*,

$$\begin{aligned} \log \eta_S &= \log \eta_D - b_D(n-1)P \\ &= \log \eta^* - b_D P - b_D(n-1)P \\ &= \log \eta^* - b_D nP \end{aligned} \tag{6.43}$$

Thus $b_D = b / n$ where b_D is the pressure coefficient for double shift of viscosity curve.

The viscosity of PS-SCG mixture at $P=P_L$ is converted by double shift using the pressure shift factor,

$$a_P = \exp\left[b_D(P_L - P_{eq})\right] \quad or \quad a_P = \exp\left[b_D(P_L - P_{atm})\right] \tag{6.44}$$

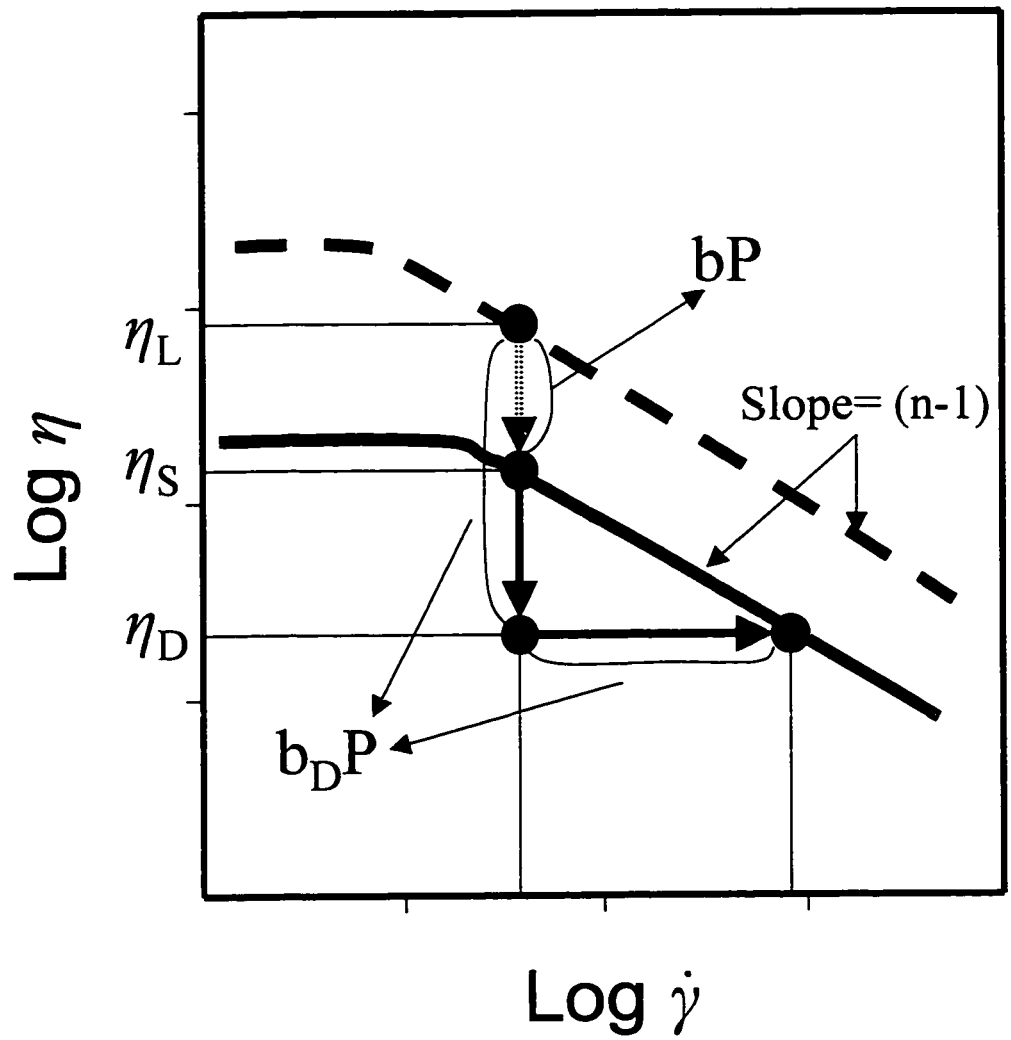

Figure 6.19
Single Shift and Double Shift of Viscosity Curve using Pressure Coefficients b and b_D.

Equation (6.44) can also be used for the pressure shift of pure PS viscosity. . The viscosity at an equilibrium pressure of PS-SCG mixture for given composition and temperature is calculated by double shift using Equation (6.44) and becomes the reference viscosity for the computation of concentration shift factor. The pressure-shifted viscosities of pure PS at selected pressures are shown in Figures 6.20(a) and 6.20(b).

The procedure to obtain Schuemmer-pressure corrected viscosity of PS-SCG is summarized in Figure 6.21.

Figures 6.22(a) through 6.22(f) represent the Schuemmer-pressure corrected viscosity of PS-CO_2, PS-R152a, and PS-R134a mixtures at $P=P_{eq}$ or $P=P_{atm}$ compared with the Bagley-Schuemmer-Pressure corrected viscosity of pure PS at the same temperature and at $P=P_{atm.}$

6.3.4 Shift Factors and Master Curves

The Schuemmer-pressure corrected viscosity of PS-SCG mixture at an arbitrary pressure can be shifted to the viscosity of pure PS at a given pressure by a curve fitting analysis producing a shift factor. Such a shift factor, which was introduced in Section 4.1, stands for the product of concentration shift factor, pressure shift factor and temperature shift factor. The contribution of each shift factor is cancelled if the corresponding independent variable is kept constant.

Figures 6.23(a) through 6.23(f) exhibit the shifted viscosity data of PS-SCG mixtures at $P=P_{eq}$ (PS-CO_2 and PS-R152a) or $P=P_{atm}$ (PS-R134a) unto the pure PS viscosity model at $P=P_{atm}$. The evaluated shift factor for PS-CO_2 and PS-R152a is the product of concentration and pressure shift factors whereas that of PS-R134a represents exactly the concentration shift factor. The concentration shift factor will be compared

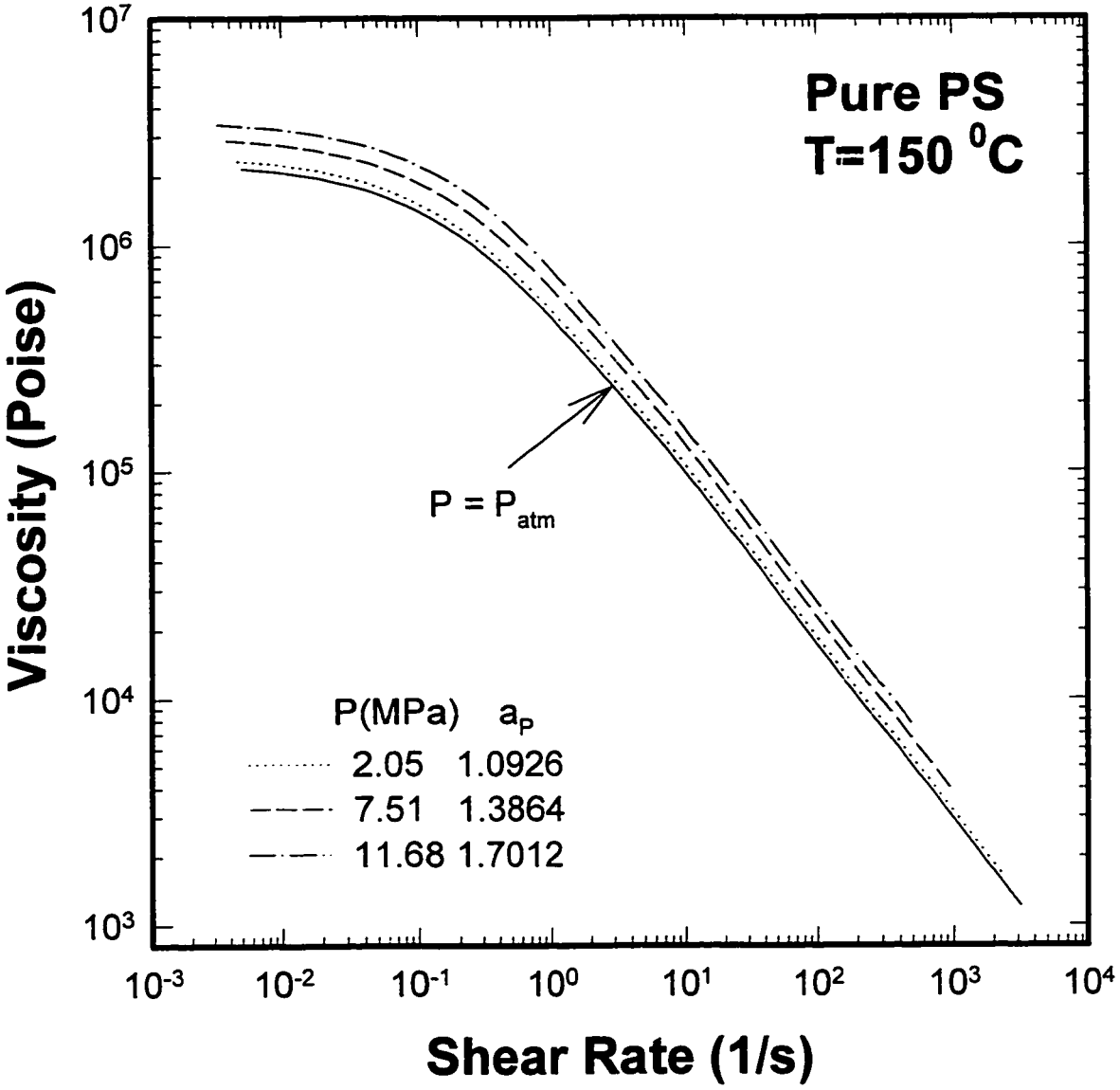

Figure 6.20(a)
Viscosities of pure PS at elevated Pressures estimated by Pressure Shift using Pressure Coefficient for T=150 ^{0}C.

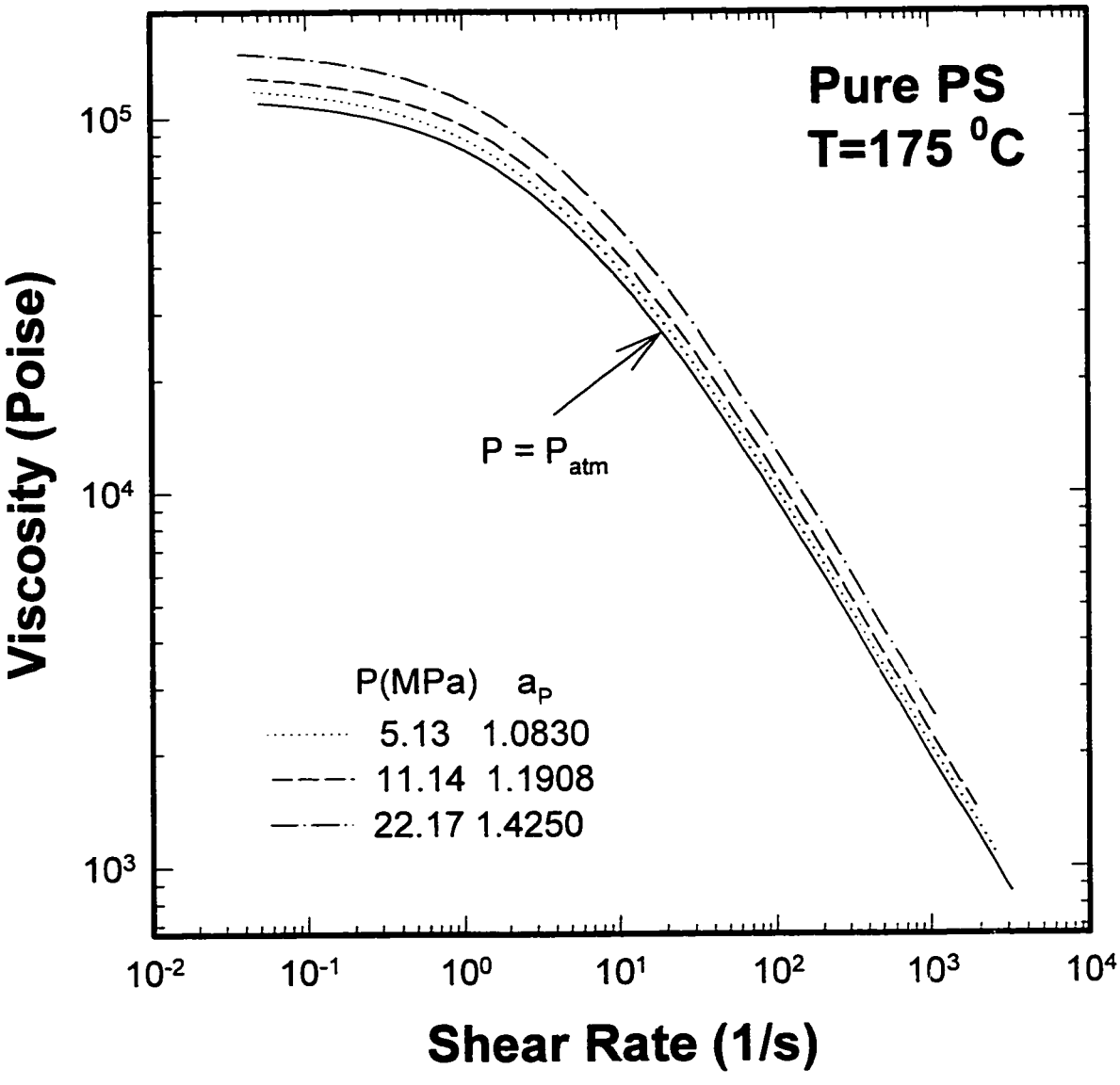

Figure 6.20(b)
Viscosities of pure PS at elevated Pressures estimated by Pressure Shift using Pressure Coefficient for T=175 ^{0}C.

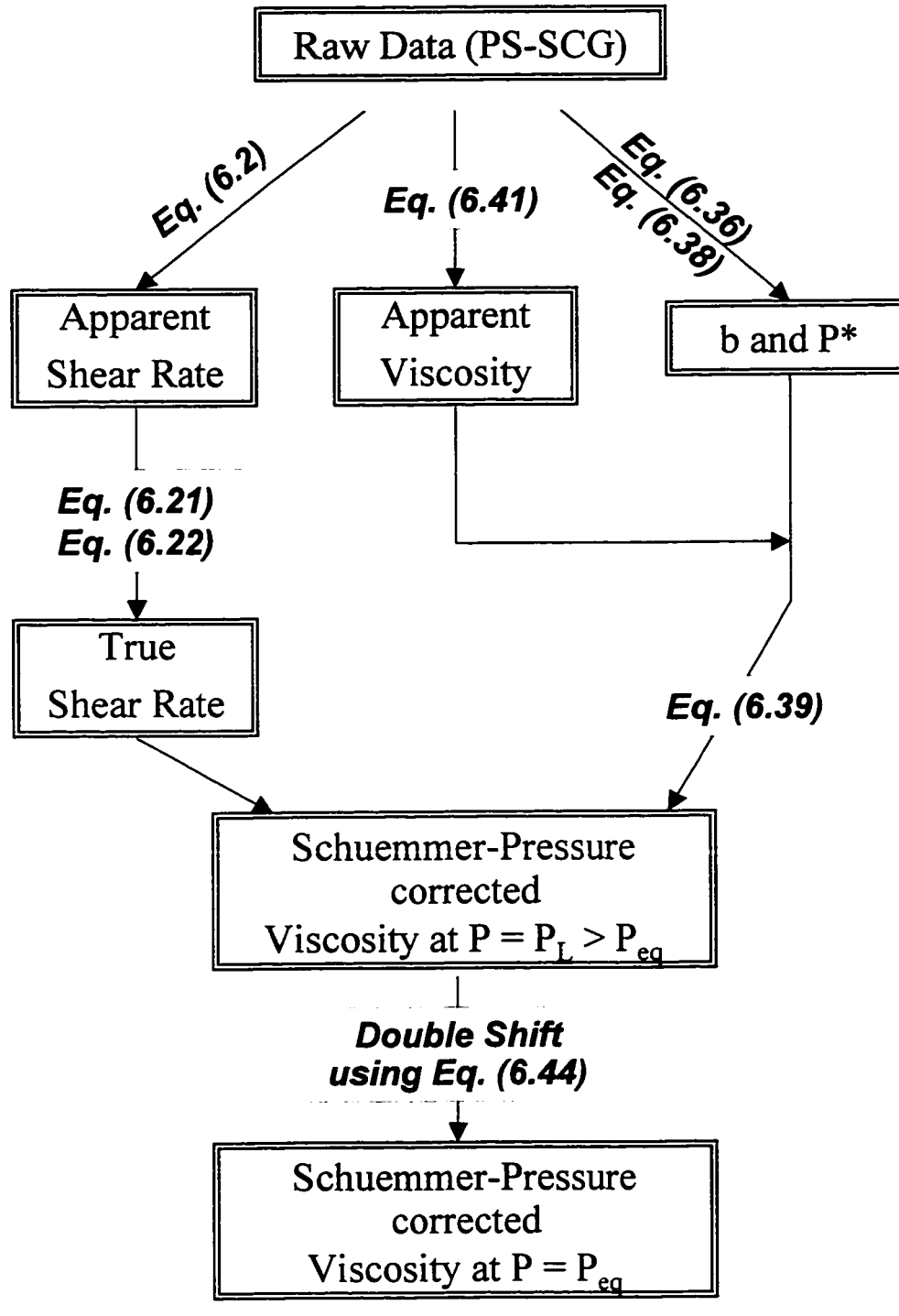

Figure 6.21
Procedure to obtain Schuemmer-Pressure corrected Viscosity of PS-SCG at $P=P_{atm}$ or $P=P_{eq}$.

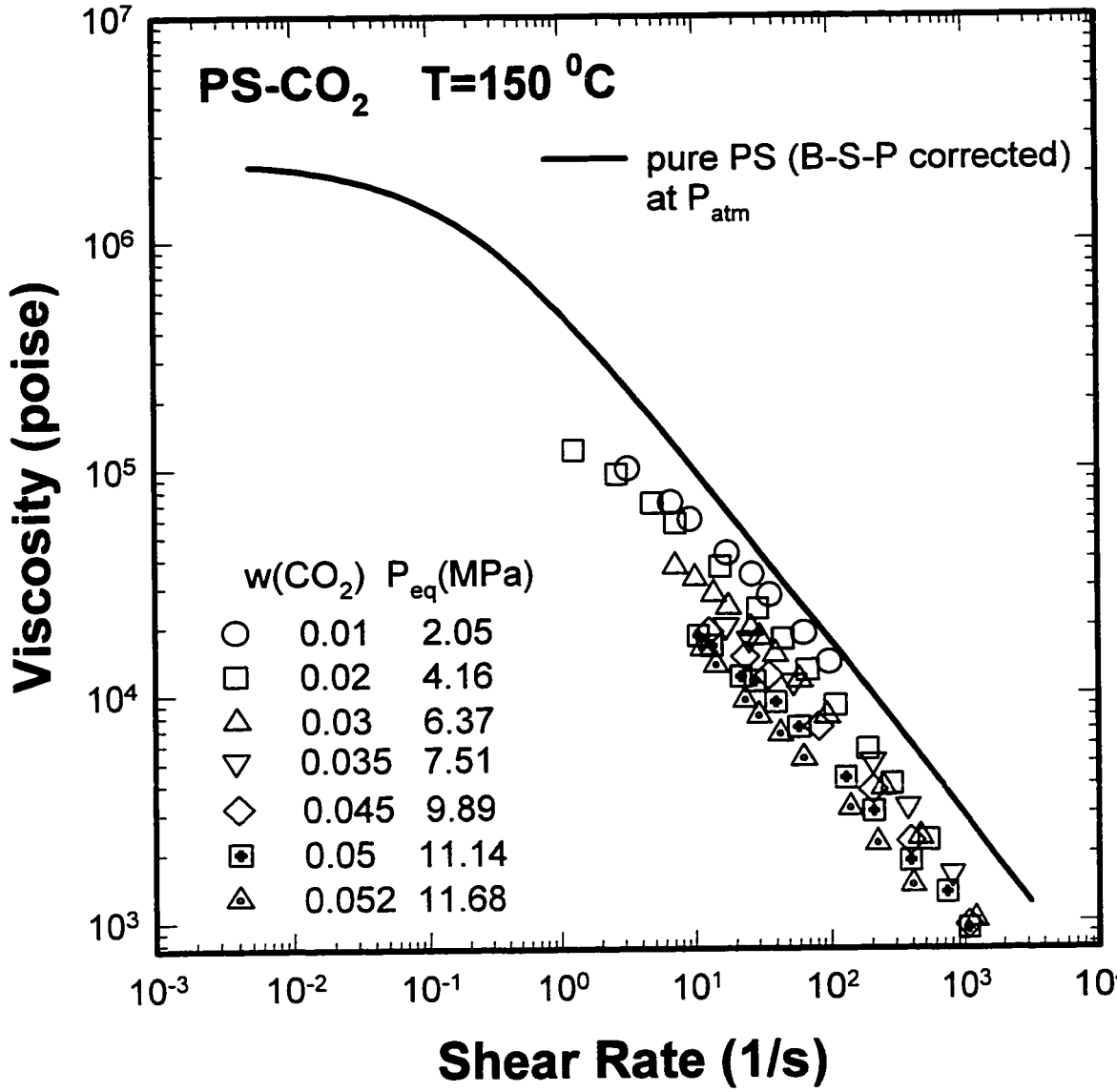

Figure 6.22(a)
Schuemmer-Pressure corrected Viscosities of PS-CO_2 at $P=P_{eq}$ (Equilibrium Pressure) and at T=150 ^{0}C compared with Bagley-Schuemmer-Pressure corrected Viscosity of pure PS at $P=P_{atm}$.

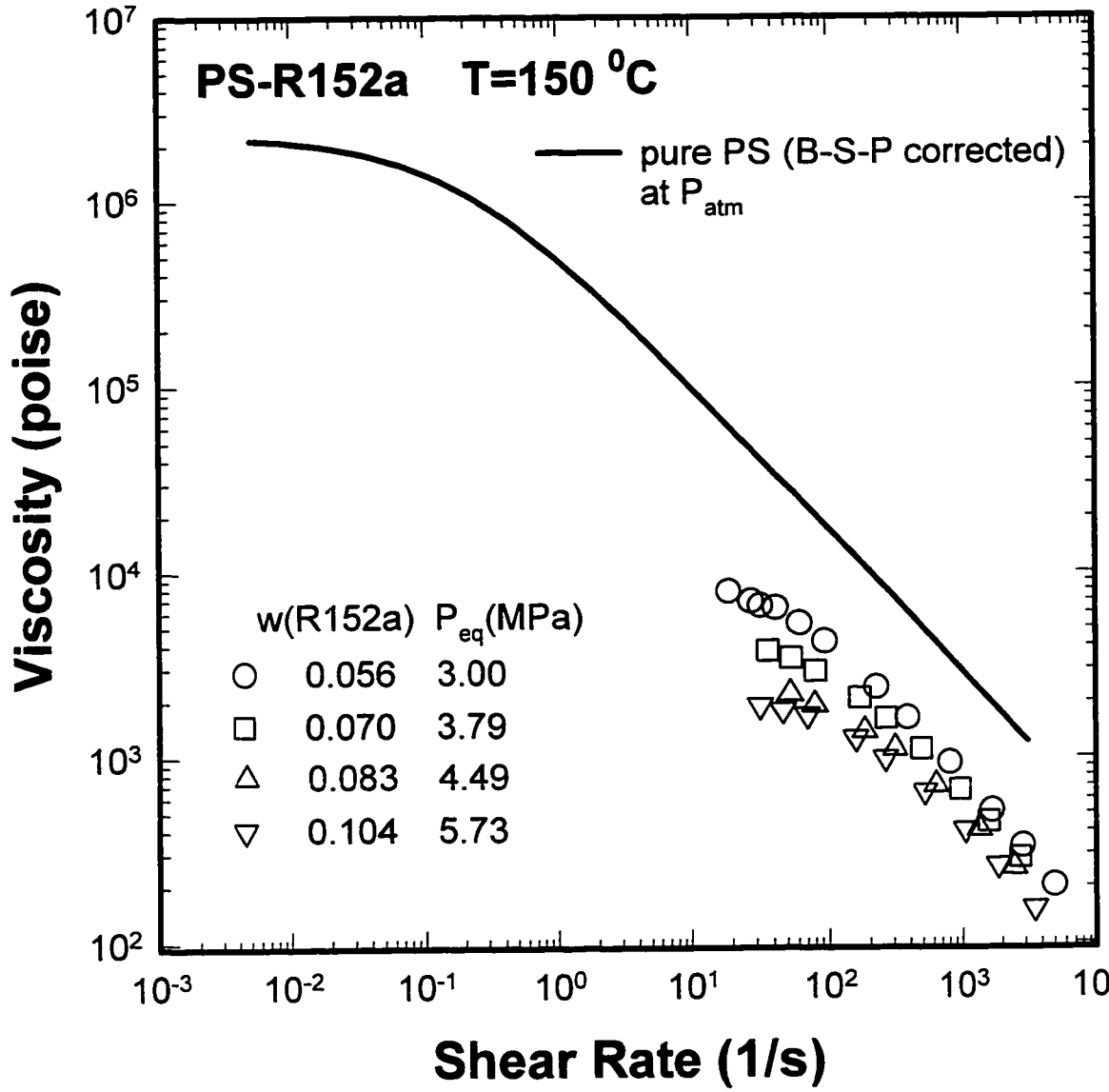

Figure 6.22(b)
Schuemmer-Pressure corrected Viscosities of PS-R152a at $P=P_{eq}$ (Equilibrium Pressure) and at T=150 °C compared with Bagley-Schuemmer-Pressure corrected Viscosity of pure PS at $P=P_{atm}$.

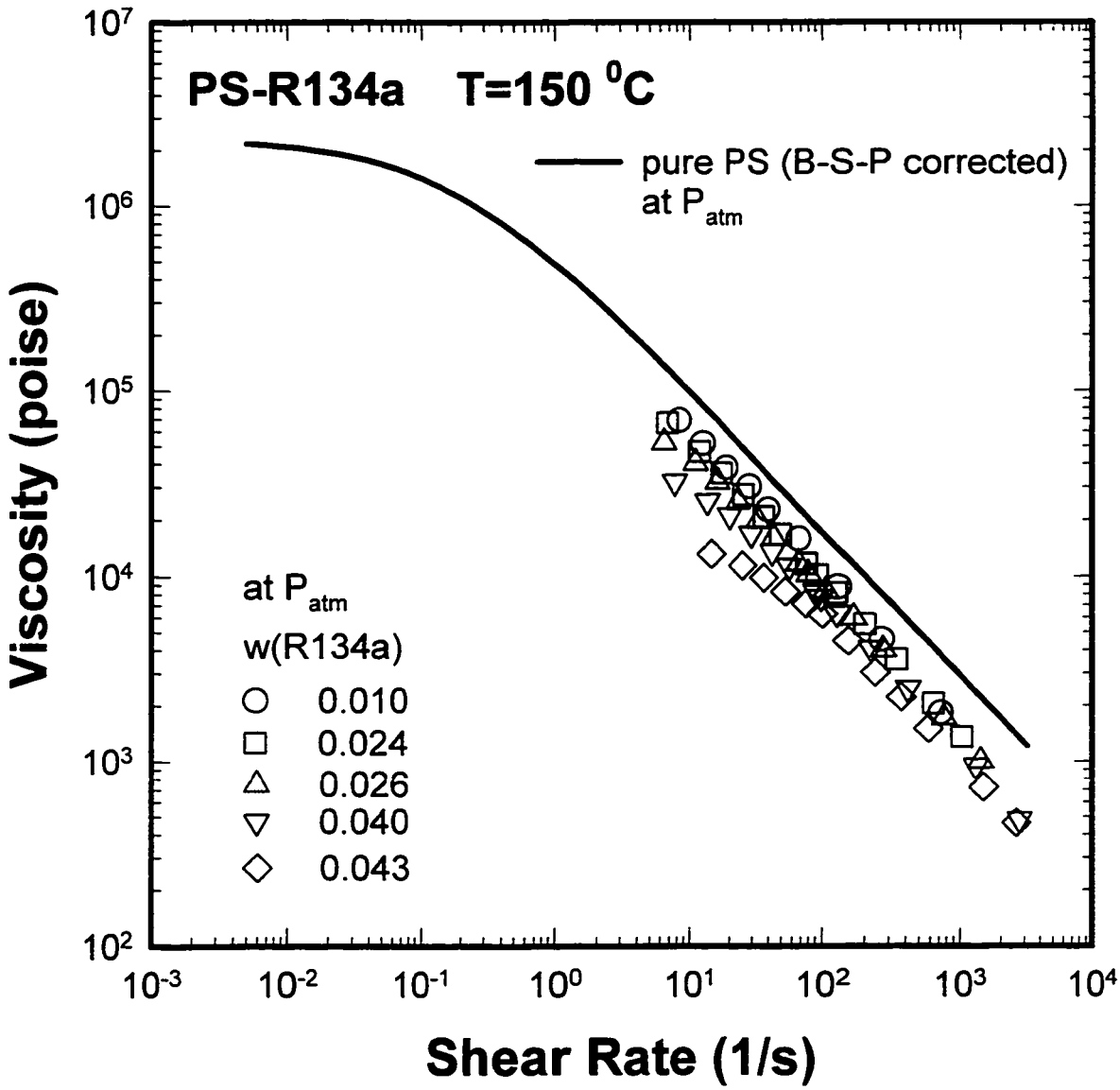

Figure 6.22(c)
Schuemmer-Pressure corrected Viscosities of PS-R134a at $P=P_{atm}$ and at T=150 °C compared with Bagley-Schuemmer-Pressure corrected Viscosity of pure PS at $P=P_{atm}$.

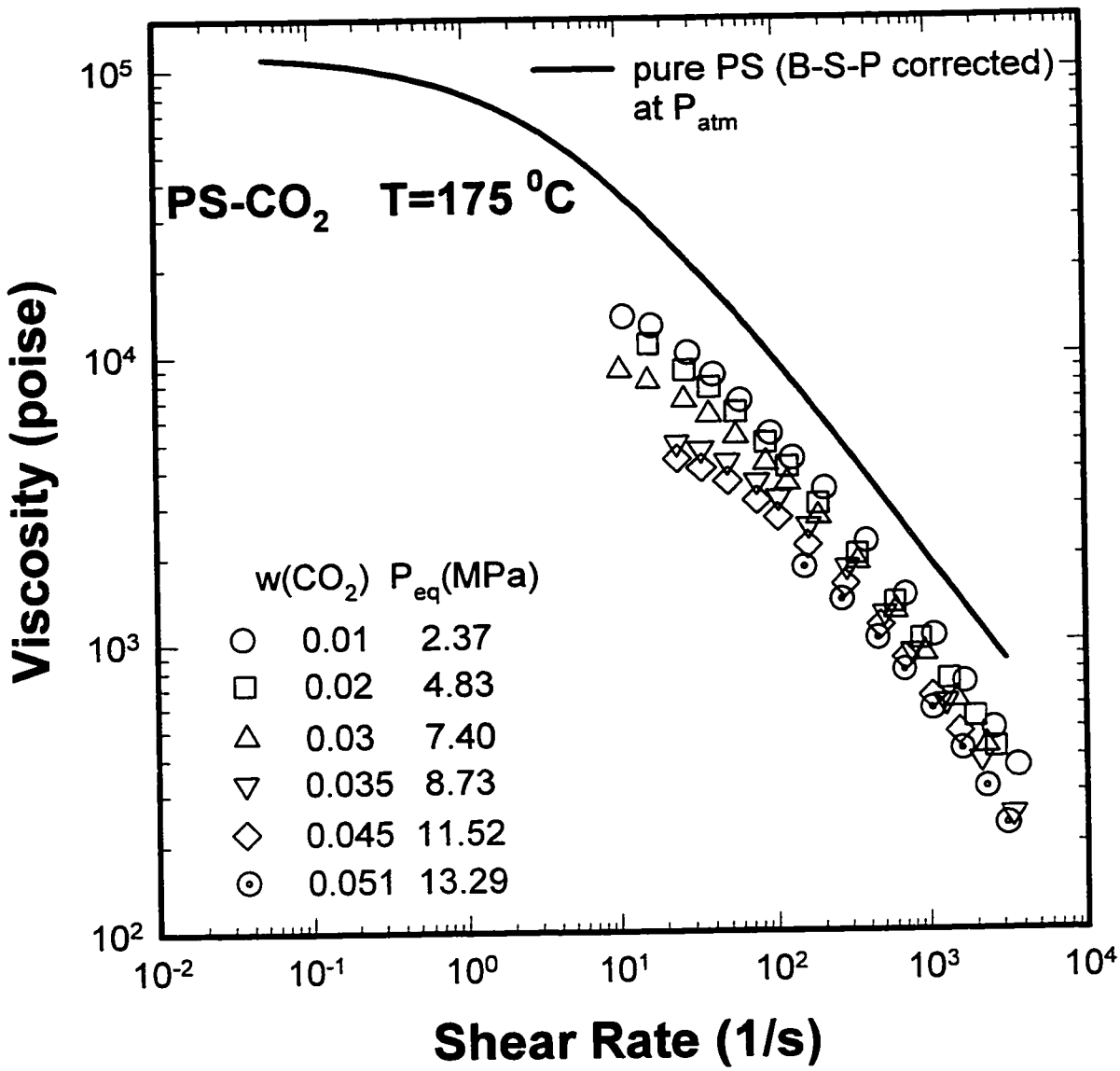

Figure 6.22(d)
Schuemmer-Pressure corrected Viscosities of PS-CO_2 at $P=P_{eq}$(Equilibrium Pressure) and at T=175 ^{0}C compared with Bagley-Schuemmer-Pressure corrected Viscosity of pure PS at $P=P_{atm}$.

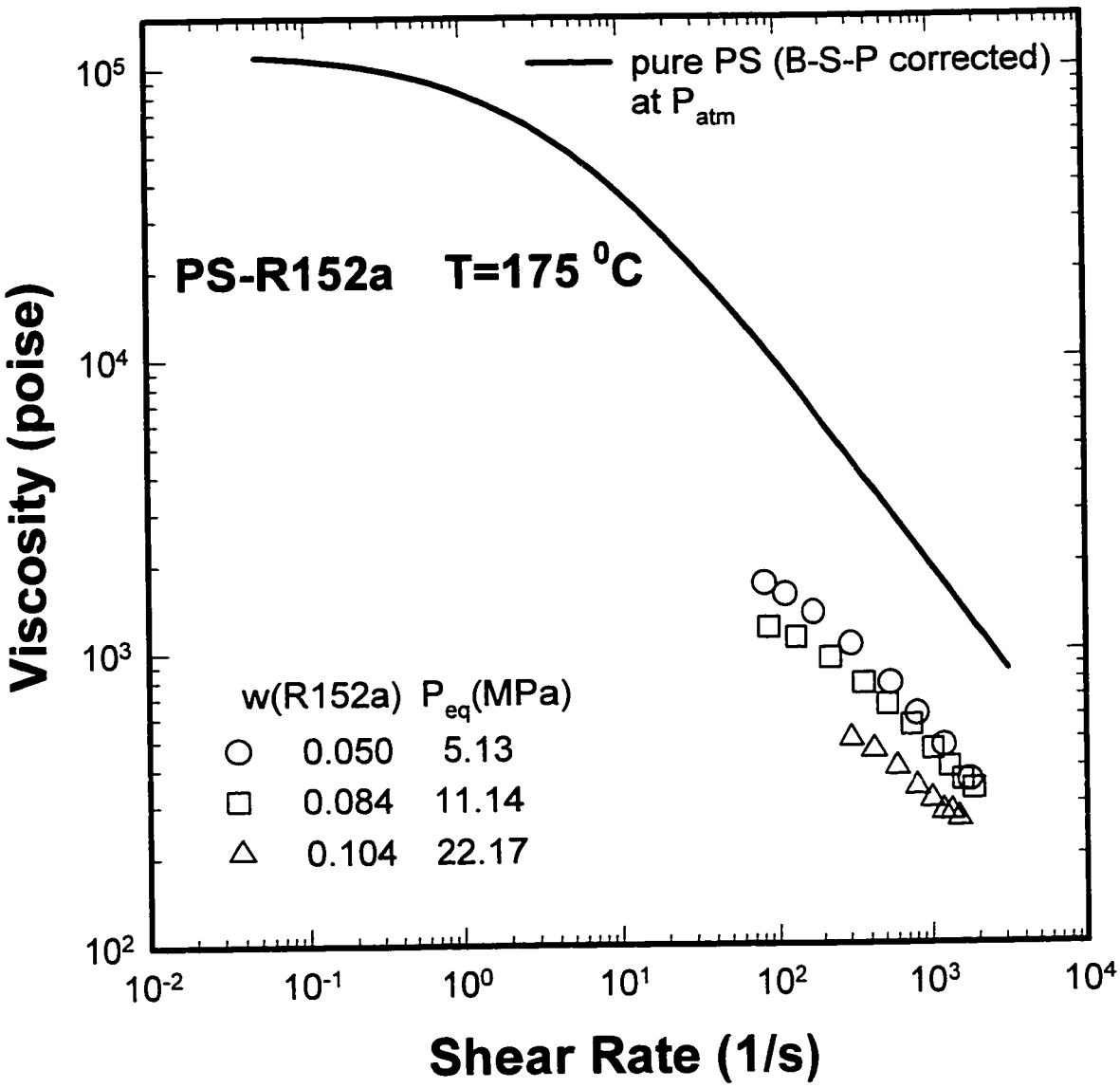

Figure 6.22(e)
Schuemmer-Pressure corrected Viscosities of PS-R152a at $P=P_{eq}$ (Equilibrium Pressure and at T=175 °C compared with Bagley-Schuemmer-Pressure corrected Viscosity of pure PS at $P=P_{atm}$.

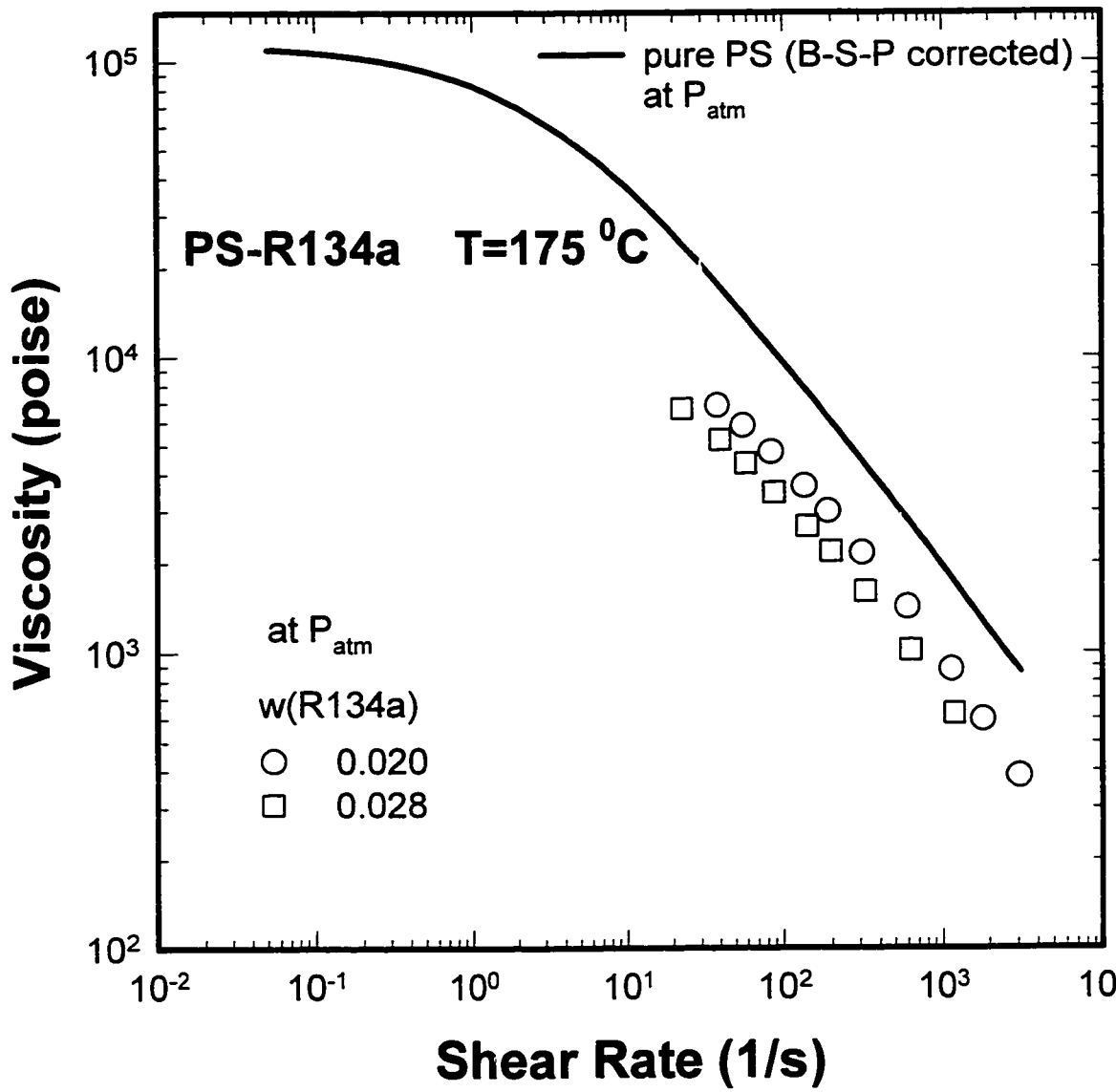

Figure 6.22(f)
Schuemmer-Pressure corrected Viscosities of PS-R134a at $P=P_{atm}$ and at T=175 ^{0}C compared with Bagley-Schuemmer-Pressure corrected Viscosity of pure PS at $P=P_{atm}$.

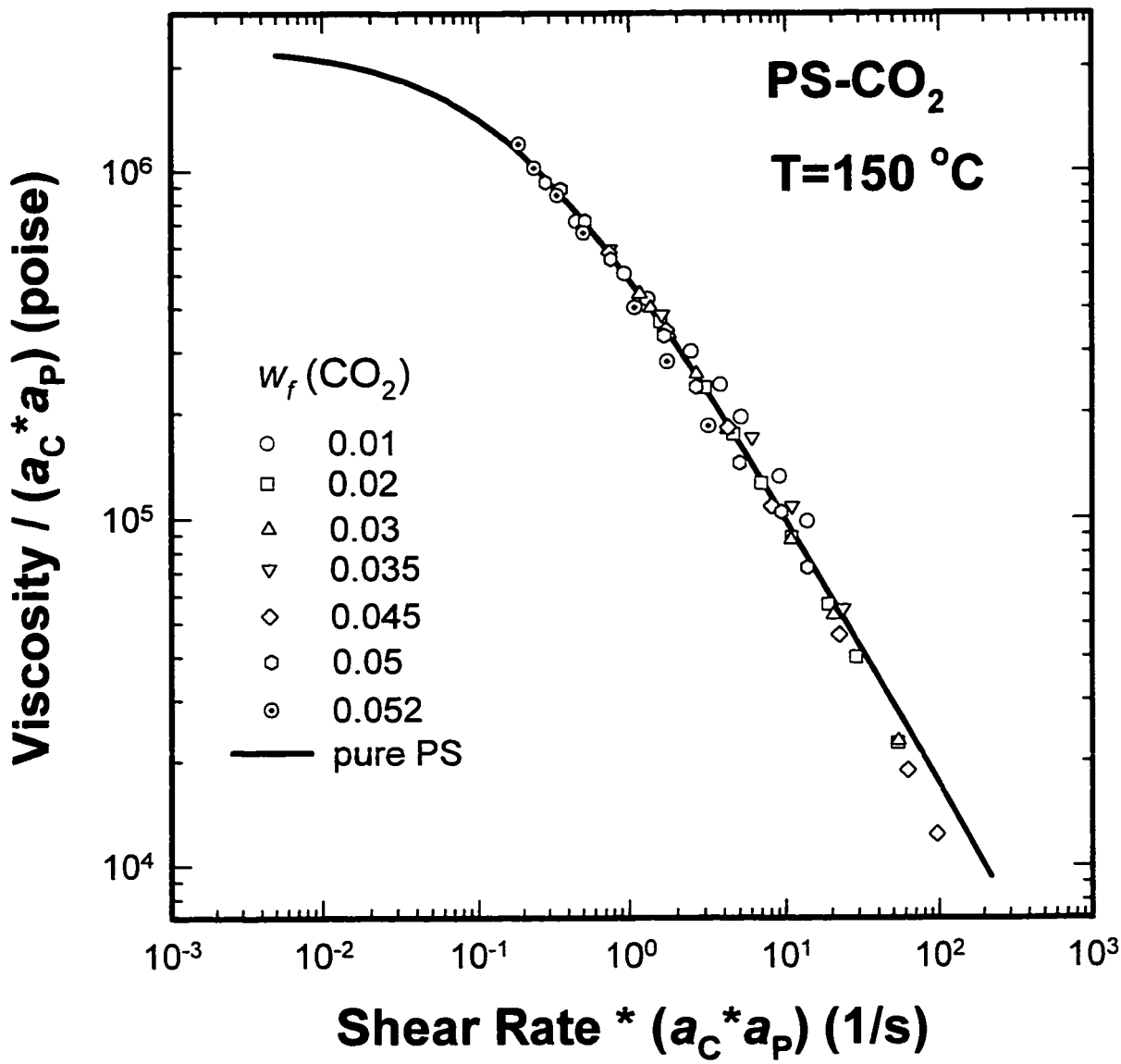

Figure 6.23(a)
Master Curve of Schuemmer-Pressure corrected Viscosities of PS-CO_2 shifted on Bagley-Schuemmer-Pressure corrected Viscosity of pure PS at $P=P_{atm}$ and T=150 ^{0}C.

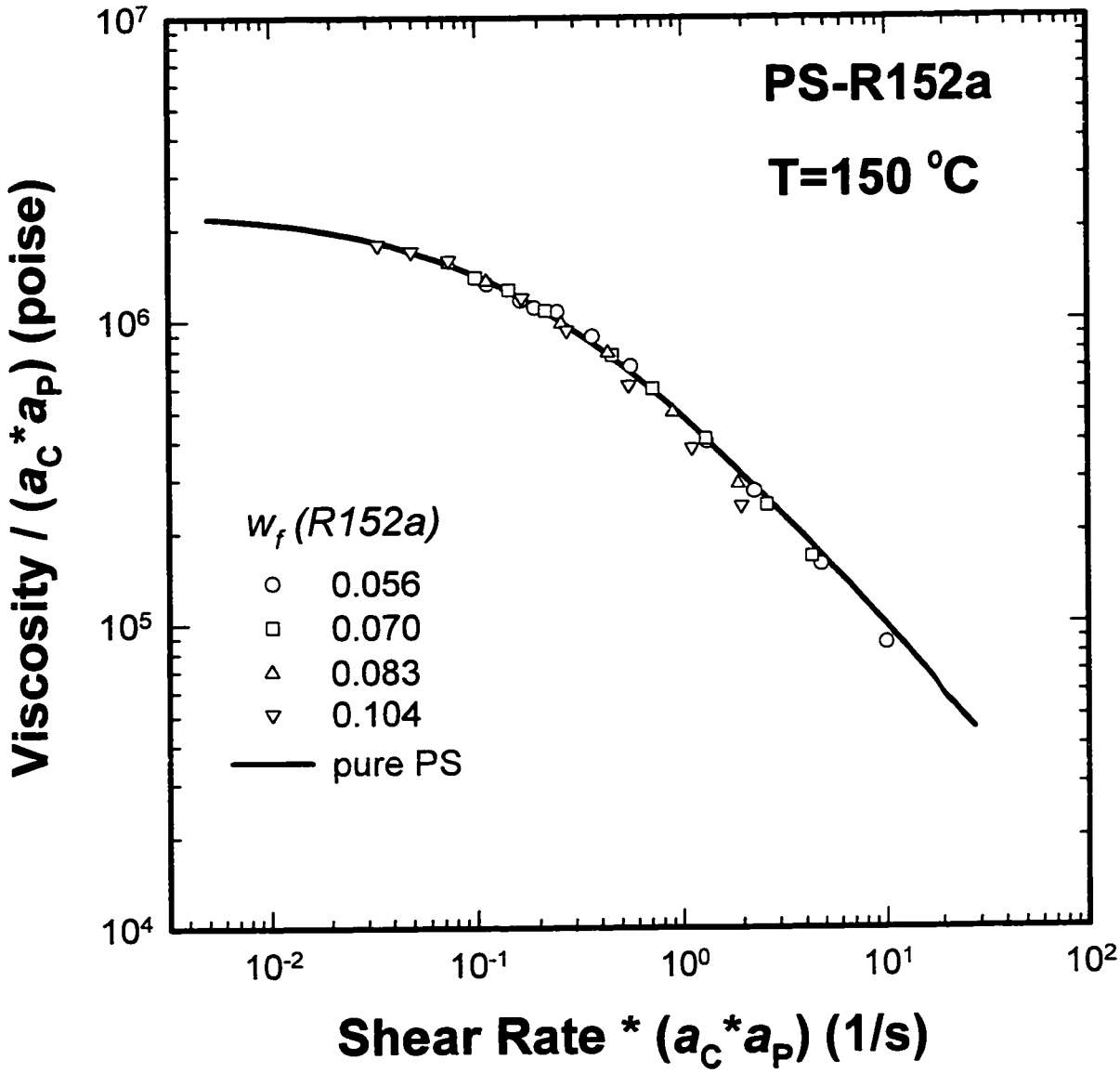

Figure 6.23(b)
Master Curve of Schuemmer-Pressure corrected Viscosities of PS-R152a shifted on Bagley-Schuemmer-Pressure corrected Viscosity of pure PS at $P=P_{atm}$ and T=150 ^{0}C.

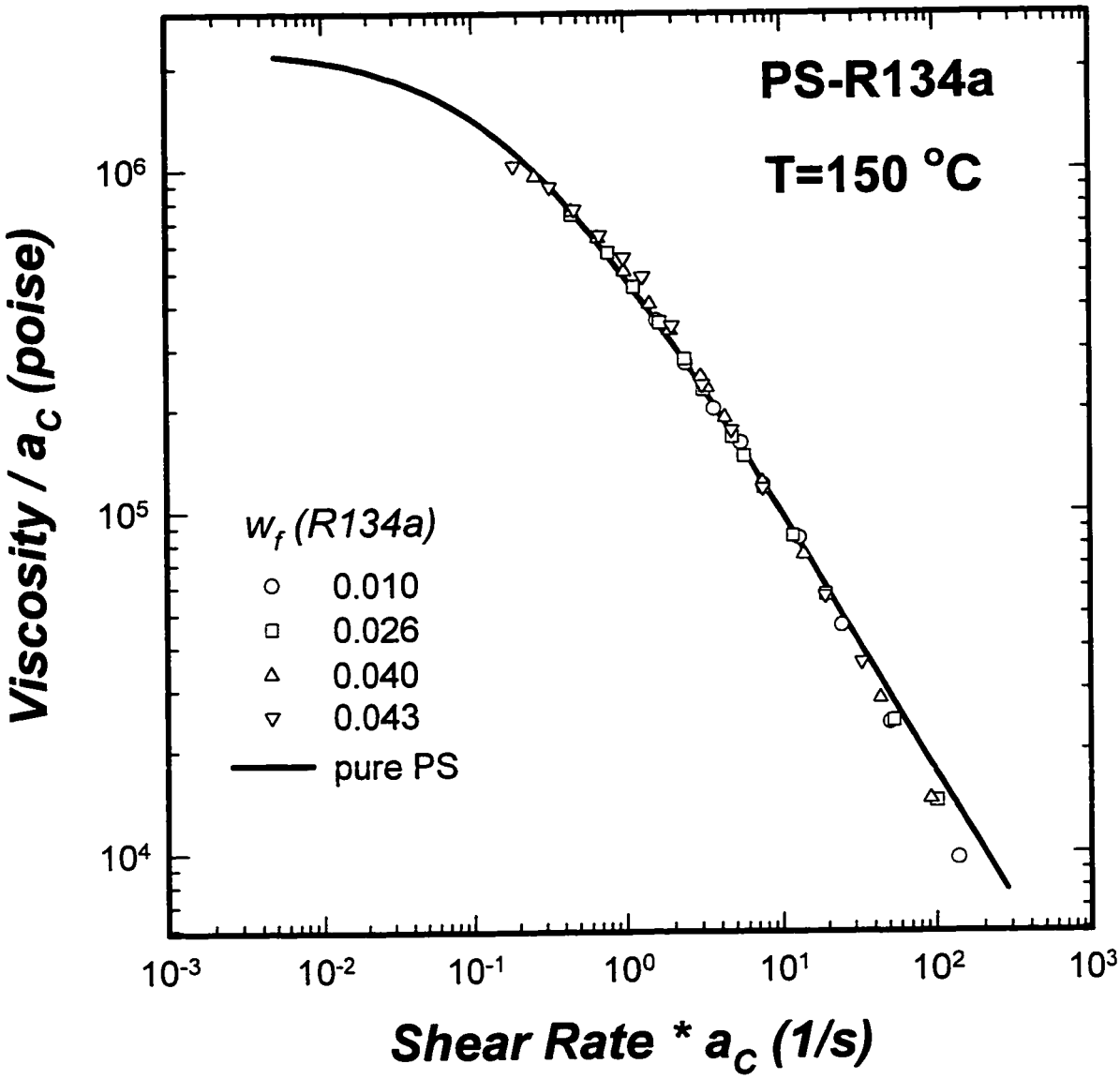

Figure 6.23(c)
Master Curve of Schuemmer-Pressure corrected Viscosities of PS-R134a shifted on Bagley-Schuemmer-Pressure corrected Viscosity of pure PS at $P=P_{atm}$ and T=150 ^{0}C.

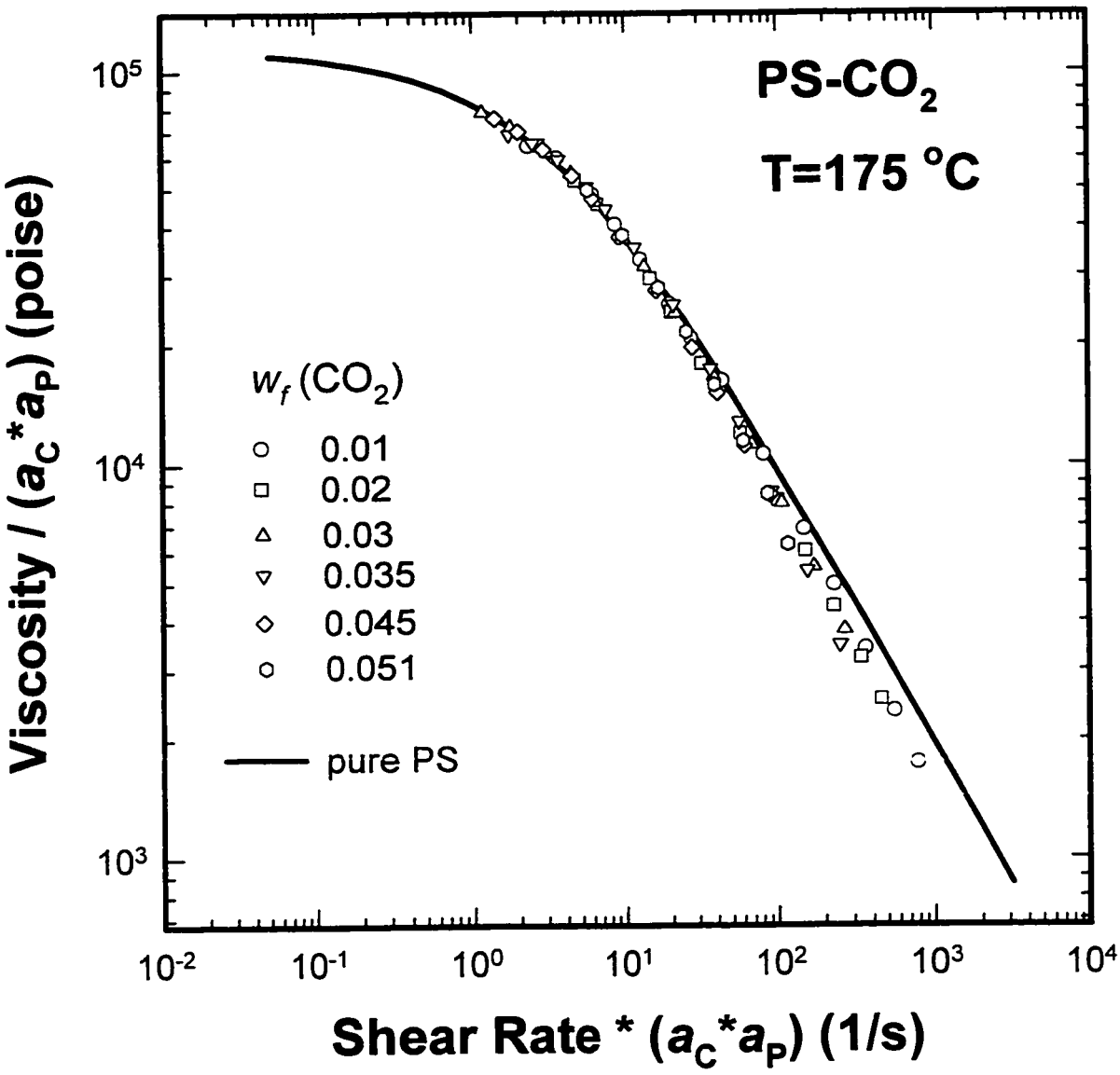

Figure 6.23(d)
Master Curve of Schuemmer-Pressure corrected Viscosities of PS-CO_2 shifted on Bagley-Schuemmer-Pressure corrected Viscosity of pure PS at $P=P_{atm}$ and T=175 ^{0}C.

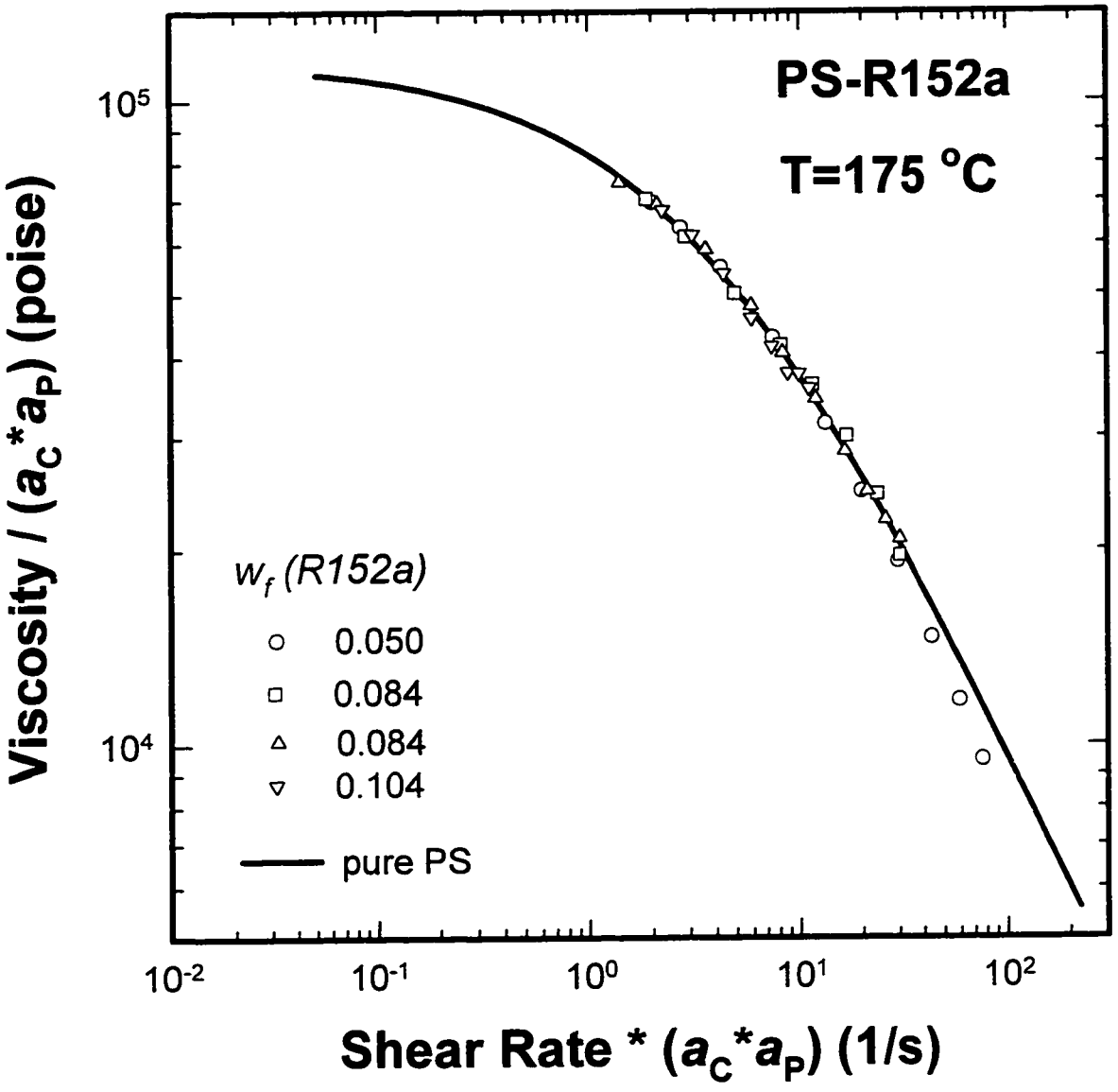

Figure 6.23(e)
Master Curve of Schuemmer-Pressure corrected Viscosities of PS-R152a shifted on Bagley-Schuemmer-Pressure corrected Viscosity of pure PS at P=P_{atm} and T=175 ^{0}C.

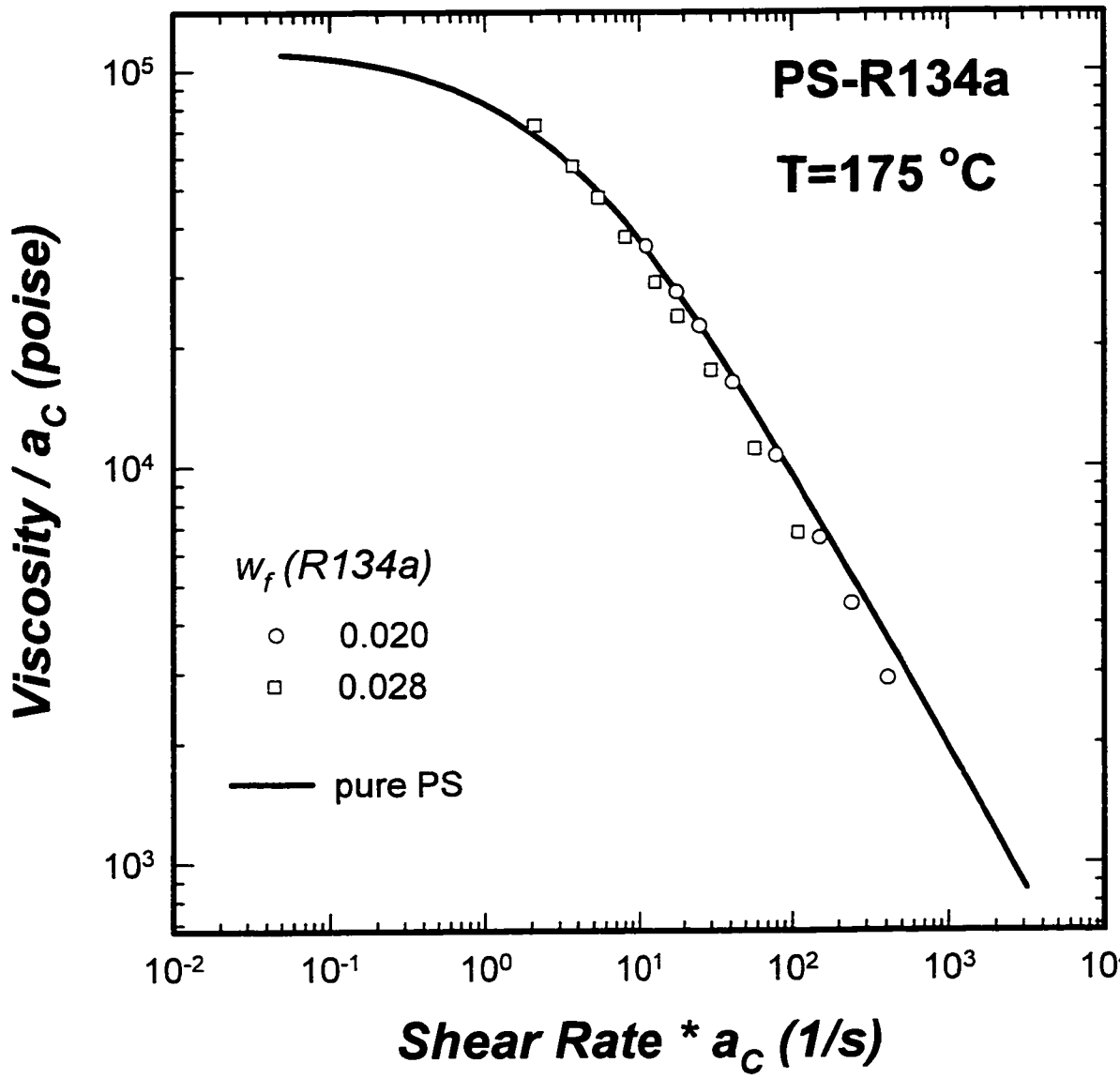

Figure 6.23(f)
Master Curve of Schuemmer-Pressure corrected Viscosities of PS-R134a shifted on Bagley-Schuemmer-Pressure corrected Viscosity of pure PS at $P=P_{atm}$ and T=175 ^{0}C.

with the theoretical prediction of viscosity reduction calculated by the extended free volume model in Chapter 7.

Every data point at each temperature is depicted together in Figure 6.24 for T=150 ^{0}C and Figure 6.25 for T=175 ^{0}C. By the incorporation of temperature shift factor, the data points in Figure 6.25 at T=175 ^{0}C can be shifted unto the pure PS viscosity model at T=150 ^{0}C giving a complete master curve in Figure 6.26. Consequently the close match of all shifted viscosity data of PS-SCG mixtures in the current study indicates that the combined application of shift factors, a_T, a_P, and a_C, is successful for PS-SCG.

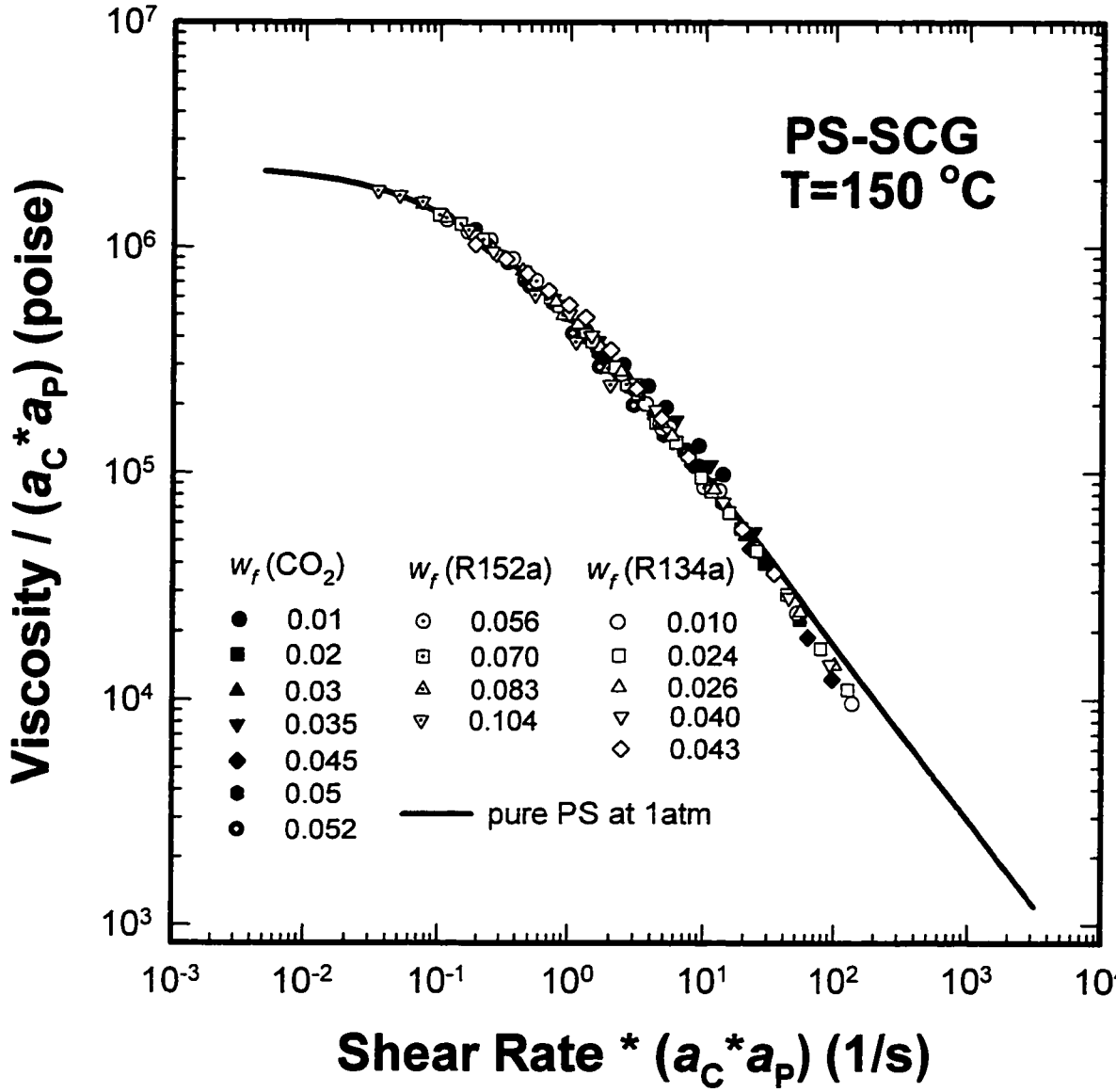

Figure 6.24
Master Curve of Schuemmer-Pressure corrected Viscosities of PS-SCG at T=150 ^{0}C shifted on Bagley-Schuemmer-Pressure corrected Viscosity of pure PS at P=P_{atm} and T=150 ^{0}C.

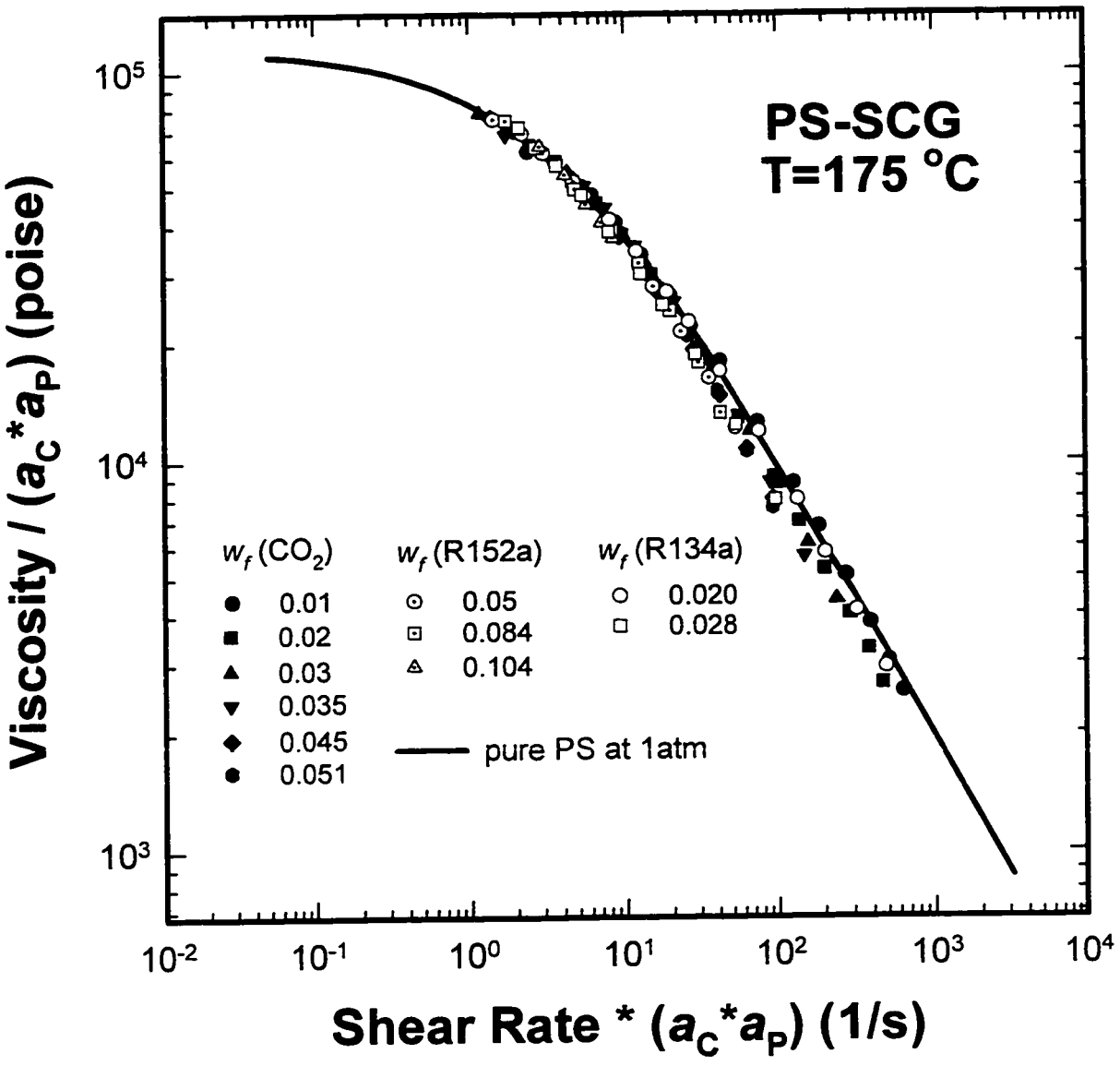

Figure 6.25
Master Curve of Schuemmer-Pressure corrected Viscosities of PS-SCG at T=175 ^{0}C shifted on Bagley-Schuemmer-Pressure corrected Viscosity of pure PS at P=P_{atm} and T=175 ^{0}C.

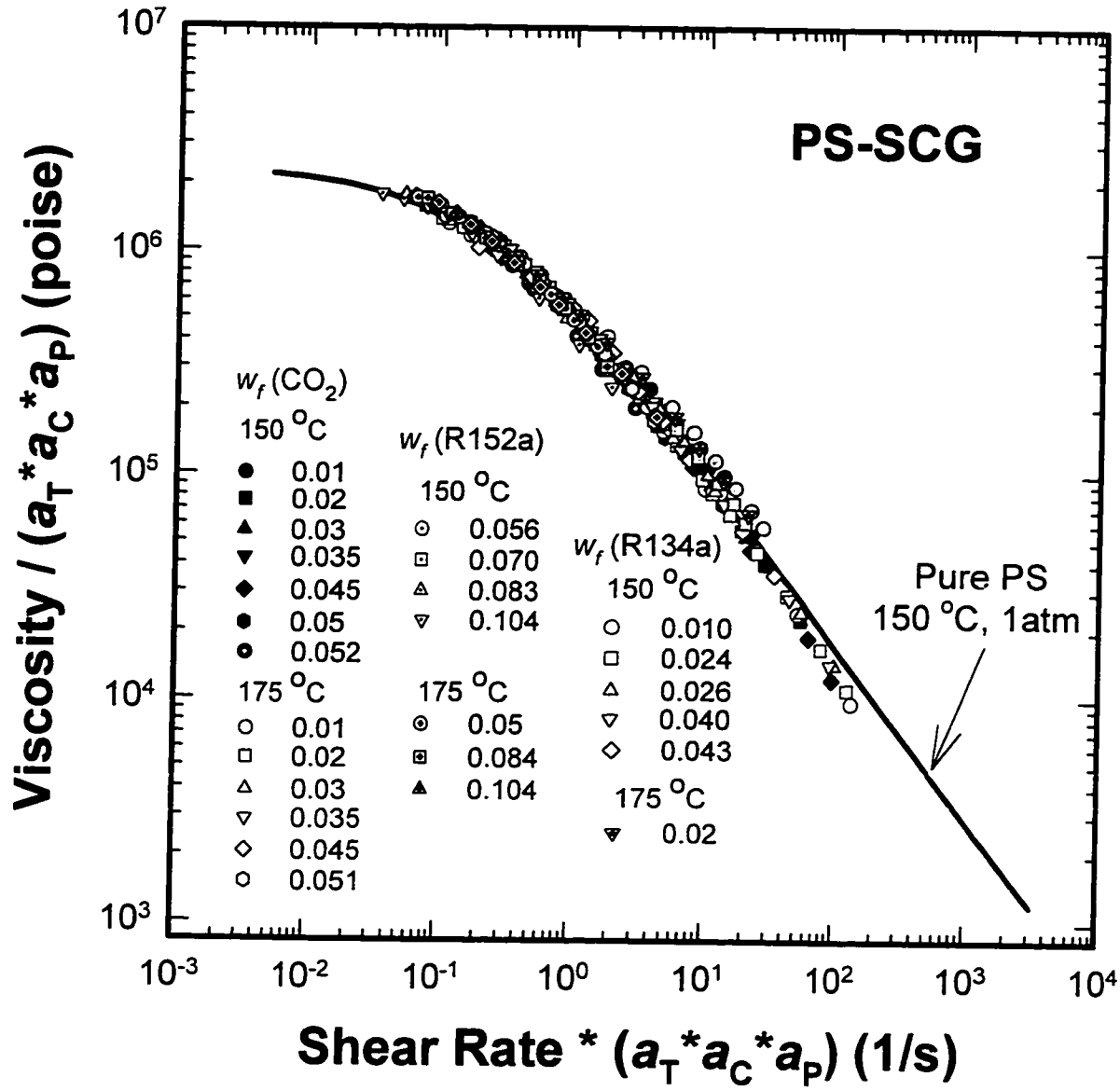

Figure 6.26
Master Curve of Schuemmer-Pressure corrected Viscosities of PS-SCG at T=150 and 175 ^{0}C shifted on Bagley-Schuemmer-Pressure corrected Viscosity of pure PS at P=P_{atm} and T=150 ^{0}C.

CHAPTER 7

VISCOSITY REDUCTION AND FREE VOLUME RHEOLOGICAL MODEL

The viscosity reduction by added supercritical gases which was experimentally proven in the current study can be examined theoretically by the free volume rheological model. Equation (4.15) represents the estimated viscosity reduction calculated by the ratio of viscosity of the PS-SCG mixture to that of pure PS, which is equivalent to ($a_C \cdot a_P \cdot a_T$). If the temperature and the pressure are kept constant, i.e., a_P and a_T become unity, the viscosity ratio in Equation (4.15) is equivalent to the concentration shift factor, a_C.

The equilibrium pressure for a given composition and temperature was chosen as the reference pressure for PS-CO2 and PS-R152a mixtures, and the atmospheric pressure for PS-R134a mixture. The only effect of diluent onto viscosity reduction, a_C, will be presented and discussed in this chapter.

$$\frac{\eta_m}{\eta_P} = w_P^n \left(\frac{\rho_m}{\rho_P}\right)^n \exp\left[\frac{1}{f_m} - \frac{1}{f_P}\right] \tag{4.22}$$

In order to apply Equation (4.22), densities of pure components and the mixture, the occupied volumes of pure components, and the exponent, n should be available.

7.1 Parameter Estimations for Free-Volume Rheological Model

7.1.1 Computation of Mixture Density

As stated in Chapter 4, while densities of pure components are obtained directly using the Sanchez-Lacombe equation of state for pure component, the evaluation of mixture density needs the binary interaction parameter. The binary interaction parameter,

δ_{ij}, was evaluated through the non-linear curve fitting of available solubility data shown in Figure 5.4 and 5.5 by Khan [1997]. Computed binary interaction parameters for PS-CO_2 and PS-R152a systems at 150 and 175 ^{0}C are tabulated in Table 7.1.

Table 7.1
Evaluated Binary Interaction Parameters

	T (^{0}C)	P (MPa)	δ_{ij}	Reference
PS-CO_2	35 50	1 – 7 1 – 7	0.100 0.098	Wissinger and Paulaitus (1987)
	100 140 180	1 – 25 1 – 25 1 – 25	0.0980 0.0961 0.1100	Sato et al. (1996)
	150 175	1 – 25 1 – 25	0.1048 0.1089	Interpolation
PS-R152a	135 160	1 – 16 1 – 16	0.046 0.087	Garg et al. (1994)
	150 175	1 – 16 1 – 16	0.0685 0.1054	Interpolation

The densities of PS-SCG mixtures and pure components were estimated for each equilibrium condition which was computed for pressures ranging 0.25 to 25 MPa at an increment of 0.25 MPa at 150 and 175 ^{0}C respectively.

7.1.2 Exponential Factor

The exponent n in Equation (4.15) was computed by the iso-free volume experiment using mono-dispersed polystyrene introduced in Section 5.7. The free volume rheological model is modified for the iso-free volume case as:

$$\frac{\eta_m}{\eta_P} = w_P{}^n \tag{7.1}$$

Exclusive reviews [Boyer, 1963; Kaelble, 1970; Haward, 1970] on the concept of free volume are subjected to polymers including polystyrene. Figure 7.1 shows the fitted data indicating that n varies from 3.33 to 3.59 depending on the initial slope determination. In the current study, the value of n was fixed to 3.4 which is between the minimum and maximum values from the experiment and confirmed by many previous investigations [van Krevelen, 1990].

7.1.3 Occupied Volume of Polystyrene

The occupied volume is an important characteristic in determining free volume fraction. In the current study, the occupied volume of polystyrene was evaluated from a series of Newtonian viscosity data over a wide range of temperatures measured by the Weissenberg Rheogoniometer. The Kelly-Bueche free volume, which relates the viscosity of pure polymer to the specific volume and the occupied volume, is given as

$$\eta = B\exp\left(\frac{V}{V - V_0}\right) \tag{7.2}$$

where B is a constant.

By the curve fitting of experimental viscosity data, the occupied volume was obtained as 0.941 cm^3/g as depicted for pure polystyrene in Figure 7.2.

An occupied volume of 0.933 cm^3/g is obtained by curve fitting the average values of temperature shift factors of PS measured in several investigations for temperatures ranging from 150 to 260 ^0C [Meister, 1992]. Williams [1951] gave 0.940 cm^3/g in his theoretical analysis of WLF equation for polystyrene. The volume of closest molecular packing of polystyrene, which represents the occupied volume

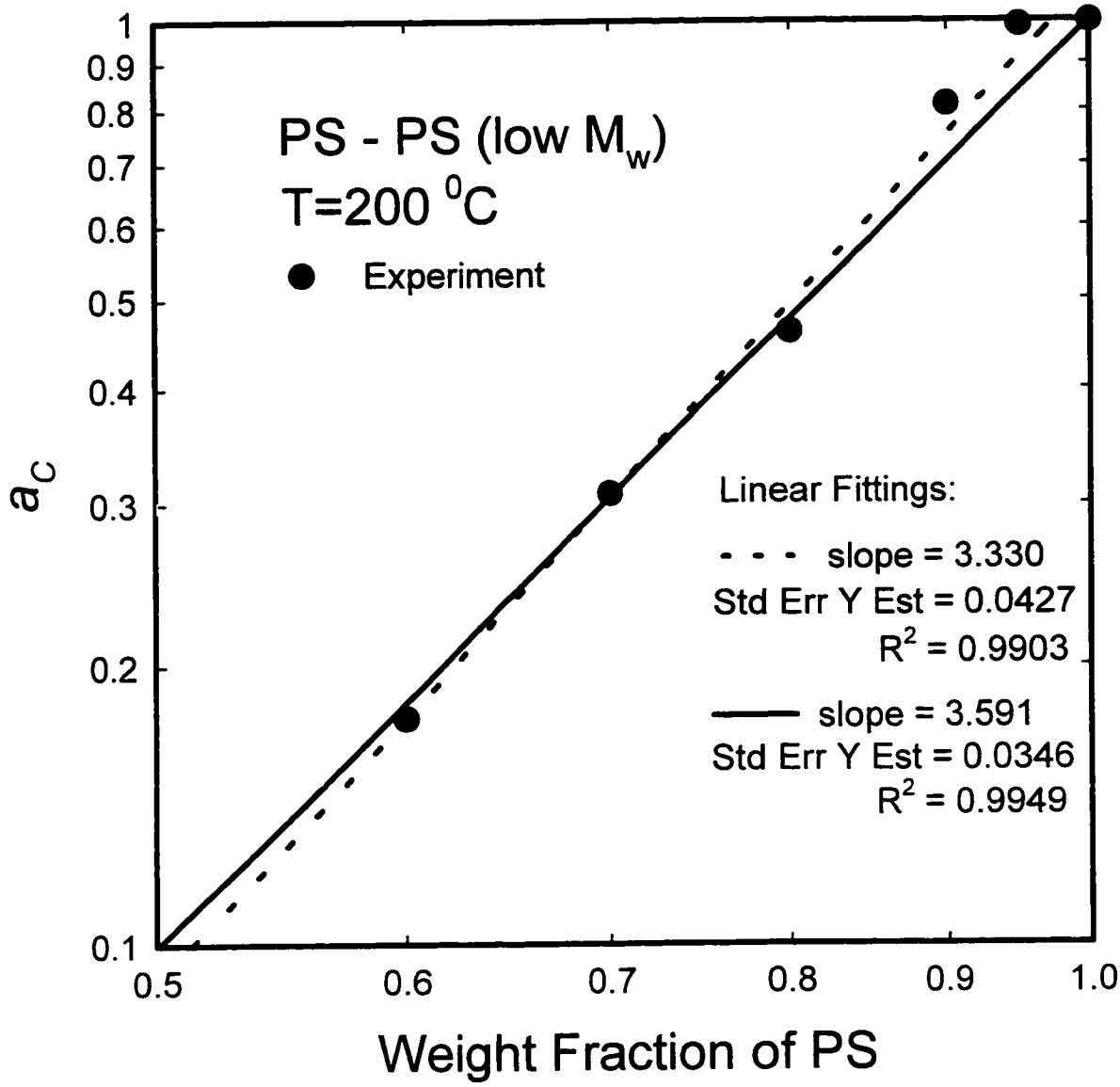

Figure 7.1
Viscosity Reduction of PS by addition of Lower Molecular Weight PS having same Free Volume at T=200 ^{0}C.

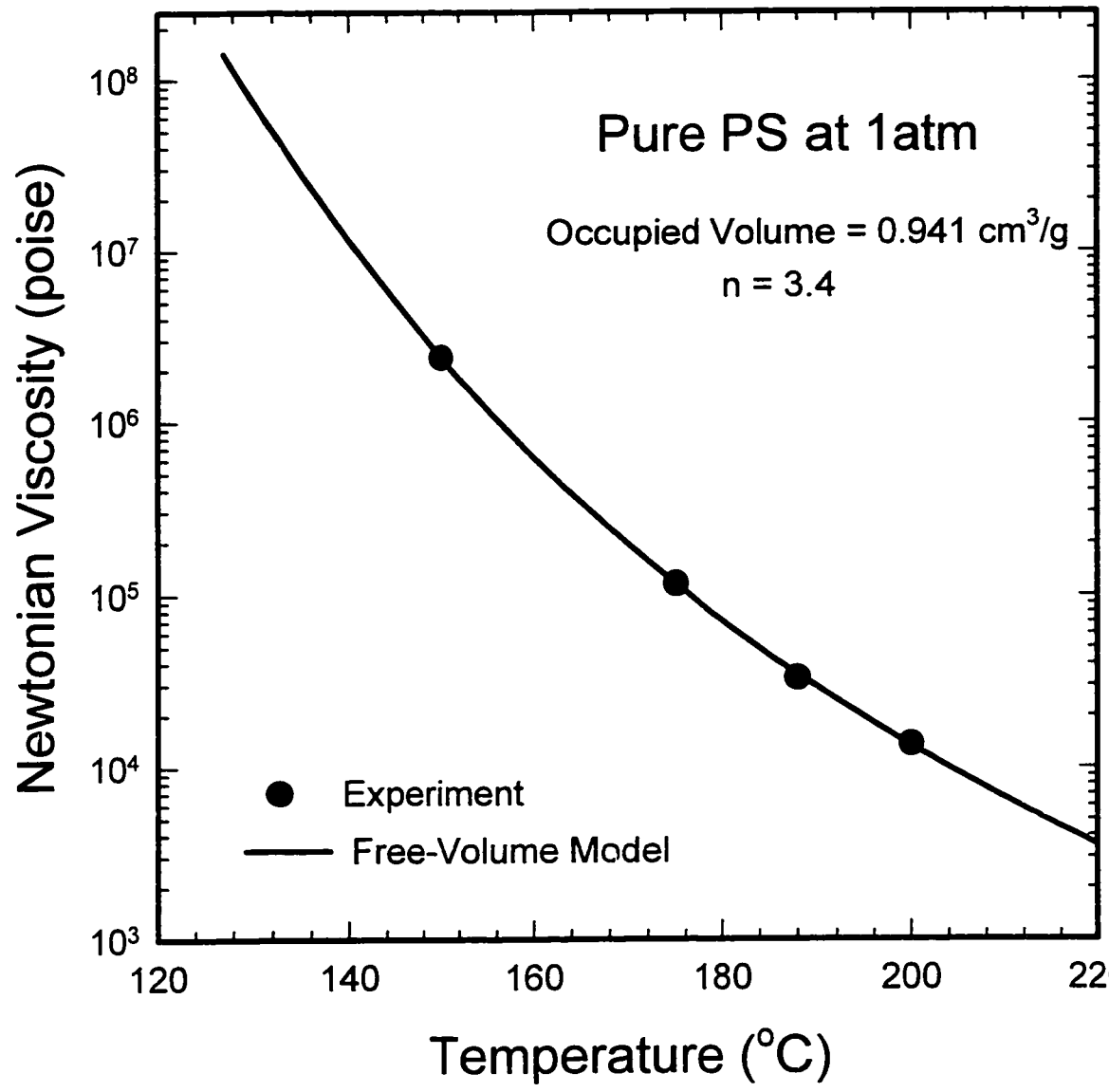

Figure 7.2
Temperature-dependent Viscosity of pure PS for Evaluation of Occupied Volume of pure PS by Free Volume Rheological Model.

thermodynamically, has been reported as 0.849 cm^3/g [Bondi, 1964A], 0.82 cm^3/g [Blitz, 1934], and 0.85 cm^3/g [Haward et al., 1966]. As mentioned by Utracki [1985], the free volume for the rheological modeling should be obtained rheologically and might be different from the thermodynamic free volume.

7.1.4 Occupied Volume of Supercritical Gases

Occupied volumes of supercritical gases are shown in Table 4.1 and 4.2. The occupied volume should be precisely computed for the accurate estimation of the free volume and the viscosity reduction. For the current study, the occupied volume of carbon dioxide was selected as 0.5995 cm^3/g. Two different values of occupied volumes by the group contribution method in Table 3.4 were used for R152a, i.e., 0.6277 cm^3/g and 0.7509 cm^3/g.

7.2 Polystyrene – Carbon Dioxide

The experimental viscosity reductions due to dissolved carbon dioxide at 150 and 175 ^0C are compared with the theoretical prediction using the free volume rheological model in Figure 7.3. The error bars in Figure 7.3 reflect the span of pressure coefficient with standard deviation shown in Figure 6.17, which influences the pressure correction, the pressure shift, and accordingly the evaluation of concentration shift factor.

As the temperature increases, the free volume fraction of pure polystyrene becomes greater causing less contribution of dissolved gas to the reduction of viscosity as shown in Figure 7.3. The free volume rheological model predicts the viscosity reduction fairly at compositions lower than 4 weight percent of carbon dioxide for both

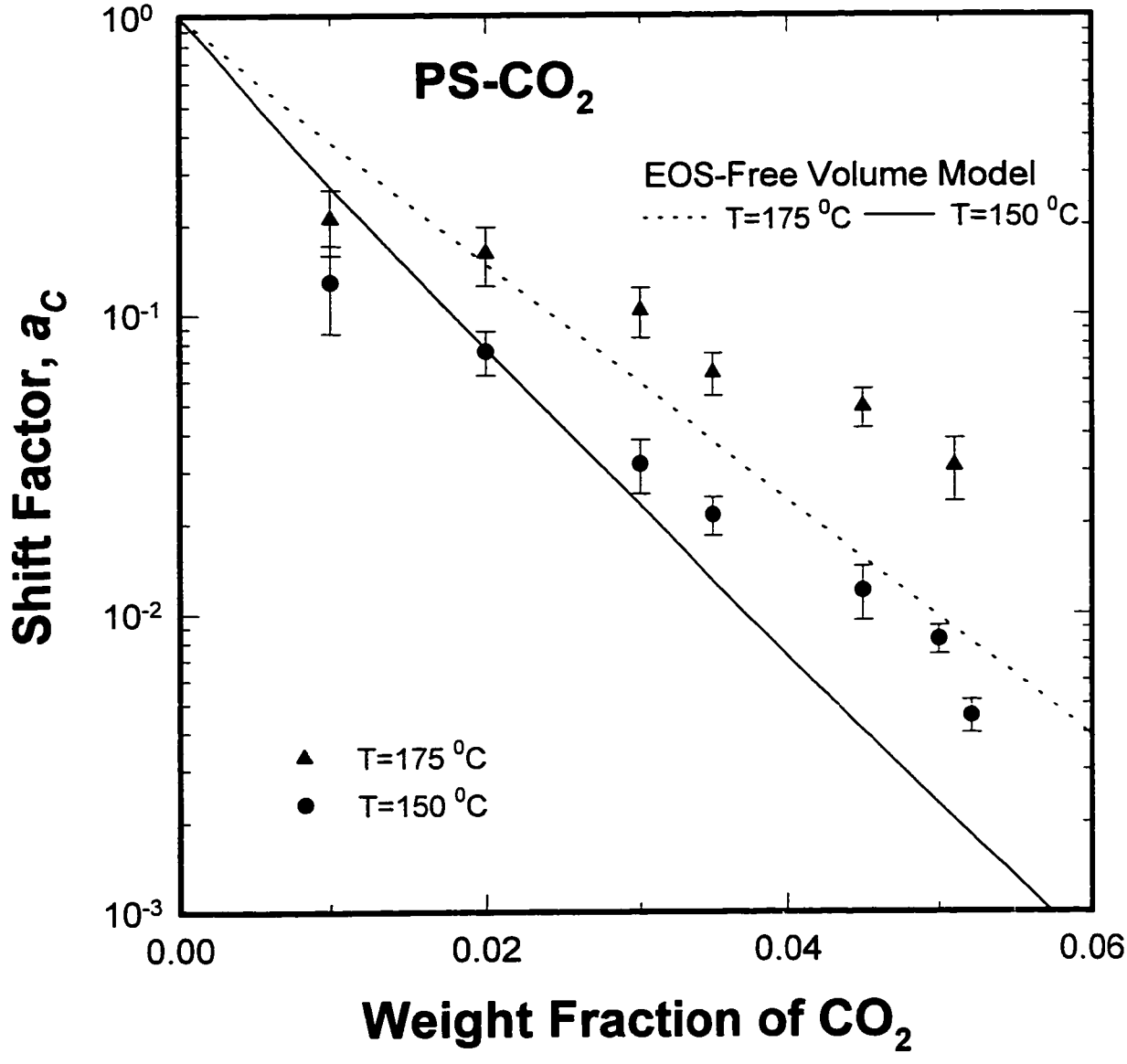

Figure 7.3
Viscosity Reduction of PS-CO_2 obtained by Experiments and Free Volume Rheological Model Prediction at T=150 and 175 ^{0}C.

temperatures. The theoretical viscosity reduction shows a linear dependence unto the weight fraction in log-log scale, while the experimental results exhibit a gradual decay of shift factor for higher compositions.

At higher compositions, over 4 weight percent, the experimental shift factor decreases gradually with the weight fraction. From the experimental point of view, such a pattern of shift factor can be explained by recognizing the higher back-pressures needed for higher gas contents. As the dissolved amount of gas increases, the equilibrium pressure is also increased, demanding much higher back-pressure, which was kept higher than corresponding equilibrium pressure, in order to insure a single phase mixture extruded during measurement. Figure 7.4 indicates the variation of equilibrium pressure for PS-SCG estimated by the Sanchez-Lacombe equation of state model for mixture at T=150 and 175 ^{0}C. Due to the limitation of back-pressure (maximum 18 MPa) which is set for the maximum allowable load limit of the load cell, the extra pressure exerted over the equilibrium pressure is smaller for higher compositions. It can not be concluded that the insufficient back-pressure would be the only elucidation for the gradual change of experimental shift factor. In Section 7.6 the Chow's model presents a pattern of shift factors showing slow change at moderate compositions.

The theoretical prediction of viscosity reduction induced by dissolved carbon dioxide are depicted for different values of occupied volumes of carbon dioxide at 150 ^{0}C and compared with experimental results in Figure 7.5. The occupied volume of diluent has to be determined accurately, since it influences the theoretical prediction of viscosity reduction significantly. As in the case of pure polystyrene, there are differences between thermodynamic and rheological occupied volumes. It may be postulated that the

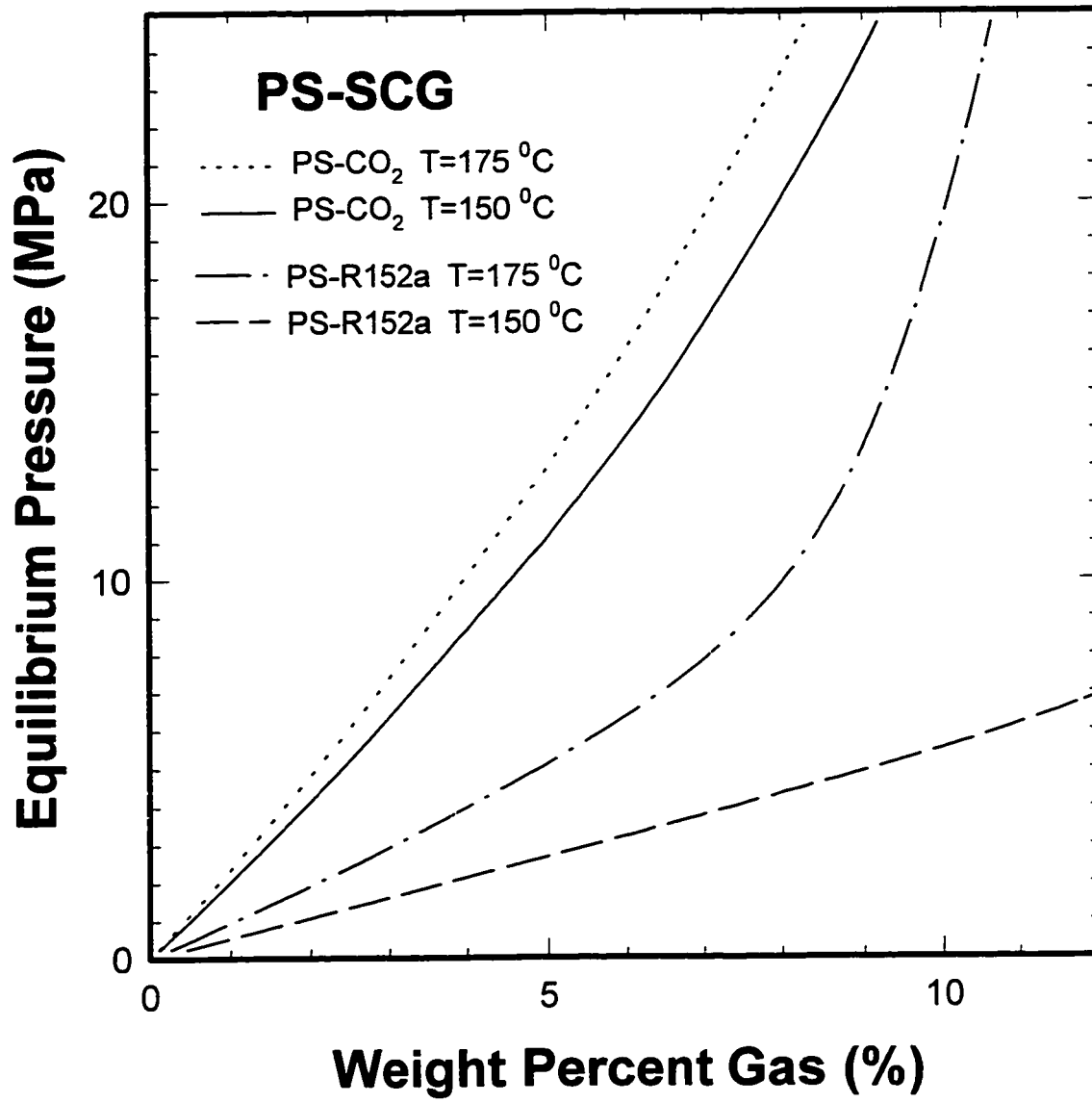

Figure 7.4
Equilibrium Pressures for PS-CO_2 and PS-R152a Mixtures at T=150 and 175 ^{0}C computed by Equation of State Model.

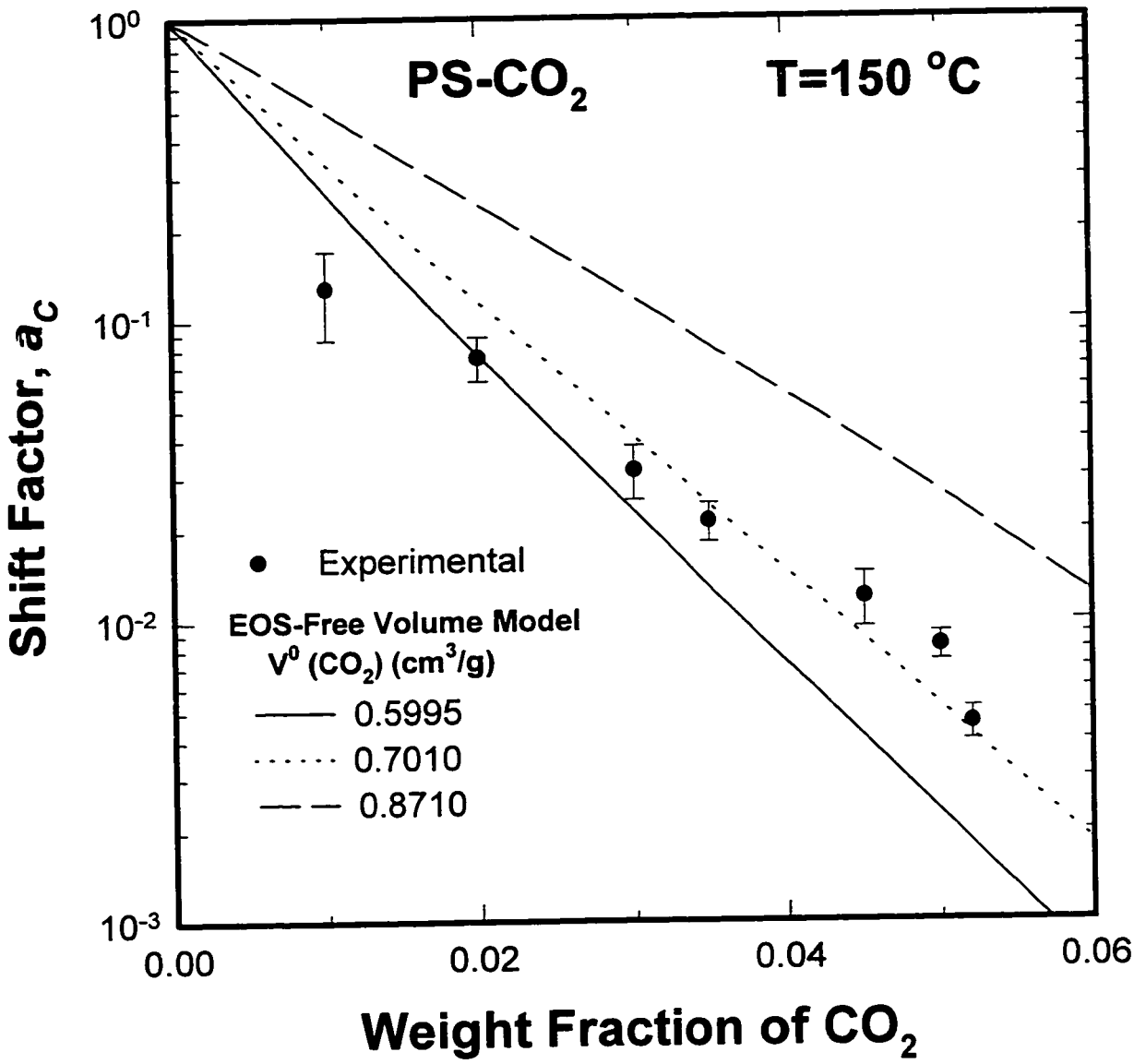

Figure 7.5
Viscosity Reduction estimated by Free Volume Rheological Model for PS-CO_2 with different Occupied Volumes of CO_2 at T=150 ^{0}C.

discrepancy between thermodynamic occupied volume and rheological one also exist for supercritical gases.

7.3 Polystyrene-Difluoroethane

It was demonstrated from the desorption curves for PS-SCG mixtures, Figure 4.2, that R152a exhibits a remarkable solubility and compatibility to PS yielding enhanced free volume fraction and consequently a great viscosity reduction. The viscosity reductions of PS-R152a mixture at T=150 and 175 ^{0}C are presented in Figure 7.6 with theoretical predictions based on two different occupied volumes of R152a. At T=150 ^{0}C, the viscosity reduction approaches three-orders of magnitude around 10 weight percent of R152a and experimental shift factors show close matches with theoretical predictions with some deviations at the highest composition.

The theoretical predictions demonstrate a linear relationship with slight curvature for 150 ^{0}C and for 175 ^{0}C a relatively rapid decay of viscosity reduction is estimated in the ranges over 8 weight percent which can be related to the abrupt increase of the equilibrium pressure shown in Figure 7.4.

The two experimental data points for 175 ^{0}C over 8 weight percent were measured under relatively insufficient back-pressure conditions due to the increased equilibrium pressures for the compositions. In this case the disagreement between experimental and theoretical shift factors can be attributed to the erroneous experimental data due to back-pressure insufficiency.

The occupied volume of 0.6227 cm^3/g, which was calculated by the group contribution method using the molar van der Waals volumes suggested by Bondi [1964],

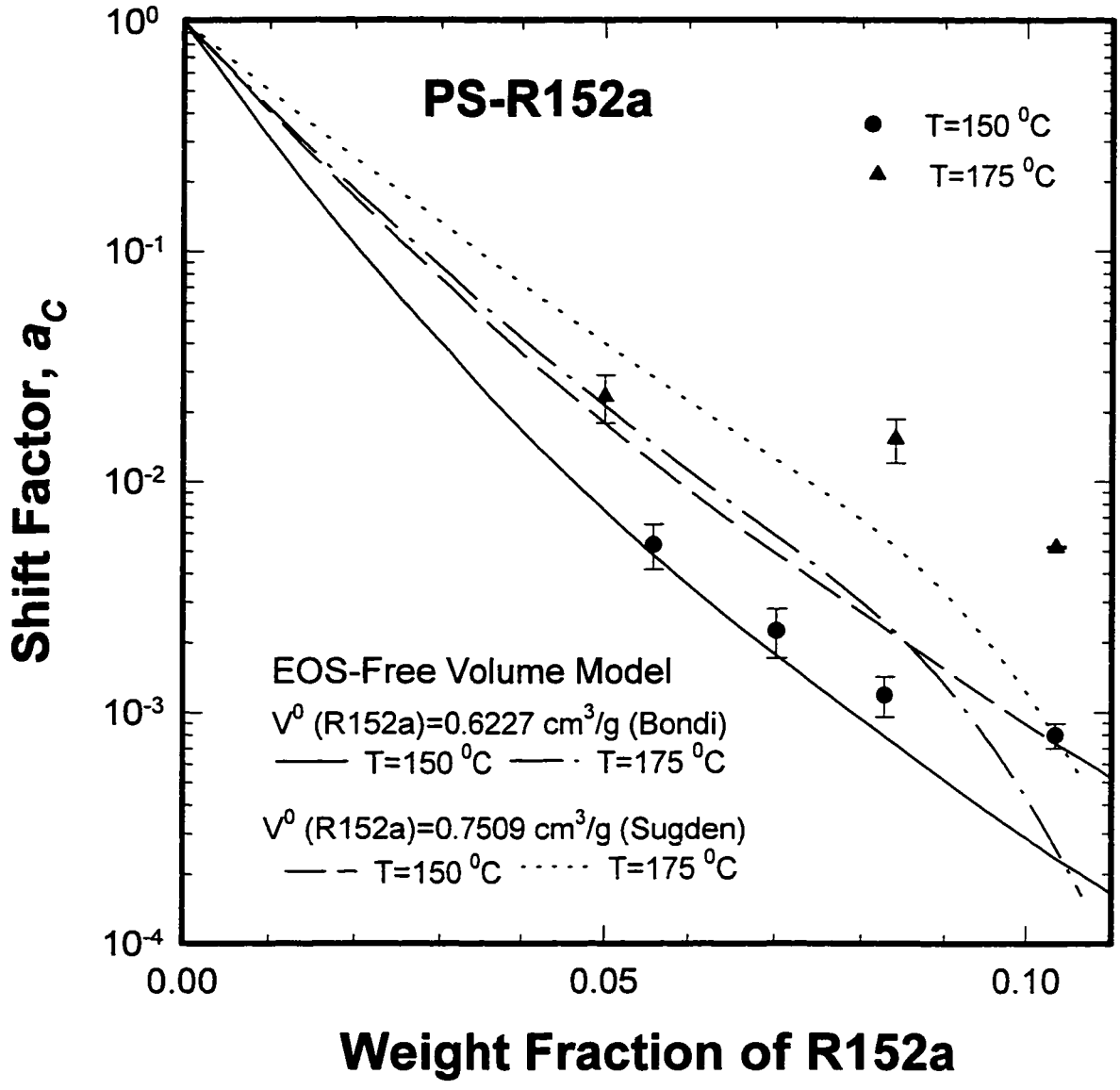

Figure 7.6
Viscosity Reduction of PS-R152a by Experiments and Free Volume Rheological Model Prediction at T=150 and 175 °C.

generates better curve fitting at 150 ^{0}C than the other one. Only the first data point is fitted exactly at 175 ^{0}C, but the two data points at higher composition probably have experimental errors. Therefore the occupied volume of 0.6227 cm^3/g might be judged as more reasonable one in comparison with 0.7509 cm^3/g which was also computed by the group contribution method using molar occupied volumes given by Sugden [1927].

7.4 Polystyrene-tetrafluoroethane

Since the solubility data of R134a in polystyrene was not available, the Sanchez-Lacombe equation of state model could not be applied and consequently theoretical estimation of viscosity reduction by the free volume rheological model was not performed. Without knowledge of equilibrium pressures the measurement was done at high back-pressures ranging 15 to 18 MPa.

Only experimental data are represented in Figures 7.7. Relatively more fluctuations in the experimental viscosity reduction can be seen and the effect of pressure coefficient is substantial compared with other PS-SCG mixtures indicating the measurement with higher degree of non-homogeneous mixtures.

7.5 Chain Dilution and Free Volume Effect

From the iso-free volume experiment with mono-dispersed polystyrenes of widely different molecular weights, the exclusive effect of dilution of chain entanglement can be evaluated. The viscosity reduction by the dilution of chain entanglement is less than one order of magnitude as shown in Figure 7.8. Therefore, it is evident that the great reduction of viscosity of PS-SCG mixtures is brought mainly by the increment of free

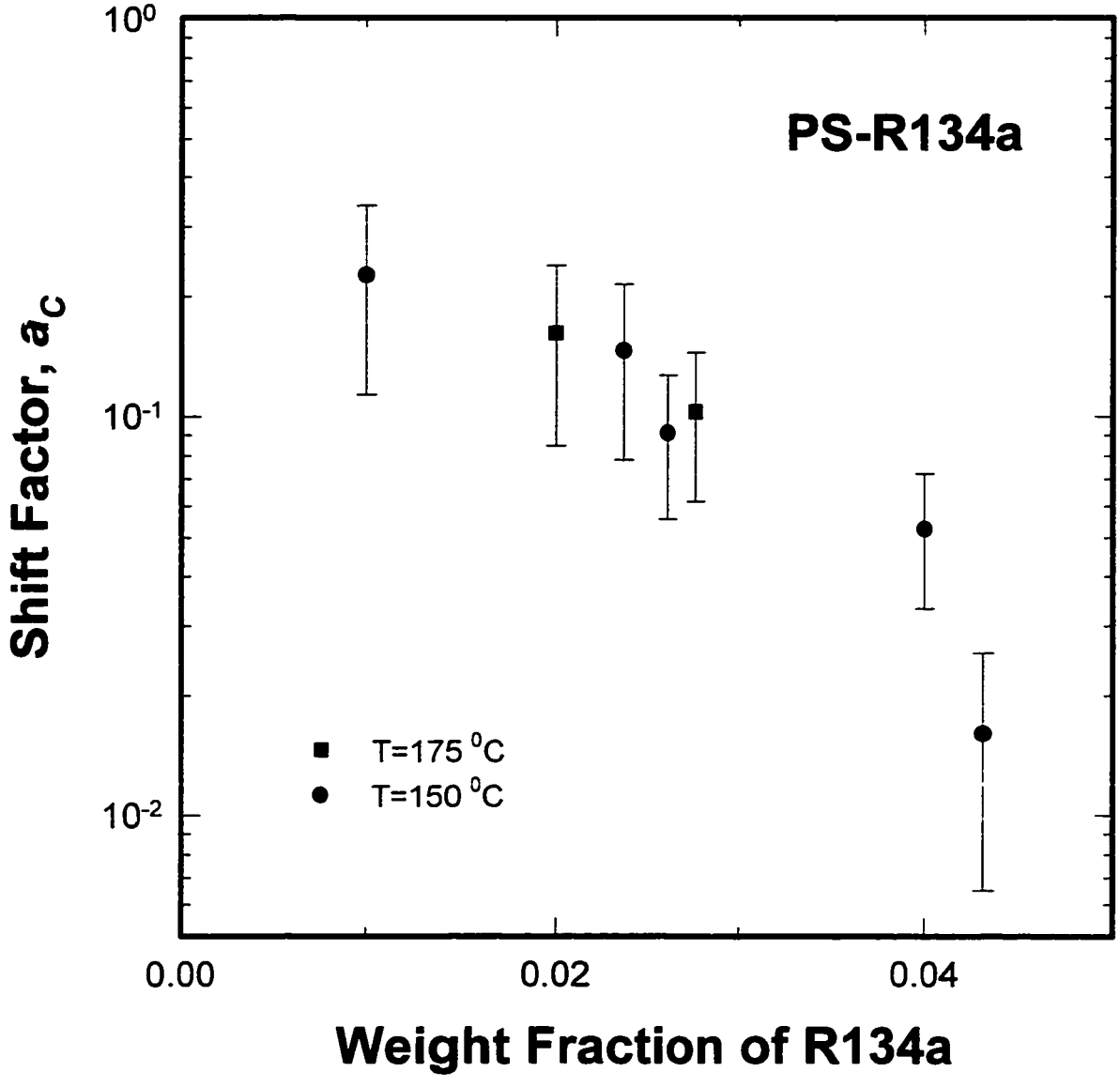

Figure 7.7
Viscosity Reduction of PS-R134a by Experiments at T=150 and 175 °C.

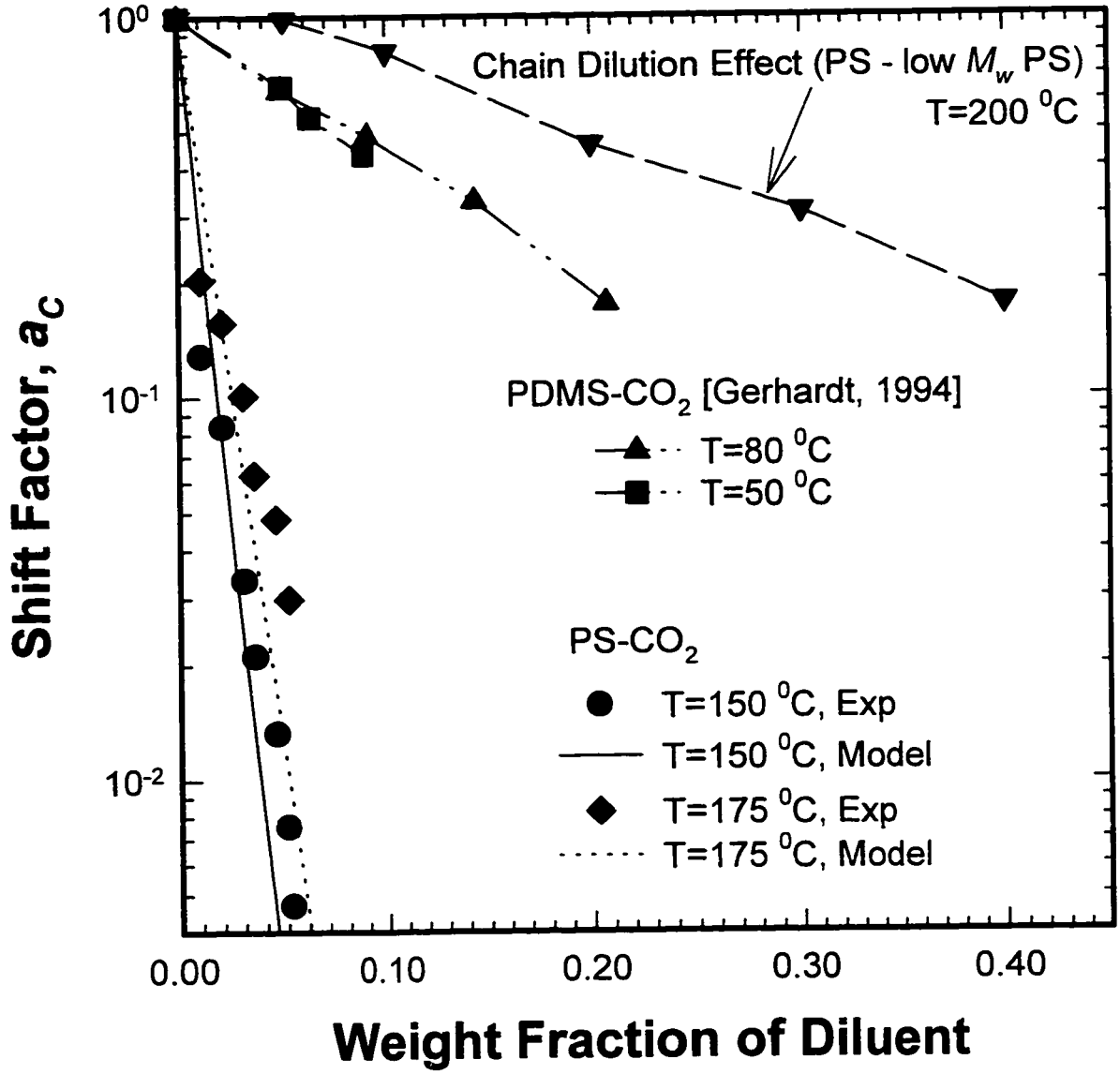

Figure 7.8
Viscosity Reductions due to CO_2 for PS-CO_2 and PDMS-CO_2 Mixtures compared with the Contribution of low M_w-PS having same Free Volume Fraction with PS making an Iso-Free Volume Solution.

volume due to the dissolved supercritical gas.

As Kwag et al. [1995] reported, the viscosity reduction becomes great for the polymer and diluent mixture when the viscosity measurement is conducted at temperatures near the T_g of pure polymer since the pure polymer has only a little fractional free volume at this temperature regime. This statement is confirmed by the comparison with the viscosity reduction of PDMS-CO_2 mixtures at 50 and 80 ^{0}C [Gerhardt, 1994] and that of PS-CO_2 at 150 and 175 ^{0}C in Figure 7.8. The relatively small reduction of viscosity of PDMS-CO_2 is explained by the fact that the pure PDMS at 50 and 80 ^{0}C is far from and way above its glass transition temperature (T_g of PDMS = -128 ^{0}C) and comprising larger amount of free volume. In contrast the pure PS at 150 and 175 ^{0}C is much more glassy and having limited free volume fraction. Therefore a large viscosity reduction was possible through the free volume enhancement brought by added carbon dioxide.

7.6 Theoretical Models using WLF Equation

The Chow's formula [1980], Equation (2.21) through (2.23) which provide the depression of T_g for diluted polymeric system, can be examined through the comparison of viscosity reduction or shift factor with the equivalent a_T of the diluted polystyrene calculated using the WLF equation with the estimated T_g.

$$\ln\left(\frac{T_g}{T_{g0}}\right) = \beta\{(1-\theta)\ln(1-\theta) + \theta(1-\theta)\} \tag{2.21}$$

$$\beta = zR / M_p \Delta C_{pp} \tag{2.22}$$

$$\theta = (M_p / zM_d)(w/(1-w) \tag{2.23}$$

The depression of T_g produces a single line for PS-SCG mixtures regardless of species of gases as shown in Figure 7.9. It is assumed that the estimated T_g of diluted polystyrene by Chow's model is valid at the equilibrium pressure of a certain composition.

The concentration shift factor was calculated by Equation (4.7) for PS-SCG mixtures

$$\ln a_C = \ln\left[\frac{\eta_0(T, P_{eq}, c)}{\eta_0(T, P_{eq}, c_0)}\right] = -\frac{C_1\{T - T_g(P_{eq}, c)\}}{C_2 + \{T - T_g(P_{eq}, c_0)\}} \tag{4.7}$$

The calculated concentration-shift factor are compared with the experimental results and the predictions by the free volume rheological model in Figure 7.10 and 7.11 for T=150 ^{0}C and T=175 ^{0}C respectively.

The viscosity reduction is dependent only on the molecular weight of added species and the interaction between polystyrene and gases are not considered. The viscosity reduction calculated based on the depressed T_g by the Chow's model exhibits an initial rapid decrease of shift factor followed by gradual decrease at higher compositions, which is similarly represented by experimental data points. Although the experimental shift factors overall locate close to the curve of Chow's model for PS-CO_2 for both temperatures, the application of Chow's model to the evaluation of viscosity reduction should be performed with caution that it is an ideal theoretical estimation which does not include the interaction between components.

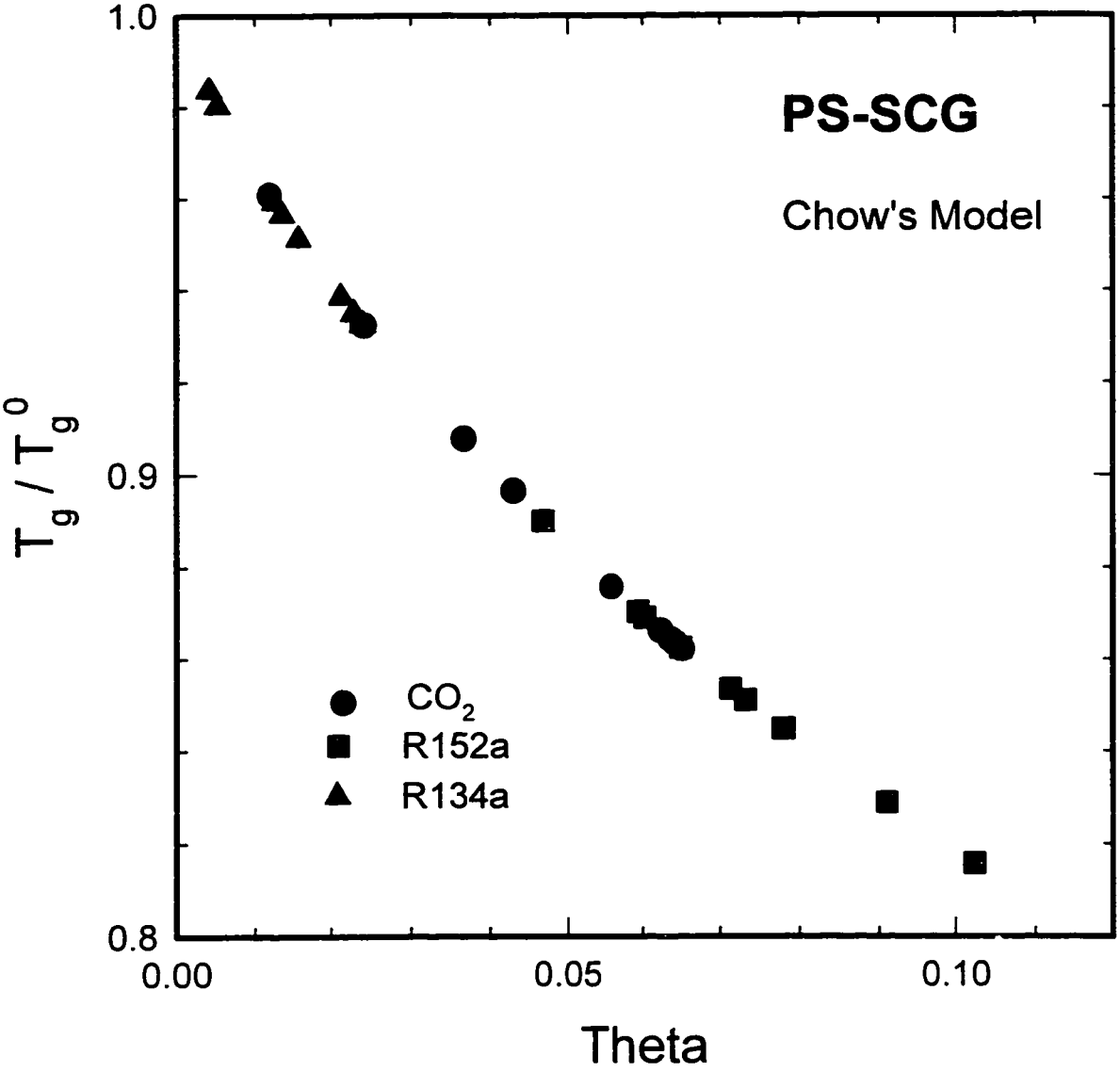

Figure 7.9
Depression of T_g estimated by Chow's Model for PS-CO_2, PS-R152a, and PS-R134a.

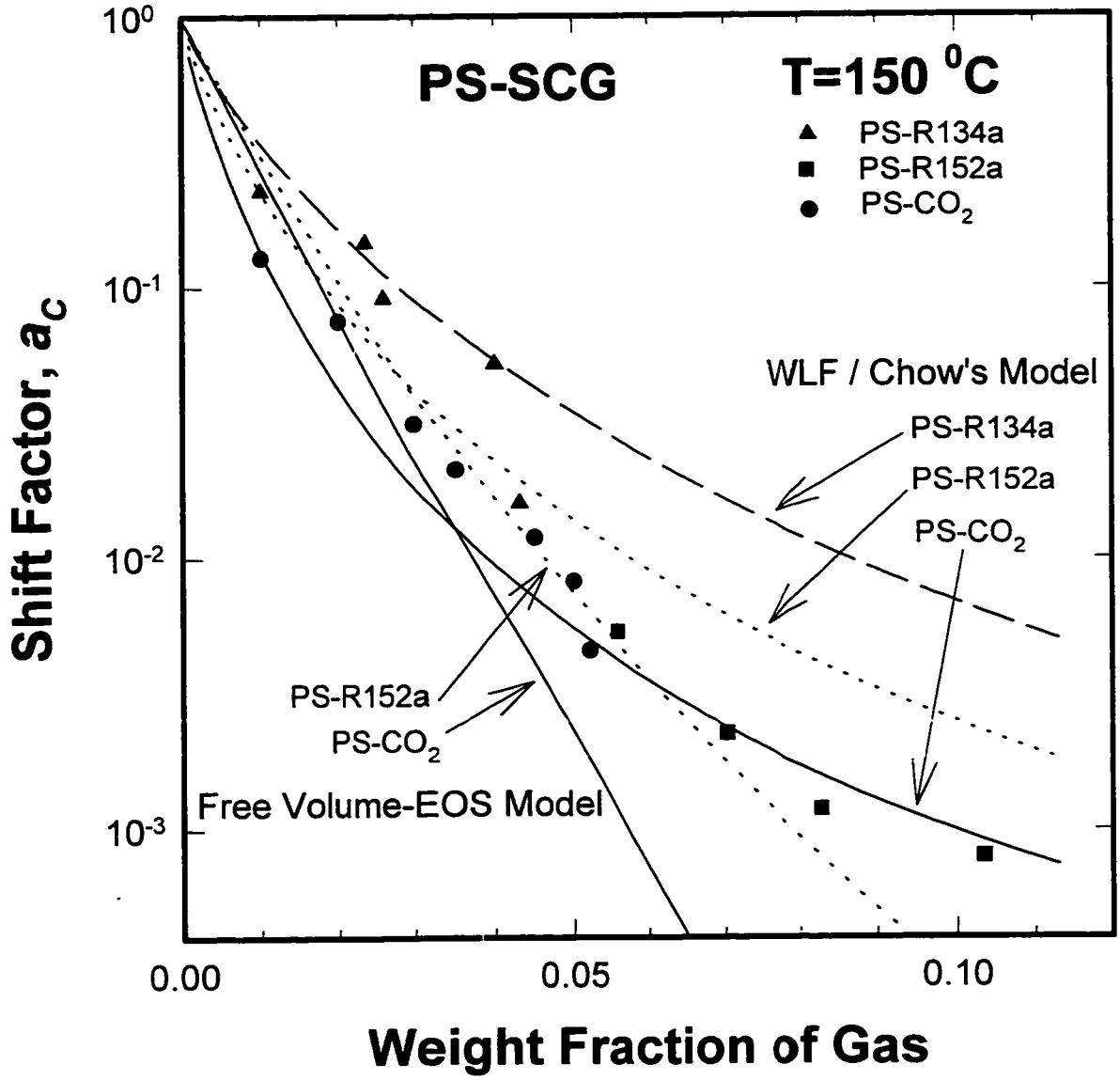

Figure 7.10
Viscosity Reduction of PS-SCG Mixtures obtained by Experiments, Free Volume Rheological Model, and WLF Equation with Chow's Model at T=150 °C.

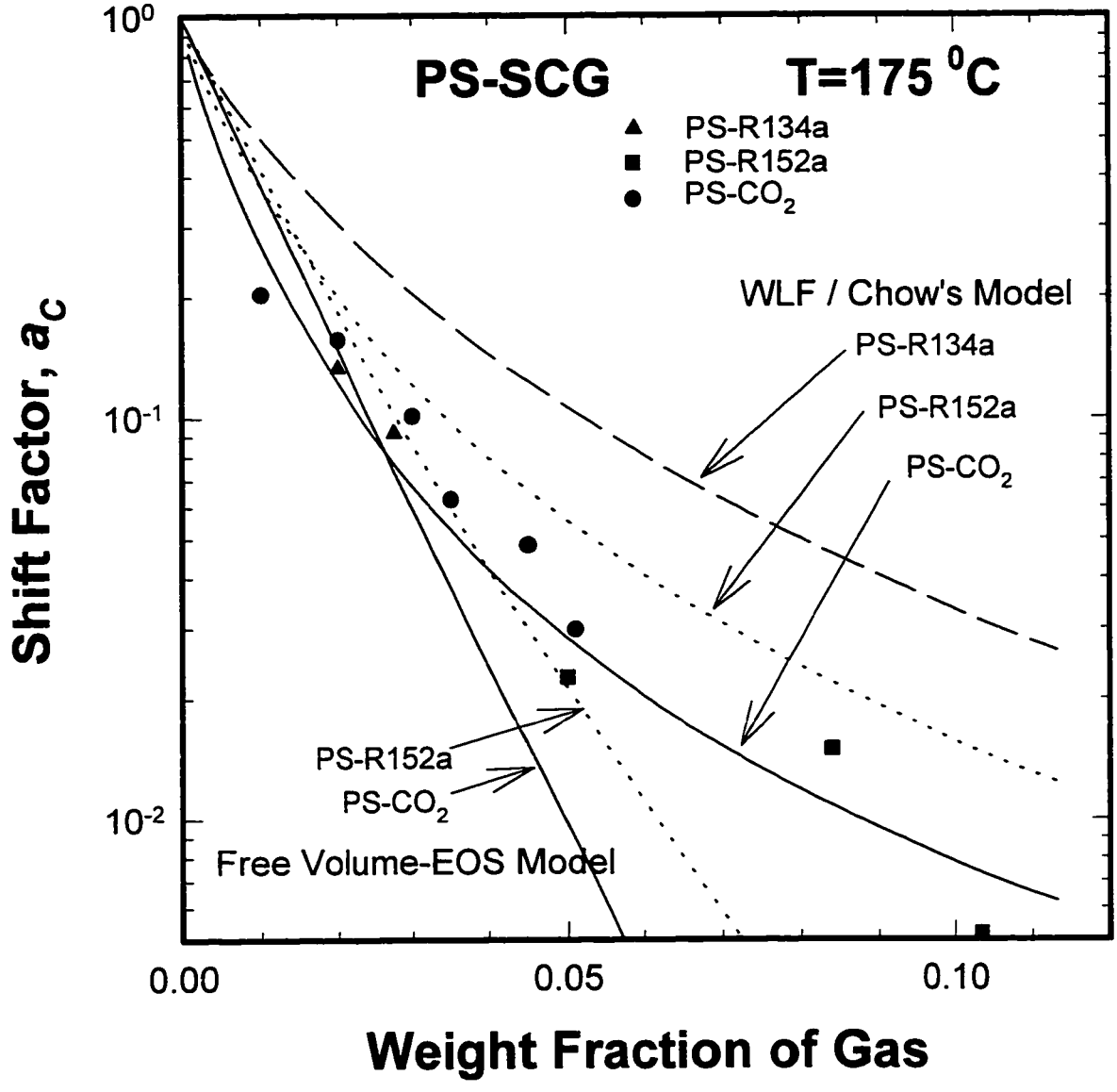

Figure 7.11
Viscosity Reduction of PS-SCG Mixtures obtained by Experiments, Free Volume Rheological Model, and WLF Equation with Chow's Model at T=175 ^{0}C.

CHAPTER 8

CONCLUSIONS

Shear viscosities of polystyrene melt with dissolved supercritical gases were experimentally measured using a modified pressurized capillary rheometer. The theoretical predictions were performed by the free volume rheological model. The major conclusions are summarized as:

- The solubility and compatibility of 1,1-difluoroethane (R152a) to polystyrene is superior to those of carbon dioxide or 1,1,1,2-tetrafluoroethane (R134a).
- The pressurized capillary rheometer is excellent to produce the viscosity data for polystyrene-supercritical gas mixtures at elevated temperatures and pressures, which have not been reported in literature previously. A significant reduction of viscosity brought by dissolved gas was observed, reaching as much as 3 orders of magnitude decrease in viscosity.
- A modified pressure correction procedure is developed based on the work of Penwell, et al. in order to consider the pressure effect on viscosity measurement. The method evaluates a pressure coefficient, which represents the effect of pressure on viscosity, and an effective pressure representing the pressure point in the pressure distribution where the local pressure gradient is equal to the measured apparent pressure gradient. Then the viscosity data is corrected by a pressure shift factor, which is calculated by the pressure coefficient and effective pressure. The pressure correction procedure successfully eliminates the apparent and abnormal shear-thickening behavior and

produces perfect overlap of data obtained in the different length dies.

- The composition-dependent shift factor scaling method, which is similar to classical viscoelastic scaling techniques for the evaluation of temperature effect on viscosity (time-temperature superposition), was adopted in order to evaluate the effect of gas concentration on viscosity. The method successfully consolidates the viscosity data of gas-loaded systems onto a single master curve, confirming that viscosity reduction by presence of dissolved gas can be represented quantitatively through the concentration shift factor. Similarly the effect of pressure of mixed systems is represented by the pressure-dependent shift factor which is calculated using the pressure coefficient obtained from the pressure correction procedure. Thus a single or multiple shift factors are used to analyze the combined effects of temperature, pressure and concentration on viscosity and each effect can be assessed separately.
- The effect of free volume on viscosity was found to be much greater than the effect of chain dilution. The viscosity reduction was maximized when the measurement temperature approaches the glass transition temperature of pure polymer, because of significant free volume increases due to the presence of dissolved gas. For 5 weight percent of CO_2 of PDMS-CO_2 solution at 50 ^{0}C ($T - T_g$ = 178 ^{0}C), the composition-dependent shift factor is 0.65 whereas, it reaches 0.0075 for the same concentration of PS-CO_2 solution at 150 ^{0}C ($T - T_g$ = 50 ^{0}C).
- The free volume rheological model with the Sanchez Lacombe equation of state is successful in predicting the viscosity reduction due to dissolved supercritical gases. The theoretical prediction is greatly influenced by the occupied volume of diluent. The occupied volume of pure component should be obtained through a rheological

experiment or theory.

- The viscosity reduction can be approximately predicted by the WLF equation with known T_g of gas-loaded system, estimated by Chow's model. However, it should be noticed that the interaction between polymer and gas is not considered in the calculation of T_g, by Chow's formula.

Recommendations:

- The extension of viscosity measurement for more than two-phase systems such as two or more gases with one polymer, or a polymer blend with one gas, or polymer blend with mixture of gases would be valuable for more practical applications.
- Improvement of free volume model as well as thermodynamic models should be accompanied for investigations of multi-component polymeric systems.
- Other rheological properties such as elongational viscosity can be investigated for gas-loaded polymer melts.
- The rheological characterization of diluted polymer systems under processing conditions, such as plastic foam processes with blowing agents, would be a challenging study that is practically important and involves the non-equilibrium state of mixing.

APPENDIX I
EXPERIMENTAL RHEOLOGICAL DATA FOR PURE POLYSTYRENE

AI.1 Capillary Rheometer Data for pure PS

Table AI.1(a)
Raw Data and Apparent Viscosity for pure PS: T=150 ^{0}C and (L/D)=40[a]

Apparent Shear Rate $\dot{\gamma}_{wa}(s^{-1})$	Load Cell Force (L/D=40) F (lb_f)	Wall Friction Force F_w (lb_f)	Pressure Drop [b] ΔP (*psi*)	Apparent Wall Shear Stress τ_{wa}(dyne/cm^2)	Apparent Viscosity η_a (*poise*)
0.35	97.00	2.73	853.54	364959	**960628**
0.5	116.95	3.00	1031.69	441133	**812429**
1.0	159.50	3.62	1411.40	603488	**552838**
1.5	197.30	4.03	1749.89	748219	**456985**
2.5	255.25	4.62	2269.22	970277	**355344**
4.0	323.45	5.24	2881.09	1231903	**281870**
5.5	388.50	5.71	3465.84	1481928	**247090**
7.5	465.50	6.21	4158.52	1778109	**217883**
10.0	558.50	6.70	4996.06	2136223	**196961**
12.5	651.00	7.12	5829.83	2492728	**184499**
17.5	922.00	7.79	8277.42	3539274	**189621**

[a] D=0.0496 *in.* and L=1.9990 *in.*

[b] $\Delta P = 4\,(F - F_w) / (\pi D_p^2)$; D_p=3/8 *in.*

Table AI.1(b)
Orifice Pressure Drops and Schuemmer-Bagley corrected Viscosities for pure PS: T=150 ^{0}C and (L/D)=40[a]

Schuemmer-corrected Shear Rate $\dot{\gamma}_w$ (s^{-1})	Load Cell Force (L/D=0) F_0 (lb_f)	Orifice Pressure Drop [b] ΔP_0 (*psi*)	Pressure (Bagley-corrected) $\Delta P - \Delta P_0$ (*psi*)	Wall Shear Stress τ_w(dyne/cm^2)	Bagley-corrected Viscosity η (*poise*)
0.29	10.15	67.21	786.33	336220	**960628**
0.42	12.02	81.67	950.03	406214	**812429**
0.83	16.70	118.46	1292.94	552838	**552838**
1.25	20.24	146.74	1603.15	685478	**456985**
2.08	25.78	191.58	2077.64	888360	**355344**
3.32	32.22	244.21	2636.88	1127481	**281870**
4.57	37.46	287.51	3178.33	1358994	**247090**
6.23	43.40	336.75	3821.77	1634121	**217883**
8.30	49.74	389.65	4606.40	1969615	**196961**
10.38	55.29	436.16	5393.67	2306235	**184499**
14.53	64.85	516.63	7760.79	3318372	**189621**

[a] D=0.0496 *in.* and L=1.9990 *in.*

[b] $\Delta P_0 = 4\,(F_0 - F_w) / (\pi D_p^2)$; D_p=3/8 *in.*

Table AI.1(c)
Bagley-Schuemmer-Pressure corrected Viscosities for pure PS:
T=150 ^{0}C and (L/D)=40[a]

Pressure Correction Parameters: m_0 =425820 *poise*; b=2.5056E-04 psi^{-1}; n=0.3892

Schuemmer-corrected Shear Rate $\dot{\gamma}_w$ (s^{-1})	Effective Pressure P^* (*psi*)	Pressure Correction Factor [b] a_P	**Bagley-Pressure-corrected Viscosity** [c] η (***poise***)
0.29	386.71	1.1017	**871914**
0.42	465.60	1.1237	**722969**
0.83	629.03	1.1707	**472223**
1.25	774.78	1.2143	**376350**
2.08	993.85	1.2828	**277012**
3.32	1246.11	1.3665	**206276**
4.57	1484.25	1.4505	**170349**
6.23	1759.55	1.5541	**140201**
8.30	2084.08	1.6857	**116841**
10.38	2397.61	1.8235	**101179**
14.53	3270.29	2.2692	**83564**

[a] D=0.0496 *in.* and L=1.9990 *in.*

[b] $a_P = exp\ \{b(P^* - P_L)\}$ where P_L is zero for pure PS melts

Table AI.2(a)
Raw Data and Apparent Viscosity for pure PS:
T=150 ^{0}C and (L/D)=75[a]

Apparent Shear Rate $\dot{\gamma}_{wa}$ (s^{-1})	Load Cell Force (L/D=40) F (lb_f)	Wall Friction Force F_w (lb_f)	Pressure Drop [b] ΔP (*psi*)	Apparent Wall Shear Stress τ_{wa}(dyne/cm^2)	**Apparent Viscosity** η_a (***poise***)
0.10	85.20	1.95	753.75	173964	**1739637**
0.20	122.35	2.35	1086.51	250763	**1253815**
0.35	184.10	2.73	1642.16	379006	**1082875**
0.50	233.92	3.00	2090.79	482549	**965098**
0.75	306.10	3.35	2741.21	632664	**843552**
1.00	366.85	3.62	3288.81	759050	**759050**
1.50	469.14	4.03	4211.16	971927	**647951**
2.50	669.34	4.62	6018.46	1389046	**555618**
4.00	1038.84	5.24	9358.30	2159872	**539968**

[a] D=0.0502 *in.* and L=3.7482 *in.*

[b] $\Delta P = 4\ (F - F_w) / (\pi D_p^2)$; D_p=3/8 *in.*

Table AI.2(b)
Orifice Pressure Drops and Schuemmer-Bagley corrected Viscosities for pure PS: T=150 ^{0}C and (L/D)=75[a]

Schuemmer-corrected Shear Rate $\dot{\gamma}_w$ (s^{-1})	Load Cell Force (L/D=0) F_0 (lb_f)	Orifice Pressure Drop [b] ΔP_0 (*psi*)	Pressure (Bagley-corrected) $\Delta P - \Delta P_0$ (*psi*)	Wall Shear Stress τ_w(dyne/cm^2)	Bagley-corrected Viscosity η (*poise*)
0.08	5.61	0.08	33.10	166325	**1663246**
0.17	7.79	0.17	49.24	239399	**1196996**
0.29	10.15	0.29	67.21	363494	**1038553**
0.42	12.02	0.42	81.67	463701	**927402**
0.62	14.57	0.62	101.61	609213	**812283**
0.83	16.70	0.83	118.46	731711	**731711**
1.25	20.24	1.25	146.74	938060	**625374**
2.08	25.78	2.08	191.58	1344830	**537932**
3.32	32.22	3.32	244.21	2103508	**525877**

[a] D=0.0502 *in.* and L=3.7482 *in.*
[b] $\Delta P_0 = 4\,(F_0 - F_w) / (\pi D_p^2)$; D_p=3/8 *in.*

Table AI.2(c)
Bagley-Schuemmer-Pressure corrected Viscosities for pure PS: T=150 ^{0}C and (L/D)=75[a]

Pressure Correction Parameters: m_0 =425820 *poise*; b=2.5056E-04 psi^{-1}; n=0.3892

Schuemmer-corrected Shear Rate $\dot{\gamma}_w$ (s^{-1})	Effective Pressure P^* (*psi*)	Pressure Correction Factor [b] a_P	Bagley-Pressure-corrected Viscosity [c] η (*poise*)
0.08	354.91	1.0930	**1521725**
0.17	507.41	1.1356	**1054088**
0.29	761.61	1.2103	**858126**
0.42	962.51	1.2727	**728666**
0.62	1247.32	1.3669	**594259**
0.83	1480.79	1.4492	**504896**
1.25	1861.21	1.5942	**392287**
2.08	2565.06	1.9016	**282879**
3.32	3724.66	2.5428	**206810**

[a] D=0.0502 *in.* and L=3.7482 *in.*
[b] $a_P = exp\,\{b(P^* - P_L)\}$ where P_L is zero for pure PS melts

Table AI.3(a)
Raw Data and Apparent Viscosity for pure PS:
T=175 ^{0}C and (L/D)=40[a]

Apparent Shear Rate $\dot{\gamma}_{wa}(s^{-1})$	Load Cell Force (L/D=40) F (lb_f)	Wall Friction Force F_w (lb_f)	Pressure Drop [b] ΔP (*psi*)	Apparent Wall Shear Stress τ_{wa}(dyne/cm^2)	**Apparent Viscosity** η_a (***poise***)
35	202.07	7.1	1765.26	754792	**21565**
50	241.33	8.4	2109.01	901775	**18036**
100	337.57	10.1	2964.93	1267751	**12678**
150	411.33	11.4	3621.06	1548297	**10322**
250	511.00	13.1	4508.06	1927564	**7710**
400	630.67	14.8	5576.15	2384259	**5961**
550	701.00	15.6	6205.71	2653450	**4824**
750	798.00	16.8	7073.10	3024329	**4032**
1000	870.33	16.3	7732.54	3306295	**3306**
1250	943.33	19.5	8364.52	3576518	**2861**
2000	1070.00	23.5	9475.17	4051408	**2026**

[a] D=0.0496 *in.* and L=1.9990 *in.*
[b] $\Delta P = 4\,(F - F_w) / (\pi D_p^2)$; D_p=3/8 *in.*

Table AI.3(b)
Orifice Pressure Drops and Schuemmer-Bagley corrected Viscosities for pure PS:
T=175 ^{0}C and (L/D)=40[a]

Schuemmer-corrected Shear Rate $\dot{\gamma}_w$ (s^{-1})	Load Cell Force (L/D=0) F_0 (lb_f)	Orifice Pressure Drop [b] ΔP_0 (*psi*)	Pressure (Bagley-corrected) $\Delta P - \Delta P_0$ (*psi*)	Wall Shear Stress τ_w(dyne/cm^2)	**Bagley-corrected Viscosity** η (***poise***)
29.05	23.50	148.49	1616.77	691301	**19751**
41.50	25.70	156.64	1952.38	834800	**16696**
83.00	32.30	201.00	2763.93	1181806	**11818**
124.50	37.25	234.05	3387.01	1448222	**9655**
207.50	49.50	329.57	4178.49	1786646	**7147**
332.00	63.85	444.11	5132.04	2194368	**5486**
456.50	80.13	584.22	5621.49	2403648	**4370**
622.50	93.47	694.15	6378.95	2727522	**3637**
830.00	108.20	832.08	6900.47	2950514	**2951**
1037.50	118.00	891.83	7472.69	3195186	**2556**
1660.00	142.00	1072.92	8402.25	3592649	**1796**

[a] D=0.0496 *in.* and L=1.9990 *in.*
[b] $\Delta P_0 = 4\,(F_0 - F_w) / (\pi D_p^2)$; D_p=3/8 *in.*

Table AI.3(c)
Bagley-Schuemmer-Pressure corrected Viscosities for pure PS: T=175 ^{0}C and (L/D)=40[a]

Pressure Correction Parameters: m_0 =416894 *poise*; b=9.1394E-05 psi^{-1}; n=0.2202

Schuemmer-corrected Shear Rate γ°_w (s^{-1})	Effective Pressure P^* (*psi*)	Pressure Correction Factor [b] a_P	Bagley-Pressure-corrected Viscosity [c] η (*poise*)
29.05	798.43	1.0757	**18361**
41.50	961.68	1.0919	**15291**
83.00	1352.89	1.1316	**10444**
124.50	1649.85	1.1627	**8303**
207.50	2022.84	1.2031	**5940**
332.00	2465.91	1.2528	**4379**
456.50	2690.67	1.2788	**3418**
622.50	3034.96	1.3197	**2756**
830.00	3269.50	1.3483	**2188**
1037.50	3524.52	1.3801	**1852**
1660.00	3933.59	1.4326	**1254**

[a] D=0.0496 *in.* and L=1.9990 *in.*

[b] $a_P = exp\ \{b(P^* - P_L)\}$ where P_L is zero for pure PS melts

Table AI.4(a)
Raw Data and Apparent Viscosity for pure PS: T=175 ^{0}C and (L/D)=75[a]

Apparent Shear Rate γ°_{wa}(s^{-1})	Load Cell Force (L/D=40) F (lb_f)	Wall Friction Force F_w (lb_f)	Pressure Drop [b] ΔP (*psi*)	Apparent Wall Shear Stress τ_{wa}(dyne/cm^2)	Apparent Viscosity η_a (*poise*)
5.5	145.33	4.57	1274.51	294153	**53482**
7.5	180.33	4.96	1587.82	366464	**48862**
10	218.67	5.36	1931.29	445737	**44574**
12.5	251.57	5.69	2226.18	513797	**41104**
20	332.73	6.46	2954.16	681812	**34091**
35	451.00	7.50	4015.50	926768	**26479**
55	580.33	8.47	5177.76	1195014	**21728**
100	794.00	9.94	7099.00	1638433	**16384**
150	1020.67	11.08	9140.95	2109709	**14065**
250	1338.33	12.71	12002.43	2770132	**11081**
400	1623.33	14.41	14567.42	3362125	**8405**

[a] D=0.0502 *in.* and L=3.7482 *in.*

[b] $\Delta P = 4\ (F - F_w) / (\pi D_p^2)$; D_p=3/8 *in.*

Table AI.4(b)
Orifice Pressure Drops and Schuemmer-Bagley corrected Viscosities for pure PS: T=175 ^{0}C and (L/D)=75[a]

Schuemmer-corrected Shear Rate $\dot{\gamma}_w$ (s^{-1})	Load Cell Force (L/D=0) F_0 (lb_f)	Orifice Pressure Drop [b] ΔP_0 (*psi*)	Pressure (Bagley-corrected) $\Delta P - \Delta P_0$ (*psi*)	Wall Shear Stress τ_w(dyne/cm^2)	Bagley-corrected Viscosity η (*poise*)
4.57	4.14	37.51	1236.99	285495	**51908**
6.23	5.13	46.42	1541.40	355751	**47433**
8.30	6.20	56.17	1875.12	432774	**43277**
10.38	7.16	64.86	2161.32	498828	**39906**
16.60	9.61	86.98	2867.17	661736	**33087**
29.05	13.44	121.71	3893.79	898678	**25677**
45.65	17.48	158.27	5019.49	1158486	**21063**
83.00	24.51	221.91	6877.09	1587217	**15872**
124.50	30.67	277.67	8863.28	2045623	**13637**
207.50	40.48	366.51	11635.92	2685543	**10742**
332.00	52.05	471.23	14096.18	3253365	**8133**

[a] D=0.0502 *in.* and L=3.7482 *in.*

[b] $\Delta P_0 = 4\,(F_0 - F_w) / (\pi D_p^2)$; D_p=3/8 *in.*

Table AI.4(c)
Bagley-Schuemmer-Pressure corrected Viscosities for pure PS: T=175 ^{0}C and (L/D)=75[a]

Pressure Correction Parameters: m_0 =416894 *poise*; b=9.1394E-05 psi^{-1}; n=0.2202

Schuemmer-corrected Shear Rate $\dot{\gamma}_w$ (s^{-1})	Effective Pressure P^* (*psi*)	Pressure Correction Factor [b] a_P	Bagley-Pressure-corrected Viscosity [c] η (*poise*)
4.57	612.67	1.0576	**49081**
6.23	761.65	1.0721	**44244**
8.30	924.18	1.0881	**39772**
10.38	1062.88	1.1020	**36212**
16.60	1402.30	1.1367	**29107**
29.05	1889.22	1.1885	**21605**
45.65	2413.97	1.2469	**16893**
83.00	3259.03	1.3470	**11784**
124.50	4134.10	1.4591	**9346**
207.50	5307.14	1.6242	**6614**
332.00	6301.61	1.7788	**4572**

[a] D=0.0502 *in.* and L=3.7482 *in.*

[b] $a_P = exp\,\{b(P^* - P_L)\}$ where P_L is zero for pure PS melts

Table AI.5(a)
Raw Data and Apparent Viscosity for pure PS:
T=188 ^{0}C and (L/D)=40[a]

Apparent Shear Rate $\dot{\gamma}_{wa}$ (s^{-1})	Load Cell Force (L/D=40) F (lb_f)	Wall Friction Force F_w (lb_f)	Pressure Drop [b] ΔP (*psi*)	Apparent Wall Shear Stress τ_{wa}(dyne/cm^2)	**Apparent Viscosity** η_a (***poise***)
35	122.67	6.80	1049.07	448565	**12816**
50	139.50	7.70	1193.34	510249	**10205**
100	199.83	9.50	1723.31	736854	**7369**
150	242.15	11.00	2092.87	894872	**5966**
250	303.50	12.80	2632.04	1125413	**4502**
400	371.00	14.60	3226.90	1379763	**3449**
550	423.33	15.30	3694.39	1579656	**2872**
750	484.00	14.50	4250.92	1817617	**2423**
1000	521.00	16.30	4569.63	1953890	**1954**
1250	554.00	17.80	4854.83	2075839	**1661**
2000	650.00	20.00	5704.11	2438975	**1219**

[a] D=0.0496 *in.* and L=1.9990 *in.*
[b] $\Delta P = 4\,(F - F_w) / (\pi D_p^2)$; D_p=3/8 *in.*

Table AI.5(b)
Orifice Pressure Drops and Schuemmer-Bagley corrected Viscosities for pure PS:
T=188 ^{0}C and (L/D)=40[a]

Schuemmer-corrected Shear Rate $\dot{\gamma}_w$ (s^{-1})	Load Cell Force (L/D=0) F_0 (lb_f)	Orifice Pressure Drop [b] ΔP_0 (*psi*)	Pressure (Bagley-corrected) $\Delta P - \Delta P_0$ (*psi*)	Wall Shear Stress τ_w(dyne/cm^2)	**Bagley-corrected Viscosity** η (***poise***)
29.05	10.5	33.50	1015.57	434241	**12407**
41.50	13.5	52.51	1140.82	487795	**9756**
83.00	18.5	81.49	1641.82	702012	**7020**
124.50	21.3	93.26	1999.61	854996	**5700**
207.50	24.7	107.74	2524.30	1079343	**4317**
332.00	30.5	143.96	3082.94	1318208	**3296**
456.50	35.3	181.08	3513.31	1502228	**2731**
622.50	43.0	258.04	3992.88	1707282	**2276**
830.00	52.2	325.04	4244.58	1814907	**1815**
1037.50	58.5	368.50	4486.33	1918273	**1535**
1660.00	77.0	516.09	5188.03	2218306	**1109**

[a] D=0.0496 *in.* and L=1.9990 *in.*
[b] $\Delta P_0 = 4\,(F_0 - F_w) / (\pi D_p^2)$; D_p=3/8 *in.*

Table AI.5(c)
Bagley-Schuemmer-Pressure corrected Viscosities for pure PS: T=188 ^{0}C and (L/D)=40[a]

Pressure Correction Parameters: m_0 =262040 *poise*; b=6.7435E-05 psi^{-1}; n=0.2414

Schuemmer-corrected Shear Rate $\dot{\gamma}_w$ (s^{-1})	Effective Pressure P^* (*psi*)	Pressure Correction Factor[b] a_P	Bagley-Pressure-corrected Viscosity[c] η (*poise*)
29.05	504.89	1.0346	**11992**
41.50	566.75	1.0390	**9390**
83.00	813.34	1.0564	**6645**
124.50	988.57	1.0689	**5332**
207.50	1244.25	1.0875	**3970**
332.00	1514.77	1.1075	**2976**
456.50	1721.99	1.1231	**2432**
622.50	1951.67	1.1407	**1996**
830.00	2071.70	1.1499	**1578**
1037.50	2186.66	1.1589	**1324**
1660.00	2518.46	1.1851	**936**

[a] D=0.0496 *in.* and L=1.9990 *in.*

[b] $a_P = exp\ \{b(P^* - P_L)\}$ where P_L is zero for pure PS melts

Table AI.6(a)
Raw Data and Apparent Viscosity for pure PS: T=188 ^{0}C and (L/D)=75[a]

Apparent Shear Rate $\dot{\gamma}_{wa}$(s^{-1})	Load Cell Force (L/D=40) F (lb_f)	Wall Friction Force F_w (lb_f)	Pressure Drop[b] ΔP (*psi*)	Apparent Wall Shear Stress τ_{wa}(dyne/cm^2)	Apparent Viscosity η_a (*poise*)
5.5	61.55	4.51	516.46	119198	**21672**
7.5	78.90	4.88	670.18	154676	**20623**
10	98.00	5.25	839.74	193809	**19381**
20	158.20	6.27	1375.56	317476	**15874**
35	227.13	6.80	1994.93	460425	**13155**
55	297.40	8.13	2619.10	604483	**10991**
100	411.33	9.50	3638.26	839701	**8397**
150	506.00	11.00	4481.80	1034389	**6896**
250	650.00	12.80	5769.30	1331541	**5326**
400	798.33	14.60	7096.04	1637748	**4094**
550	904.33	15.30	8049.44	1857791	**3378**
750	1025.00	14.50	9149.22	2111617	**2815**
1000	1127.50	16.30	10060.97	2322047	**2322**
1250	1200.00	17.80	10703.81	2470414	**1976**
1500	1240.00	18.95	11055.58	2551602	**1701**
2000	1350.00	20.00	12042.02	2779268	**1390**

[a] D=0.0502 *in.* and L=3.7482 *in.*

[b] $\Delta P = 4\ (F - F_w) / (\pi D_p^2)$; D_p=3/8 *in.*

Table AI.6(b)
Orifice Pressure Drops and Schuemmer-Bagley corrected Viscosities for pure PS: T=188 ^{0}C and (L/D)=75[a]

Schuemmer-corrected Shear Rate $\dot{\gamma}_w$ (s^{-1})	Load Cell Force (L/D=0) F_0 (lb_f)	Orifice Pressure Drop [b] ΔP_0 (*psi*)	Pressure (Bagley-corrected) $\Delta P - \Delta P_0$ (*psi*)	Wall Shear Stress τ_w(dyne/cm^2)	Bagley-corrected Viscosity η (*poise*)
4.57	4.51	0.02	516.45	119194	**21672**
6.23	5.21	2.99	667.18	153985	**20531**
8.30	5.96	6.39	833.35	192335	**19233**
16.6	8.23	17.72	1357.84	313385	**15669**
29.05	10.68	35.17	1959.76	452309	**12923**
45.65	13.19	45.82	2573.29	593909	**10798**
83.0	17.43	71.77	3566.49	823138	**8231**
124.5	21.05	91.00	4390.80	1013387	**6756**
207.5	26.71	125.93	5643.38	1302478	**5210**
332.0	33.25	168.84	6927.20	1598780	**3997**
456.5	38.57	210.66	7838.78	1809171	**3289**
622.5	44.56	272.20	8877.01	2048793	**2732**
830.0	50.96	313.79	9747.18	2249625	**2250**
1037.5	56.54	350.77	10353.05	2389458	**1912**
1245.0	61.55	385.77	10669.82	2462568	**1642**
1660.0	70.39	456.20	11585.82	2673979	**1337**

[a] D=0.0502 *in.* and L=3.7482 *in.* [b] $\Delta P_0 = 4\,(F_0 - F_w) / (\pi D_p^2)$; D_p=3/8 *in.*

Table AI.6(c)
Bagley-Schuemmer-Pressure corrected Viscosities for pure PS: T=188 ^{0}C and (L/D)=75[a]

Pressure Correction Parameters: m_0 =262040 *poise*; b=6.7435E-05 psi^{-1}; n=0.2414

Schuemmer-corrected Shear Rate $\dot{\gamma}_w$ (s^{-1})	Effective Pressure P^* (*psi*)	Pressure Correction Factor [b] a_P	Bagley-Pressure-corrected Viscosity [c] η (*poise*)
4.57	257.47	1.0175	**21299**
6.23	332.34	1.0227	**20076**
8.30	414.72	1.0284	**18703**
16.6	673.74	1.0465	**14973**
29.05	969.09	1.0675	**12106**
45.65	1268.04	1.0893	**9913**
83.0	1747.52	1.1251	**7316**
124.5	2141.27	1.1553	**5848**
207.5	2732.31	1.2023	**4333**
332.0	3329.01	1.2517	**3193**
456.5	3747.14	1.2875	**2555**
622.5	4217.75	1.3290	**2055**
830.0	4607.59	1.3644	**1649**
1037.5	4876.57	1.3894	**1376**
1245.0	5016.40	1.4025	**1171**
1660.0	5417.65	1.4410	**928**

[a] D=0.0502 *in.* and L=3.7482 *in.*

[b] $a_P = exp\,\{b(P^* - P_L)\}$ where P_L is zero for pure PS melts

Table AI.7(a)
Raw Data and Apparent Viscosity for pure PS:
T=200 ^{0}C and (L/D)=40[a]

Apparent Shear Rate $\dot{\gamma}_{wa}(s^{-1})$	Load Cell Force (L/D=40) F (lb_f)	Wall Friction Force F_w (lb_f)	Pressure Drop [b] ΔP (*psi*)	Apparent Wall Shear Stress τ_{wa}(dyne/cm^2)	Apparent Viscosity η_a (*poise*)
35	68.50	6.2	564.07	241188	**6891**
50	85.05	7.2	704.87	301388	**6028**
100	126.75	9.0	1066.13	455856	**4559**
150	157.25	10.4	1329.60	568513	**3790**
250	200.24	12.5	1699.80	726805	**2907**
400	243.25	13.8	2077.47	888290	**2221**
550	278.28	14.5	2388.31	1021200	**1857**
750	318.00	14.8	2745.22	1173805	**1565**
1000	356.47	15.5	3087.16	1320014	**1320**
1250	385.78	16.4	3344.40	1430005	**1144**
2000	459.56	18.8	3990.67	1706336	**853**

[a] D=0.0496 *in.* and L=1.9990 *in.*
[b] $\Delta P = 4\,(F - F_w) / (\pi D_p^2)$; D_p=3/8 *in.*

Table AI.7(b)
Orifice Pressure Drops and Schuemmer-Bagley corrected Viscosities for pure PS:
T=200 ^{0}C and (L/D)=40[a]

Schuemmer-corrected Shear Rate $\dot{\gamma}_w(s^{-1})$	Load Cell Force (L/D=0) F_0 (lb_f)	Orifice Pressure Drop [b] ΔP_0 (*psi*)	Pressure (Bagley-corrected) $\Delta P - \Delta P_0$ (*psi*)	Wall Shear Stress τ_w(dyne/cm^2)	Bagley-corrected Viscosity η (*poise*)
29.05	6.2	0.00	564.07	241188	**6891**
41.50	7.2	0.00	704.87	301388	**6028**
83.00	10.1	9.96	1056.17	451597	**4516**
124.50	13.6	28.97	1300.63	556125	**3707**
207.50	17.5	45.27	1654.53	707448	**2830**
332.00	20.5	60.66	2016.81	862352	**2156**
456.50	23.0	76.96	2311.35	988293	**1797**
622.50	26.3	104.12	2641.09	1129284	**1506**
830.00	29.3	124.95	2962.22	1266589	**1267**
1037.50	32.2	143.06	3201.35	1368837	**1095**
1660.00	42.4	213.68	3776.99	1614971	**807**

[a] D=0.0496 *in.* and L=1.9990 *in.*
[b] $\Delta P_0 = 4\,(F_0 - F_w) / (\pi D_p^2)$; D_p=3/8 *in.*

Table AI.7(c)
Bagley-Schuemmer-Pressure corrected Viscosities for pure PS: T=200 ^{0}C and (L/D)=40[a]

Pressure Correction Parameters: m_0 =147101 *poise*; b=7.4247E-05 psi^{-1}; n=0.2794

Schuemmer-corrected Shear Rate $\dot{\gamma}_w$ (s^{-1})	Effective Pressure P^* (*psi*)	Pressure Correction Factor [b] a_P	Bagley-Pressure-corrected Viscosity [c] η (*poise*)
29.05	281.05	1.0211	**6749**
41.50	350.90	1.0264	**5873**
83.00	524.63	1.0397	**4343**
124.50	645.08	1.0491	**3534**
207.50	818.80	1.0627	**2663**
332.00	995.82	1.0767	**2002**
456.50	1139.15	1.0883	**1651**
622.50	1298.98	1.1012	**1367**
830.00	1453.97	1.1140	**1137**
1037.50	1568.98	1.1235	**975**
1660.00	1844.39	1.1468	**704**

[a] D=0.0496 *in.* and L=1.9990 *in.*

[b] $a_P = exp\ \{b(P^* - P_L)\}$ where P_L is zero for pure PS melts

Table AI.8(a)
Raw Data and Apparent Viscosity for pure PS: T=200 ^{0}C and (L/D)=75[a]

Apparent Shear Rate $\dot{\gamma}_{wa}$(s^{-1})	Load Cell Force (L/D=40) F (lb_f)	Wall Friction Force F_w (lb_f)	Pressure Drop [b] ΔP (*psi*)	Apparent Wall Shear Stress τ_{wa}(dyne/cm^2)	Apparent Viscosity η_a (*poise*)
10	55.20	4.86	455.74	105185	**10518**
20	88.50	5.83	748.48	172747	**8637**
35	131.73	6.20	1136.60	262324	**7495**
50	174.75	7.20	1517.02	350125	**7003**
100	261.47	9.00	2285.87	527573	**5276**
150	328.50	10.40	2880.12	664726	**4432**
250	429.00	12.50	3771.05	870350	**3481**
400	531.67	13.80	4688.84	1082173	**2705**
550	613.00	14.50	5418.91	1250671	**2274**
750	698.80	14.80	6193.04	1429338	**1906**
1000	774.25	15.50	6869.83	1585541	**1586**
1250	839.00	16.40	7447.94	1718967	**1375**
1500	868.50	18.08	7699.84	1777103	**1185**
2000	957.33	18.80	8497.62	1961230	**981**
2500	1010.0	20.67	8957.56	2067382	**827**

[a] D=0.0502 *in.* and L=3.7482 *in.*

[b] $\Delta P = 4\ (F - F_w) / (\pi D_p^2)$; D_p=3/8 *in.*

Table AI.8(b)
Orifice Pressure Drops and Schuemmer-Bagley corrected Viscosities for pure PS: T=200 ^{0}C and (L/D)=75[a]

Schuemmer-corrected Shear Rate $\dot{\gamma}_w$ (s^{-1})	Load Cell Force (L/D=0) F_0 (lb_f)	Orifice Pressure Drop [b] ΔP_0 (*psi*)	Pressure (Bagley-corrected) $\Delta P - \Delta P_0$ (*psi*)	Wall Shear Stress τ_w(dyne/cm^2)	Bagley-corrected Viscosity η (*poise*)
8.3	3.29	0.00 [c]	469.98	108470	**10847**
16.6	4.55	0.00 [c]	760.11	175432	**8772**
29.05	6.20	0.00	1136.60	262324	**7495**
41.5	7.20	0.00	1517.02	350125	**7003**
83.0	10.10	9.96	2275.91	525275	**5253**
124.5	13.60	28.97	2851.15	658039	**4387**
207.5	17.50	45.27	3725.78	859901	**3440**
332.0	20.50	60.66	4628.18	1068172	**2670**
456.5	23.00	76.96	5341.95	1232909	**2242**
622.5	26.30	104.12	6088.91	1405307	**1874**
830.0	29.30	124.95	6744.89	1556704	**1557**
1037.5	32.20	143.06	7304.89	1685950	**1349**
1245.0	34.01	144.23	7555.60	1743815	**1163**
1660.0	42.40	213.68	8283.94	1911914	**956**
2075.0	43.15	203.55	8754.00	2020403	**808**

[a] D=0.0502 *in.* and L=3.7482 *in.* [b] $\Delta P_0 = 4\,(F_0 - F_w) / (\pi D_p^2)$; D_p=3/8 *in.*
[c] $(F_0 - F_w)$ has negative values, but forced to zero.

Table AI.8(c)
Bagley-Schuemmer-Pressure corrected Viscosities for pure PS: T=200 ^{0}C and (L/D)=75[a]

Pressure Correction Parameters: m_0 =147101 *poise*; b=7.4247E-05 psi^{-1}; n=0.2794

Schuemmer-corrected Shear Rate $\dot{\gamma}_w$ (s^{-1})	Effective Pressure P^* (*psi*)	Pressure Correction Factor [b] a_P	Bagley-Pressure-corrected Viscosity [c] η (*poise*)
8.3	234.31	1.0175	**10660**
16.6	378.27	1.0285	**8529**
29.05	564.30	1.0428	**7187**
41.5	751.39	1.0574	**6623**
83.0	1121.93	1.0869	**4833**
124.5	1400.44	1.1096	**3954**
207.5	1819.97	1.1447	**3005**
332.0	2247.89	1.1816	**2260**
456.5	2582.81	1.2114	**1850**
622.5	2929.96	1.2430	**1507**
830.0	3232.00	1.2712	**1225**
1037.5	3487.77	1.2956	**1041**
1245.0	3601.66	1.3066	**890**
1660.0	3930.34	1.3389	**714**
2075.0	4140.76	1.3599	**594**

[a] D=0.0502 *in.* and L=3.7482 *in.*
[b] $a_P = exp\,\{b(P^* - P_L)\}$ where P_L is zero for pure PS melt

AI.2 Weissenbeg Rheogoniometer Data for pure PS

For all oscillatory measurements, displacement was 0.01 rad.

G' = storage modulus; G" = loss modulus; ω = angular velocity;

η' = dynamic viscosity; η'' = elastic viscosity; η^* = complex viscosity.

Table AI.9(a)
Oscillatory Measurement Data for pure PS: T=150 ^{0}C

freq. (Hz)	ω (rad/s)	G' (dyne/cm^2)	η' (poise)	G" (dyne/cm^2)	η'' (poise)	η^* (poise)
0.00101	0.0063	1215	192234	13564	214591	2154509
0.00169	0.0106	2838	267462	21860	205983	2077131
0.00282	0.0177	6133	346640	34450	194707	1977692
0.00470	0.0295	12594	426637	52731	178637	1836611
0.00772	0.0485	24186	498626	77915	160629	1681905
0.01300	0.0817	44838	548943	113356	138778	1492408
0.02183	0.1372	78494	572275	158625	115647	1290325
0.03661	0.2300	128818	560013	212768	92497	1081288
0.05973	0.3753	195444	520775	271951	72463	892356
0.09996	0.6281	288349	459105	338426	53883	707901

Table AI.9(b)
Oscillatory Measurement Data for pure PS: T=175 ^{0}C

freq. (Hz)	ω (rad/s)	G' (dyne/cm^2)	η' (poise)	G" (dyne/cm^2)	η'' (poise)	η^* (poise)
0.00994	0.0624	541.9	107900	6736	8680	108235
0.01654	0.1039	1141	106100	11030	10980	106702
0.02712	0.1704	2384	103000	17560	13990	103997
0.04432	0.2785	4928	98530	27430	17700	100079
0.07106	0.4465	9577	92090	41120	21450	94562
0.11740	0.7376	18560	83820	61840	25160	87529
0.19520	1.2265	34540	74120	90920	28150	79300
0.32100	2.0169	59690	63180	127400	29590	69755
0.50470	3.1711	94310	53280	168900	29740	61003
0.84110	5.2848	150000	42280	223400	28380	50917
1.39400	8.7588	224900	32510	284800	25680	41432
2.30900	14.5079	321900	24140	350100	22190	32782
3.77400	23.7127	439500	17610	417600	18530	25567
6.02100	37.8311	572600	12790	483900	15140	19817
9.90700	62.2475	736500	9028	562000	11830	14883

Table AI.9(c)
Oscillatory Measurement Data for pure PS: T=188 ^{0}C

freq. (Hz)	ω (rad/s)	G' (dyne/cm^2)	η' (poise)	G" (dyne/cm^2)	η'' (poise)	η^* (poise)
0.00996	0.0626	99.87	32290	2020	1596	32331
0.02028	0.1274	207.6	31490	4011	1630	31520
0.03170	0.1992	399.8	31190	6212	2007	31253
0.04921	0.3092	795.8	30830	9533	2574	30939
0.07509	0.4718	1556	30120	14210	3298	30298
0.11790	0.7408	3155	29090	21550	4259	29401
0.18600	1.1687	6279	27750	32430	5373	28265
0.29170	1.8328	11860	25990	47630	6473	26781
0.45310	2.8469	20970	23700	67460	7366	24814
0.68670	4.3147	35050	21470	92650	8122	22958
1.08200	6.7984	58260	18670	126800	8574	20526
1.44400	9.0729	80550	17100	155100	8881	19263
1.70000	10.6814	92100	15740	168100	8623	17945
2.17400	13.6596	119700	14480	197800	8762	16926
2.67600	16.8138	140400	12870	216400	8347	15342
2.91000	18.2841	154900	12630	230900	8473	15207
4.16400	26.1632	202700	10310	269900	7747	12901
6.38300	40.1056	279900	8132	326100	6980	10715
9.94000	62.4549	377200	6232	389200	6039	8678

Table AI.9(d)
Oscillatory Measurement Data for pure PS: T=200 ^{0}C

freq. (Hz)	ω (rad/s)	G' (dyne/cm^2)	η' (poise)	G" (dyne/cm^2)	η'' (poise)	η^* (poise)
0.00996	0.0626	35.48	13520	845.5	567.	13528
0.01651	0.1037	59.71	13380	1388	575.	13393
0.02723	0.1711	98.64	13270	2270	576.	13280
0.04458	0.2801	188.4	13210	3700	672.	13226
0.07134	0.4482	350.4	13060	5856	781.	13088
0.11790	0.7408	794.3	12860	9526	107	12904
0.19520	1.2265	1795	12600	15460	146	12690
0.32100	2.0169	3901	12110	24420	193	12261
0.51260	3.2208	7854	11520	37110	243	11777
0.83950	5.2747	15470	10640	56150	293	11042
1.39100	8.7399	29210	9466	82740	334	10040
2.30900	14.5079	52640	8182	118700	362	8950
3.77400	23.7127	87550	6843	162300	369	7777
6.00000	37.6991	135400	5587	210600	359	6641
9.94000	62.4549	206200	4337	270800	330	5450

APPENDIX II
PARAMETERS OF MODIFIED CROSS MODEL FOR PURE POLYSTYRENE

Modified Cross Model:

$$\frac{\eta}{\eta_0} = \frac{1}{\left(1+(K\dot{\gamma})^m\right)} \tag{2.4}$$

Table AII.1
Modified Cross Model Parameters for pure PS Melt Viscosity: Complex Viscosity measured by Weissenberg Rheogoniometer

	T=150 ^{0}C	T=175 ^{0}C	T=188 ^{0}C	T=200 ^{0}C
η_0 (poise)	2387321	115652	32914	13589
K(s)	5.7238	0.2643	0.0699	0.0281
m (-)	0.6781	0.6916	0.7067	0.7596

Table AII.2
Modified Cross Model Parameters for pure PS Melt Viscosity: Complex Viscosity and Bagley-Schuemmer corrected Viscosity

	T=150 ^{0}C	T=175 ^{0}C	T=188 ^{0}C	T=200 ^{0}C
η_0 (poise)	2397391	115394	32897	13658
K(s)	5.9939	0.2654	0.0705	0.0296
m (-)	0.6829	0.7006	0.7120	0.7435

Table AII.3
Modified Cross Model Parameters for pure PS Melt Viscosity: Complex Viscosity and Bagley-Schuemmer-Pressure corrected Viscosity

	T=150 ^{0}C	T=175 ^{0}C	T=188 ^{0}C	T=200 ^{0}C
η_0 (poise)	2311099	115197	32971	13706
K(s)	5.5853	0.2792	0.0746	0.0294
m (-)	0.7731	0.7212	0.7088	0.7313

APPENDIX III
PARAMETERS FOR WLF EQUATION

by Williams [1953]

WLF Equation:

$$\ln \frac{\eta_0(T)}{\eta_0(T_g)} = -\frac{C_1(T-T_g)}{C_2+(T-T_g)} \tag{2.30}$$

Temperature dependence of free volume is assumed as:

$$f = f_g + \alpha (T - T_g) \tag{AIII.1}$$

where f is the relative free volume, α is a thermal expansion coefficient, f_g is the relative free volume at T_g.

Instead of using f_g=0.025 and α =4.8 x10^{-4}, the Doolittle equation [1952] is applied to melt viscosity and dilatometric data on polystyrene in order to determine the effect of molecular weight.

Doolittle's equation of viscosity is

$$\eta = A e^{B/f} \tag{AIII.2}$$

where A and B are constants and independent of temperature, and f, the relative free volume, is $(v - v_0)/ v_0$, where v_0 is the occupied volume.

For temperature range above T_g, the specific volume of polymers is given

$$v = v_g + \frac{dv}{dT}(T - T_g) \tag{AIII.3}$$

The relative free volume is given as:

$$f = \frac{v_g - v_0}{v_0} + \frac{1}{v_0}\frac{dv}{dT}(T - T_g) \tag{AIII.4}$$

Then the expression for viscosity becomes

$$\log\eta = \log A + \frac{B}{2.303\left[\frac{v_g - v_0}{v_0} + \frac{1}{v_0}\frac{dv}{dT}(T - T_g)\right]} \qquad \text{(AIII.5)}$$

Equation (AIII.5) was applied to the data of Fox and Flory [1948] on the polystyrene melt viscosity. Following expressions were given by Fox and Flory:

$$T_g, \text{ at 1 atm} = 100 - 10^5 / M_w \qquad \text{(AIII.6)}$$

$$v_g = 0.943 + 2.4\ 10^{-4}\ T_g \qquad \text{(AIII.7)}$$

$$dv/dT = (5.5 + 643 / M_w)^* 0.0001 \qquad \text{(AIII.8)}$$

$$B = 0.91 \qquad \text{(AIII.9)}$$

The slight variation of v_0 with molecular weight is expressed by

$$v_0 = 0.940 \exp(-11.5 / M_w) \qquad \text{(AIII.10)}$$

Calculation for polystyrene with M_w =132000 yields:

T_g = 99.24; v_0 = 0.9668; dv/dT = 0.00055; v_0 = 0.9400;

α = 0.000586; f_g = 0.00286;

and the WLF parameters are given as C_1 = 13.81 and C_2 =48.87.

APPENDIX IV
EXPERIMENTAL RHEOLOGICAL DATA FOR POLYSTYRENE-SCG

AIV.1 Capillary Rheometer Data for PS-CO_2

Table AIV.1(a)
Raw Data, Apparent Viscosities, and Schuemmer-corrected Shear Rates for PS-CO_2 : w(CO_2)=0.01, T=150 ^{0}C, and (L/D)=40[a]

Apparent Shear Rate $\dot{\gamma}_{wa}(s^{-1})$	Load Cell Force (L/D=40) F (lb_f)	Exit Pressure [b] P_L (*psi*)	Wall Shear Stress [c] τ_w(dyne/cm^2)	Schuemmer-corrected Shear Rate $\dot{\gamma}_w$ (s^{-1})	Apparent Viscosity η_a (*poise*)
2	357	2184	431329	**1.66**	**215665**
4	420	2193	667938	**3.32**	**166984**
5.5	458	2193	813242	**4.57**	**147862**
10	554	2198	1178916	**8.30**	**117892**
15	661	2192	1592742	**12.45**	**106183**
20	726	2193	1841636	**16.60**	**92082**
35	910	2136	2573288	**29.05**	**73523**
50	1145	2220	3443506	**41.50**	**68870**

[a] D=0.0496 *in.* and L=1.9990 *in.* [b] P_{BACK}= 9.79 MPa [c] Equaiton (6.41)

Table AIV.1(b)
Schuemmer-Pressure corrected Viscosities at P=P_L and P=P_{eq} for PS-CO_2 : w(CO_2)=0.01, T=150 ^{0}C, and (L/D)=40[a]

Pressure Coefficient: b=2.1445E-04 psi^{-1}

Schuemmer-corrected Shear Rate $\dot{\gamma}_w$ (s^{-1})	Effective Pressure P^* (*psi*)	Pressure Correction Factor [b] a_P	Pressure-corrected Viscosity at P=P_L [c] η (*poise*)	Pressure Correction Factor [d] a_P	Schuemmer-Pressure corrected Viscosity Data at P=P_{eq} (2.05 MPa) [e]	
					Shear Rate $\dot{\gamma}_w$ (s^{-1})	Viscosity at η (*poise*)
1.66	495.22	1.1130	**193772**	1.9314	**3.21**	**100327**
3.32	759.11	1.1783	**141715**	2.0025	**6.65**	**70770**
4.57	918.44	1.2196	**121238**	2.0354	**9.29**	**59566**
8.30	1310.32	1.3274	**88813**	2.1072	**17.49**	**42147**
12.45	1738.20	1.4560	**72926**	2.1533	**26.81**	**33868**
16.60	1987.66	1.5367	**59921**	2.1932	**36.41**	**27322**
29.05	2687.39	1.7876	**41128**	2.2213	**64.53**	**18515**
41.50	3456.66	2.1110	**32624**	2.3649	**98.14**	**13795**

[a] D=0.0496 *in.* and L=1.9990 *in.* [b] $a_P = exp\{b(P^* - P_L)\}$
[c] single-shifted (viscosity only) [d] $a_P = exp\{b_D (P_L - P_{eq})\}$; $b_D = b / n$
[e] double-shifted

Table AIV.2(a)
Raw Data, Apparent Viscosities, and Schuemmer-corrected Shear Rates for PS-CO_2 : w(CO_2)=0.02, T=150 ^{0}C, and (L/D)=40[a]

Apparent Shear Rate $\dot{\gamma}_{wa}(s^{-1})$	Load Cell Force (L/D=40) F (lb_f)	Exit Pressure [b] P_L (*psi*)	Wall Shear Stress [c] τ_w(dyne/cm^2)	Schuemmer-corrected Shear Rate $\dot{\gamma}_w$ (s^{-1})	Apparent Viscosity η_a (*poise*)
1	275	2005	193474	**0.83**	**193474**
2	311	2009	328276	**1.66**	**164138**
3.5	346.8	2015	461579	**2.91**	**131880**
5	376	2021	570094	**4.15**	**114019**
10	451	2038	848780	**8.30**	**84878**
17.5	523	2052	1117335	**14.53**	**63848**
25	575	2059	1312631	**20.75**	**52505**
35	627	2072	1505254	**29.05**	**43007**
50	692	2082	1748978	**41.50**	**34980**
75	781	2098	2082105	**62.25**	**27761**
100	846	2104	2327611	**83.00**	**23276**
150	922	2109	2614178	**124.50**	**17428**

[a] D=0.0496 *in.* and L=1.9990 *in.* [b] P_{BACK}= 11.37 MPa [c] Equaiton (6.41)

Table AIV.2(b)
Schuemmer-Pressure corrected Viscosities at $P=P_L$ and $P=P_{eq}$ for PS-CO_2 : w(CO_2)=0.02, T=150 ^{0}C, and (L/D)=40[a]

Pressure Coefficient: b=2.1445E-04 psi^{-1}

Schuemmer-corrected Shear Rate $\dot{\gamma}_w$ (s^{-1})	Effective Pressure P^* (*psi*)	Pressure Correction Factor [b] a_P	Pressure-corrected Viscosity at $P=P_L$ [c] η (*poise*)	Pressure Correction Factor [d] a_P	Schuemmer-Pressure corrected Viscosity Data at $P=P_{eq}$ (4.16 MPa) [e]	
					Shear Rate $\dot{\gamma}_w$ (s^{-1})	Viscosity at η (*poise*)
0.83	224.40	1.0496	**184335**	1.5259	**1.27**	**120806**
1.66	378.58	1.0851	**151271**	1.5972	**2.65**	**94709**
2.91	529.29	1.1209	**117655**	1.6716	**4.86**	**70383**
4.15	650.69	1.1506	**99092**	1.7304	**7.18**	**57266**
8.30	957.18	1.2293	**69048**	1.8813	**15.61**	**36703**
14.53	1245.38	1.3081	**48811**	2.0517	**29.80**	**23791**
20.75	1450.58	1.3673	**38402**	2.1930	**45.51**	**17511**
29.05	1649.37	1.4271	**30135**	2.3716	**68.90**	**12707**
41.50	1895.83	1.5050	**23242**	2.6145	**108.50**	**8889**
62.25	2223.62	1.6153	**17187**	3.0153	**187.70**	**5700**
83.00	2458.57	1.6992	**13698**	3.4096	**283.00**	**4018**
124.50	2725.81	1.8000	**9682**	4.2587	**530.21**	**2273**

[a] D=0.0496 *in.* and L=1.9990 *in.* [b] $a_P = exp\ \{b(P^* - P_L)\}$
[c] single-shifted (viscosity only) [d] $a_P = exp\ \{b_D\ (P_L - P_{eq})\}$; $b_D = b / n$
[e] double-shifted

Table AIV.3(a)
Raw Data, Apparent Viscosities, and Schuemmer-corrected Shear Rates for PS-CO_2 : w(CO_2)=0.03, T=150 ^{0}C, and (L/D)=40[a]

Apparent Shear Rate $\dot{\gamma}_{wa}(s^{-1})$	Load Cell Force (L/D=40) F (lb_f)	Exit Pressure [b] P_L (*psi*)	Wall Shear Stress [c] τ_w(dyne/cm^2)	Schuemmer-corrected Shear Rate $\dot{\gamma}_w$ (s^{-1})	Apparent Viscosity η_a (*poise*)
5.5	334.4	2166	346175	**4.57**	**62941**
7.5	362	2184	443412	**6.23**	**59122**
10	386	2196	529269	**8.30**	**52927**
12.5	407	2205	605121	**10.38**	**48410**
17.5	444	2221	738922	**14.53**	**42224**
20	460	2228	796773	**16.60**	**39839**
25	486	2237	891655	**20.75**	**35666**
35	536	2256	1073970	**29.05**	**30685**
50	572	2276	1201148	**41.50**	**24023**
100	704	2326	1682638	**83.00**	**16826**
150	816	2353	2099169	**124.50**	**13994**
250	983	2397	2719011	**207.50**	**10876**

[a] D=0.0496 *in.* and L=1.9990 *in.* [b] P_{BACK}= 11.98 MPa [c] Equaiton (6.41)

Table AIV.3(b)
Schuemmer-Pressure corrected Viscosities at P=P_L and P=P_{eq} for PS-CO_2 : w(CO_2)=0.03, T=150 ^{0}C, and (L/D)=40[a]

Pressure Coefficient: b=2.1445E-04 psi^{-1}

Schuemmer-corrected Shear Rate $\dot{\gamma}_w$ (s^{-1})	Effective Pressure P^* (*psi*)	Pressure Correction Factor [b] a_P	Pressure-corrected Viscosity at P=P_L [c] η (*poise*)	Pressure Correction Factor [d] a_P	Schuemmer-Pressure corrected Viscosity Data at P=P_{eq} (6.37 MPa) [e]	
					Shear Rate $\dot{\gamma}_w$ (s^{-1})	Viscosity at η (*poise*)
4.57	399	1.0896	**57765**	1.5664	**7.15**	**36876**
6.23	509	1.1157	**52991**	1.6205	**10.09**	**32701**
8.30	605	1.1390	**46466**	1.6756	**13.91**	**27732**
10.38	690	1.1599	**41735**	1.7242	**17.89**	**24205**
14.53	837	1.1974	**35264**	1.8125	**26.33**	**19456**
16.60	901	1.2138	**32822**	1.8535	**30.77**	**17708**
20.75	1004	1.2410	**28739**	1.9280	**40.01**	**14907**
29.05	1199	1.2944	**23706**	2.0710	**60.16**	**11447**
41.50	1334	1.3324	**18030**	2.2704	**94.22**	**7941**
83.00	1830	1.4823	**11351**	2.9460	**244.52**	**3853**
124.50	2241	1.6193	**8642**	3.7005	**460.72**	**2335**
207.50	2823	1.8353	**5926**	5.8582	**1215.58**	**1012**

[a] D=0.0496 *in.* and L=1.9990 *in.* [b] $a_P = exp\ \{b(P^* - P_L)\}$
[c] single-shifted (viscosity only) [d] $a_P = exp\ \{b_D\ (P_L - P_{eq})\}$; $b_D = b / n$
[e] double-shifted

Table AIV.4(a)
Raw Data, Apparent Viscosities, and Schuemmer-corrected Shear Rates for PS-CO_2 : w(CO_2)=0.035, T=150 ^{0}C, and (L/D)=40[a]

Apparent Shear Rate $\dot{\gamma}_{wa}(s^{-1})$	Load Cell Force (L/D=40) F (lb_f)	Exit Pressure [b] P_L (*psi*)	Wall Shear Stress [c] τ_w(dyne/cm^2)	Schuemmer-corrected Shear Rate $\dot{\gamma}_w$ (s^{-1})	Apparent Viscosity η_a (*poise*)
17.5	309	1644	463059	**14.53**	26461
25	364	1749	628066	**20.75**	25123
50	451	1834	921761	**41.50**	18435
150	753	2174	1931868	**124.5**	12879
250	915	2208	2536629	**207.5**	10147
400	1090	2556	3057071	**332.0**	7643

[a] D=0.0496 *in.* and L=1.9990 *in.*
[b] P_{BACK}= 8.36 MPa
[c] Equaiton (6.41)

Table AIV.4(b)
Schuemmer-Pressure corrected Viscosities at $P=P_L$ and $P=P_{eq}$ for PS-CO_2 : w(CO_2)=0.035, T=150 ^{0}C, and (L/D)=40[a]

Pressure Coefficient: b=2.1445E-04 psi^{-1}

Schuemmer-corrected Shear Rate $\dot{\gamma}_w$ (s^{-1})	Effective Pressure P^* (*psi*)	Pressure Correction Factor [b] a_P	Pressure-corrected Viscosity at $P=P_L$ [c] η (*poise*)	Pressure Correction Factor [d] a_P	Schuemmer-Pressure corrected Viscosity Data at $P=P_{eq}$ (7.51 MPa) [e]	
					Shear Rate $\dot{\gamma}_w$ (s^{-1})	Viscosity at η (*poise*)
14.53	530.99	1.1209	**23607**	1.1820	**17.17**	**19972**
20.75	715.14	1.1661	**21544**	1.2346	**25.62**	**17450**
41.50	1036.34	1.2494	**14755**	1.3091	**54.33**	**11271**
124.5	2077.72	1.5627	**8241**	1.6424	**204.48**	**5018**
207.5	2655.32	1.7692	**5735**	1.7925	**371.94**	**3199**
332.0	3125.86	1.9575	**3904**	2.4077	**799.35**	**1622**

[a] D=0.0496 *in.* and L=1.9990 *in.*
[b] $a_P = exp\ \{b(P^* - P_L)\}$
[c] single-shifted (viscosity only)
[d] $a_P = exp\ \{b_D\ (P_L - P_{eq})\}$; $b_D = b / n$
[e] double-shifted

Table AIV.5(a)
Raw Data, Apparent Viscosities, and Schuemmer-corrected Shear Rates for PS-CO_2 : w(CO_2)=0.045, T=150 ^{0}C, and (L/D)=40[a]

Apparent Shear Rate $\dot{\gamma}_{wa}$(s^{-1})	Load Cell Force (L/D=40) F (lb_f)	Exit Pressure [b] P_L (*psi*)	Wall Shear Stress [c] τ_w(dyne/cm^2)	Schuemmer-corrected Shear Rate $\dot{\gamma}_w$ (s^{-1})	Apparent Viscosity η_a (*poise*)
10	400	2825	314850	**8.30**	**31485**
17.5	448	2883	471679	**14.53**	**26953**
25	487	2930	599543	**20.75**	**23982**
50	575	3077	870599	**41.50**	**17412**
100	701	3309	1251042	**83.00**	**12510**
150	799	3584	1507332	**124.50**	**10049**
250	973	4123	1942621	**207.50**	**7770**
400	1147	4528	2434819	**332.00**	**6087**

[a] D=0.0496 *in.* and L=1.9990 *in.*
[b] P_{BACK}= 14.84 MPa
[c] Equaiton (6.41)

Table AIV.5(b)
Schuemmer-Pressure corrected Viscosities at P=P_L and P=P_{eq} for PS-CO_2 : w(CO_2)=0.045, T=150 ^{0}C, and (L/D)=40[a]

Pressure Coefficient: b=2.1445E-04 psi^{-1}

Schuemmer-corrected Shear Rate $\dot{\gamma}_w$ (s^{-1})	Effective Pressure P^* (*psi*)	Pressure Correction Factor [b] a_P	Pressure-corrected Viscosity at P=P_L [c] η (*poise*)	Pressure Correction Factor [d] a_P	Schuemmer-Pressure corrected Viscosity Data at P=P_{eq} (9.89 MPa) [e]	
					Shear Rate $\dot{\gamma}_w$ (s^{-1})	Viscosity at η (*poise*)
8.30	363.33	1.0810	**29126**	1.5450	**12.82**	**18852**
14.53	540.70	1.1229	**24003**	1.6407	**23.83**	**14630**
20.75	683.54	1.1578	**20713**	1.7216	**35.72**	**12031**
41.50	981.08	1.2340	**14110**	1.9730	**81.88**	**7152**
83.00	1386.72	1.3461	**9293**	2.4610	**204.27**	**3776**
124.50	1652.15	1.4250	**7052**	3.1276	**389.39**	**2255**
207.50	2088.72	1.5647	**4966**	5.1636	**1071.45**	**962**
332.00	2561.10	1.7315	**3515**	8.9692	**2977.77**	**392**

[a] D=0.0496 *in.* and L=1.9990 *in.*
[b] $a_P = exp\ \{b(P^* - P_L)\}$
[c] single-shifted (viscosity only)
[d] $a_P = exp\ \{b_D\ (P_L - P_{eq})\}$; $b_D = b / n$
[e] double-shifted

Table AIV.6(a)
Raw Data, Apparent Viscosities, and Schuemmer-corrected Shear Rates for PS-CO_2 : w(CO_2)=0.05, T=150 ^{0}C, and (L/D)=40[a]

Apparent Shear Rate $\dot{\gamma}_{wa}$ (s^{-1})	Load Cell Force (L/D=40) F (lb_f)	Exit Pressure [b] P_L (*psi*)	Wall Shear Stress [c] τ_w(dyne/cm^2)	Schuemmer-corrected Shear Rate $\dot{\gamma}_w$ (s^{-1})	Apparent Viscosity η_a (*poise*)
10	333	2378	246323	**8.30**	**24632**
12.5	344	2388	283034	**10.38**	**22643**
20	363	2407	344768	**16.60**	**17238**
25	387	2427	427204	**20.75**	**17088**
35	410	2447	504565	**29.05**	**14416**
50	435	2472	587019	**41.50**	**11740**
100	501	2544	803591	**83.00**	**8036**
150	547	2599	952637	**124.50**	**6351**
250	610	2711	1140779	**207.50**	**4563**
400	790	2827	1779777	**332.00**	**4449**
550	808	2823	1844959	**456.50**	**3354**

[a] D=0.0496 *in.* and L=1.9990 *in.* [b] P_{BACK}= 12.98 MPa [c] Equaiton (6.41)

Table AIV.6(b)
Schuemmer-Pressure corrected Viscosities at P=P_L and P=P_{eq} for PS-CO_2 : w(CO_2)=0.05, T=150 ^{0}C, and (L/D)=40[a]

Pressure Coefficient: b=2.1445E-04 psi^{-1}

Schuemmer-corrected Shear Rate $\dot{\gamma}_w$ (s^{-1})	Effective Pressure P^* (*psi*)	Pressure Correction Factor [b] a_P	Pressure-corrected Viscosity at P=P_L [c] η (*poise*)	Pressure Correction Factor [d] a_P	Schuemmer-Pressure corrected Viscosity Data at P=P_{eq} (11.14 MPa) [e]	
					Shear Rate $\dot{\gamma}_w$ (s^{-1})	Viscosity at η (*poise*)
8.30	285.08	1.0629	**23174**	1.2827	**10.65**	**18066**
10.38	327.06	1.0725	**21111**	1.2970	**13.46**	**16277**
16.60	397.36	1.0888	**15833**	1.3299	**22.08**	**11905**
20.75	490.66	1.1108	**15384**	1.3530	**28.07**	**11371**
29.05	577.61	1.1316	**12739**	1.3863	**40.27**	**9189**
41.50	669.64	1.1542	**10172**	1.4292	**59.31**	**7117**
83.00	908.23	1.2146	**6616**	1.5521	**128.82**	**4263**
124.50	1069.79	1.2574	**5051**	1.6582	**206.44**	**3046**
207.50	1270.66	1.3126	**3476**	1.8810	**390.30**	**1848**
332.00	1927.66	1.5109	**2945**	2.1961	**729.12**	**1341**
456.50	1992.51	1.5320	**2190**	2.3567	**1075.82**	**929**

[a] D=0.0496 *in.* and L=1.9990 *in.* [b] $a_P = exp\ \{b(P^* - P_L)\}$
[c] single-shifted (viscosity only) [d] $a_P = exp\ \{b_D\ (P_L - P_{eq})\}$; $b_D = b / n$
[e] double-shifted

Table AIV.7(a)
Raw Data, Apparent Viscosities, and Schuemmer-corrected Shear Rates for PS-CO_2 : w(CO_2)=0.052, T=150 ^{0}C, and (L/D)=40[a]

Apparent Shear Rate $\dot{\gamma}_{wa}$(s^{-1})	Load Cell Force (L/D=40) F (lb_f)	Exit Pressure [b] P_L (*psi*)	Wall Shear Stress [c] τ_w(dyne/cm^2)	Schuemmer-corrected Shear Rate $\dot{\gamma}_w$ (s^{-1})	Apparent Viscosity η_a (*poise*)
10	324	2333	230636	**8.30**	**23064**
12.5	330	2344	247562	**10.38**	**19805**
20	343	2357	288633	**16.60**	**14432**
25	351	2365	314258	**20.75**	**12570**
35	371	2379	382570	**29.05**	**10931**
50	390	2394	446071	**41.50**	**8921**
100	438	2429	608779	**83.00**	**6088**
150	463	2453	689781	**124.50**	**4599**
250	514	2492	862680	**207.50**	**3451**

[a] D=0.0496 *in.* and L=1.9990 *in.*
[b] P_{BACK}= 12.18 MPa
[c] Equaiton (6.41)

Table AIV.7(b)
Schuemmer-Pressure corrected Viscosities at P=P_L and P=P_{eq} for PS-CO_2 : w(CO_2)=0.052, T=150 ^{0}C, and (L/D)=40[a]

Pressure Coefficient: b=2.1445E-04 psi^{-1}

Schuemmer-corrected Shear Rate $\dot{\gamma}_w$ (s^{-1})	Effective Pressure P^* (*psi*)	Pressure Correction Factor [b] a_P	Pressure-corrected Viscosity at P=P_L [c] η (*poise*)	Pressure Correction Factor [d] a_P	Schuemmer-Pressure corrected Viscosity Data at P=P_{eq} (11.68 MPa) [e]	
					Shear Rate $\dot{\gamma}_w$ (s^{-1})	Viscosity at η (*poise*)
8.30	267.10	1.0588	**21782**	1.3716	**11.38**	**15881**
10.38	286.50	1.0632	**18627**	1.3915	**14.44**	**13386**
16.60	333.46	1.0740	**13438**	1.4319	**23.77**	**9385**
20.75	362.67	1.0807	**11632**	1.4548	**30.19**	**7995**
29.05	440.23	1.0988	**9948**	1.4947	**43.42**	**6655**
41.50	511.92	1.1158	**7996**	1.5434	**64.05**	**5181**
83.00	693.83	1.1601	**5248**	1.6689	**138.52**	**3144**
124.50	783.43	1.1825	**3889**	1.7691	**220.25**	**2198**
207.50	972.55	1.2314	**2802**	1.9458	**403.75**	**1440**

[a] D=0.0496 *in.* and L=1.9990 *in.*
[b] $a_P = exp\ \{b(P^* - P_L)\}$
[c] single-shifted (viscosity only)
[d] $a_P = exp\ \{b_D\ (P_L - P_{eq})\}$; $b_D = b / n$
[e] double-shifted

Table AIV.8(a)

Raw Data, Apparent Viscosities, and Schuemmer-corrected Shear Rates for PS-CO_2 : w(CO_2)=0.01, T=175 ^{0}C, and (L/D)=40[a]

Apparent Shear Rate $\dot{\gamma}_{wa}$(s^{-1})	Load Cell Force (L/D=40) F (lb_f)	Exit Pressure [b] P_L (*psi*)	Wall Shear Stress [c] τ_w(dyne/cm^2)	Schuemmer-corrected Shear Rate $\dot{\gamma}_w$ (s^{-1})	Apparent Viscosity η_a (*poise*)
10	218.8	1500	184779	**8.30**	**18478**
15	241.7	1510	266775	**12.45**	**17785**
25	272.1	1521	376366	**20.75**	**15055**
35	294.9	1528	459136	**29.05**	**13118**
50	322.1	1538	557249	**41.50**	**11145**
75	356.4	1551	680811	**62.25**	**9077**
100	385	1565	782692	**83.00**	**7827**
150	454	1617	1023166	**124.50**	**6821**
250	542	1715	1315652	**207.50**	**5263**
400	634	1778	1638279	**332.00**	**4096**
550	712	1832	1912188	**456.50**	**3477**
750	779	1880	2145780	**622.50**	**2861**
1000	841	1896	2373673	**830.00**	**2374**

[a] D=0.0496 *in.* and L=1.9990 *in.* [b] P_{BACK}= 7.43 MPa [c] Equaiton (6.41)

Table AIV.8(b)

Schuemmer-Pressure corrected Viscosities at P=P_L and P=P_{eq} for PS-CO_2 : w(CO_2)=0.01, T=175 ^{0}C, and (L/D)=40[a]

Pressure Coefficient: b=1.6398E-04 psi^{-1}

Schuemmer-corrected Shear Rate $\dot{\gamma}_w$ (s^{-1})	Effective Pressure P^* (*psi*)	Pressure Correction Factor [b] a_P	Pressure-corrected Viscosity at P=P_L [c] η (*poise*)	Pressure Correction Factor [d] a_P	Schuemmer-Pressure corrected Viscosity Data at P=P_{eq} (2.37 MPa) [e]	
					Shear Rate $\dot{\gamma}_w$ (s^{-1})	Viscosity at η (*poise*)
8.30	214.80	1.0359	**17838**	1.3121	**10.89**	**13595**
12.45	309.30	1.0520	**16905**	1.3384	**16.66**	**12631**
20.75	434.82	1.0739	**14019**	1.3770	**28.57**	**10180**
29.05	529.02	1.0906	**12028**	1.4070	**40.87**	**8549**
41.50	640.03	1.1107	**10035**	1.4451	**59.97**	**6944**
62.25	778.81	1.1362	**7989**	1.4978	**93.24**	**5334**
83.00	892.38	1.1576	**6761**	1.5450	**128.24**	**4376**
124.50	1157.38	1.2090	**5642**	1.6470	**205.05**	**3426**
207.50	1473.93	1.2734	**4133**	1.8493	**383.73**	**2235**
332.00	1815.77	1.3468	**3041**	2.0989	**696.84**	**1449**
456.50	2100.01	1.4111	**2464**	2.3591	**1076.91**	**1044**
622.50	2338.09	1.4673	**1950**	2.7138	**1689.34**	**719**
830.00	2566.57	1.5233	**1558**	3.1370	**2603.74**	**497**

[a] D=0.0496 *in.* and L=1.9990 *in.* [b] $a_P = exp\ \{b(P^* - P_L)\}$

[c] single-shifted (viscosity only) [d] $a_P = exp\ \{b_D\ (P_L - P_{eq})\}$; $b_D = b / n$

[e] double-shifted

Table AIV.9(a)

Raw Data, Apparent Viscosities, and Schuemmer-corrected Shear Rates for PS-CO_2 : w(CO_2)=0.02, T=175 ^{0}C, and (L/D)=40[a]

Apparent Shear Rate $\dot{\gamma}_{wa}$(s^{-1})	Load Cell Force (L/D=40) F (lb_f)	Exit Pressure [b] P_L (*psi*)	Wall Shear Stress [c] τ_w(dyne/cm^2)	Schuemmer-corrected Shear Rate $\dot{\gamma}_w$ (s^{-1})	Apparent Viscosity η_a (*poise*)
15	240.6	1614	218139	**12.45**	**14543**
25	266	1628	307091	**20.75**	**12284**
35	288	1635	386764	**29.05**	**11050**
50	312	1647	471633	**41.50**	**9433**
75	343	1662	581565	**62.25**	**7754**
100	367	1676	665637	**83.00**	**6656**
150	404	1708	790778	**124.50**	**5272**
250	463	1770	986387	**207.50**	**3946**
400	536	1837	1233747	**332.00**	**3084**
550	588	1879	1412131	**456.50**	**2568**
750	642	1931	1593685	**622.50**	**2125**
1000	697	1951	1792767	**830.00**	**1793**
1250	741	1953	1957858	**1037.50**	**1566**

[a] D=0.0496 *in.* and L=1.9990 *in.* [b] P_{BACK}= 9.03 MPa [c] Equaiton (6.41)

Table AIV.9(b)

Schuemmer-Pressure corrected Viscosities at P=P_L and P=P_{eq} for PS-CO_2 : w(CO_2)=0.02, T=175 ^{0}C, and (L/D)=40[a]

Pressure Coefficient: b=1.6398E-04 psi^{-1}

Schuemmer-corrected Shear Rate $\dot{\gamma}_w$ (s^{-1})	Effective Pressure P^* (*psi*)	Pressure Correction Factor [b] a_P	Pressure-corrected Viscosity at P=P_L [c] η (*poise*)	Pressure Correction Factor [d] a_P	Schuemmer-Pressure corrected Viscosity Data at P=P_{eq} (4.83 MPa) [e]	
					Shear Rate $\dot{\gamma}_w$ (s^{-1})	Viscosity at η (*poise*)
12.45	253.31	1.1615	**13951**	1.2762	**15.89**	**10932**
20.75	355.58	1.1641	**11588**	1.3069	**27.12**	**8867**
29.05	446.68	1.1655	**10270**	1.3295	**38.62**	**7724**
41.50	543.20	1.1678	**8629**	1.3591	**56.40**	**6349**
62.25	667.43	1.1706	**6950**	1.3991	**87.10**	**4968**
83.00	761.82	1.1733	**5875**	1.4342	**119.04**	**4096**
124.50	901.36	1.1795	**4548**	1.5005	**186.81**	**3031**
207.50	1117.13	1.1916	**3285**	1.6251	**337.21**	**2021**
332.00	1385.93	1.2047	**2457**	1.7939	**595.57**	**1370**
456.50	1576.96	1.2130	**1982**	1.9460	**888.34**	**1019**
622.50	1768.98	1.2234	**1590**	2.1577	**1343.15**	**737**
830.00	1976.76	1.2275	**1296**	2.3797	**1975.19**	**545**
1037.50	2146.87	1.2279	**1101**	2.5828	**2679.62**	**426**

[a] D=0.0496 *in.* and L=1.9990 *in.* [b] $a_P = exp\ \{b(P^* - P_L)\}$

[c] single-shifted (viscosity only) [d] $a_P = exp\ \{b_D\ (P_L - P_{eq})\}$; $b_D = b / n$

[e] double-shifted

Table AIV.10(a)

Raw Data, Apparent Viscosities, and Schuemmer-corrected Shear Rates for PS-CO_2 : w(CO_2)=0.03, T=175 ^{0}C, and (L/D)=40[a]

Apparent Shear Rate $\dot{\gamma}_{wa}$(s^{-1})	Load Cell Force (L/D=40) F (lb_f)	Exit Pressure [b] P_L (*psi*)	Wall Shear Stress [c] τ_w(dyne/cm^2)	Schuemmer-corrected Shear Rate $\dot{\gamma}_w$ (s^{-1})	Apparent Viscosity η_a (*poise*)
10	268.8	2121	113076	**8.30**	**11308**
15	282.7	2133	159375	**12.45**	**10625**
25	305.7	2151	237325	**20.75**	**9493**
35	325	2164	303980	**29.05**	**8685**
50	347.2	2179	380598	**41.50**	**7612**
75	377	2198	484173	**62.25**	**6456**
100	402	2211	572544	**83.00**	**5725**
150	440	2239	703268	**124.50**	**4688**
250	498	2270	908260	**207.50**	**3633**
400	565	2332	1134530	**332.00**	**2836**
550	622	2439	1304477	**456.50**	**2372**
750	678	2536	1474533	**622.50**	**1966**
1000	723	2569	1629343	**830.00**	**1629**

[a] D=0.0496 *in.* and L=1.9990 *in.* [b] P_{BACK}= 12.62 MPa [c] Equaiton (6.41)

Table AIV.10(b)

Schuemmer-Pressure corrected Viscosities at P=P_L and P=P_{eq} for PS-CO_2 : w(CO_2)=0.03, T=175 ^{0}C, and (L/D)=40[a]

Pressure Coefficient: b=1.6398E-04 psi^{-1}

Schuemmer-corrected Shear Rate $\dot{\gamma}_w$ (s^{-1})	Effective Pressure P^* (*psi*)	Pressure Correction Factor [b] a_P	Pressure-corrected Viscosity at P=P_L [c] η (*poise*)	Pressure Correction Factor [d] a_P	Schuemmer-Pressure corrected Viscosity Data at P=P_{eq} (7.40 MPa) [e]	
					Shear Rate $\dot{\gamma}_w$ (s^{-1})	Viscosity at η (*poise*)
8.30	131.75	1.1873	**11066**	1.2417	**10.31**	**8912**
12.45	185.42	1.1897	**10307**	1.2628	**15.72**	**8162**
20.75	275.42	1.1932	**9074**	1.2954	**26.88**	**7005**
29.05	352.01	1.1957	**8198**	1.3211	**38.38**	**6205**
41.50	439.65	1.1987	**7083**	1.3534	**56.17**	**5233**
62.25	557.42	1.2024	**5892**	1.3983	**87.04**	**4214**
83.00	657.27	1.2050	**5140**	1.4362	**119.20**	**3579**
124.50	803.91	1.2105	**4109**	1.5066	**187.57**	**2728**
207.50	1031.29	1.2167	**3068**	1.6241	**337.00**	**1889**
332.00	1278.65	1.2291	**2300**	1.8100	**600.93**	**1271**
456.50	1461.95	1.2509	**1866**	2.0624	**941.48**	**905**
622.50	1643.23	1.2709	**1502**	2.4161	**1503.99**	**622**
830.00	1806.41	1.2778	**1212**	2.8130	**2334.76**	**431**

[a] D=0.0496 *in.* and L=1.9990 *in.* [b] $a_P = exp\ \{b(P^* - P_L)\}$

[c] single-shifted (viscosity only) [d] $a_P = exp\ \{b_D\ (P_L - P_{eq})\}$; $b_D = b / n$

[e] double-shifted

Table AIV.11(a)
Raw Data, Apparent Viscosities, and Schuemmer-corrected Shear Rates for PS-CO_2 : w(CO_2)=0.035, T=175 ^{0}C, and (L/D)=40[a]

Apparent Shear Rate $\dot{\gamma}_{wa}$(s^{-1})	Load Cell Force (L/D=40) F (lb_f)	Exit Pressure [b] P_L (*psi*)	Wall Shear Stress [c] τ_w(dyne/cm^2)	Schuemmer-corrected Shear Rate $\dot{\gamma}_w$ (s^{-1})	Apparent Viscosity η_a (*poise*)
25	270.8	2043	148144	**20.75**	**5926**
35	286.7	2055	202064	**29.05**	**5773**
50	306	2066	269165	**41.50**	**5383**
75	331.3	2079	357885	**62.25**	**4772**
100	352.6	2089	433215	**83.00**	**4332**
150	386	2108	549978	**124.50**	**3667**
250	435	2136	721410	**207.50**	**2886**
400	487	2171	901154	**332.00**	**2253**
550	529	2213	1040824	**456.50**	**1892**
750	575	2314	1170455	**622.50**	**1561**
1000	606	2355	1267645	**830.00**	**1268**

[a] D=0.0496 *in.* and L=1.9990 *in.* [b] P_{BACK}= 11.79 MPa [c] Equaiton (6.41)

Table AIV.11(b)
Schuemmer-Pressure corrected Viscosities at P=P_L and P=P_{eq} for PS-CO_2 : w(CO_2)=0.035, T=175 ^{0}C, and (L/D)=40[a]

Pressure Coefficient: b=1.6398E-04 psi^{-1}

Schuemmer-corrected Shear Rate $\dot{\gamma}_w$ (s^{-1})	Effective Pressure P^* (*psi*)	Pressure Correction Factor [b] a_P	Pressure-corrected Viscosity at P=P_L [c] η (*poise*)	Pressure Correction Factor [d] a_P	Schuemmer-Pressure corrected Viscosity Data at P=P_{eq} (8.73 MPa) [e]	
					Shear Rate $\dot{\gamma}_w$ (s^{-1})	Viscosity at η (*poise*)
20.75	172.41	1.1357	**5761**	1.1618	**24.11**	**4958**
29.05	234.76	1.1380	**5555**	1.1781	**34.22**	**4715**
41.50	312.05	1.1400	**5115**	1.1983	**49.73**	**4268**
62.25	413.71	1.1425	**4459**	1.2267	**76.36**	**3635**
83.00	499.57	1.1443	**3991**	1.2519	**103.90**	**3188**
124.50	631.83	1.1479	**3306**	1.2989	**161.71**	**2545**
207.50	824.16	1.1532	**2521**	1.3869	**287.77**	**1818**
332.00	1023.46	1.1598	**1905**	1.5247	**506.21**	**1249**
456.50	1176.67	1.1678	**1560**	1.6940	**773.29**	**921**
622.50	1317.58	1.1873	**1257**	2.0529	**1277.96**	**612**
830.00	1422.41	1.1954	**1004**	2.5950	**2153.82**	**387**

[a] D=0.0496 *in.* and L=1.9990 *in.* [b] $a_P = exp\ \{b(P^* - P_L)\}$
[c] single-shifted (viscosity only) [d] $a_P = exp\ \{b_D\ (P_L - P_{eq})\}$; $b_D = b / n$
[e] double-shifted

Table AIV.12(a)
Raw Data, Apparent Viscosities, and Schuemmer-corrected Shear Rates for PS-CO_2 : w(CO_2)=0.045, T=175 ^{0}C, and (L/D)=40[a]

Apparent Shear Rate $\dot{\gamma}_{wa}(s^{-1})$	Load Cell Force (L/D=40) F (lb_f)	Exit Pressure [b] P_L (*psi*)	Wall Shear Stress [c] τ_w(dyne/cm^2)	Schuemmer-corrected Shear Rate $\dot{\gamma}_w$ (s^{-1})	Apparent Viscosity η_a (*poise*)
25	307.8	2417	131435	**20.75**	**5257**
35	320.5	2427	173822	**29.05**	**4966**
50	336.6	2437	228962	**41.50**	**4579**
75	358.7	2452	304438	**62.25**	**4059**
100	376	2461	364710	**83.00**	**3647**
150	403	2478	457551	**124.50**	**3050**
250	444	2503	599295	**207.50**	**2397**
400	488	2528	752344	**332.00**	**1881**
550	521	2557	862729	**456.50**	**1569**
750	560	2628	978089	**622.50**	**1304**
1000	601	2662	1116986	**830.00**	**1117**

[a] D=0.0496 *in.* and L=1.9990 *in.*
[b] P_{BACK}= 12.58 MPa
[c] Equaiton (6.41)

Table AIV.12(b)
Schuemmer-Pressure corrected Viscosities at $P=P_L$ and $P=P_{eq}$ for PS-CO_2 : w(CO_2)=0.045, T=175 ^{0}C, and (L/D)=40[a]

Pressure Coefficient: b=1.63989E-04 psi^{-1}

Schuemmer-corrected Shear Rate $\dot{\gamma}_w$ (s^{-1})	Effective Pressure P^* (*psi*)	Pressure Correction Factor [b] a_P	Pressure-corrected Viscosity at $P=P_L$ [c] η (*poise*)	Pressure Correction Factor [d] a_P	Schuemmer-Pressure corrected Viscosity Data at $P=P_{eq}$ (11.52 MPa) [e]	
					Shear Rate $\dot{\gamma}_w$ (s^{-1})	Viscosity at η (*poise*)
20.75	153.05	1.1300	**5127**	1.1691	**24.26**	**4386**
29.05	202.13	1.1319	**4804**	1.1836	**34.38**	**4059**
41.50	265.78	1.1337	**4384**	1.2014	**49.86**	**3649**
62.25	352.54	1.1365	**3831**	1.2266	**76.36**	**3123**
83.00	421.51	1.1382	**3404**	1.2474	**103.53**	**2729**
124.50	527.22	1.1414	**2798**	1.2846	**159.93**	**2178**
207.50	687.38	1.1461	**2142**	1.3489	**279.90**	**1588**
332.00	858.63	1.1508	**1634**	1.4351	**476.45**	**1138**
456.50	981.06	1.1563	**1336**	1.5260	**696.60**	**875**
622.50	1108.03	1.1698	**1087**	1.6882	**1050.88**	**644**
830.00	1259.61	1.1763	**909**	1.8737	**1555.15**	**485**

[a] D=0.0496 *in.* and L=1.9990 *in.*
[b] $a_P = exp\ \{b(P^* - P_L)\}$
[c] single-shifted (viscosity only)
[d] $a_P = exp\ \{b_D\ (P_L - P_{eq})\}$; $b_D = b / n$
[e] double-shifted

Table AIV.13(a)

Raw Data, Apparent Viscosities, and Schuemmer-corrected Shear Rates for PS-CO_2 : w(CO_2)=0.05, T=175 ^{0}C, and (L/D)=40[a]

Apparent Shear Rate $\dot{\gamma}_{wa}(s^{-1})$	Load Cell Force (L/D=40) F (lb_f)	Exit Pressure [b] P_L (*psi*)	Wall Shear Stress [c] τ_w(dyne/cm^2)	Schuemmer-corrected Shear Rate $\dot{\gamma}_w$ (s^{-1})	Apparent Viscosity η_a (*poise*)
150	403	2718	355271	**124.50**	**2368**
250	443	2755	488013	**207.50**	**1952**
400	489	2817	632983	**332.00**	**1582**
550	530	2903	749968	**456.50**	**1364**
750	570	2985	864495	**622.50**	**1153**
1000	608	3037	984082	**830.00**	**984**
1250	629	3043	1058420	**1037.50**	**847**

[a] D=0.0496 *in.* and L=1.9990 *in.*

[b] P_{BACK}= 15.00 MPa

[c] Equaiton (6.41)

Table AIV.13(b)

Schuemmer-Pressure corrected Viscosities at $P=P_L$ and $P=P_{eq}$ for PS-CO_2 : w(CO_2)=0.051, T=175 ^{0}C, and (L/D)=40[a]

Pressure Coefficient: b=1.6398E-04 psi^{-1}

Schuemmer-corrected Shear Rate $\dot{\gamma}_w$ (s^{-1})	Effective Pressure P^* (*psi*)	Pressure Correction Factor [b] a_P	Pressure-corrected Viscosity at $P=P_L$ [c] η (*poise*)	Pressure Correction Factor [d] a_P	Schuemmer-Pressure corrected Viscosity Data at $P=P_{eq}$ (13.29 MPa) [e]	
					Shear Rate $\dot{\gamma}_w$ (s^{-1})	Viscosity at η (*poise*)
124.50	410.73	1.1381	**2214**	1.2127	**150.98**	**1826**
207.50	561.77	1.1450	**1780**	1.2716	**263.86**	**1400**
332.00	725.22	1.1567	**1405**	1.3676	**454.06**	**1027**
456.50	855.98	1.1731	**1185**	1.4933	**681.71**	**794**
622.50	983.01	1.1890	**981**	1.6815	**1046.70**	**583**
830.00	1114.60	1.1992	**820**	1.9461	**1615.25**	**421**
1037.50	1195.87	1.2004	**696**	2.2434	**2327.56**	**310**

[a] D=0.0496 *in.* and L=1.9990 *in.*

[b] $a_P = exp\{b(P^* - P_L)\}$

[c] single-shifted (viscosity only)

[d] $a_P = exp\{b_D (P_L - P_{eq})\}$; $b_D = b / n$

[e] double-shifted

AIV.2 Capillary Rheometer Data for PS-R152a

Table AIV.14(a)
Raw Data, Apparent Viscosities, and Schuemmer-corrected Shear Rates for PS-R152a : w(R152a)=0.056, T=150 ^{0}C, and (L/D)=40[a]

Apparent Shear Rate $\dot{\gamma}_{wa}(s^{-1})$	Load Cell Force (L/D=40) F (lb_f)	Exit Pressure [b] P_L (*psi*)	Wall Shear Stress [c] τ_w(dyne/cm^2)	Schuemmer-corrected Shear Rate $\dot{\gamma}_w(s^{-1})$	Apparent Viscosity η_a (*poise*)
12.5	303	2238	188485	**10.38**	**15079**
17.5	321	2260	246164	**14.53**	**14066**
20	329	2267	273043	**16.60**	**13652**
25	344	2278	348482	**20.75**	**13939**
35	369	2301	434567	**29.05**	**12416**
50	400	2323	544166	**41.50**	**10883**
100	466	2387	770058	**83.00**	**7701**
150	515	2429	940271	**124.50**	**6268**
250	590	2500	1198091	**207.50**	**4792**
400	662	2533	1460438	**332.00**	**3651**

[a] D=0.0496 *in.* and L=1.9990 *in.* [b] P_{BACK}= 12.06 MPa [c] Equaiton (6.41)

Table AIV.14(b)
Schuemmer-Pressure corrected Viscosities at $P=P_L$ and $P=P_{eq}$ for PS-R152a : w(R152a)=0.056, T=150 ^{0}C, and (L/D)=40[a]

Pressure Coefficient: b=2.1445E-04 psi^{-1}

Schuemmer-corrected Shear Rate $\dot{\gamma}_w(s^{-1})$	Effective Pressure P^* (*psi*)	Pressure Correction Factor [b] a_P	Pressure-corrected Viscosity at $P=P_L$ [c] η (*poise*)	Pressure Correction Factor [d] a_P	Schuemmer-Pressure corrected Viscosity Data at $P=P_{eq}$ (3.00 MPa) [e]	
					Shear Rate $\dot{\gamma}_w(s^{-1})$	Viscosity at η (*poise*)
10.38	218.68	1.0479	**14390**	1.8278	**18.96**	**7873**
14.53	284.90	1.0628	**13235**	1.9079	**27.71**	**6937**
16.60	315.66	1.0698	**12761**	1.9421	**32.24**	**6571**
20.75	401.59	1.0897	**12792**	2.0042	**41.59**	**6383**
29.05	498.97	1.1126	**11160**	2.1179	**61.53**	**5269**
41.50	621.91	1.1422	**9528**	2.2625	**93.89**	**4211**
83.00	871.62	1.2048	**6391**	2.6884	**223.14**	**2377**
124.50	1056.52	1.2534	**5001**	3.0738	**382.68**	**1627**
207.50	1331.28	1.3293	**3605**	3.8690	**802.82**	**932**
332.00	1604.32	1.4092	**2591**	5.0429	**1674.25**	**514**

[a] D=0.0496 *in.* and L=1.9990 *in.* [b] $a_P = exp\ \{b(P^* - P_L)\}$
[c] single-shifted (viscosity only) [d] $a_P = exp\ \{b_D\ (P_L - P_{eq})\}$; $b_D = b / n$
[e] double-shifted

Table AIV.15(a)
Raw Data, Apparent Viscosities, and Schuemmer-corrected Shear Rates for PS-R152a : w(R152a)=0.070, T=150 ^{0}C, and (L/D)=40[a]

Apparent Shear Rate $\dot{\gamma}_{wa}(s^{-1})$	Load Cell Force (L/D=40) F (lb_f)	Exit Pressure [b] P_L (*psi*)	Wall Shear Stress [c] τ_w(dyne/cm^2)	Schuemmer-corrected Shear Rate $\dot{\gamma}_w$ (s^{-1})	Apparent Viscosity η_a (*poise*)
25	315.2	2427	173421	**20.75**	**6937**
35	332.1	2438	233278	**29.05**	**6665**
50	352.2	2454	303245	**41.50**	**6065**
100	384	2333	475837	**83.00**	**4758**
150	408	2270	594162	**124.50**	**3961**
250	455	2253	781210	**207.50**	**3125**
400	523	2401	978900	**332.00**	**2447**
550	571	2489	1125382	**456.50**	**2046**
750	627	2601	1292470	**622.50**	**1723**

[a] D=0.0496 *in.* and L=1.9990 *in.*
[b] P_{BACK}= 12.48 MPa
[c] Equaiton (6.41)

Table AIV.15(b)
Schuemmer-Pressure corrected Viscosities at $P=P_L$ and $P=P_{eq}$ for PS-R152a : w(R152a)=0.070, T=150 ^{0}C, and (L/D)=40[a]

Pressure Coefficient: b=2.1445E-04 psi^{-1}

Schuemmer-corrected Shear Rate $\dot{\gamma}_w$ (s^{-1})	Effective Pressure P^* (*psi*)	Pressure Correction Factor [b] a_P	Pressure-corrected Viscosity at $P=P_L$ [c] η (*poise*)	Pressure Correction Factor [d] a_P	Schuemmer-Pressure corrected Viscosity Data at $P=P_{eq}$ (3.79 MPa) [e]	
					Shear Rate $\dot{\gamma}_w$ (s^{-1})	Viscosity at η (*poise*)
20.75	201.33	1.0438	**6646**	1.7706	**36.74**	**3753**
29.05	270.15	1.0592	**6292**	1.8398	**53.45**	**3420**
41.50	350.14	1.0775	**5629**	1.9296	**80.08**	**2917**
83.00	545.44	1.1232	**4236**	2.0361	**168.99**	**2081**
124.50	677.66	1.1553	**3429**	2.1262	**264.71**	**1613**
207.50	883.93	1.2072	**2588**	2.3496	**487.55**	**1102**
332.00	1098.26	1.2636	**1937**	2.9154	**967.93**	**664**
456.50	1254.65	1.3064	**1566**	3.4903	**1593.32**	**449**
622.50	1430.54	1.3563	**1271**	4.4337	**2760.00**	**287**

[a] D=0.0496 *in.* and L=1.9990 *in.*
[b] $a_P = exp\ \{b(P^* - P_L)\}$
[c] single-shifted (viscosity only)
[d] $a_P = exp\ \{b_D\ (P_L - P_{eq})\}$; $b_D = b / n$
[e] double-shifted

Table AIV.16(a)
Raw Data, Apparent Viscosities, and Schuemmer-corrected Shear Rates for PS-R152a : w(R152a)=0.083, T=150 ^{0}C, and (L/D)=40[a]

Apparent Shear Rate $\dot{\gamma}_{wa}(s^{-1})$	Load Cell Force (L/D=40) F (lb_f)	Exit Pressure [b] P_L (*psi*)	Wall Shear Stress [c] τ_w(dyne/cm^2)	Schuemmer-corrected Shear Rate $\dot{\gamma}_w$ (s^{-1})	Apparent Viscosity η_a (*poise*)
35	390	3110	143890	**29.05**	**4111**
50	406	3135	191502	**41.50**	**3830**
100	450	3189	330600	**83.00**	**3306**
150	491	3242	461144	**124.50**	**3074**
250	544	3326	622545	**207.50**	**2490**
400	604	3430	802106	**332.00**	**2005**
550	655	3535	948438	**456.50**	**1724**

[a] D=0.0496 *in.* and L=1.9990 *in.*
[b] P_{BACK}= 17.18 MPa
[c] Equaiton (6.41)

Table AIV.16(b)
Schuemmer-Pressure corrected Viscosities at P=P_L and P=P_{eq} for PS-R152a : w(R152a)=0.083, T=150 ^{0}C, and (L/D)=40[a]

Pressure Coefficient: b=2.1445E-04 psi^{-1}

Schuemmer-corrected Shear Rate $\dot{\gamma}_w$ (s^{-1})	Effective Pressure P^* (*psi*)	Pressure Correction Factor [b] a_P	Pressure-corrected Viscosity at P=P_L [c] η (*poise*)	Pressure Correction Factor [d] a_P	Schuemmer-Pressure corrected Viscosity Data at P=P_{eq} (4.49 MPa) [e]	
					Shear Rate $\dot{\gamma}_w$ (s^{-1})	Viscosity at η (*poise*)
29.05	167.26	1.0362	**3968**	1.8145	**52.71**	**2187**
41.50	222.16	1.0483	**3653**	1.9182	**79.60**	**1905**
83.00	381.30	1.0844	**3049**	2.2082	**183.28**	**1381**
124.50	528.96	1.1189	**2748**	2.4844	**309.31**	**1106**
207.50	709.24	1.1626	**2142**	3.0514	**633.17**	**702**
332.00	906.85	1.2124	**1654**	4.0570	**1346.92**	**408**
456.50	1065.61	1.2540	**1375**	5.4316	**2479.55**	**253**

[a] D=0.0496 *in.* and L=1.9990 *in.*
[b] $a_P = exp\ \{b(P^* - P_L)\}$
[c] single-shifted (viscosity only)
[d] $a_P = exp\ \{b_D\ (P_L - P_{eq})\}$; $b_D = b / n$
[e] double-shifted

Table AIV.17(a)
Raw Data, Apparent Viscosities, and Schuemmer-corrected Shear Rates for PS-R152a : w(R152a)=0.104, T=150 ^{0}C, and (L/D)=40[a]

Apparent Shear Rate $\dot{\gamma}_{wa}$ (s^{-1})	Load Cell Force (L/D=40) F (lb_f)	Exit Pressure [b] P_L (*psi*)	Wall Shear Stress [c] τ_w(dyne/cm^2)	Schuemmer-corrected Shear Rate $\dot{\gamma}_w$ (s^{-1})	Apparent Viscosity η_a (*poise*)
25	331	2801	74457	**20.75**	**2978**
35	343	2839	103800	**29.05**	**2966**
50	358	2872	146753	**41.50**	**2935**
100	396	2958	254839	**83.00**	**2548**
150	424	3020	335201	**124.50**	**2235**
250	467	3134	450751	**207.50**	**1803**
400	519	3278	588209	**332.00**	**1471**
550	561	3427	685380	**456.50**	**1246**
750	603	3576	782448	**622.50**	**1043**

[a] D=0.0496 *in.* and L=1.9990 *in.*
[b] P_{BACK}= 16.41 MPa
[c] Equaiton (6.41)

Table AIV.17(b)
Schuemmer-Pressure corrected Viscosities at P=P_L and P=P_{eq} for PS-R152a : w(R152a)=0.104, T=150 ^{0}C, and (L/D)=40[a]

Pressure Coefficient: b=2.1445E-04 psi^{-1}

Schuemmer-corrected Shear Rate $\dot{\gamma}_w$ (s^{-1})	Effective Pressure P^* (*psi*)	Pressure Correction Factor [b] a_P	Pressure-corrected Viscosity at P=P_L [c] η (*poise*)	Pressure Correction Factor [d] a_P	Schuemmer-Pressure corrected Viscosity Data at P=P_{eq} (5.73 MPa) [e]	
					Shear Rate $\dot{\gamma}_w$ (s^{-1})	Viscosity at η (*poise*)
20.75	86.80	1.0185	**2924**	1.5507	**32.18**	**1886**
29.05	120.86	1.0259	**2891**	1.6125	**46.84**	**1793**
41.50	170.57	1.0367	**2831**	1.6883	**70.06**	**1677**
83.00	294.87	1.0643	**2394**	1.9037	**158.01**	**1258**
124.50	386.56	1.0851	**2059**	2.0967	**261.04**	**982**
207.50	517.31	1.1155	**1616**	2.4945	**517.61**	**648**
332.00	671.18	1.1524	**1276**	3.1766	**1054.65**	**402**
456.50	778.86	1.1789	**1057**	4.0854	**1865.01**	**259**
622.50	885.52	1.2058	**865**	5.6885	**3541.08**	**152**

[a] D=0.0496 *in.* and L=1.9990 *in.*
[b] $a_P = exp\{b(P^* - P_L)\}$
[c] single-shifted (viscosity only)
[d] $a_P = exp\{b_D (P_L - P_{eq})\}$; $b_D = b / n$
[e] double-shifted

Table AIV.18(a)
Raw Data, Apparent Viscosities, and Schuemmer-corrected Shear Rates for PS-R152a : w(R152a)=0.05, T=175 ^{0}C, and (L/D)=40[a]

Apparent Shear Rate $\dot{\gamma}_{wa}(s^{-1})$	Load Cell Force (L/D=40) F (lb_f)	Exit Pressure [b] P_L (*psi*)	Wall Shear Stress [c] τ_w(dyne/cm^2)	Schuemmer-corrected Shear Rate $\dot{\gamma}_w$ (s^{-1})	Apparent Viscosity η_a (*poise*)
75	282	2063	173944	**62.25**	**2319**
100	295.8	2078	218100	**83.00**	**2181**
150	319.8	2099	297617	**124.50**	**1984**
250	356	2134	416503	**207.50**	**1666**
400	411	2285	558261	**332.00**	**1396**
550	448	2359	664891	**456.50**	**1209**
750	488	2418	789253	**622.50**	**1052**
1000	524	2460	905372	**830.00**	**905**

[a] D=0.0496 *in.* and L=1.9990 *in.*
[b] P_{BACK}= 11.94 MPa
[c] Equaiton (6.41)

Table AIV.18(b)
Schuemmer-Pressure corrected Viscosities at $P=P_L$ and $P=P_{eq}$ for PS-R152a : w(R152a)=0.052, T=175 ^{0}C, and (L/D)=40[a]

Pressure Coefficient: b=1.6398E-04 psi^{-1}

Schuemmer-corrected Shear Rate $\dot{\gamma}_w$ (s^{-1})	Effective Pressure P^* (*psi*)	Pressure Correction Factor [b] a_P (for Single Shift)	Pressure-corrected Viscosity at $P=P_L$ [c] η (*poise*)	Pressure Correction Factor [d] a_P (for Double Shift)	Schuemmer-Pressure corrected Viscosity Data at $P=P_{eq}$ (5.13 MPa) [e]	
					Shear Rate $\dot{\gamma}_w$ (s^{-1})	Viscosity at η (*poise*)
62.25	202.27	1.0337	**2244**	1.3142	**81.81**	**1707**
83.00	253.26	1.0424	**2092**	1.3412	**111.32**	**1560**
124.50	344.71	1.0582	**1875**	1.3868	**172.66**	**1352**
207.50	480.56	1.0820	**1540**	1.4652	**304.02**	**1051**
332.00	641.17	1.1109	**1256**	1.6247	**539.41**	**773**
456.50	760.99	1.1329	**1067**	1.7587	**802.84**	**607**
622.50	899.66	1.1590	**908**	1.9258	**1198.84**	**471**
830.00	1028.11	1.1836	**765**	2.1295	**1767.46**	**359**

[a] D=0.0496 *in.* and L=1.9990 *in.*
[b] $a_P = exp\{b(P^* - P_L)\}$
[c] single-shifted (viscosity only)
[d] $a_P = exp\{b_D (P_L - P_{eq})\}$; $b_D = b / n$
[e] double-shifted

Table AIV.19(a)
Raw Data, Apparent Viscosities, and Schuemmer-corrected Shear Rates for PS-R152a : w(R152a)=0.084, T=175 ^{0}C, and (L/D)=40[a]

Apparent Shear Rate $\dot{\gamma}_{wa}(s^{-1})$	Load Cell Force (L/D=40) F (lb_f)	Exit Pressure [b] P_L (*psi*)	Wall Shear Stress [c] τ_w(dyne/cm^2)	Schuemmer-corrected Shear Rate $\dot{\gamma}_w$ (s^{-1})	Apparent Viscosity η_a (*poise*)
100	244.3	1840	129339	**83.00**	**1293**
150	263.1	1874	183166	**124.50**	**1221**
250	291.8	1920	268313	**207.50**	**1073**
400	324.7	1976	365134	**332.00**	**913**
550	354	2049	442382	**456.50**	**804**
750	397	2179	547999	**622.50**	**731**
1000	429	2248	637088	**830.00**	**637**
1250	454	2278	716650	**1037.50**	**573**
1500	477	2285	798908	**1245.00**	**533**
1750	500	2274	889300	**1452.50**	**508**

[a] D=0.0496 *in.* and L=1.9990 *in.*
[b] P_{BACK}= 11.12 MPa
[c] Equaiton (6.41)

Table AIV.19(b)
Schuemmer-Pressure corrected Viscosities at $P=P_L$ and $P=P_{eq}$ for PS-R152a : w(R152a)=0.084, T=175 ^{0}C, and (L/D)=40[a]

Pressure Coefficient: b=1.6398E-04 psi^{-1}

Schuemmer-corrected Shear Rate $\dot{\gamma}_w$ (s^{-1})	Effective Pressure P^* (*psi*)	Pressure Correction Factor [b] a_P (for single Shift)	Pressure-corrected Viscosity at $P=P_L$ [c] η (*poise*)	Pressure Correction Factor [d] a_P (for double Shift)	Schuemmer-Pressure corrected Viscosity Data at $P=P_{eq}$ (11.14 MPa) [e]	
					Shear Rate $\dot{\gamma}_w$ (s^{-1})	Viscosity at η (*poise*)
83.00	150.62	1.0250	1262	1.0473	86.93	1205
124.50	212.93	1.0355	1179	1.0586	131.80	1114
207.50	311.07	1.0523	1020	1.0763	223.33	948
332.00	421.99	1.0716	852	1.1002	365.26	774
456.50	509.99	1.0872	740	1.1308	516.19	654
622.50	629.59	1.1088	659	1.1871	738.95	555
830.00	729.83	1.1271	565	1.2294	1020.42	460
1037.50	818.85	1.1437	501	1.2578	1304.93	399
1245.00	910.38	1.1610	459	1.2760	1588.60	360
1452.50	1010.39	1.1802	431	1.2849	1866.25	335

[a] D=0.0496 *in.* and L=1.9990 *in.*
[b] $a_P = exp\ \{b(P^* - P_L)\}$
[c] single-shifted (viscosity only)
[d] $a_P = exp\ \{b_D\ (P_L - P_{eq})\}$; $b_D = b / n$
[e] double-shifted

Table AIV.20(a)
Raw Data, Apparent Viscosities, and Schuemmer-corrected Shear Rates for PS-R152a : w(R152a)=0.104, T=175 ^{0}C, and (L/D)=40[a]

Apparent Shear Rate $\dot{\gamma}_{wa}(s^{-1})$	Load Cell Force (L/D=40) F (*lb$_f$*)	Exit Pressure [b] P_L (*psi*)	Wall Shear Stress [c] τ_w(dyne/cm^2)	Schuemmer-corrected Shear Rate $\dot{\gamma}_w$ (s^{-1})	Apparent Viscosity η_a (*poise*)
400	379	2857	190010	**332.00**	**475**
550	399	2903	242798	**456.50**	**441**
750	430	3036	300676	**622.50**	**401**
1000	450	3091	349295	**830.00**	**349**
1250	465	3101	398695	**1037.50**	**319**
1500	473	3080	434853	**1245.00**	**290**
1750	479	2987	494493	**1452.50**	**283**
2000	482	2928	528316	**1660.00**	**264**

[a] D=0.0496 *in.* and L=1.9990 *in.*
[b] P_{BACK}= 15.86 MPa
[c] Equaiton (6.41)

Table AIV.20(b)
Schuemmer-Pressure corrected Viscosities at P=P_L and P=P_{eq} for PS-R152a : w(R152a)=0.104, T=175 ^{0}C, and (L/D)=40[a]

Pressure Coefficient: b=1.6398E-04 psi^{-1}

Schuemmer-corrected Shear Rate $\dot{\gamma}_w$ (s^{-1})	Effective Pressure P^* (*psi*)	Pressure Correction Factor [b] a_P	Pressure-corrected Viscosity at P=P_L [c] η (*poise*)	Pressure Correction Factor [d] a_P	Schuemmer-Pressure corrected Viscosity Data at P=P_{eq} (22.17 MPa) [e]	
					Shear Rate $\dot{\gamma}_w$ (s^{-1})	Viscosity at η (*poise*)
332.00	220.84	1.0369	**458**	1.0895	**304.72**	**499**
456.50	281.72	1.0473	**422**	1.0828	**421.60**	**456**
622.50	348.22	1.0588	**379**	1.0500	**592.85**	**398**
830.00	403.89	1.0685	**327**	1.0368	**800.54**	**339**
1037.50	460.28	1.0784	**296**	1.0357	**1001.79**	**306**
1245.00	501.44	1.0857	**267**	1.0442	**1192.24**	**279**
1452.50	569.11	1.0978	**257**	1.0787	**1346.53**	**278**
1660.00	607.37	1.1047	**239**	1.1037	**1504.03**	**264**

[a] D=0.0496 *in.* and L=1.9990 *in.*
[b] $a_P = exp\ \{b(P^* - P_L)\}$
[c] single-shifted (viscosity only)
[d] $a_P = exp\ \{b_D\ (P_L - P_{eq})\}$; $b_D = b / n$
[e] double-shifted

AIV.3 Capillary Rheometer Data for PS-R134a

Table AIV.21(a)
Raw Data, Apparent Viscosities, and Schuemmer-corrected Shear Rates for PS-R134a : w(R134a)=0.010, T=150 ^{0}C, and (L/D)=40[a]

Apparent Shear Rate $\dot{\gamma}_{wa}$ (s^{-1})	Load Cell Force (L/D=40) F (lb_f)	Exit Pressure [b] P_L (*psi*)	Wall Shear Stress [c] τ_w(dyne/cm^2)	Schuemmer-corrected Shear Rate $\dot{\gamma}_w$ (s^{-1})	Apparent Viscosity η_a (*poise*)
4	467	2175	857762	**3.32**	**214440**
5.5	505	2182	1000073	**4.57**	**181831**
7.5	547	2189	1157762	**6.23**	**154368**
10	630	2193	1475452	**8.30**	**147545**
12.5	660	2201	1586574	**10.38**	**126926**
17.5	797	2202	2113927	**14.53**	**120796**
25	862	2211	2358695	**20.75**	**94348**
35	950	2202	2700095	**29.05**	**77146**
50	1076	2193	3216993	**41.50**	**64340**

[a] D=0.0496 *in.* and L=1.9990 *in.*
[b] P_{BACK}= 11.40 MPa
[c] Equaiton (6.41)

Table AIV.21(b)
Schuemmer-Pressure corrected Viscosities at P=P_L and P=P_{atm} for PS-R134a : w(R134a)=0.010, T=150 ^{0}C, and (L/D)=40[a]

Pressure Coefficient: b=2.1445E-04 psi^{-1}

Schuemmer-corrected Shear Rate $\dot{\gamma}_w$ (s^{-1})	Effective Pressure P^* (*psi*)	Pressure Correction Factor [b] a_P	Pressure-corrected Viscosity at P=P_L [c] η (*poise*)	Pressure Correction Factor [d] a_P	Schuemmer-Pressure corrected Viscosity Data at P=P_{atm} [e]	
					Shear Rate $\dot{\gamma}_w$ (s^{-1})	Viscosity at η (*poise*)
3.32	966.85	1.2324	**174000**	2.5211	**8.37**	**69017**
4.57	1120.29	1.2740	**142728**	2.7558	**12.58**	**51792**
6.23	1288.01	1.3210	**116857**	3.0585	**19.04**	**38207**
8.30	1618.60	1.4189	**103989**	3.4334	**28.50**	**30287**
10.38	1731.95	1.4540	**87292**	3.8335	**39.77**	**22771**
14.53	2253.89	1.6277	**74213**	4.6791	**67.96**	**15861**
20.75	2487.30	1.7119	**55113**	6.2793	**130.29**	**8777**
29.05	2803.69	1.8331	**42085**	9.1944	**267.10**	**4577**
41.50	3262.84	2.0243	**31783**	17.3212	**718.83**	**1835**

[a] D=0.0496 *in.* and L=1.9990 *in.*
[b] $a_P = exp\{b(P^* - P_L)\}$
[c] single-shifted (viscosity only)
[d] $a_P = exp(b_D P_L)$; $b_D = b / n$
[e] double-shifted

Table AIV.22(a)
Raw Data, Apparent Viscosities, and Schuemmer-corrected Shear Rates for PS-R134a : w(R134a)=0.024, T=150 ^{0}C, and (L/D)=40[a]

Apparent Shear Rate $\dot{\gamma}_{wa}(s^{-1})$	Load Cell Force (L/D=40) F (lb_f)	Exit Pressure [b] P_L (*psi*)	Wall Shear Stress [c] τ_w(dyne/cm^2)	Schuemmer-corrected Shear Rate $\dot{\gamma}_w$ (s^{-1})	Apparent Viscosity η_a (*poise*)
2.5	415	2217	640828	**2.08**	**256331**
4	463	2233	817411	**3.32**	**204353**
5.5	500	2244	954141	**4.57**	**173480**
7.5	542	2256	1109692	**6.23**	**147959**
10	581	2266	1254475	**8.30**	**125448**
12.5	615	2273	1381510	**10.38**	**110521**
17.5	669	2285	1582835	**14.53**	**90448**
20	694	2289	1676811	**16.60**	**83841**
25	752	2294	1921285	**20.75**	**76851**
35	844	2304	2246050	**29.05**	**64173**
50	960	2317	2685931	**41.50**	**53719**
74.54	1088	2318	3176530	**61.87**	**42615**
100	1253	2317	3812095	**83.00**	**38121**

[a] D=0.0496 *in.* and L=1.9990 *in.* [b] P_{BACK}= 13.76 MPa [c] Equaiton (6.41)

Table AIV.22(b)
Schuemmer-Pressure corrected Viscosities at $P=P_L$ and $P=P_{atm}$ for PS-R134a : w(R134a)=0.024, T=150 ^{0}C, and (L/D)=40[a]

Pressure Coefficient: b=2.1445E-04 psi^{-1}

Schuemmer-corrected Shear Rate $\dot{\gamma}_w$ (s^{-1})	Effective Pressure P^* (*psi*)	Pressure Correction Factor [b] a_P	Pressure-corrected Viscosity at $P=P_L$ [c] η (*poise*)	Pressure Correction Factor [d] a_P	Schuemmer-Pressure corrected Viscosity Data at $P=P_{atm}$ [e]	
					Shear Rate $\dot{\gamma}_w$ (s^{-1})	Viscosity at η (*poise*)
2.08	729.22	1.1701	**219063**	3.2751	**6.80**	**66887**
3.32	923.09	1.2200	**167497**	3.5886	**11.91**	**46675**
4.57	1071.12	1.2596	**137729**	3.8472	**17.56**	**35800**
6.23	1237.33	1.3055	**113335**	4.1490	**25.83**	**27316**
8.30	1389.92	1.3491	**92984**	4.4785	**37.17**	**20762**
10.38	1522.15	1.3881	**79619**	4.7752	**49.54**	**16673**
14.53	1728.54	1.4512	**62324**	5.3197	**77.27**	**11716**
16.60	1823.56	1.4813	**56601**	5.5711	**92.48**	**10160**
20.75	2066.83	1.5610	**49233**	6.0436	**125.40**	**8146**
29.05	2381.34	1.6704	**38418**	6.9499	**201.89**	**5528**
41.50	2791.86	1.8249	**29437**	8.2744	**343.39**	**3558**
61.87	3229.24	2.0052	**21252**	10.3101	**637.87**	**2061**
83.00	3764.92	2.2505	**16939**	12.4859	**1036.33**	**1357**

[a] D=0.0496 *in.* and L=1.9990 *in.* [b] $a_P = exp\{b(P^* - P_L)\}$
[c] single-shifted (viscosity only) [d] $a_P = exp(b_D P_L)$; $b_D = b / n$
[e] double-shifted

Table AIV.23(a)
Raw Data, Apparent Viscosities, and Schuemmer-corrected Shear Rates for PS-R134a : w(R134a)=0.026, T=150 ^{0}C, and (L/D)=40[a]

Apparent Shear Rate $\dot{\gamma}_{wa}(s^{-1})$	Load Cell Force (L/D=40) F (lb_f)	Exit Pressure [b] P_L (*psi*)	Wall Shear Stress [c] τ_w(dyne/cm^2)	Schuemmer-corrected Shear Rate $\dot{\gamma}_w$ (s^{-1})	Apparent Viscosity η_a (*poise*)
2.5	373	2276	452780	**2.08**	**181112**
4	422	2292	633235	**3.32**	**158309**
5.5	455	2303	754479	**4.57**	**137178**
7.5	492	2315	890673	**6.23**	**118756**
10	528	2327	1022987	**8.30**	**102299**
12.5	556	2336	1125938	**10.38**	**90075**
17.5	604	2350	1303179	**14.53**	**74467**
20	625	2356	1381028	**16.60**	**69051**
25	664	2363	1550877	**20.75**	**62035**
35	751	2372	1856713	**29.05**	**53049**
50	844	2394	2203704	**41.50**	**44074**
100	1100	2423	3174226	**83.00**	**31742**
150	1300	2411	3948114	**124.5**	**26321**

[a] D=0.0496 *in.* and L=1.9990 *in.* [b] P_{BACK}= 13.50 MPa [c] Equaiton (6.41)

Table AIV.23(b)
Schuemmer-Pressure corrected Viscosities at $P=P_L$ and $P=P_{atm}$ for PS-R134a : w(R134a)=0.026, T=150 ^{0}C, and (L/D)=40[a]

Pressure Coefficient: b=2.1445E-04 psi^{-1}

Schuemmer-corrected Shear Rate $\dot{\gamma}_w$ (s^{-1})	Effective Pressure P^* (*psi*)	Pressure Correction Factor [b] a_P	Pressure-corrected Viscosity at $P=P_L$ [c] η (*poise*)	Pressure Correction Factor [d] a_P	Schuemmer-Pressure corrected Viscosity Data at $P=P_{atm}$ [e]	
					Shear Rate $\dot{\gamma}_w$ (s^{-1})	Viscosity at η (*poise*)
2.08	519.41	1.1183	**161948**	3.0966	**6.43**	**52298**
3.32	720.82	1.1679	**135549**	3.3492	**11.12**	**40472**
4.57	854.36	1.2020	**114127**	3.5527	**16.22**	**32125**
6.23	1002.66	1.2410	**95696**	3.7850	**23.56**	**25283**
8.30	1145.01	1.2796	**79946**	4.0374	**33.51**	**19801**
10.38	1254.59	1.3102	**68752**	4.2608	**44.21**	**16136**
14.53	1440.85	1.3638	**54604**	4.6569	**67.64**	**11725**
16.60	1521.71	1.3877	**49759**	4.8374	**80.30**	**10286**
20.75	1696.11	1.4408	**43055**	5.1689	**107.25**	**8330**
29.05	2003.22	1.5393	**34463**	5.7616	**167.37**	**5981**
41.50	2341.02	1.6555	**26624**	6.6318	**275.22**	**4015**
83.00	3227.51	2.0036	**15842**	9.1914	**762.88**	**1724**
124.5	3875.59	2.3037	**11426**	11.3911	**1418.19**	**1003**

[a] D=0.0496 *in.* and L=1.9990 *in.* [b] $a_P = exp\{b(P^* - P_L)\}$
[c] single-shifted (viscosity only) [d] $a_P = exp(b_D P_L)$; $b_D = b / n$
[e] double-shifted

Table AIV.24(a)
Raw Data, Apparent Viscosities, and Schuemmer-corrected Shear Rates for PS-R134a : w(R134a)=0.040, T=150 ^{0}C, and (L/D)=40[a]

Apparent Shear Rate $\dot{\gamma}_{wa}$ (s^{-1})	Load Cell Force (L/D=40) F (lb_f)	Exit Pressure [b] P_L (*psi*)	Wall Shear Stress [c] τ_w(dyne/cm^2)	Schuemmer-corrected Shear Rate $\dot{\gamma}_w$ (s^{-1})	Apparent Viscosity η_a (*poise*)
2.5	405	2866	324494	**2.08**	**129798**
4	443	2876	464929	**3.32**	**116232**
5.5	478	2888	593488	**4.57**	**107907**
7.5	512	2897	719351	**6.23**	**95914**
10	551	2909	863279	**8.30**	**86328**
12.5	587	2918	997202	**10.38**	**79776**
17.5	644	2937	1207148	**14.53**	**68980**
20	635	2796	1231496	**16.60**	**61575**
25	653	2744	1345486	**20.75**	**53819**
35	740	2874	1599585	**29.05**	**45702**
50	842	2998	1937805	**41.50**	**38756**
100	1060	3044	2753946	**83.00**	**27539**
150	1183	3052	3221185	**124.5**	**21475**

[a] D=0.0496 *in.* and L=1.9990 *in.* [b] P_{BACK}= 14.83 MPa [c] Equaiton (6.41)

Table AIV.24(b)
Schuemmer-Pressure corrected Viscosities at P=P_L and P=P_{atm} for PS-R134a : w(R134a)=0.040, T=150 ^{0}C, and (L/D)=40[a]

Pressure Coefficient: b=2.1445E-04 psi^{-1}

Schuemmer-corrected Shear Rate $\dot{\gamma}_w$ (s^{-1})	Effective Pressure P^* (*psi*)	Pressure Correction Factor [b] a_P	Pressure-corrected Viscosity at P=P_L [c] η (*poise*)	Pressure Correction Factor [d] a_P	Schuemmer-Pressure corrected Viscosity Data at P=P_{atm} [e]	
					Shear Rate $\dot{\gamma}_w$ (s^{-1})	Viscosity at η (*poise*)
2.08	374.30	1.0836	**119779**	3.7444	**7.77**	**31989**
3.32	533.11	1.1212	**103667**	4.1104	**13.65**	**25221**
4.57	676.79	1.1563	**93319**	4.4230	**20.19**	**21099**
6.23	815.90	1.1914	**80507**	4.7768	**29.74**	**16854**
8.30	973.10	1.2322	**70058**	5.1769	**42.97**	**13533**
10.38	1117.56	1.2710	**62764**	5.5391	**57.47**	**11331**
14.53	1340.54	1.3333	**51734**	6.2182	**90.32**	**8320**
16.60	1366.13	1.3407	**45928**	5.9456	**98.70**	**7725**
20.75	1485.16	1.3754	**39131**	6.2009	**128.67**	**6310**
29.05	1746.02	1.4546	**31420**	7.7182	**224.21**	**4071**
41.50	2083.77	1.5639	**24781**	9.9819	**414.25**	**2483**
83.00	2855.16	1.8455	**14923**	15.8252	**1313.49**	**943**
124.5	3269.87	2.0173	**10645**	22.1776	**2761.11**	**480**

[a] D=0.0496 *in.* and L=1.9990 *in.* [b] $a_P = exp\ \{b(P^* - P_L)\}$
[c] single-shifted (viscosity only) [d] $a_P = exp\ (b_D P_L)$; $b_D = b / n$
[e] double-shifted

Table AIV.25(a)
Raw Data, Apparent Viscosities, and Schuemmer-corrected Shear Rates for PS-R134a : w(R134a)=0.043, T=150 ^{0}C, and (L/D)=40[a]

Apparent Shear Rate $\dot{\gamma}_{wa}(s^{-1})$	Load Cell Force (L/D=40) F (lb_f)	Exit Pressure [b] P_L (*psi*)	Wall Shear Stress [c] τ_w(dyne/cm^2)	Schuemmer-corrected Shear Rate $\dot{\gamma}_w$ (s^{-1})	Apparent Viscosity η_a (*poise*)
2.5	398	2982	247718	**2.08**	**99087**
4	436	2998	385587	**3.32**	**96397**
5.5	466	3007	496072	**4.57**	**90195**
7.5	502	3026	625402	**6.23**	**83387**
10	549	3043	798163	**8.30**	**79816**
12.5	594	3058	964362	**10.38**	**77149**
17.5	626	3076	1077951	**14.53**	**61597**
25	649	3094	1156273	**20.75**	**46251**
35	703	3116	1379052	**29.05**	**39401**
50	750	3134	1523408	**41.50**	**30468**
100	915	3194	2128379	**83.00**	**21284**
150	1045	3219	2615450	**124.5**	**17436**

[a] D=0.0496 *in.* and L=1.9990 *in.* [b] P_{BACK}= 18.85 MPa [c] Equaiton (6.41)

Table AIV.25(b)
Schuemmer-Pressure corrected Viscosities at P=P_L and P=P_{atm} for PS-R134a : w(R134a)=0.043, T=150 ^{0}C, and (L/D)=40[a]

Pressure Coefficient: b=2.1445E-04 psi^{-1}

Schuemmer-corrected Shear Rate $\dot{\gamma}_w$ (s^{-1})	Effective Pressure P^* (*psi*)	Pressure Correction Factor [b] a_P	Pressure-corrected Viscosity at P=P_L [c] η (*poise*)	Pressure Correction Factor [d] a_P	Schuemmer-Pressure corrected Viscosity Data at P=P_{atm} [e]	
					Shear Rate $\dot{\gamma}_w$ (s^{-1})	Viscosity at η (*poise*)
2.08	286.67	1.0634	**93179**	7.0565	**14.64**	**13205**
3.32	443.63	1.0998	**87648**	7.6612	**25.44**	**11441**
4.57	568.07	1.1296	**79850**	8.1181	**37.06**	**9836**
6.23	712.22	1.1650	**71575**	8.6773	**54.02**	**8249**
8.30	902.25	1.2135	**65775**	9.2547	**76.81**	**7107**
10.38	1082.33	1.2613	**61168**	9.7634	**101.29**	**6265**
14.53	1203.87	1.2946	**47581**	10.5880	**153.79**	**4494**
20.75	1286.95	1.3178	**35096**	11.5910	**240.51**	**3028**
29.05	1520.04	1.3854	**28441**	12.7461	**370.28**	**2231**
41.50	1668.54	1.4302	**21303**	14.1284	**586.33**	**1508**
83.00	2269.52	1.6269	**13082**	18.0418	**1497.47**	**725**
124.5	2728.76	1.7953	**9712**	20.9716	**2610.96**	**463**

[a] D=0.0496 *in.* and L=1.9990 *in.* [b] $a_P = exp\ \{b(P^* - P_L)\}$
[c] single-shifted (viscosity only) [d] $a_P = exp\ (b_D P_L)$; $b_D = b / n$
[e] double-shifted

Table AIV.26(a)
Raw Data, Apparent Viscosities, and Schuemmer-corrected Shear Rates for PS-R134a : w(R134a)=0.020, T=175 ^{0}C, and (L/D)=40[a]

Apparent Shear Rate $\dot{\gamma}_{wa}(s^{-1})$	Load Cell Force (L/D=40) F (*lbf*)	Exit Pressure [b] P_L (*psi*)	Wall Shear Stress [c] τ_w(dyne/cm^2)	Schuemmer-corrected Shear Rate $\dot{\gamma}_w$ (s^{-1})	Apparent Viscosity η_a (*poise*)
25	345.2	2270	339374	**20.75**	**13575**
35	370	2278	429460	**29.05**	**12270**
50	399	2288	534541	**41.50**	**10691**
75	437	2300	672855	**62.25**	**8971**
100	470	2307	794762	**83.00**	**7948**
150	519	2323	973202	**124.50**	**6488**
250	609	2343	1306782	**207.50**	**5227**
400	696	2360	1629721	**332.00**	**4074**
550	755	2370	1848887	**456.50**	**3362**
750	829	2422	2107869	**622.50**	**2810**

[a] D=0.0496 *in.* and L=1.9990 *in.*
[b] P_{BACK}= 12.36 MPa
[c] Equaiton (6.41)

Table AIV.26(b)
Schuemmer-Pressure corrected Viscosities at P=P_L and P=P_{atm} for PS-R134a : w(R134a)=0.020, T=175 ^{0}C, and (L/D)=40[a]

Pressure Coefficient: b=1.6398E-04 psi^{-1}

Schuemmer-corrected Shear Rate $\dot{\gamma}_w$ (s^{-1})	Effective Pressure P^* (*psi*)	Pressure Correction Factor [b] a_P	Pressure-corrected Viscosity at P=P_L [c] η (*poise*)	Pressure Correction Factor [d] a_P	Schuemmer-Pressure corrected Viscosity Data at P=P_{atm} [e]	
					Shear Rate $\dot{\gamma}_w$ (s^{-1})	Viscosity at η (*poise*)
20.75	392.41	1.0687	**12702**	1.8497	**38.38**	**6867**
29.05	495.08	1.0875	**11283**	1.9259	**55.95**	**5859**
41.50	614.05	1.1096	**9635**	2.0229	**83.95**	**4763**
62.25	769.35	1.1392	**7875**	2.1591	**134.40**	**3647**
83.00	905.00	1.1657	**6818**	2.2766	**188.96**	**2995**
124.50	1101.51	1.2051	**5384**	2.4913	**310.16**	**2161**
207.50	1462.33	1.2811	**4080**	2.8756	**596.68**	**1419**
332.00	1803.56	1.3573	**3002**	3.4236	**1136.65**	**877**
456.50	2030.64	1.4106	**2383**	3.9860	**1819.62**	**598**
622.50	2294.33	1.4750	**1905**	4.9437	**3077.43**	**385**

[a] D=0.0496 *in.* and L=1.9990 *in.*
[b] $a_P = exp\ \{b(P^* - P_L)\}$
[c] single-shifted (viscosity only)
[d] $a_P = exp\ (b_D P_L)$; $b_D = b / n$
[e] double-shifted

Table AIV.27(a)

Raw Data, Apparent Viscosities, and Schuemmer-corrected Shear Rates for PS-R134a : w(R134a)=0.028, T=175 ^{0}C, and (L/D)=40[a]

Apparent Shear Rate $\dot{\gamma}_{wa}(s^{-1})$	Load Cell Force (L/D=40) F (lb_f)	Exit Pressure [b] P_L (*psi*)	Wall Shear Stress [c] τ_w(dyne/cm^2)	Schuemmer-corrected Shear Rate $\dot{\gamma}_w$ (s^{-1})	Apparent Viscosity η_a (*poise*)
15	306.8	2281	189450	**12.45**	**12630**
25	329.7	2301	266158	**20.75**	**10646**
35	347.4	2313	327046	**29.05**	**9344**
50	368	2331	396187	**41.50**	**7924**
75	397	2349	497093	**62.25**	**6628**
100	422	2364	584609	**83.00**	**5846**
150	461	2387	721342	**124.50**	**4809**
250	516	2420	913865	**207.50**	**3655**
400	571	2456	1104795	**332.00**	**2762**

[a] D=0.0496 *in.* and L=1.9990 *in.*

[b] P_{BACK}= 13.62 MPa

[c] Equaiton (6.41)

Table AIV.27(b)

Schuemmer-Pressure corrected Viscosities at $P=P_L$ and $P=P_{atm}$ for PS-R134a : w(R134a)=0.028, T=175 ^{0}C, and (L/D)=40[a]

Pressure Coefficient: b=1.6398E-04 psi^{-1}

Schuemmer-corrected Shear Rate $\dot{\gamma}_w$ (s^{-1})	Effective Pressure P^* (*psi*)	Pressure Correction Factor [b] a_P	Pressure-corrected Viscosity at $P=P_L$ [c] η (*poise*)	Pressure Correction Factor [d] a_P	Schuemmer-Pressure corrected Viscosity Data at $P=P_{atm}$ [e]	
					Shear Rate $\dot{\gamma}_w$ (s^{-1})	Viscosity at η (*poise*)
12.45	220.15	1.0380	**12168**	1.8228	**22.69**	**6675**
20.75	308.50	1.0536	**10104**	1.9271	**39.99**	**5243**
29.05	378.31	1.0662	**8764**	2.0090	**58.36**	**4362**
41.50	457.23	1.0805	**7333**	2.1150	**87.77**	**3467**
62.25	571.75	1.1017	**6016**	2.2603	**140.70**	**2662**
83.00	670.43	1.1203	**5218**	2.3876	**198.17**	**2186**
124.50	823.44	1.1497	**4183**	2.6133	**325.36**	**1601**
207.50	1036.44	1.1919	**3067**	3.0144	**625.48**	**1017**
332.00	1244.86	1.2348	**2237**	3.5818	**1189.16**	**625**

[a] D=0.0496 *in.* and L=1.9990 *in.*

[b] $a_P = exp\ \{b(P^* - P_L)\}$

[c] single-shifted (viscosity only)

[d] $a_P = exp\ (b_D P_L)$; $b_D = b / n$

[e] double-shifted

APPENDIX V
COMPOSITION-DEPENDENT SHIFT FACTORS

Table AV.1(a)
Composition-dependent Shift Factors: PS-CO_2 at T=150 ^{0}C

w(CO_2)	b_{avg} =2.1445 10^{-4}	b_{low} =1.5776 10^{-4}	b_{high} =2.7114 10^{-4}	Average of a_C
0.010	0.1286	0.1711	0.0867	0.1288
0.020	0.0840	0.0883	0.0627	0.0783
0.030	0.0335	0.0381	0.0252	0.0323
0.035	0.0212	0.0246	0.0183	0.0213
0.045	0.0133	0.0144	0.0095	0.0124
0.050	0.0078	0.0091	0.0073	0.0081
0.052	0.0046	0.0051	0.0040	0.0046

Table AV.1(b)
Composition-dependent Shift Factors: PS-CO_2 at T=175 ^{0}C

w(CO_2)	b_{avg} =1.6398 10^{-4}	b_{low} =0.6679 10^{-4}	b_{high} =2.6117 10^{-4}	Average of a_C
0.010	0.2033	0.2634	0.1586	0.2084
0.020	0.1566	0.1974	0.1249	0.1596
0.030	0.1010	0.1230	0.0835	0.1025
0.035	0.0628	0.0742	0.0534	0.0635
0.045	0.0483	0.0562	0.0417	0.0487
0.051	0.0299	0.0384	0.0237	0.0307

Table AV.2(a)
Composition-dependent Shift Factors: PS-R152a at T=150 ^{0}C

w(CO_2)	b_{avg} =2.1445 10^{-4}	b_{low} =1.5776 10^{-4}	b_{high} =2.7114 10^{-4}	Average of a_C
0.056	0.0052	0.0065	0.0042	0.0053
0.070	0.0023	0.0028	0.0017	0.0023
0.083	0.0012	0.0014	0.0010	0.0012
0.103	0.0008	0.0009	0.0007	0.0008

Table AV.2(b)
Composition-dependent Shift Factors: PS-R152a at T=175 ^{0}C

$w(CO_2)$	b_{avg} =1.6398 10^{-4}	b_{low} =0.6679 10^{-4}	b_{high} =2.6117 10^{-4}	Average of a_C
0.050	0.0227	0.0289	0.0179	0.0232
0.084	0.0150	0.0187	0.0120	0.0152
0.104	0.0052	0.0053	0.0052	0.0052

Table AV.3(a)
Composition-dependent Shift Factors: PS-R134a at T=150 ^{0}C

$w(CO_2)$	b_{avg} =2.1445 10^{-4}	b_{low} =1.5776 10^{-4}	b_{high} =2.7114 10^{-4}	Average of a_C
0.010	0.1905	0.3398	0.1136	0.2146
0.024	0.1226	0.2145	0.0781	0.1384
0.026	0.0708	0.1267	0.0557	0.0844
0.040	0.0335	0.0721	0.0331	0.0462
0.043	0.0129	0.0256	0.0065	0.0150

Table AV.3(b)
Composition-dependent Shift Factors: PS-R134a at T=175 ^{0}C

$w(CO_2)$	b_{avg} =1.6398 10^{-4}	b_{low} =0.6679 10^{-4}	b_{high} =2.6117 10^{-4}	Average of a_C
0.020	0.1331	0.2392	0.0848	0.1524
0.028	0.0918	0.1443	0.0615	0.0992

Table AV.4
Composition-dependent Shift Factors: PS-low M_w PS at T=200 ^{0}C

w(low M_w PS)	a_C
0.05	0.9891
0.10	0.8115
0.20	0.4607
0.30	0.3077
0.40	0.1757

REFERENCES

Andrade, E.N. da Costa, *Nature*, **125**, 309, 582 (1930).

Bae, Y.C. and Gulari, Es., *J. Appl. Polym. Sci.*, **63**, 459 (1997).

Bae, Y.C., "Viscosity Reduction of Polymeric Liquids by Dissolved Gases," Ph.D. Dissertation, Wayne State University, Detroit, MI (1989).

Bae, Y.C., *Polymer*, **37**, 3011 (1996).

Bagley, E.B., *J. Appl. Phys.*, **28**, 624 (1~57).

Bagley, E.B., *Trans. Sec. Rheol.*, **5**, 355 (1961).

Ballman, R.L., *Nature*, **202**, 289 (1964).

Barnes, H.A., Hutton, J.F., and Walters, K., The Introduction to Rheology, Elsevier Scientific, New York (1989), Chapter 2.

Berens, A.R. and Huvard, G.S., Supercritical Fluid Science and Technology, ACS Symp. Ser. 406, Johnston, K.P. and Penninger, J.M.L. Eds., Amer. Chem. Soc., Washington, DC (1989), Chapter 14.

Biltz, W., Rauchemie Der Festen Stoffe, J.W. Edwards, Pub., Ann Arbor (1944), from Leopold Voss, Leipzig (1934).

Binding, D.M., *J. Non-Newtonian Fluid Mech.*, **27**, 173 (1988).

Bird, R.B., Armstrong, R.C., and Hasager, O., Dynamics of Polymeric Liquids, Vol. 1: Fluid Mechanics, 2nd ed., John Wiley and Sons, New York (1987), Chap. 3,10.

Blyler, L.L., and Kwei, T.K., *J. Polym. Sci.*, Part C., **35**, 165 (1979).

Bondi, A., *J. Phys. Chem.*, **68**, 411(1964)B.

Bondi, A., *J. Polym. Sci.*, **A2**, 3159(1964)A.

Bondi, A., Physical Properties of Molecular Crystals, Liquids and Glasses, Wiely, New York (1968). Chap. 3 and 4.

Boyer, R. F., *Rubber Chem. Technol.*, **36**, 1322(1962).

Briscoe, B.J. and Kelly, C.T., *Material Sci. & Eng.*, **A168**, 111 (1993).

Brydson, J.A., Flow Properties of Polymer Melts, 2nd Ed., George Goldwin Limited associated with Plastic and Rubber Institute, London (1981), Chap. 4 and 5.

Bueche, F., *J. Appl. Phys.*, **26**, 738 (1955).

Bueche, F., *J. Chem. Phys.*, **20**,1959 (1952).

Bueche, F., *J. Chem. Phys.*, **21**, 1850 (1953).

Bueche, F., *J. Chem. Phys.*, **25**, 599 (1956).

Bueche, F., Physical Properties of Polymers, Wiley, New York, 1962. p.117.

Carreau, P.J., *Trans. Soc. Rheol.*, **16**, 99 (1972).

Chiou, J.S., Barlow, J.W., and Paul, D.R., *J. Appl. Polym. Sci.*, **30**, 2633 (1985).

Chmiel, H., and Schuemmer, P., *Chemie-Ing.-Techn.*, **43**, 1257 (1971).

Chow, T.S., *Macromolecules*, **13**, 362 (1980).

Christmann, L. and Knappe, W., *Colloid Polym. Sci.*, **252**, 705 (1974).

Christmann, L. and Weber, G., *Rheol. Acta*, **17**, 16 (1978).

Clark, M.R. and DeSimone, J.M., *Macromolecules*, **28**, 3002 (1995).

Cogswell, F.N. and McGowan, J.C., *Br. Polym. J.*, **4**, 183 (1972).

Cogswell, F.N., Polymer Melt Rheology: A Guide for Industrial Practice, Plastics and Rubber Institute, John Wiley & Sons, New York (1981), Chapter 3.

Cogswell, F.N., *Polym. Eng. Sci.*, **12**, 64 (1972) A.

Cogswell, F.N., *Trans. Soc. Rheol.*, **16**, 383 (1972) B.

Cohen, M.H., and Turnbull, D., *J. Chem. Phys.*, **31**, 1164 (1959).

Condo, P.D., Sanchez, I.C., Panayiotou, C.G., and Johnston, K.P., *Macromolecules*, **25**, 6119 (1992).

Cox, W.P. and Merz, E.H., *J. Polym. Sci.*, **28**, 619 (1958).

Cross, M.M., *J. Colloid Sci.*, **20**, 417 (1965).

Daneshvar, M., "High Pressure Phase Equilibria of Highly Asymmetric Polymer – Supercritical Fluid Systems," Ph.D. Dissertation, Wayne State University, Detroit, Michigan (1989).

Daneshvar, M., Kim, S., and Gulari, E., *J. Phys. Chem.*, **94**, 2124 (1990).

Darby, R., Viscoelastic Fluids: An Introduction to Their Properties and Behavior, Marcell Dekker, New York (1976), Chapter 2.

Davies, A.R., Farah I.M., Rides, M., and Thomas, K., *Makromol. Chem. Macromol. Symp.*, **68**, 25 (1993).

Dealy, J.M., Rheometers for Molten Plastics, Van Nostrand Rheinhold, New York (1982).

Desimone, J.M., Guan, Z., Elsbernd, C.S., *Science*, **257**, 945 (1992).

Doolittle, A.K., *J. Appl. Phys.*, **37**, 1003 (1951).

Durill, P.L. and Griskey, R.G., *AIChE J.*, **12**, 1147 (1966).

Ferry, J.D., Viscoelastic Properties of Polymers, 3rd ed., John Wiley and Sons, New York(1980), Chap. 17.

Fleming, G.K. and Koros, W.J., *Macromolecules*, **19**, 2285 (1986).

Foster, R.W. and Lindt, J.T., *Polym. Eng. Sci.*, **27**, 1292 (1987).

Fox, T.G., and Flory, P.J., *J. Phys. Chem.*, **70**, 2384 (1948).

Fridman, M.L., Sabsai, O.Yu., Nikolaeva, N.E., and Barshten, G.R., *J. Cellular Plast.*, **25**, 574 (1989).

Fujita, H., and Maekawa, E., *J. Phys. Chem.*, **66**, 1053 (1962).

Garg, A., "Thermodynamics of Polymer Melts Swollen with Supercritical Gases, Ph.D. Dissertation, Wayne State University, Detroit (1993).

Garg, A., Gulari, E., and Manke, C.W., *Macromolecules*, **27**, 5643 (1994).

Gee. G., *Polymer*, **7**, 177 (1966).

Gerhardt, L.J., "A Rheological Investigation of Polydimethylsiloxane Swollen with Supercritical Carbon Dioxide," Ph.D. Dissertation, Wayne State University, Detroit, Michigan (1994).

Gerhardt, L.J., Manke, C.W., Gulair, E., *J. Polym. Sci., Polym. Phys. Ed.*, **35**, 523 (1997).

Gibbs, J.H. and DiMarzio, E.A., *J. Chem. Phys.*, **28**, 373 (1958).

Glasstone, S., Laidler, K.J., and Eyring, H., Theory of Rate Processes, McGraw Hill, New York (1941), Chapter 9.

Goel, S.K. and Beckman, J., *Polymer*, **34**, 1410 (1993).

Goldhammer, D.A., *J. Physik. Chem.*, **20**, 577 (1910).

Graessley, W.W., *Adv. Polym. Sci.*, **16**, 1 (1974).

Graessley, W.W., *J. Chem. Phys.*, **43**, 2696 (1965).

Graessley, W.W., *J. Chem. Phys.*, **47**, 1942 (1967).

Guan, Z., Combes, J.R., Menceloglu, Y.Z., and DeSimone, J.M., *Macromolecules*, **26**, 2663 (1993).

Hachisuka, H., Sato, T., Imai, T., Tsujita, Y., Takizawa, A., and Kinoshita, T., *Polym. J.*, **22**, 77 (1990).

Han, C.D., and Ma, C.-Y., *J. Appl. Polym. Sci.*, **28**, 551 (1983)A.

Han, C.D., and Ma, C.-Y., *J. Appl. Polym. Sci.*, **28**, 831 (1983)B.

Han, C.D., *Trans. Soc. Rheol.*, **18**, 163 (1974).

Handa, Y.P., Capowski, S., and O'Neill, M.L., *Thermochimica Acta*, **226**, 177 (1993).

Handa, Y.P., Lampron, S., and O'Neill, M.L., *J. Polym. Sci., Polym. Phys. Ed.*, **32**, 2549 (1994).

Hatzikiriakos, S.G., and Dealy, J.M., *J. Rheol.*, **36**, 703 (1992).

Haward, R.N., Breuer, H., and Rehage, G., *J. Polym. Sci., Polym. Let.*, **4**, 375 (1966).

Haward, R.N., *J. Macromal Sci.-Revs. Macromol Chem.*, **C4**, 191(1970).

Helwege, K., Knappe, W., Paul, P., and Semjonow, *Rheol. Acta*, **6**, 165 (1967).

Herrmann, H.-D. and Knappe, W., *Rheol. Acta*, **8**, 384 (1969).

Heuse, R., *Z. Physik. Chem. (A)*, **147**, 273 (1930).

Hirose, T., Mizoguchi, K., and Kamiya, Y., *J. Polym. Sci., Polym. Phys. Ed.*, **24**, 2107 (1986).

Hunter, E., and Richards, R.B., U.S. Patent 2,457,238 (1945).

Jaarmo, S., Rantakyla, M., and Aaltonen, O., Proc. 4th Intl. Symp. Supercritical Fluids, Sendai, Japan, May 11-14, Vol. A., 263 (1997).

Johnson, M.F., Evans, W.W., Jordan, I., and Ferry, J.D., *J. Colloid Sci.*, **7**, 498 (1952).

Kadijk, S.E. and van Den Brule, B.H.A.A., *Polym. Eng. Sci.*, **34**, 1535 (1994).

Kaelble, D.H., Rheology, Vol.5, ed. Eirich, F.R., Academic Press, New York, (1970), Chapter 5.

Kamal, M.R., and Nyun, H., *Rheol. Acta*, **12**, 263 (1973).

Karl, V.-H., *Angew. Makromol. Chem.*, **79**, 11 (1979).

Kazatchkov, I.B., Hatzikiriakos, S.G., and Stewart, C.W., *Polym. Eng. Sci.*, **35**, 1863 (1995).

Kelley, F.N., and Bueche, F., *J. Polym. Sci.*, **50**, 549 (1961).

Kendall, J. and DeSimone, J.M., Proc. 4th Intl. Symp. Supercritical Fluids, Sendai, Japan, May 11-14, Vol. C., 771 (1997).

Khan, V., private communication (1997).

Kim, S., "High Pressure Phase Equilibrium Measurements and Thermodynamic Modeling of PDMS-C02 Systems," Ph.D. Dissertation, Wayne State University, Detroit (1992).

Kumar, S.K., Chabria, S.P., Reid, R.C., and Suter, U.W., *Macromolecules*, **20**, 2550 (1987).

Kwag, C. and Vlachopoulos, J., *Polym. Eng. Sci.*, **31**, 1015 (1991).

Kwag, C., Gerhardt, L.J., Khan, V., Gulari, E., Manke, C.W., *Polym. Mater. Sci. Eng.*, **74**, 183 (1996).

Laun, H.M. and Hirsch, G., *Rheol. Acta*, **28**, 267 (1989).

Laun, H.M. and Schuch, H., *J. Rheol.*, **33**, 119 (1989).

Laun, H.M., *Rheol. Acta*, **22**, 171 (1983).

Lomellini, P., *Polymer*, **33**, 4983 (1992).

Lord, H.A., *Polym. Eng. Sci.*, **19**, 469 (1979).

Magill, J.H. and Greet, R.J., *Ind. & Eng. Chem.*, **8**, 701 (1969).

Matthews, A.P., *J. Phys. Chem.*, **20**, 554 (1916).

McHugh, M.A., and Krukonis, V.J., Supercritical Fluids Extraction: Principles and Practice," Butterworths, Boston (1986).

Meister, B.J., Encyclopedia of Polymer Science and Engineering, 2nd ed., eds by Mark, H.F., Bikales, N.M., Overberger, C.G., Menges, G., and Kroschwitz, J.E., Vol.16 - Styrene Polymers, p125-128, John Wiley and Sons, New York (1992).

Mendelson, R.A., *J. Rheol.*, **23**, 545 (1979).

Mendelson, R.A., *J. Rheol.*, **24**, 765 (1980).

Miller, A.A., *Macromolecules*, **4**, 757 (1971).

Mishima, K., Matsuyama, K., Uchiyama, H., and Ide, M., Proc. 4th Intl. Symp. Supercritical Fluids, Sendai, Japan, May 11-14, Vol. A., 267 (1997).

Newitt, D.M. and Weale, K.E., *J. Chem. Soc.*, 1541 (1948).

Nishimura, N., *J. Polym. Sci., Part A*, **3**, 237 (1965).

Onogi, S., Kimura, S., Kato, T., Matsuda, T., and Miyanaga, N., *J. Polym. Sci.*, **C15**, 381 (1966).

Oyanagi, Y., and White, J.L., J *J. Appl. Polym. Sci.*, **23**, 1013 (1979).

Panayiotou, C., and Vera, J.H., *Polymer J.*, **14**, 681 (1982).

Penwell, R.C., Porter, R.S., and Middleman, S., *J. Polym. Sci.*, A-2, **9**, 731 (1971).

Penwell, R.C., and Porter, R.S., *J. Polym. Sci., A-2*, **9**, 463 (1971).

Rabinowitsch, B., *Z. Phys. Chem.*, **145**,1 (1929).

Reid, C.P., Prausnitz, J.M., and Sherwood, T.K., The Properties of Gases and Liquids, 3rd ed., McGraw-Hill, New York (1977), Chap. 12.

Reiner, M., Deformation, Strain. and Flow, Wiley-Interscience, New York (1960), p. 246.

Riande, E., Markovitz, H., Plazek, D.J., and Raghupathi, N., *J. Polym. Sci.*, **50**, 405 (1975).

Rodriguez, F., Principle of Polymer Science, 2nd ed., McGraw-Hill, New York (1982), Chap. 3.

Sanchez, I.C., and Lacombe, R.H., *J. Phys. Chem.*, **80**, 2352 (1976).

Sanchez, I.C., and Lacombe, R.H., *Macromolecules*, **11**, 1145 (1978).

Saraf, V.P., and Kiran, E., *J. Supercritical Fluids*, **1**, 37 (1988).

Sato, Y., Yurugi, M., Fujiwara, K., Takishima, S., and Masuoka, H., *Fluid Phase Equil.*, **125**, 129 (1996).

Schouten, J.A., Scholten, J., Nelissen, L., and Nies, E., *Polym. Comm.*, **32**, 421 (1991).

Schuemmer, P., and Worthoff, R.H., *Chem. Eng. Sci.*, **33**, 759 (1978).

Sefcik, M.D., *J. Polym. Sci., Polym. Phys. Ed.*, **24**, 957 (1986).

Semjonow, von V., *Rheol. Acta*, **2**, 138 (1962).

Shah, V.M., Hardy, B.J., and Stern, S.A., *J. Polym. Sci., Polym. Phys. Ed.*, **24**, 2033 (1986).

Shah, V.M., Hardy, B.J., and Stern, S.A., *J. Polym. Sci., Polym. Phys. Ed.*, **31**, 313 (1993).

Shieh, Y.-T., Su, J.-H., Manivannan, G., Lee P.H.C., Sawan, S.P., and Spall, W.D., *J. Appl. Polym. Sci.*, **59**, 695 (1996) A.

Shieh, Y.-T., Su, J.-H., Manivannan, G., Lee P.H.C., Sawan, S.P., and Spall, W.D., *J. Appl. Polym. Sci.*, **59**, 707 (1996) B.

Simha, A.Q., and Simha, R., *J. Appl. Phys.*, **42**, 4592 (1971).

Shroff, R.N., Cancio, L.V., and Shida, M., *Trans. Soc. Rheol.*, **21**, 429 (1977).

Shuler, S.F., Binding, D.M., and Pipes, R.B., *Polym. Composites*, **15**, 427 (1994).

Sisko, A.W., *Ind. & Eng. Chem.*, **50**, 1789 (1958).

Smith, P.B. and Moll, D.J., *Macromolecules*, **23**, 3250 (1990).

Spencer, R.S., and Williams, J.L., *J. Colloid Sci.*, **2**, 1 17 (1947).

Stratton, R.A., *J. Colloid Interface Sci.*, **22**, 517 (1966)

Sugden, S., *J. Chem. Soc.*, 1780 and 1786 (1927).

Suh, K.W., private communication (1997).

Tremblay, B., *J. Non-Newtonian Fluid Mech.*, **33**, 137 (1989).

Tremblay, B., *Polym. Eng. Sci.*, **32**, 65 (1992).

Utracki, L.A., *Polym. Eng. Sci.*, **25**, 655 (1985).

Van Krevelen, D.W., Properties of Polymers: Their Correlation with Chemical Structure; Their Numerical Estimation and Prediction from additive Group Contributions, Third Ed., Elsevier Science, New York (1990), Chapter 15 and 16.

Vinogradov, G.V. and Malkin, A.Y., Rheology of Polymers: Viscoelasticity and Flow of Polymers, Springer-Verlag, Berlin (1980), Chapter 3.

Wang, W.V. and Kramer, E.J., and Sachse, W.H., *J. Polym. Sci., Part B*, **20**, 1371 (1982).

Westover, R.F., *SPE Trans.*, **1**, 14 (1961).

Whorlow, R.W., Rheological Techniques, Ellis Horwood, New York (1992), Chap. 1.

Williams, M.C., *AIChE J.*, **13**, 534 (1967).

Williams, M.L., *J. Appl. Phys.*, **29**, 1395 (1953).

Williams, M.L., Landel, R.F., and ferry, J.D., *J. Am. Chem. Soc.*, **77**, 3701 (1955)

Wissinger, R.G. and Paulaitis, M.E., *J. Polym. Sci., Polym. Phys. Ed.*, **25**, 2497 (1987).

Wissinger, R.G., and Paulitis, M.E., *Ind. Eng. Chem., Res.*, **30**, 842 (1991)

Yamada, M. and Porter, R.S., *J. Appl. Polym. Sci.*, **18**, 1711 (1974).

ABSTRACT

RHEOLOGY OF MOLTEN POLYSTYRENE
WITH DISSOLVED GASES

by

CHOONGYONG KWAG

May, 1998

Co-advisors: Dr. Esin Gulari and Dr. Charles W. Manke

Major: Chemical Engineering

Degree: Doctor of Philosophy

Dissolved gases in polymers behave as excellent plasticizers, reducing viscosity significantly through the chain dilution effect and the addition of free volume. Rheological measurements and theoretical modeling are presented for molten polystyrene with dissolved gases, including carbon dioxide, 1,1-difluoroethane (R152a), and 1,1,1,2-tetrafluoroethane (R134a), which are considered to be environmentally acceptable for replacing previous ozone-depleting hydrochlorocarbon (HFC) refrigerants.

A modified pressurized capillary rheometer was employed for the viscosity measurement of molten polystyrene with dissolved gases under elevated pressures and at various temperatures. Experimental results show a significant reduction of viscosity due to dissolved gas, reaching as much as 3 orders of magnitude decrease in viscosity.

The composition-dependent shift factor scaling method, which is similar to classical viscoelastic scaling techniques (time-temperature superposition), was adopted in order to evaluate the effect of gas concentration on viscosity. The method successfully consolidates the viscosity data of gas-loaded systems onto a single master curve,

confirming that viscosity reduction by presence of dissolved gas can be represented quantitatively through the concentration shift factor.

The extended free volume model was developed for the theoretical prediction of viscosity reduction by the dissolved gas. Free volumes were calculated from the specific volumes and the occupied volumes of pure components and mixtures. The specific volumes of polymer-gas mixtures were computed by the Sanchez-Lacombe equation of state model, which was parameterized using the solubility data of gases in molten polystyrene. The theoretical viscosity reduction was compared with the experimentally obtained shift factor.

The effect of free volume on viscosity was found to be much greater than the effect of chain dilution. The viscosity reduction was maximized when the measurement temperature approaches the glass transition temperature of pure polymer, because of significant free volume increases due to the presence of dissolved gas.

In addition, an extensive pressure correction procedure was developed in order to obtain representative viscosity data from capillary rheometry, and this method was successfully applied to both pure and gas loaded polystyrene melts.

AUTOBIOGRAPHICAL STATEMENT

Name: Choongyong Kwag

Date of Birth: March 29, 1959

Education:

- Ph.D., Chemical Engineering, Wayne State University, Detroit, MI, 1998
- M.S., Chemical Engineering, Seoul National University, Seoul, Korea, 1983
- B.E., Ajou University, Suwon, Korea, 1980

Experience:

- Graduate Research Assistant, Wayne State University, Detroit, MI 1992-1997
- Research Engineer, LG Cable Co., Anyang, Korea, 1984-1988

Research Interest:

- Polymer Rheology and Processing
- Polymer Solutions
- Supercritical Fluid Applications